THE ROLE OF ZOOPLANKTON FOR CARBON EXPORT, NUTRIENT RECYCLING AND PHYTOPLANKTON BLOOM PHENOLOGY IN AN OCEAN BIOGEOCHEMICAL MODEL

Dissertation zur Erlangung des akademischen Grades eines Doktors der Naturwissenschaften

DR. RER. NAT.

am Fachbereich 2 der Universität Bremen

ONUR KARAKUŞ

Gutachterinnen:

Dr. Judith Hauck, AWI

Prof. Dr. Corinne Le Quéré, UEA

Bremen, Mai 2022

Datum des Kolloquiums: 20. Juli 2022

Universität Bremen

ALFRED-WEGENER-INSTITUT
HELMHOLTZ-ZENTRUM FÜR POLAR- UND MEERESFORSCHUNG

ONUR KARAKUŞ

THE ROLE OF ZOOPLANKTON FOR CARBON EXPORT, NUTRIENT RECYCLING AND PHYTOPLANKTON BLOOM PHENOLOGY IN AN OCEAN BIOGEOCHEMICAL MODEL

Onur Karakuş: *The Role of Zooplankton for Carbon Export, Nutrient Recycling and Phytoplankton Bloom Phenology in an Ocean Biogeochemical Model*, Bremen, May 2022

To the memory of my parents...
Özlemle ve sevgiyle...

ABSTRACT

Marine zooplankton, i.e., heterotrophic marine plankton, serve as trophic links between primary producers and higher trophic levels, and as recyclers for nutrients and carbon in the pelagic ecosystem. In addition, they play a major role for the carbon export flux due to fecal pellet production and fragmentation of particles. They are distributed all over the ocean and constitute a large variety of organisms. Because of large uncertainties in the estimation of parameters and the forms of equations, zooplankton are often parameterized in strongly simplified forms in ocean biogeochemical models. Nowadays, however, increasing data availability from experiments and observations makes it possible to implement different zooplankton functional types in models. This thesis presents the implementation of new zooplankton functional types into an ocean biogeochemical model. Subsequently, the sensitivity of net primary production, carbon export and nutrients to the implementation of these new zooplankton functional types was analyzed.

In my thesis, I use a global setup of the biogeochemical model Regulated Ocean Ecosystem Model (REcoM) coupled with the Finite Element Sea-Ice Ocean Model (FESOM). I implemented an explicit parametrization of micro-, meso-, and polar macrozooplankton based on process rates and biomass observations from the literature, as well as a representation of fast-sinking detritus. This extended version of REcoM was used to analyze the role of zooplankton for carbon export, nutrient recycling, and phytoplankton bloom phenology. In a second step, a new sinking routine that considers the roles of mineral ballasting and seawater viscosity on the particle sinking speed and the effect of oxygen on remineralization rates was added to the model. This set-up was used to assess the role of each factor (ballast minerals, seawater viscosity, and oxygen concentration) for the export and transfer efficiencies of carbon, i.e. the amount of particulate organic carbon that is exported across the euphotic depth and reaches the deep ocean.

The implementation of the new zooplankton groups changes the carbon transfer efficiency and net primary production in the model. *Publication I* and *III* highlight the influence of zooplankton on the transfer efficiency of carbon. *Publication I* shows that the transfer efficiency of carbon reaches up to 50% due to the high biomass of polar macrozooplankton in the Southern Ocean. Similarly, it was illustrated in *Publication III* that the high mesozooplankton biomass increases the transfer efficiency of carbon to 80% in the Equatorial Pacific. In addition, the model results presented in *Publication I* and *II* show the stimulation of net primary production due to the fast recycling of nutrients. After the parametrization of three zooplankton functional types, the new state of the model leads to a 25% increase in annual mean net primary production.

In addition to the effects on annual mean bulk fluxes, the more complex representation of zooplankton also affects the timing of phytoplankton blooms and biogeochemical fluxes. Zooplankton fecal pellets constitute an important share of sinking particulate organic carbon depending on the season in the Southern Ocean. In *Publication I*, it is shown that the typical shift from a dominance of phytodetrital aggregates in spring to zooplankton fecal pellets later in the year is now reasonably reproduced by the model after the implementation of polar macrozooplankton. Zooplankton grazing can play a decisive role in phytoplankton bloom phenology since it is a loss mechanism for phytoplankton. In *Publication II*, it is shown that the increased loss rates of phytoplankton due to stronger zooplankton grazing lead to the later start of the spring bloom. In addition, nutrient recycling by zooplankton prevents the fast exhaustion of nutrients by phytoplankton and consequently leads to a later end date of

the bloom. In the end, the more complex parametrization of zooplankton provides a modeled phytoplankton bloom phenology closer to observations. The results also indicate that the explaining mechanism behind the bloom phenology changes. While the start of the spring bloom is explained better with the 'Critical Depth Hypothesis' in the low grazing scenario, the system aligns with the 'Dilution-Recoupling Hypothesis' in the high grazing loss simulation.

Finally, the global spatial distribution of export and transfer efficiencies are analyzed in *Publication III*. In particular, I examined the impact of ballast minerals, seawater viscosity, and oxygen-dependent remineralization on export and transfer efficiencies. These three processes are often not considered in biogeochemical models. My results show that the global mean of export efficiency across the euphotic zone stays similar (13%) when the effects of mineral ballasting, seawater viscosity, and oxygen-dependent remineralization are added to the model. However, the global mean carbon transfer efficiency is more sensitive to these processes and varies between 25% and 32% in different simulations dependent on the representation of these processes. The magnitude of the effect of each process varies spatially. While the effect of ballast minerals can increase the transfer efficiency by a factor of nine in high latitudes and subtropical gyres, including oxygen-dependent remineralization can increase the transfer efficiency by 28% in low latitudes. The influence of seawater viscosity on the transfer efficiency is smaller compared to the other effects, and it increases the transfer efficiency 8% in subtropical gyres.

The thesis highlights that the zooplankton compartment in biogeochemical models should not only be treated as a closure term, and zooplankton functional types should be implemented in the global ocean biogeochemical models by using available datasets from the literature. It further underscores that missing out process representations of mechanisms that underlie carbon export has considerable effects on estimated carbon transfer efficiencies in biogeochemical models. Thus, further attention should be paid on the representation of missing processes related to particle formation and sinking.

ZUSAMMENFASSUNG

Marines Zooplankton, d.h. heterotrophes marines Plankton, dient als Bindeglied zwischen Primärproduzenten und höheren trophischen Ebenen sowie als Recycler von Nährstoffen und Kohlenstoff im pelagischen Ökosystem. Darüber hinaus spielt es eine wichtige Rolle für den Kohlenstoffexport durch das Ausscheiden von Kotballen und durch Partikelfragmentierung. Es ist im gesamten Ozean verbreitet und umfasst eine Vielzahl an Organismen. Wegen großer Unsicherheiten in der Abschätzung von Parametern und der Form von Gleichungen wird Zooplankton meist nur sehr vereinfacht in biogeochemischen Ozeanmodellen dargestellt. Die zunehmende Verfügbarkeit von experimentellen und Beobachtungsdaten macht es heutzutage jedoch möglich, verschiedene funktionelle Gruppen von Zooplankton in Modelle zu implementieren. Diese Arbeit präsentiert die Implementierung von zwei neuen funktionellen Zooplanktongruppen in ein biogeochemisches Ozeanmodell. Die Sensitivität von Netto-Primärproduktion, Kohlenstoffexport und Nährstoffen gegenüber der Implementierung dieser neuen funktionellen Zooplanktongruppen wurde analysiert.

In meiner Arbeit verwende ich das biogeochemische Model "Regulated Ocean Ecosystem Model" (REcoM), welches mit dem "Finite Element Sea-Ice Ocean Model" (FESOM) gekoppelt ist. Ich habe eine explizite Parametrisierung von Mikro-, Meso- und polarem Makrozooplankton basierend auf Prozessraten und Biomassebeobachtungen aus der Literatur, sowie eine neue Zustandsvariable von schnell sinkendem Detritus implementiert. Diese erweiterte Version von REcoM wurde für die Analyse der Rolle von Zooplankton im Kohlenstoffexport, im Nährstoffrecycling und in der Phänologie von Phytoplanktonblüten verwendet. In einem weiteren Schritt wurde eine neue Sinkroutine zum Modell hinzugefügt, welche den Effekt von Sauerstoff auf Remineralisierungsraten und den Einfluss von Meerwasserviskosität und Mineralen als Ballast auf die Geschwindigkeit von Partikelexport berücksichtigt. Diese Modellversion wurde verwendet, um die Rolle der einzelnen Faktoren (Minerale als Ballast, Meerwasserviskosität und Sauerstoffkonzentration) für den Export und die Transfereffizienz von Kohlenstoff, d.h. die Menge an partikulärem organischen Material, welche aus der euphotischen Zone bis in den tiefen Ozean exportiert wird, zu analysieren.

Die Implementierung der neuen Zooplanktongruppen verändert die Transfereffizienz von Kohlenstoff und die Netto-Primärproduktion im Modell. Die *Publikationen I* und *III* heben den Einfluss von Zooplankton auf die Transfereffizienz von Kohlenstoff hervor. *Publikation I* zeigt, dass die Transfereffizienz von Kohlenstoff aufgrund der großen Biomasse von polarem Makrozooplankton im Südozean bis zu 50% erreicht. Gleichermaßen wurde in *Publikation III* demonstriert, dass die große Biomasse von Mesozooplankton im äquatorialen Pazifik die Transfereffizienz von Kohlenstoff auf 80% erhöht. Darüber hinaus zeigen die Modellergebnisse aus den *Publikationen I* und *II* eine Stimulation der Netto-Primärproduktion aufgrund des schnellen Recyclings von Nährstoffen. Nach der Parametrisierung von drei funktionellen Zooplanktongruppen erhöht sich die durchschnittliche jährliche Netto-Primärproduktion im Modell um 25%.

Zusätzlich zu den Effekten auf die durchschnittlichen Stoffflüsse beeinflusst die komplexere Darstellung von Zooplankton auch den Zeitpunkt von Phytoplanktonblüten und die biogeochemischen Kreisläufe. Kotballen von Zooplankton machen saisonal einen wichtigen Anteil des sinkenden partikulären organischen Kohlenstoffs im Südozean aus. In *Publikation I* wird gezeigt, dass der typische Wechsel in den Hauptkomponenten des partikulären Kohlenstoffexports von Aggregaten aus totem Phytoplankton im Frühling zu Kotballen von

Zooplankton im späteren Jahresverlauf durch die Implementierung von polarem Makrozooplankton solide reproduziert wird. Fraßdruck durch Zooplankton kann eine entscheidende Rolle für die Phänologie von Phytoplanktonblüten spielen. In *Publikation II* wird gezeigt, dass der steigende Fraßdruck auf Phytoplankton zu einem späteren Start der Frühjahrsblüte führt. Darüber hinaus verhindert das Recycling von Nährstoffen durch Zooplankton das schnelle Aufbrauchen von Nährstoffen durch Phytoplankton und führt daher zu einem späteren Ende der Phytoplanktonblüte. Schlussendlich führt eine komplexere Parametrisierung von Zooplankton zu einer Phytoplanktonblüten-Phänologie im Modell, die besser mit Beobachtungen übereinstimmt. Die Ergebnisse zeigen außerdem, dass der grundlegende Mechanismus der Blütenphänologie verändert wird. Während im Szenario mit geringem Fraßdruck der Beginn der Frühjahrsblüte besser durch die 'Critical Depth Hypothesis' ('Hypothese der kritischen Tiefe') erklärt wird, entspricht das System mit starkem Fraßdruck der 'Dilution-Recoupling Hypothesis' ('Rückkopplungshypothese durch Verdünnung').

Schließlich wurde in *Publikation III* die globale räumliche Verteilung von Export und Transfereffizienzen analysiert. Im Speziellen habe ich den Einfluss von Mineralen als Ballast, Meerwasserviskosität und sauerstoffabhängiger Remineralisierung auf Export- und Transfereffizienzen untersucht. Diese drei Prozesse werden in biogeochemischen Modellen häufig nicht berücksichtigt. Meine Ergebnisse zeigen, dass die durchschnittliche globale Exporteffizienz durch die euphotische Zone etwa gleich bleibt (13%), wenn die Effekte von Ballastmineralen, Meerwasserviskosität und sauerstoffabhängiger Remineralisierung zum Modell hinzugefügt werden. Die durchschnittliche globale Transfereffizienz ist allerdings sensitiver und variiert zwischen 25% und 32% in verschiedenen Simulationen abhängig von der Repräsentation der drei Prozesse. Das Ausmaß des Effekts jedes einzelnen Prozesses ist räumlich variabel. In den hohen Breiten und den subtropischen Wirbeln kann die Transfereffizienz durch den Effekt von Ballastmineralien um ein Neunfaches, und in den niedrigen Breiten durch den Effekt der sauerstoffabhängigen Remineralisierung um 28% erhöht werden. Der Einfluss der Meerwasserviskosität auf die Transfereffizienz ist kleiner im Vergleich zu den anderen Prozessen und kann die Transfereffizienz in den subtropischen Wirbeln um 8% erhöhen.

Die Arbeit bekräftigt, dass Zooplankton in biogeochemischen Modellen nicht nur als Schließterm angesehen werden sollte und dass funktionelle Zooplanktongruppen mithilfe verfügbarer Datensätze aus der Literatur in globale Ozeanmodelle implementiert werden sollten. Darüber hinaus unterstreicht die Arbeit, dass das Weglassen von Prozessen, welche grundlegend für den Kohlenstoffexport sind, erhebliche Effekte auf die Abschätzung von Transfereffizienzen von Kohlenstoff in biogeochemischen Modellen haben kann. Deshalb sollte ein besonderes Augenmerk auf die Repräsentierung von bislang fehlenden Prozessen bezüglich der Partikelbildung und der Sinkprozesse gelegt werden.

ACKNOWLEDGEMENTS

This thesis wouldn't have been possible without the incredible support of so many people.

First and foremost, I would like to express my deepest gratitude to my Ph.D. supervisor Judith Hauck for providing guidance and permanent support during the whole period. A big thanks go to members of my thesis advisory committee: Dieter Wolf-Gladrow, Wilhelm Hagen, Christoph Völker, and Morten Iversen for always being there for scientific discussions.

I would also like to thank Cara Nissen for the numerous discussions on my manuscripts and presentations. That was always very helpful. A bouquet of thanks to Christine Klaas, Bettina Fach, and Eva Alvarez for taking their time for scientific discussion. I would also like to thank Corinne Le Quéré for agreeing to review my thesis .

Thanks to people in AWI Rechenzentrum that always support modelers.

A very special thank to my great PhD, office mate Miriam Siefert. One of the most important outcomes of this PhD is the friendship with you Dr. Seifert! Thanks for all the great time and memories. Do not forget anytime: Kafamiz rahat, Hayat bize güzel!

Big thanks to the MarESys/REcoM people for brunchs, lunchs, kayaking tour and also a couple of scientific discussions: Tanvi Nagwekar , Özgür Gürses, Claudia Hinrichs, Nabir Mamnun, Laurent Oziel, Ying Ye, Chris Danek and Frauke Bunsen. And of course, a lot of thanks to the 'Biogeos' for a warm working atmosphere and the graduate school POLMAR for offering great courses.

I thank from the bottom of my heart all the fantastic friends making life amazing in Bremen/Bremerhaven! A PhD time without these amazing people would be so much harder. Thanks to all my friends, close by or far away, that make life beautiful.

Last but not least, I would like to express my enormous gratitude to my family. Thank you for your endless support.

CONTENTS

GENERAL INTRODUCTION

1.1 THE CARBON CYCLE AND GLOBAL CLIMATE CHANGE

Before the industrial revolution, the concentration of atmospheric carbon dioxide (CO_2) was almost constant at 280 parts per million (ppm), only varying by about ten ppm over a few thousand years (*Siegenthaler et al.*, 2005). In the year 2020, the average concentration of atmospheric CO_2 reached 412.4 ppm, which is about 47% higher than the preindustrial CO_2 concentration (*IPCC*, 2021). This increase in CO_2 concentration was caused by human activities such as burning of fossil fuels and land-use change. The average CO_2 emissions from human activities amounted to 10.9 ± 0.9 Pg C yr^{-1} in the decade 2010-2019, and 46% of these emissions accumulated in the atmosphere. The remainder was taken up by the ocean (23%) as well as vegetation and soils in the terrestrial biosphere (31%, *IPCC*, 2021). This perturbation of the global carbon cycle causes an increase in Earth's global average temperature due to the greenhouse effect (*Foote*, 1856). The greenhouse effect traps heat through absorption by so-called greenhouse gases (i.e. atmospheric CO_2, water vapor, nitrous oxide, methane) and prevents the heat from escaping out of the atmosphere. The rise of global average temperature impacts Earth's climate and weather patterns resulting in floods, droughts, sea level rise, melting of glaciers and sea-ice retreat (*IPCC*, 2021). The severe consequences of the human-induced rise of atmospheric CO_2 concentrations make it important to understand the global carbon cycle.

Carbon is stored in the Earth's crust, sediments, aquatic systems, terrestrial biosphere, and atmosphere in the Earth System. These components can be referred to as 'carbon pools' (sometimes also referred to as reservoirs or stocks). The movement of carbon across these pools is called 'flux'. The global carbon cycle links the four main pools of carbon: Earth's crust, terrestrial biosphere, ocean, and atmosphere. The largest amount of carbon is stored in the Earth's crust, which amounts to 90 million petagram of carbon (Pg C). The fluxes from this pool occur on a geological time scale (*Sundquist*, 1985). The terrestrial biosphere stores approximately 2150 Pg C in organic form, mainly in plants and soils (*IPCC*, 2021). The fluxes in and out of this pool happen due to plants' photosynthesis, respiration of organisms, and soil respiration. The atmosphere holds a considerably lower amount of carbon (830 Pg C, *IPCC*, 2021) than the other pools, and most of the atmospheric carbon is in the form of CO_2. Lastly, the Earth's oceans contain around 38,000 Pg C, most of it in dissolved inorganic forms (i.e. $CO_{2(aq)}$, bicarbonate HCO_3^-, and carbonate CO_3^{2-}) in the intermediate and deep ocean (37100 Pg C, *IPCC*, 2021) as well as about 700 Pg C as dissolved organic carbon. Although the amount of carbon stored in the surface ocean is relatively small (900 Pg C, *IPCC*, 2021), this carbon can be directly exchanged with the atmosphere.

1.2 THE MARINE CARBON CYCLE

The carbon cycle is a key element cycle in the ocean, and it describes the exchange of carbon between its various pools. Its interaction with the atmosphere has fundamental importance for the Earth's climate. Open ocean waters exert a major role in storing carbon and in regulating the concentrations of CO_2 in the atmosphere because of air-sea fluxes of CO_2 (*Sarmiento and Gruber*, 2006). Two mechanisms govern the magnitude of the air-sea CO_2 flux as well as the carbon storage in the ocean: the solubility pump and the biological carbon pump (*Volk and Hoffert*, 1985).

The solubility pump regulates the absorption or release of CO_2 at the interface between the surface ocean and atmosphere. The solubility pump enriches the deep ocean with dissolved inorganic carbon in the high latitudes, where the water temperatures are low and consequently CO_2 is more soluble (*Zeebe and Wolf-Gladrow*, 2001). High latitudes are the regions where deep water formation happens and this mechanism carries water that has equilibrated with

atmospheric CO_2 levels to the deep ocean (*Sarmiento and Gruber*, 2006). In upwelling regions at lower latitudes, carbon-rich waters are brought back to the surface. The water warms up in these areas, releasing CO_2 into the atmosphere.

Marine pelagic ecosystems channel the carbon through the biological carbon pump (BCP) which describes the transfer of particulate and dissolved organic carbon from the surface to the deep ocean (*Volk and Hoffert*, 1985; *Buesseler et al.*, 2020). It is driven by unicellular algae (marine phytoplankton) that use sunlight as an energy source to form organic carbon from inorganic carbon compounds in their cells (*Karl*, 2007). This process is called primary production, and it forms the base of trophic levels in pelagic ecosystems and of the biological carbon pump. Although marine phytoplankton account for only 0.2% of the global plant biomass, they are responsible for about half of the global net primary production (*Field et al.*, 1998). Other organisms depend on the energy from particulate organic carbon that was initially fixed by primary producers. These organisms are called heterotrophs and perform secondary production, which is the consumers' incorporation of biomass. Zooplankton are the main secondary producers in the pelagic environment. Primary production, secondary production, and trophic interactions affect the fate of particulate and dissolved carbon in the ocean.

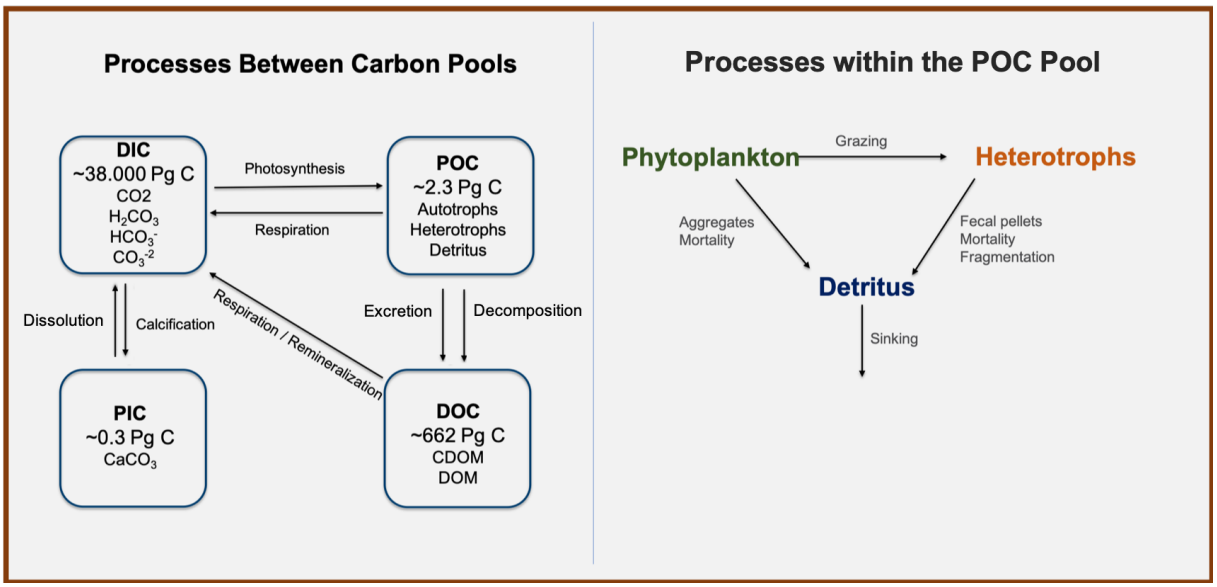

FIGURE 1.1: The key pools and processes that affect the ocean biological carbon pump. There are four different carbon pools: dissolved inorganic carbon (DIC), dissolved organic carbon (DOC), particulate inorganic carbon (PIC), and particulate organic carbon (POC). The processes, such as calcification, respiration, remineralization, photosynthesis, and excretion, determine the fluxes among the carbon pools. Within the POC pool, processes like grazing, fecal pellet production, natural mortality, gravitational sinking, and fragmentation redistribute the carbon between phytoplankton, heterotrophs and detritus.

The marine carbon cycle consists of four main carbon pools (Fig. 1.1, *Brewin et al.*, 2021), namely dissolved inorganic carbon (DIC: 38,000 Pg C, *Hedges*, 1992), dissolved organic carbon (DOC: 662 Pg C, *Carlson and Hansell*, 2015), particulate organic carbon (POC: 2.3 Pg C, *Stramska*, 2009) and particulate inorganic carbon (PIC: 0.03 Pg C, *Hopkins et al.*, 2019). The DIC pool, as the largest pool, includes carbon dioxide (CO_2), carbonic acid (H_2CO_3), as well as carbonate (CO_3^{2-}) and bicarbonate ions (HCO_3^-, *Zeebe and Wolf-Gladrow*, 2009). Phytoplankton take up bicarbonate (the main component of DIC) and CO_2 as substrates for photosynthesis and generate organic matter. The processes of respiration and remineralization release CO_2 from the DOC and POC pools back to the DIC pool. The second-largest carbon pool in the ocean is the

DOC pool which includes colored dissolved organic matter (CDOM), the optically measurable component of DOC. Furthermore, the metabolic waste of marine organisms, dissolved organic carbon resulting from excretion and degradation of particulate organic carbon, is a major component of the dissolved organic carbon pool (*Carlson and Hansell*, 2015). Although the standing stock of POC is relatively small compared to other carbon pools, the fluxes into and out of the POC pool are high. For example, the estimates of global ocean net primary production vary between 35 and 70 Pg C yr^{-1} (*Carr et al.*, 2006; *Kulk et al.*, 2020). The magnitude of the particulate organic carbon that is exported from the euphotic zone is estimated to be between 4 and 12 Pg C y^{-1} (*Laws et al.*, 2000; *Henson et al.*, 2011; *DeVries and Weber*, 2017). The POC pool is highly dynamic and has the highest turnover rate of any organic carbon pool in the planet (*Sarmiento and Gruber*, 2006). Small changes in the POC reservoir in the ocean can affect the carbon cycle substantially (*Stramska and Cieszyńska*, 2015; *Behrenfeld et al.*, 2005).

Within the POC pool, key processes such as grazing, aggregation, natural mortality, fecal pellet production, and gravitational sinking redistribute the particulate organic carbon produced by marine phytoplankton to other ecosystem components and deep ocean. Natural mortality of phytoplankton due to viral cell lysis or viral infection (*Brussaard*, 2004), aggregation of phytoplankton cells due to the coagulation and flocculation (*Smetacek*, 1985; *Kiørboe et al.*, 1990), fragmentation of larger particles through biological or physical processes such as feeding, as well as swimming (*Goldthwait et al.*, 2004; *Mayor et al.*, 2014) can affect the fluxes of particulate organic carbon. Zooplankton grazing can transfer up to 60% of the annual primary production to heterotrophic organisms through grazing (*Calbet*, 2008). The ingested carbon by zooplankton is used for secondary production by zooplankton, and the rest is converted to different forms of carbon. Respiration, for instance, converts particulate organic carbon to dissolved inorganic carbon. Besides, marine organisms release dissolved organic carbon through excretion. A critical process of the BCP is the sinking of detrital particles that determines the transfer of carbon to the mesopelagic zone, and it is sometimes called the gravitational pump (*Buesseler et al.*, 2020).

1.2.1 *Downward Flux of Particulate Organic Carbon*

Particulate organic carbon is exported to the deep ocean by several mechanisms such as gravitational, eddy-subduction, mesopelagic migrant, seasonal lipid and mixed-layer pumps (*Boyd et al.*, 2019). Among these mechanisms, the gravitational settling of the particulate organic carbon is considered to be the main mechanism of particle export. The gravitational pump describes the downward sinking of particulate organic carbon from the surface ocean to the deep ocean with a sinking rate that depends on size and density of the particles (*Siegel et al.*, 2016).

A major portion of carbon and nutrients bound in biomass by primary production is recycled in the upper ocean. Only a small fraction (less than 20%) of it sinks out from the upper ocean to depth as marine snow, taking along minerals, nutrients, and organic carbon (*Omand et al.*, 2020). The sinking particles can be made of intact phytoplankton cells (*Rembauville et al.*, 2016; *Leblanc et al.*, 2018), aggregates of phytoplankton (*Riley et al.*, 2012; *Laurenceau-Cornec et al.*, 2015) and fecal pellets of zooplankton (*Cavan et al.*, 2015). Although single dead or living phytoplankton cells that are not grazed or unaggregated can be found in sediment traps (*Durkin et al.*, 2016), they are generally not reported since phytoplankton enumeration methods require a substantial amount of cells (*Le Moigne et al.*, 2016). The major constituents of sinking particulate organic carbon are phytodetrital aggregates and zooplankton fecal pellets (*Kiørboe and Hansen*, 1993; *Laurenceau-Cornec et al.*, 2015). Aggregation of phytoplankton cells happens due to stickiness. When their concentration and stickiness are high enough, phytoplankton cells collide and

form large phytodetrital aggregates (*Jackson*, 1990; *Burd and Jackson*, 2009). *Laurenceau-Cornec et al.* (2015) found that phytodetrital aggregates form 50% of the total amount of particles and dominate the sinking particles in most of the stations in the Southern Ocean. The second major path is through zooplankton fecal pellets or fecal aggregates, which are the reaggregation of phytodetritus and zooplankton fecal pellets (*Turner*, 2002; *Laurenceau-Cornec et al.*, 2015). A large contribution of the fecal pellets to the organic carbon fluxes was recorded in high latitudes (*Ebersbach and Trull*, 2008; *Laurenceau-Cornec et al.*, 2015). The proportion of zooplankton fecal pellets to total carbon fluxes is highly variable, but most values are below 40% in the global ocean (*Turner*, 2015).

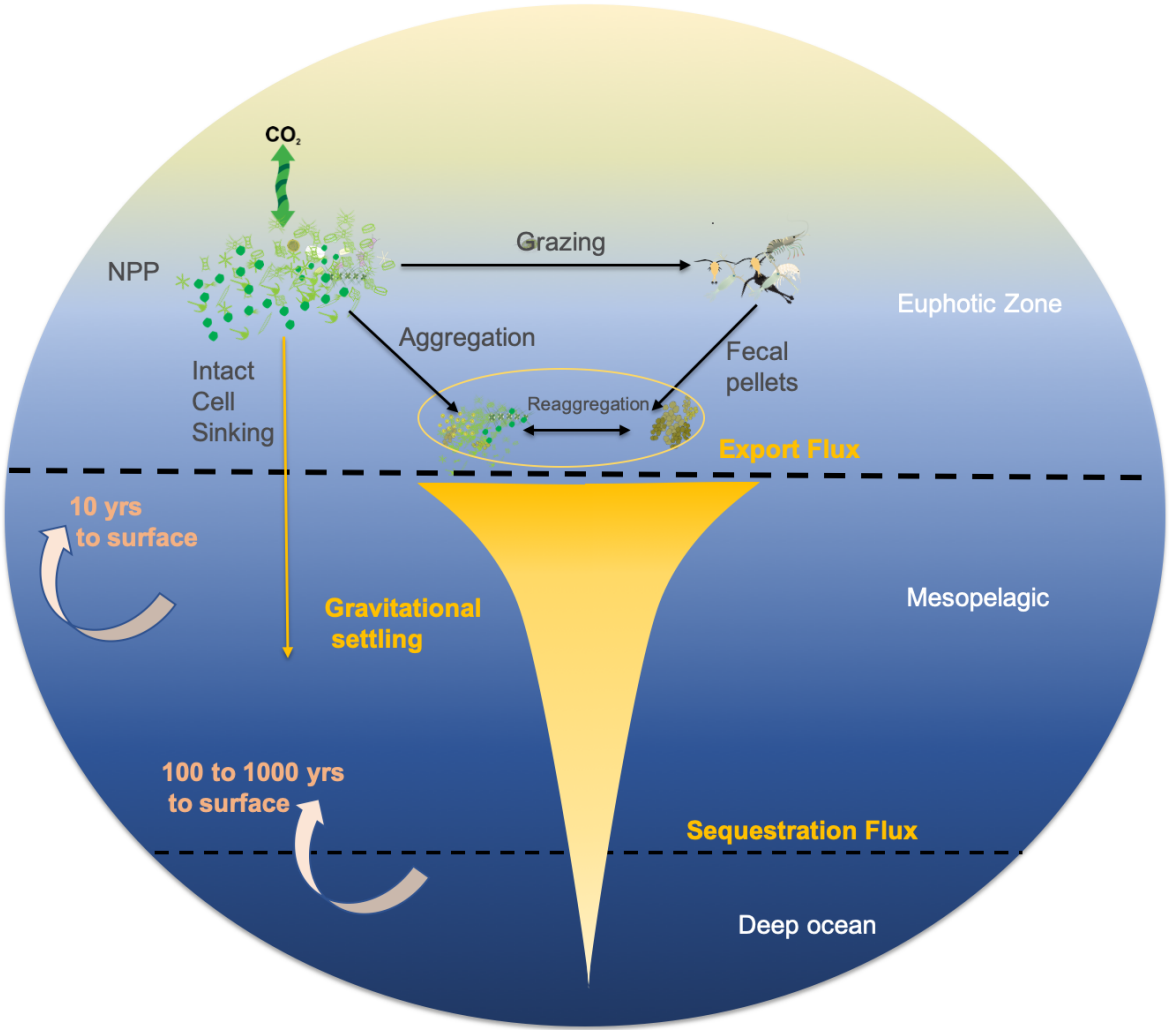

FIGURE 1.2: Schematic of particulate organic carbon pathways in the ocean. Phytoplankton fixes carbon in organically-bound forms, which is referred to as net primary production (NPP). A part of this organic matter is transferred to zooplankton by grazing. Zooplankton produces sinking fecal pellets, and phytoplankton produce sinking aggregates. The fecal pellets and aggregates can reaggregate. All three components (phytoplankton aggregates, zooplankton fecal pellets, and reaggregates) of the sinking particles can reach the deep ocean due to gravitational settling. Intact phytoplankton cells can also sink, although they account for only a small proportion of the sinking particulate organic carbon. The turnover of sequestered carbon below the sequestration depth (>1000 m) to the surface takes 100 years or more.

While the turnover of the exported carbon from the mesopelagic zone to the euphotic zone takes decades, it takes hundreds to thousands of years from the deep ocean (below 1000 m) to

the surface (Fig. 1.2, *Passow and Carlson*, 2012). Once the carbon reaches the deep ocean, it is isolated from the atmosphere for centuries. Therefore, it is vital to investigate the efficiency of the biological carbon pump. It can be assessed by using two metrics called export efficiency and transfer efficiency (*Buesseler et al.*, 2020). While the export efficiency quantifies the strength of the particle flux from the surface ocean, the transfer efficiency measures the fraction of particulate organic carbon transported to the deep ocean. The export efficiency/ratio (e-ratio) is the ratio between the POC flux at a certain depth level and the net primary production above this depth level, which is usually chosen as relatively shallow (euphotic depth or fixed 100 m). The export efficiency is highly variable in the global ocean. While it is generally higher (15-25%) in high latitudes, it decreases in low latitudes (*Henson et al.*, 2012; *Laufkötter et al.*, 2016). The export efficiency is thought to be positively correlated with the net primary production and negatively correlated with sea surface temperature (*Laws et al.*, 2011; *Henson et al.*, 2012). However, on a regional scale in the Southern Ocean, it was found that the e-ratio is negatively correlated with NPP (*Maiti et al.*, 2013). The second metric, the 'transfer efficiency,' is the ratio between the POC flux in the deep ocean (>1000 m) and the POC flux at a shallower depth (fixed 100 m, or euphotic depth). The POC flux around 1000 m is also called 'sequestration flux,' because it results in a turnover of carbon that takes longer than 100 years (*Passow and Carlson*, 2012). The transfer efficiency of carbon shows similar spatial variability in the global ocean as the export efficiency, i.e., high transfer efficiency in high latitudes and low transfer efficiency in the subtropics (*Weber et al.*, 2016; *Maerz et al.*, 2020). The sequestration flux and consequently transfer efficiency depends on input rates of nutrients to the ocean, the export flux at the base of the euphotic zone, the carbon fixation and remineralization rates, and the flux attenuation at and above 1000 m (*Passow and Carlson*, 2012). Specifically, ballast minerals (*Weber et al.*, 2016), temperature (*Iversen and Ploug*, 2013) and oxygen levels (*Devol and Hartnett*, 2001) play a major role in the determination of the transfer efficiency.

1.2.2 *Modelling the Particulate Organic Carbon Fluxes*

The attenuation of sinking particulate organic carbon is one of the major topics of biological carbon pump studies. There are already several particle flux attenuation models such as depth-attenuation (*Suess*, 1980) , exponential (*Banse*, 1990), power-law (*Martin et al.*, 1987), ballast model (*Armstrong et al.*, 2001a) and double exponential models (*Lutz et al.*, 2002). While the double exponential model (*Lutz et al.*, 2002) captures both fast and slow attenuating fluxes, the other models use a single carbon pool. Among these models, Martin's power-law is the most used formulation (*Martin et al.*, 1987) to describe the particulate organic carbon export in the global ocean. The "Martin curve" was derived from measurements from an open ocean station in the Pacific, and this formulation suggests a 90% decline of POC flux between a depth of 100 m and 1000 m (*Martin et al.*, 1987).

Besides these mechanistic models that are often applied to observational studies, ocean biogeochemical and Earth System Models are commonly used to investigate the integrated global carbon export flux (*Palevsky and Doney*, 2018), the export ratio (*Henson et al.*, 2015; *Laufkötter et al.*, 2016), transfer efficiency (*Laufkötter et al.*, 2017), and their temporal and spatial variability (*Henson et al.*, 2015). The total estimated global carbon export in CMIP5 and CMIP6 models shows a large range of 2.4-11.9 Pg C yr^{-1} as a result of the different ecosystem structures of the models (*Séférian et al.*, 2020). Although there is large uncertainty about the integrated global carbon export production, models are useful to investigate mechanisms that are difficult to derive from instantaneous measurements. For example, the time lag between primary production and export production was illustrated by using a single biogeochemical model (*Henson et al.*, 2015).

However, only a subset of the processes that affect particle formation, sinking, and remineralization are represented in the models that are used in the CMIP6 simulations. *Henson et al.* (2022) summarized the processes and their effects on global carbon export. For example, the relatively complex biological interactions (e.g., particle fragmentation, vertical migration of zooplankton and fish, particle stickiness, and variable stoichiometry of the particles) are just represented in two of the 19 CMIP6 models. Temperature and oxygen-dependent remineralization rates are used in more than half of the models. The neglect of processes causes positive or negative biases in the present-day modeled global export simulations. While not considering fish and zooplankton vertical migration specifically causes an underestimation of present-day global export in the models, the underrepresentation of processes such as particle fragmentation or oxygen-dependent remineralization results in an overestimation.

1.3 MARINE ZOOPLANKTON

Zooplankton are the animal component of the planktonic community, often in microscopic sizes, that inhabit the ocean. They are distributed all over the ocean, from the surface to depth (*Hernández-León et al.*, 2020). Zooplankton constitute a large variety of organisms. If meroplankton (organisms that have both planktonic and benthic stages of life cycles) is included, the number of zooplankton species reaches some ten thousands (*Lenz*, 2000). There are two systematic groups: protozooplankton (unicelluar) and metazooplankton (multicellular) (*Lenz*, 2000). The systematic group protozooplankton consists of the main zooplankton taxa of heterotrophic flagellates, ciliata, foraminifera, and radiolaria. Cnidaria (e.g., polychaeta larvae), mollusca (e.g., veliger larvae), crustacea (e.g., copepoda), and tunicata form the metazooplankton systematic groups. All of the main taxonomic groups can be in the form of meroplankton which have a planktic or benthic stages or holoplankton that is planktic in their entire life cycle. While 27% of the total zooplankton species are holoplankton (16% protozooplankton, 11% metazooplankton), the remaining 73% consist of the meroplankton (*Lenz*, 2000).

Marine zooplankton covers different size classes, which are in the range of tiny 2 μm ciliates to large 2 m jellyfish. According to one of the most accepted size classifications by *Sieburth et al.* (1978), there are the following five size classes: nano (2-20 μm, e.g., flagellates), micro (20-200 μm, e.g., ciliates), meso (0.2-20 mm, e.g., copepods), macro (2-20 cm, e.g., krill) and mega (0.2-2 m, e.g., jellyfish). While the main constituents of nano-zooplankton are the flagellates that feed on bacteria, the other protozoans belong to the microzooplankton class. Copepods are the dominant zooplankton in the mesozooplankton group and macrozooplankton consists of euphausiids, but also of pelagic members of cnidarians, amphipods, and decapods. Only a few species, such as jellyfish, pelagic tunicates, and chain-forming salps, can reach a large size and belong to the mega-zooplankton group.

In the following subsections, I will describe the roles of zooplankton in carbon cycle, nutrient recycling and phytoplankton bloom phenology. Subsequently, I will describe the effect of warming on zooplankton in the global ocean.

1.3.1 *Marine Zooplankton and the Carbon Cycle*

The pelagic food web, which contains thousands of different living organisms, plays a central role in the ocean carbon cycle. In this complex ecosystem, zooplankton has a major role in the pathways of the carbon flow. These pathways drive the spatial and temporal variability of nutrient recycling, carbon export production, and grazing coupling (*Steinberg and Landry*, 2017). Zooplankton transfer carbon in different forms, i.e. particulate organic carbon (POC), dissolved

organic carbon (DOC) and dissolved inorganic carbon (DIC), and can convert carbon from one of these forms to another. While particulate organic carbon is transferred due to predator-prey interaction and egestion, metabolic waste excretion and respiration affect the dissolved organic and inorganic carbon content of the seawater. In the following, each paragraph will describe the roles of zooplankton in the carbon cycle.

Zooplankton grazing, fecal pellet production and vertical migration directly affect the transfer of particulate organic carbon in the ocean. One of the ways of particulate organic carbon transfer is a result of feeding relationships. Microzooplankton is the major consumer of phytoplankton and bacteria in the global ocean, and consumes 60% of the annual primary production (*Calbet*, 2008). Microzooplankton is mainly consumed by mesozooplankton, and this represents the main utilization pathway of the secondary production (*Steinberg and Landry*, 2017). At the same time, zooplankton can be the main food source for higher trophic level organisms such as cetaceans. A very well-known example is the Antarctic krill as prey for whales in the Southern Ocean (*Savoca et al.*, 2021). Another important role of zooplankton on particulate organic carbon transfer is due to egestion of fecal pellets. Depending on the region and season, the contribution of zooplankton fecal pellets to the carbon flux can reach up to 100% (*Turner*, 2015). The relative contributions of zooplankton fecal pellets to carbon export varies seasonally and spatially (*Ebersbach and Trull*, 2008; *Iversen et al.*, 2017; *Halfter et al.*, 2020). For example, zooplankton fecal pellets constitute the highest share of 22%-63% of the total carbon flux in spring and the lowest share of 2%-7% in summer in the Pacific Antarctic Polar Front region (*Dagg et al.*, 2003). Similarly, the carbon flux at 200 m in Kerguelen Plateau is dominated by fecal pellets ($56 \pm 19\%$ of the total flux) in early spring (*Laurenceau-Cornec et al.*, 2015). The egestion rate of zooplankton is generally assumed to be constant at 30% of assimilated food (*Steinberg and Landry*, 2017). However, the rates show a large variability depending on the species (*Bochdansky, Alexander B. and Deibel, Don and Rivkin, Richard B.* , 1999), food nutritional quality (*Purcell*, 1983) and food type (*Besiktepe and Dam*). In addition, the sinking characteristics (fast or slow degradation) of the fecal pellets and the fecal pellet production rates depend on the feeding environment (*Besiktepe and Dam*). *Atkinson et al.* (2012) showed that the egestion rates increase with increasing feeding rates of zooplankton. A last important process is the the vertical migration of zooplankton that spans diel and seasonal timescales (*Schnack-Schiel and Hagen*, 1994). The diel vertical migrators feed in the surface ocean at night (nocturnal ascend), which is then metabolized during the day in the mesopelagic zone (*Steinberg and Landry*, 2017; *Bandara et al.*, 2021). Despite the generality of this feature, the vertical migration can also be on a reversed time scale, i.e., nocturnal descent (*Ohman et al.*, 1983). Diel vertical migration is considered an active component of the biological carbon pump. The carbon flux as a result of vertical migration can reach up to 13.0-71.4% of computed sinking particulate organic carbon fluxes and hence contributes significantly to the export of carbon (*Longhurst et al.*, 1990; *Steinberg et al.*, 2000).

Zooplankton supports the microbial loop in the ocean via the release of DOC by sloppy feeding, direct excretion and fecal pellet leaching (*Steinberg and Landry*, 2017). Zooplankton-mediated release of dissolved organic carbon is one of the principal mechanisms that control the quantity of DOC in the ocean (*Carlson and Hansell*, 2015). As a result of sloppy feeding, which is the physical breakage of a food source, some of the DOC in the prey is released into the water column. This is the first step of the release of DOC by zooplankton. Sloppy feeding can make up 20% of the total DOC released by zooplankton (*Saba et al.*, 2011). Other studies show that sloppy feeding by marine copepods can make up up to 70% of the total DOC released by zooplankton (*Møller*, 2007). The amount of sloppy feeding depends on the species and the grazing strategies. For example, while for crustacean zooplankton the amount of DOC released due to sloppy feeding has the highest share of the total DOC released by zooplankton, it is lower for microzooplankton species such as ciliates (*Steinberg and Landry*,

2017). The prey concentration or the size difference between prey and predator can affect the amount of carbon that is released. For example, when the prey size is relatively larger than the predator, DOC release due to sloppy feeding is higher (*Møller*, 2005, 2007). Another important mechanism is the direct excretion of the metabolic waste of zooplankton. Excretion rates of zooplankton depend on the temperature and the body mass (*Ikeda*, 2014). According to the literature, approximately 10 to 30% of the ingested POC by zooplankton is released as DOC (*Carlson and Hansell*, 2015). An indirect source of dissolved organic carbon is the leaching of egested fecal pellets. Leaching may occur within minutes of egestion (*Møller et al.*, 2003) and continue for hours or days (*Urban-Rich*, 1999; *Thor et al.*, 2003). The leachability of particulate matter can be related to fragility (*Iversen et al.*, 2017), density (*Bruland and Silver*, 1981) and lack of a peritrophic membrane (*Caron et al.*, 1989).

Finally, respiration is another important process that plays a major role in the carbon cycle. Approximately 50% of the ingested carbon by microzooplankton and mesozooplankton is released back to the ecosystem through respiration (*Steinberg and Landry*, 2017). Global mesozooplankton respiration amounts to 17-32% of the global net primary production (*del Giorgio and Duarte*, 2002; *Hernández-León and Ikeda*, 2005). Body mass, temperature, oxygen, food concentration, light, pressure, and pH can all affect the respiration rates of zooplankton (*Ikeda*, 2014; *Hernandez-Leon and Ikeda*, 2005).

1.3.2 *Marine Zooplankton as Nutrient Recyclers*

In the previous section, the role of zooplankton on the release of dissolved organic matter as a part of the carbon cycle was introduced. Here, the role of zooplankton in macro- and micronutrient recycling will be described. All essential nutrients may potentially be recycled within the productive surface layer between primary and secondary producers (*Smetacek*, 1985). Zooplankton drive nutrient recycling by grazing, controlling the transformation and movement of nutrients over time and space and, thus, play an essential role in the recycling of macronutrients such as silicic acid and nitrogen, and micronutrients such as iron. Nutrient recycling by zooplankton directly impacts primary production, especially in regions with nutrient limitations. Zooplankton nutrient recycling can stimulate phytoplankton growth (*Coello-Camba et al.*, 2017), and nutrient regeneration can support 11-25% of the primary and bacterial production (*Verity*, 1985; *Hernández-León et al.*, 2008).

Sloppy feeding, direct excretory release, and leaching from the fecal pellets are processes that affect nutrient recycling by zooplankton. The biological availability and the relative contributions of each process change depending on the body mass, seawater temperature, food quality, prey size, and the zooplankton species. For example, higher temperature and body mass increase nutrient excretion in tropical areas (*Ikeda*, 2014). While *Saba et al.* (2009) show that having either a carnivorous or an omnivorous diet affects the NH_4^+ release of copepods, *Møller* (2007) illustrates the importance of the prey size. Recently, *Böckmann et al.* (2021) showed that in the Southern Ocean, the impact of the bioavailability of iron leached from fecal pellets depends on the group of zooplankton species that egested the fecal pellets (krill or salp). Previous experimental studies also clearly illustrate the fuelling effect of fast-recycling of nutrients by zooplankton (*Coello-Camba et al.*, 2017; *Laglera et al.*, 2017; *Böckmann et al.*, 2021). Zooplankton grazing is an important mechanism for the release of organic iron ligands in the ocean (*Sato et al.*, 2007). For instance, *Tovar-Sanchez et al.* (2007) quantify the large iron release by krill, and *Laglera et al.* (2017) illustrate the rapid recycling of particulate iron by copepods. Besides, *Schmidt et al.* (2016) study the mobilization of iron attached to the lithogenic particles by zooplankton and how gut processes can accelerate its dissolution. Although the study considers specifically

the Antarctic krill, this process is likely a widespread phenomenon among suspension-feeding zooplankton.

1.3.3 *Marine Zooplankton as Grazers of Phytoplankton*

In marine ecosystems, the term 'grazing' is used to describe the consumption of phytoplankton by zooplankton. Grazing by zooplankton determines the fate of marine phytoplankton production (*Banse*, 2013). The predation of phytoplankton occurs constantly and is much more intense in the ocean ecosystem compared to the land ecosystems (*Smetacek*, 2012; *Menden-Deuer et al.*, 2021a). This interaction between zooplankton and phytoplankton does not only affect the total phytoplankton biomass but it also has an impact on the phytoplankton composition and their succession due to selective grazing (*Ryther and Sanders*, 1980; *Verity and Smetacek*, 1996; *Behrenfeld*, 2010). While zooplankton generally graze on prey that is 10-fold smaller than their own body size, they can still graze on phytoplankton that is larger than themselves (*Hansen et al.*, 1994; *Menden-Deuer et al.*, 2005). Global average removal of primary production by herbivorous grazers ranges from 49% to 67% (*Calbet and Landry*, 2004; *Schmoker et al.*, 2013). Depending on the size class of zooplankton, their contribution to total grazing losses varies. Microzooplankton graze on 67% of the global primary production (*Calbet and Landry*, 2004), and mesozooplankton contributes with 10% to the total grazing loss in regions of high productivity (*Calbet*, 2001). The carnivory among heterotrophs (e.g., predation of protozooplankton by metazooplankton) is also important in the ecosystem. For instance, although the protozooplankton consumes most of the phytoplankton, it cannot curtail the phytoplankton bloom as a result of high grazing pressure on them by metazooplankton (*Smetacek*, 2012).

Finally, zooplankton grazing can also affect the phytoplankton bloom phenology. The phytoplankton bloom depends on the bottom-up (e.g., nutrients, temperature, light) and top-down control (grazing by zooplankton). As a result of an imbalance between the loss and growth rates, the phytoplankton bloom starts or ends. Since grazing by zooplankton is one of the major loss terms for phytoplankton, it may play a decisive role on the bloom start day. Dilution of the grazers through deepening of the mixed layer depth (MLD), for instance, can allow the bloom initiation already in autumn (*Behrenfeld*, 2010). The spring bloom of phytoplankton can terminate due to exhaustion of surface nutrients and overgrazing by heterotrophs.

1.3.4 *Climate change and Zooplankton*

The increase of heat-trapping greenhouse gas levels in the Earth's atmosphere increased the Earth's global average temperature by 1.09°C between 1850-1900 to 2011-2020 (*IPCC*, 2021). This human-induced warming causes several natural disasters such as the melting of glaciers, decreased sea ice, droughts, floods, and other extreme events. The change in the physical environment causes migration and extinction of plants and animals already today (*IPCC*, 2021).

Plankton's physiological rates, composition, abundance, and trophic efficiency are tightly linked with temperature (*Richardson*, 2008). Several time-series studies have already shown that the distribution, abundance, and phenology of zooplankton were impacted in the period between 1958 and 2002. The warming of surface waters results in poleward movement of zooplankton species (*Beaugrand et al.*, 2002; *Lindley and Daykin*, 2005). Although the poleward movement of marine populations due to warming is not always confirmed (*Edwards et al.*, 2021), the presence of warm-water species in colder regions has increased over the last 60 years (*Beaugrand et al.*, 2009). Warming events result in earlier timing of the zooplankton biomass peak across a wide range of geographical locations from the Subarctic Pacific to

the North Sea (*Mackas et al.*, 1998; *Edwards et al.*, 2006). Over the last 60 years, an increase in the abundance of tropical foraminifera is the classic example of the impact of warming on plankton abundance (*Field et al.*, 2006). Experimental studies also reveeal an increase in sexual and asexual reproduction rates of jellyfish (*Purcell*, 2005). All these changes in the distribution and abundance affect the competition between species. In a warming ocean, jellyfish may, for example, have more advantages than fish (*Parsons and Lalli*, 2002).

1.4 MATHEMATICAL MODELING OF THE MARINE ENVIRONMENT

Mathematical modeling is the concept of creating a simple mathematical representation of systems or phenomena to get insights and make projections into the future (*Fennel and Neumann*, 2015). While models describe how the world functions, they also make it easier to understand the underlying processes. Mathematical models can be used to develop scientific understanding, test the effect of changes in a system, or aid decision-making. The development of models involves two steps: identifying the most important processes in the systems and formulating their mathematical description. The first step is to decide which processes should be included or excluded in the model. The second step is to define the form of the equations. Modeling stages can be divided into four categories: building, studying, testing, and finally using. All of these stages evolve together. When the models are being used, they are rebuilt according to the newly evolving questions. Whenever a new feature is added to a model, it should be studied and tested again.

Mechanistic models are widely used in marine research to describe the general circulation (*Bryan*, 1968), biogeochemistry (*Maier-Reimer*, 1993) and ecosystem studies (*Fleming*, 1939; *Steele and Henderson*, 1992). Biogeochemical and ecosystem models are generally coupled to a circulation model to simulate the advection, mixing, and diffusion of tracers. The principle of mathematical modeling (building, studying, testing, using) also applies to studies of marine environments. The different scientific questions of various research groups lead to the development of a large variety of biogeochemical/ecosystem models. The simplicity or complexity of a model is a matter of the question that is aimed to be investigated. While some simple models can be very useful to explain questions such as seasonal dynamics (*Sarmiento et al.*, 1993; *Fasham*, 1995), some other questions need a way more complex ecosystem structure (*Doney*, 1999). For example, many of the key biogeochemical processes, such as active vertical nutrient transport by plankton migration (*Villareal et al.*, 1996), calcification (*Holligan et al.*, 1993) or nitrogen fixation (*Capone et al.*, 1997) are carried out by only specific plankton species. To represent these processes mechanistically, complex models are needed. Therefore, relatively complex models such as 'Plankton Functional Type Models' (PFT Models) have been used in the last two decades to investigate marine ecosystems and their role in biogeochemistry (*Le Quéré et al.*, 2005; *Hood et al.*, 2006).

1.4.1 *Plankton Functional Type Modeling*

Numerical ocean ecosystem/biogeochemical models have been used as a research tool since the beginning of the 1940s. One of the first examples is the model of *Riley* (1949) which describes the formation of the spring bloom in the North Atlantic. This work was expanded later by *Sverdrup* (1953). Today's models (PFT models) are mainly built on top of the pioneering studies of nutrient-phytoplankton-zooplankton-detritus (NPZD) models (e.g., *Steele*, 1958; *Fasham et al.*, 1990). Therefore, firstly the NPZD models and then examples of PFT models will be described.

The NPZ and NPZD type models, with (at least) 3 or 4 state variables, are the first examples of ocean ecosystem models. In the past when computational power was limited, these models were used to understand the relationships between phytoplankton, zooplankton, and nutrients. In these models, nutrients are generally represented with a single macronutrient such as nitrate. Furthermore, zooplankton and phytoplankton are generally represented with a single generic group where the different biogeochemical functions of distinct plankton groups are not represented. In these models, mostly the Redfield elemental ratios (constant atomic ratio of carbon, nitrogen and phosphorus in marine phytoplankton, *Redfield et al.*, 1963) are used to calculate the cycling of various elements coupled to the simulated nutrient. Although there are a number of simplifications in these models, they have been used for almost seven decades to describe the seasonal cycling of phytoplankton (*Fasham et al.*, 1990), and to investigate the model sensitivity to additional state variables and different mathematical formulas (*Edwards and Yool*, 2000; *Mitra*, 2009).

Before the invention of computers, the population dynamics of phytoplankton was first modeled by *Fleming* (1939). *Riley and Bumpus* (1946) presented the first model describing the predator-prey relations at Georges Bank after the invention of the computer. Later, more complex models were used to calculate the net primary production and biological rates (*Steele*, 1958, 1959). Similar models with more state variables were used in the North Pacific by *Frost* (1993) and in the North Atlantic by *Fasham et al.* (1990). In the 1990s, with the cheaper and more widespread use of computers, many new publications on plankton modeling were published (*Gentleman et al.*, 2003). For example, the first versions of coupled NPZD models with three-dimensional general circulation models (GCMs) started to be used in biogeochemical modeling studies (e.g., *Maier-Reimer and Hasselmann*, 1987; *Najjar et al.*, 1992; *Sarmiento et al.*, 1993; *Anderson and Sarmiento*, 1995). Nowadays, these types of models are still used in climate research as a component of Earth System Models (e.g., *Zahariev et al.*, 2008; *Ilyina et al.*, 2013; *Kawamiya et al.*, 2020)

According to the number of state variables, PFT models are one of the most complex models that are being used to explain plankton dynamics. However, process descriptions are still simple. As NPZD models, PFT models are also used quite often as a component of Earth System Models to assess the impact of climate change on phytoplankton and element cycling (*Séférian et al.*, 2020). The PFT modeling approach aims to allow models capturing the variability of the biological rates under different climatic regimes by using all the collected data of biological rates of plankton over the last decades (*Le Quéré et al.*, 2005). Nowadays, several data products provide global biomass of plankton types (e.g. *Leblanc et al.*, 2012; *Moriarty et al.*, 2013; *Moriarty and O'Brien*, 2013) or fundamental rates such as mortality and growth rates (e.g. *Buitenhuis et al.*, 2010; *Hirst and Kiorboe*, 2002; *Hirst et al.*, 2003) to make PFT modeling possible. In these models, plankton functional types are grouped according to their ecological and/or biogeochemical role rather than the phylogeny of plankton (*Le Quéré et al.*, 2005; *Hood et al.*, 2006). They are defined based on their explicit biogeochemical role, a distinct set of physiological rates, the effect on the other PFTs' performance, or the quantitative importance in the ocean (*Le Quéré et al.*, 2005). The main PFTs are defined by *Le Quéré et al.* (2005) as a guideline for modelers. According to the authors' definition, the main phytoplankton types are pico-autotrophs, nitrogen fixers, calcifiers, DMS producers, silicifiers, and mixed phytoplankton. The heterotroph PFTs are pico-heterotrophs (bacteria) and zooplankton (protozooplankton/microzooplankton, mesozooplankton and macrozooplankton, *Le Quéré et al.*, 2005). However, the number and the type of PFTs vary among the models according to the specific research questions.

In CMIP5 and CMIP6 simulations, the ocean biogeochemistry is represented by twelve different models using NPZD or PFT type of models (*Séférian et al.*, 2020), and different variants thereof. Seven of the twelve models (e.g., BEC, BLINGv2, MEDUSA-2.0, PISCES) use PFT

modeling approaches. All models have a different model trophic web, which is indicated by the different numbers of phytoplankton and zooplankton functional types. Table 1.1 summarizes the representation of PFTs and nutrient cycling of seven biogeochemical models that are used in CMIP5 and CMIP6 simulations, plus the two models PLANKTOM11 and REcoM-2. While all of the models resolve carbon, nitrogen, silicic acid, and iron cycling, phosphate cycling is resolved only in four of the models in Table 1.1. All the models represent phytoplankton with at least two PFTs (generally mixed-phytoplankton and silicifiers-diatoms), and zooplankton is represented in some models with a single state variable.

Model	Number of Phy.,	Number of Zoo.	Nutrient Cycling	Reference
BEC	4	1	C, N, P, Si, Fe	*Moore et al.* (2004)
BLINGv2	2	2	C, P, Si, Fe,	*Dunne et al.* (2020)
COBALTv2	3	3	C, N, P, Si, Fe	*Stock et al.* (2020)
MEDUSA-2.0	2	2	C, N, Si, Fe	*Yool et al.* (2013)
NOBM	4	1	C, N, Si, Fe	*Romanou et al.* (2014)
PISCES-v2	2	2	C, N, Si, Fe	*Aumont et al.* (2015)
TOPAZv2	3	1	C, N, P, Si, Fe	*Dunne et al.* (2013)
PLANKTOM-11	6	4	C, N, P, Si, Fe	*Wright et al.* (2021)
REcoM-2	2	1	C, N, Si, Fe	*Hauck et al.* (2013)

TABLE 1.1: List of PFT models that are used in biogeochemical research. The table summarizes the number of phytoplankton and zooplankton functional types, as well as the nutrients whose cycling is represented.

1.4.2 *Zooplankton Groups in Plankton Functional Type Models*

Representation of zooplankton in biogeochemical models is challenging due to uncertainties in the estimation of rates (grazing, mortality etc.), the choice of the response equations, the computational cost, and difficulties in assessing the performance of the zooplankton compartment (*Gentleman and Neuheimer*, 2008; *Everett et al.*, 2017). Therefore, zooplankton parametrizations show a wide variety among global biogeochemical models. In the most simplistic models, zooplankton processes are represented implicitly or with only one state variable as a closure term. Recently, several models integrated more than one zooplankton group with distinct physiological rates. Although zooplankton functional types are named differently across the literature, the most commonly used names for the most abundant zooplankton functional types are micro-, meso-, and macrozooplankton. In the following paragraphs, their potential biogeochemical functions and the representation as a functional group are described following *Le Quéré et al.* (2005):

Microzooplankton covers the function of the unicellular heterotrophs (5-200 μm, ciliates, or heterotrophic flagellates) in large-scale biogeochemical models. Their growth rates are similar to that of small phytoplankton and their ingestion rates are closely coupled to the production rates of their prey. Microzooplankton grazes preferentially on small phytoplankton and dampens their bloom formation. Microzooplankton is sometimes also named 'protozooplankton' or 'small zooplankton' in some of the models such as PLANKTOM (*Le Quéré et al.*, 2016) or COBALT (*Stock et al.*, 2020).

Mesozooplankton (0.2-20 mm) in the models mainly represents copepods which produce large and fast-sinking fecal pellets. In contrast to microzooplankton, mesozooplankton graze

preferentially on larger phytoplankton such as diatoms and microzooplankton. Their grazing rates are slower compared to microzooplankton. The mesozooplankton group is also called 'medium zooplankton' in the biogeochemical model COBALT (*Stock et al.*, 2020).

In comparison to micro- and mesozooplankton, macrozooplankton (2-20 cm) is less well represented in models. It can reach very high biomass values and also produces fast-sinking fecal pellets. Since it has a relatively patchy distribution and complex life cycle, it is difficult to parametrize this functional group. Macrozooplankton grazes on a large spectrum of different prey. Only few global biogeochemical models (e.g. PLANKTOM, COBALT; *Le Quéré et al.*, 2016; *Stock et al.*, 2020) represent macrozooplankton explicitly (Table 1.1).

1.4.3 *Zooplankton Processes and Parametrizations in Models*

Among ocean biogeochemical models, the parametrization of the various processes that affect the zooplankton biomass shows large diversity. However, the general structure of the rate of change in zooplankton biomass ($\frac{dZ}{dt}$) is rather universal and can be described by the following text equation:

$$\frac{dZ}{dt} = uptake - excretion - egestion - respiration - mortality \tag{1.1}$$

where the *uptake* represents the biomass source to zooplankton (Z) which is grazing. The metabolic waste, *respiration*, *excretion*, or *egestion*, are defined as sink terms in the models. In addition, *mortality* (generally including both natural mortality and predation) is defined as a closure term. All of these mentioned processes can be represented implicitly or explicitly in the models. There are many different forms of functions to represent each of these processes in the literature. Here, some of the parameters and their ranges will be presented. Besides, different types of ingestion and mortality functions will be described. In the end, the sensitivity of the models to different processes and functions will be given as a summary.

The *uptake* is generally called 'total grazing' and is a product of an ingestion function that describes how the ingestion rate will change with prey density, maximum ingestion rate, temperature function, and zooplankton biomass. Although there are different functions that describe the ingestion rate depending on the prey density (*Gentleman et al.*, 2003), most of the current biogeochemical models use a Holling type I-III (*Holling*, 1959) or Ivlev (*Ivlev*, 1961) ingestion function (*Vallina et al.*, 2014). Figure 1.3 summarizes the functional response of Holling and Ivlev type ingestion functions to increasing prey concentration. The type I functional response gives a linear accelerating ingestion rate with increasing prey density. However, type II (hyperbolic) or type III (sigmoidal) reach a plateau (saturate) at high prey concentrations. While type II gives a decelerating ingestion rate with high abundances of prey, type III decelerates the ingestion rate with low abundances of prey. The parameter 'half-saturation constant' in the Holling type functions represents the concentration where the ingestion rate is half of the maximum ingestion rate, and higher half saturation constant causes slower increase of ingestion rate. The Ivlev decay constant has a similar role as the half-saturation constant. This parameter is used for regulating how fast the ingestion rate will reach its maximum (Fig. 1.3). A higher decay constant stands for a higher grazing rate and vice-versa. The total grazing is usually temperature-dependent. For this, some models use different exponential functions for different zooplankton functional types (*Le Quéré et al.*, 2016) while other models use the same temperature function for different zooplankton functional types for simplicity (*Aumont et al.*, 2015). Few models do not use temperature-dependent grazing formulations (*Yool et al.*, 2013). In models, zooplankton can have multiple prey groups/types (phyto- and zooplankton groups, detritus) depending on the model complexity, and different

prey preferences can be assigned to the zooplankton. In this way, predator-prey selectivity can be regulated in the models. However, there is no consensus and while some models (*Le Quéré et al.*, 2016) use varying prey preferences (*Fasham et al.*, 1990), some others give constant preferences for food sources.

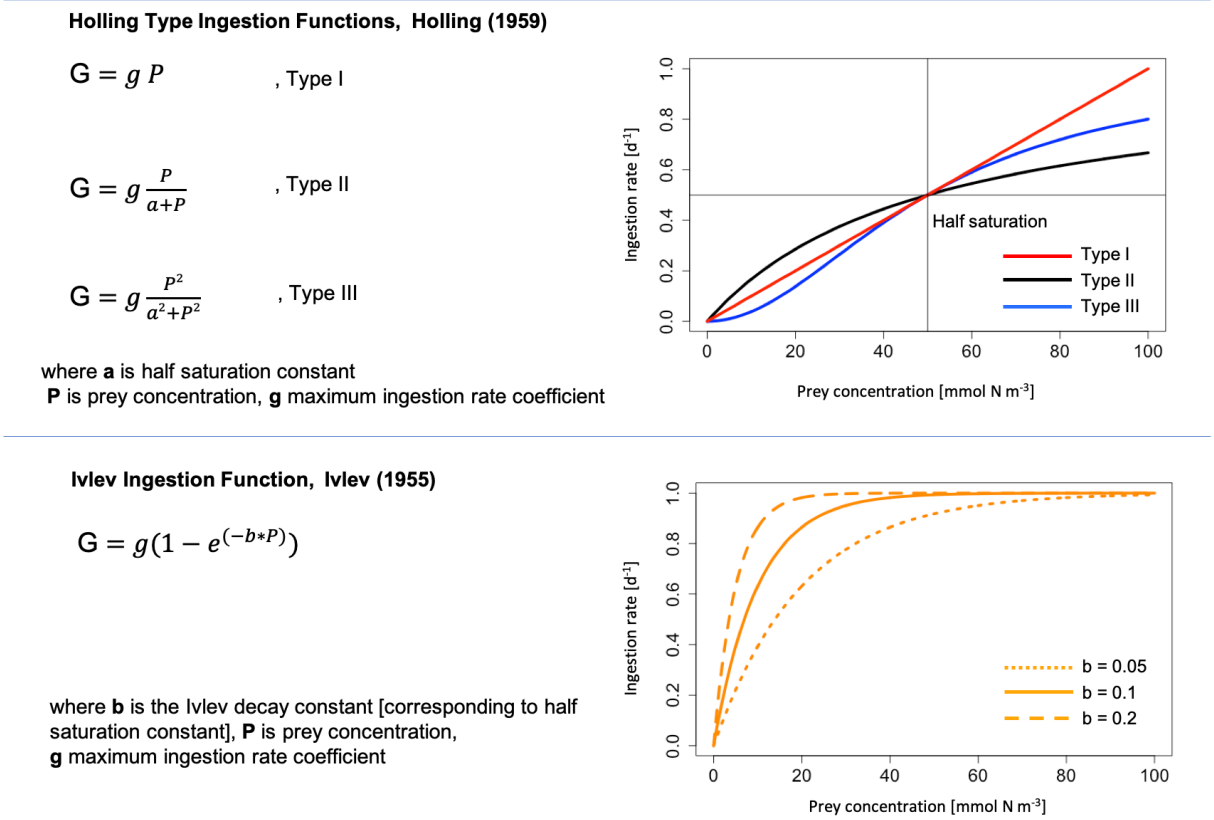

FIGURE 1.3: Ingestion rate coefficient (G, d^{-1}) as a function of the biomass concentration of a single prey (P, mmol C m^{-3}) for Holling type and Ivlev ingestion functions. Holling type I (red), Holling type II (black), and Holling type III (blue) ingestion functions are illustrated in the upper panel, where g (d^{-1}) is the maximum ingestion rate coefficient and a is the half-saturation constant (mmol C m^{-3}). The Ivlev ingestion function is shown in the lower panel, with decay rate constant b (1/mmol C m^{-3}) of 0.05, 0.1 and 0.2 illustrated by different line styles.

An 'assimilation efficiency' parameter may be used to define all sink processes (e.g., *respiration*, *excretion*, *egestion*) that are included in the models. However, since there is specific data for each of these processes, they are generally separated. In this case, 'assimilation efficiency' or 'grazing efficiency' can be used to account for sloppy feeding. Some models use variable assimilation efficiency to mimic the increase of sloppy feeding with increasing prey abundance (*Montagnes and Fenton*, 2012). The respiration and excretion rates are generally constant relative to the biomass, but some models use temperature functions to enhance respiration in warmer waters (*Le Quéré et al.*, 2016).

Mortality parameters are among the least known parameters since they are also difficult to estimate experimentally (*Carlotti et al.*, 2000). In nature, mortality of zooplankton is caused by disease, starvation, or predation (*Hirst and Kiorboe*, 2002). The parametrization of mortality generally covers all of these processes. The mortality of zooplankton is a model closure term since zooplankton is typically the highest trophic level in models (*Edwards and Yool*, 2000; *Mitra*, 2009). Different types of equations (linear, quadratic, hyperbolic, and sigmoidal) are used to describe the zooplankton mortality in the models. Figure 1.4 summarizes four functions that

describe mortality rates of zooplankton depending on the zooplankton concentration. While in the linear function, the mortality term (in the square brackets) does not change depending on the zooplankton biomass, the other three formulations represent an increasing mortality term with an increasing zooplankton biomass. The choice of the mathematical form of the mathematical form of the mortality depends mostly on the food web structure of the model (*Mitra et al.*, 2014).

Closure functions	Type	Used in
$M = [m]\, Z$	, Linear	Evans and Parslow(1985)
$M = [m_2\, Z]\, Z$	, Quadratic	Steele and Henderson (1981)
$M = [m \frac{Z}{k+Z}]\, Z$	, Hyperbolic	Frost (1987)
$M = [m \frac{Z^2}{k^2+Z^2}]\, Z$	, Sigmoidal	Malchow (1984)

where **m**, $\mathbf{m_2}$ are the mortality rate coefficients, **k** is the half saturation constant and **Z** is the zooplankton concentration

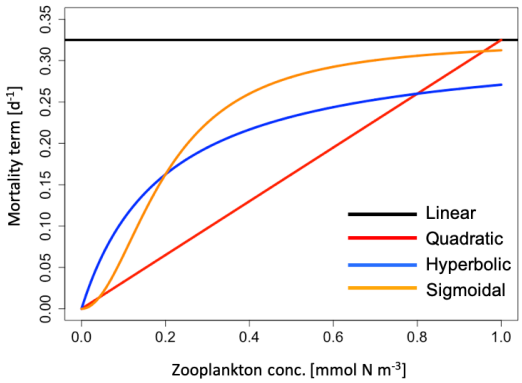

FIGURE 1.4: Mortality rate (M, mmol N m^{-3} d^{-1}) as a function of the mortality term (given in square brackets) and biomass concentration of zooplankton (Z, mmol C m^{-3}) for linear (black), quadratic (red), hyperbolic (blue) and sigmoidal (orange) formulations, where the mortality rate coefficient m is 0.325 (d^{-1}) and m_2 is 0.325 ((mmol N m^{-3})$^{-1}$ d^{-1}).

Model results are highly sensitive to different parametrization formulations of zooplankton since they directly affect phytoplankton biomass and composition. Indirectly, this also affects the use of nutrients in the models. A large number of studies investigated the sensitivity of biogeochemical models to different formulations. For example, *Anderson et al.* (2010) showed that the choice of different ingestion formulas (Holling type III or Ivlev) can cause a three times higher diatom biomass in the ocean. Furthermore, previous works showed that the parametrization of predator-prey selectivity by using different mathematical formulas can change the modelled phytoplankton diversity (*Prowe et al.*, 2012; *Vallina et al.*, 2014). Recently, *Moeller et al.* (2019) used light-dependent grazing formulations and showed that this can cause a deepening of simulated chlorophyll maxima which results in a better model-data agreement. Besides, *Steele and Henderson* (1992) and *Edwards and Yool* (2000) analysed the sensitivity of plankton and plankton cycles to the formulation of the zooplankton mortality. In addition, *Hill Cruz et al.* (2021) illustrated that changes in the zooplankton mortality can have a strong impact on the trophic interactions in the model.

1.4.4 *Evaluation of Zooplankton Model Results*

The performance of the zooplankton component of biogeochemical models is the component that is least assessed against field observations (*Everett et al.*, 2017). Biogeochemical model performances are usually compared with observations of nutrients and chlorophyll concentrations. Although there are several ways to observe zooplankton biomass or abundance such as net sampling (*Wiebe and Benfield*, 2003), continuous plankton recorder (*Richardson et al.*, 2006), optical plankton counter (*Herman et al.*, 2004) and bioacoustics (*Greene and Wiebe*, 1990), the format of the data makes it difficult for the use in model evaluations because they often quantify abundance rather than mass (*Everett et al.*, 2017).

Current developments of plankton functional type models (*Stock et al.*, 2020) increase the need for biomass data of key plankton functional types. For this purpose, the biomass data of five autotroph (picophytoplankton, diazotrophs, coccolithophores, phaeocystis, diatoms) and six heterotroph groups (picoheterotrophs, foraminifers, pteropods, micro-, meso- and macrozooplankton) was compiled in a 1°x1° global gridded data set (*Buitenhuis et al.*, 2013). The MAREDAT data products of global micro-, meso and macrozooplankton biomass (*Buitenhuis et al.*, 2010; *Moriarty and O'Brien*, 2013; *Moriarty et al.*, 2013) were used in the studies that are presented in this thesis. While the MAREDAT mesozooplankton biomass dataset includes the Coastal and Oceanic Plankton Ecology, Production, and Observation Database (COPEPOD, http://www.st.nmfs.noaa.gov/copepod), the macrozooplankton dataset contains data points from COPEPOD and KRILLBASE (*Atkinson et al.*, 2004).

1.5 AIM AND SCOPE OF THE THESIS

This thesis aims to examine the effect of zooplankton and the mechanistic description of their processes on carbon export and sequestration flux, nutrient cycling, and phytoplankton phenology in a global ocean biogeochemical model. For this purpose, three zooplankton functional groups, namely micro-, meso- and macrozooplankton, and a new particle sinking routine were implemented to the original version of the ocean biogeochemical model REcoM-2. The model was used to answer the following questions:

- What are the roles of zooplankton in carbon export and nutrient recycling?
- How does zooplankton grazing affect phytoplankton bloom phenology?
- What are the relative roles of plankton community composition and of mineral ballasting, seawater viscosity, and oxygen-dependent remineralization on carbon export efficiency and transfer efficiency?

Publication I is a model development study with a focus on the implementation of polar macrozooplankton in the model. Since Antarctic krill is one of the key species in the Southern Ocean and plays an important role in the carbon cycle, a new zooplankton group was implemented to the model and parametrized as Antarctic krill. *Publication I* revealed that macrozooplankton plays a key role in transferring carbon to the mesopelagic zone in the model Southern Ocean, in agreement with observational studies. In addition, it enhances the net primary production there due to the fast recycling of nutrients.

Publication II is also a model development study with the focus on separating the previously generic zooplankton group into micro- and mesozooplankton as additional functional types in the model. *Publication II* revealed that the fast-recycling of nutrients by zooplankton has a significant impact on the net primary production. Besides, the detailed analysis of phytoplankton bloom phenology showed that the more complex representation of zooplankton grazing changes the mechanism behind the phytoplankton bloom from light-controlled Sverdrup's system to dilution controlled Behrenfeld system in the Southern Ocean, but also delays the start and peak days of the phytoplankton bloom.

In Publication III, the model with three zooplankton functional types was used to study global patterns of export ratio and transfer efficiency of carbon. For this study, a new sinking routine was parametrized in the model. In this study, we quantified the relative roles of phytoplankton and zooplankton community composition, of seawater viscosity, particle density, and oxygen-dependent remineralization on the export ratio and transfer efficiency of sinking particulate organic carbon.

In the last chapter, the major results of the three publications are synthesized. Finally, an outlook for future scientific directions regarding the research on zooplankton modeling and biogeochemical modeling is provided.

1.6 LIST OF PUBLICATIONS AND DECLARATION OF OWN CONTRIBUTION

Publication I O. Karakuş, C. Völker, M. Iversen, W. Hagen, D. Wolf-Gladrow, B. Fach, J. Hauck: Modeling the Impact of Macrozooplankton on Carbon Export Production in the Southern Ocean, Journal of Geophysical Research: Oceans, 126(12). doi:10.1029/2021JC017315

I have implemented polar macrozooplankton as a new zooplankton group into the biogeochemical model REcoM after conceptual design with all co-authors. I have conducted the model simulations. I have conducted the data analyses and have discussed and further developed them with the help of the co-authors. I have written the manuscript in cooperation with the co-authors.

Publication II O. Karakuş, C. Völker, M. Iversen, W. Hagen, J. Hauck (2022): The role of zooplankton grazing and nutrient recycling for global ocean biogeochemistry and phytoplankton phenology; in review at JGR:Biogeosciences

I have implemented a new zooplankton group and parametrized micro- and mesozooplankton in the biogeochemical model REcoM. I have conducted model simulations and analyses of the model outputs. I have discussed results and interpretation with the co-authors. I have written the manuscript in cooperation with the co-authors

Publication III O. Karakuş, C. Nissen, W. Hagen, M. Iversen, C. Völker, Ö. Gürses, J. Hauck (2022): The Role of Ballasting, Seawater Viscosity and Oxygen for Carbon Export and Transfer Efficiencies in the Global Ocean; to be submitted to Global Biogeochemical Cycles.

I have implemented a new particle sinking routine into the biogeochemical model REcoM in close collaboration with the co-authors. I have conducted the model simulations. I have analyzed the model results, produced figures and tables and wrote the manuscript with comments and corrections from the co-authors.

2

PUBLICATION I

MODELING THE IMPACT OF MACROZOOPLANKTON ON CARBON EXPORT PRODUCTION IN THE SOUTHERN OCEAN

JGR Oceans

RESEARCH ARTICLE
10.1029/2021JC017315

Modeling the Impact of Macrozooplankton on Carbon Export Production in the Southern Ocean

Onur Karakuş[1], Christoph Völker[1], Morten Iversen[1], Wilhelm Hagen[2,3], Dieter Wolf-Gladrow[1], Bettina Fach[4], and Judith Hauck[1]

[1]Alfred-Wegener-Institut, Helmholtz-Zentrum für Polar- und Meeresforschung, Bremerhaven, Germany, [2]University of Bremen, BreMarE, Marine Zoology, Bremen, Germany, [3]University of Bremen, MARUM Center of Environmental Sciences, Bremen, Germany, [4]Middle East Technical University, Institute of Marine Sciences, Erdemli-Mersin, Turkey

Abstract Macrozooplankton and its grazing pressure shape ecosystem structures and carbon pathways in the Southern Ocean. Here, we present the implementation of "polar macrozooplankton" as a plankton functional type and a related fast-sinking detritus class (fecal pellets) into the biogeochemical model REcoM-2. We use the model to assess major carbon pathways and ecosystem structure in the Southern Ocean south of 50°S. The model represents zooplankton biomass and its spatial distribution in the Southern Ocean reasonably well in comparison to available biomass data. A distinct difference of our model from previous versions is the seasonal pattern of particle formation processes and ecosystem structures in the Southern Ocean. REcoM-2 now captures high zooplankton biomass and a typical shift from a dominance of phytodetrital aggregates in spring to zooplankton fecal pellets later in the year. At sites with high biomass of macrozooplankton, the transfer efficiency of particulate organic carbon can be as high as 50%, and the carbon content of the exported material increases. In our simulations, macrozooplankton is an important component of the Southern Ocean plankton community, contributing up to 0.12 Pg C per year (14%) to total modeled carbon export across 100 m depth. Macrozooplankton changes the phytoplankton composition and supports the recycling of macronutrients. These results support the important role of macrozooplankton such as krill in the Southern Ocean and have implications for the representation of Southern Ocean biogeochemical cycles in models.

Plain Language Summary Large zooplankton such as krill is an important component of marine ecosystems, but it is rarely represented in ocean ecosystem models. Large zooplankton grazes on phytoplankton, smaller zooplankton, and sinking particles in the ocean. To understand the role of large zooplankton for carbon cycling in the Southern Ocean, we have implemented this group into our ecosystem model and describe macrozooplankton feeding and particle formation based on observations. We find that large zooplankton supports a stable or even increased growth of phytoplankton, in spite of its grazing. This is because it also returns nutrients to phytoplankton via excretion. Besides, large zooplankton increases the transfer of carbon to the deep ocean.

Key Points:

- A new macrozooplankton parametrization is implemented into the biogeochemical model REcoM-2
- Transfer efficiency reaches up to 50% due to the high carbon content and fast sinking of macrozooplankton fecal pellets
- Macrozooplankton contributes up to 14% (0.12 Pg C yr^{-1}) to modeled carbon export at 100 m depth in the Southern Ocean south of 50°S

Supporting Information:

Supporting Information may be found in the online version of this article.

Correspondence to:

O. Karakuş,
onur.karakus@awi.de

Citation:

Karakuş, O., Völker, C., Iversen, M., Hagen, W., Wolf-Gladrow, D., Fach, B., & Hauck, J. (2021). Modeling the impact of macrozooplankton on carbon export production in the Southern Ocean. *Journal of Geophysical Research: Oceans*, *126*, e2021JC017315. https://doi.org/10.1029/2021JC017315

Received 26 FEB 2021
Accepted 1 NOV 2021

1. Introduction

The biological carbon pump plays an essential role in the cycling of carbon in the oceans (Honjo, 2004; Volk & Hoffert, 1985). It is driven by a large variety of organisms that are part of a complex ecosystem. The export of organic carbon from the surface to deeper layers proceeds via several pathways including the formation of aggregates and fecal pellets that sink gravitationally, and the downwelling of dissolved compounds (Boyd et al., 2019; Steinberg & Landry, 2017). Marine carbon cycle models are used to assess carbon fluxes in the ocean ecosystems to gain a deeper understanding of the carbon cycle. However, the complexity of marine ecosystems and the processes relevant for carbon export cannot be fully reflected in these models (Laufkötter et al., 2016). For example, zooplankton is still represented by a single variable in many global ocean biogeochemical models (Séférian et al., 2020), despite the large diversity and traits of zooplankton. A handful of models represent three plankton functional types (PFTs) of zooplankton (Le Quéré et al., 2016; Stock et al., 2020).

One of the zooplankton PFTs is macrozooplankton, defined as the size class of 2–20 cm, which reaches high biomass and shows a patchy distribution (Moriarty et al., 2013). Groups being classified as macrozooplankton

Journal of Geophysical Research: Oceans 10.1029/2021JC017315

are, for example, euphausiids, but also pelagic members of, for example, cnidarians, amphipods, and decapods. They consume a large spectrum of prey sizes with different feeding strategies and carbon assimilated by this group is transferred to higher trophic levels, transforming and transferring particulate organic carbon (Steinberg & Landry, 2017). They produce large fecal pellets with a high sinking rate, which reduces microbial degradation in the euphotic zone and leads to direct sinking to the meso- and bathypelagic (Turner, 2002). The relative contribution of zooplankton fecal pellets to the particulate organic carbon (POC) flux can comprise up to 100% in different sites of the ocean, illustrating the important role of zooplankton in the biological carbon pump (Turner, 2015).

The Southern Ocean is one of the regions, which plays a significant role in the export of particulate organic carbon (Arteaga et al., 2018; Schlitzer, 2002). Export production (EP), an important component of the biological carbon pump, transfers 15%–25% of the carbon fixed by primary production to deeper waters in the Southern Ocean (Henson et al., 2012). The estimation of export production over the 100 m depth horizon varies between 10 to 600 mg C m^{-2} d^{-1} with an average of around 150 mg C m^{-2} d^{-1} (Maiti et al., 2013). The biogenic carbon flux is dominated by the gravitational sinking of phytodetrital aggregates and zooplankton fecal pellets, although other processes such as the sinking of zooplankton carcasses, molts, and zooplankton migration also contribute (Boyd et al., 2019; Halfter et al., 2020). The relative contributions of phytodetrital aggregates and zooplankton fecal pellets to carbon export show seasonal and spatial patterns (Dagg et al., 2003; Ebersbach & Trull, 2008; Halfter et al., 2020; Iversen et al., 2017; Laurenceau-Cornec et al., 2015; Turner, 2015). For example, phytodetrital aggregates are reported to contribute 24%–74% to the export production in the Kerguelen Plateau (Ebersbach & Trull, 2008) and the relative contribution of zooplankton fecal pellets can vary from 22%–63% in spring to 2%–7% in summer in the Pacific Antarctic Polar Front region (Dagg et al., 2003). Generally, a high contribution of aggregates is related to phytoplankton blooms in the surface waters (Turner, 2015), although phytodetrital aggregates can also dominate the export flux in the Southern Ocean high-nutrient low-chlorophyll (HNLC) waters where grazing pressure is relatively low (Halfter et al., 2020). At the naturally iron-fertilized Kerguelen Plateau, a shift occurred from dominance of phytodetrital aggregates in spring to zooplankton fecal pellets later in the year (Ebersbach & Trull, 2008; Laurenceau-Cornec et al., 2015; Rembauville et al., 2015).

The Southern Ocean also hosts a high density of macrozooplankton, including the efficient grazer Antarctic krill (*Euphausia superba*) with biomass estimates ranging between 60 to 420 million tons based on acoustic and in situ (net haul density and length frequency) data (Atkinson et al., 2009; Nicol et al., 2000; Siegel et al., 2004). Krill shape the ecosystem, for example, through stimulating primary productivity with the release of iron and ammonium and affect the carbon export (Cavan et al., 2019). Furthermore, krill impact the accumulation of diatoms due to grazing, which consequently plays a decisive role in biogeochemical cycles (Smetacek et al., 2004). Krill enable short pathways between lowest (phytoplankton) and higher trophic levels (marine mammals) and contribute to an efficient carbon transfer to the deeper layers via fecal pellet production (Meyer, 2012). While the contribution of krill to particulate organic carbon production may vary between 7 and 1,300 mg C m^{-2} d^{-1} in the Southern Ocean (Belcher et al., 2019; Clarke et al., 1988), krill fecal pellets contribute on average 0.04 Pg C per yr^{-1} which equals 35% of the total export flux in the marginal ice zone (Belcher et al., 2019).

Large-scale ocean biogeochemical models differ from each other in terms of complexity, such as the number of functional types of phyto- and zooplankton and represented processes (Laufkötter et al., 2016; Le Quéré et al., 2016; Séférian et al., 2020). Due to a lack of mechanistic understanding, projections of the future biological carbon pump are associated with much larger uncertainties compared to physical and chemical variables, such as temperature, oxygen, or pH (Frölicher et al., 2016). Zooplankton groups and their parameterizations play a critical role in the performance of ecosystem models with respect to primary production (Le Quéré et al., 2016), secondary production (Anderson et al., 2013), and particulate organic carbon production and export (Laufkötter et al., 2016). Growth, transport, and impact of macrozooplankton, especially krill, have been simulated in various regional models (Arrigo et al., 2003; Fach et al., 2002; Hense et al., 2003; Hofmann & Lascara, 2000; Lancelot et al., 2000), but only a few global biogeochemical models possess representations of macrozooplankton (Le Quéré et al., 2016; Stock et al., 2014).

Here, we present a new version of the global ocean ecosystem and biogeochemistry model REcoM-2 with the implementation of a macrozooplankton group. Up to now, REcoM-2 included a single type of zooplankton

Journal of Geophysical Research: Oceans 10.1029/2021JC017315

which, based on the chosen parameterization, represented small and fast-growing zooplankton. The goal of the current paper is to analyze the effect of an additional macrozooplankton group that can create large biomass accumulations in certain regions and thereby impact the structure and functioning of ecosystems. The parameterization for this second zooplankton group is based on the temperature tolerance of Antarctic krill, hence, this group cannot represent macrozooplankton in warmer waters. The aim is therefore mainly to obtain a more realistic representation of the Southern Ocean biological carbon pump in the model. We implemented this new group and parameterized it as a macrozooplankton group resembling Antarctic krill for the following reasons: (a) the occurrence of high biomass of macrozooplankton (Antarctic krill) in the Southern Ocean (Atkinson et al., 2004) and its specific role in biogeochemical cycling as characterized by (b) the slow growth rates of this group (Le Quéré et al., 2016), (c) the efficient filter-feeding of krill (Meyer, 2012), and (d) a fecal pellet production with strong transfer efficiency to the deep ocean (Belcher et al., 2017). In this study, we analyze carbon export pathways and the role of macrozooplankton in the Antarctic ecosystem with and without this group.

2. Methods

2.1. FESOM-REcoM With Macrozooplankton and Two Sinking Particle Classes

We used the Finite Element Sea Ice Ocean Model FESOM-1.4 (Wang et al., 2014) as the physical component of the coupled ocean-ecosystem model. FESOM-1.4 uses the finite element method for solving the primitive equations on an unstructured mesh which allows calculations with higher resolutions in more dynamical areas and coarser resolution in less dynamic, for example, subtropical areas. In this study, we used the CORE-II mesh set-up which has a resolution of 20 km along the Antarctic coast and around 70 km at 60°S (Sidorenko et al., 2011). The model set-up and its performance is described by Sidorenko et al. (2011), and evaluated as part of the coordinated ocean-ice reference experiments phase II (CORE-II) globally (e.g., Griffies et al., 2014) and regionally (see Downes et al., 2015, 2018; Farneti et al. (2015) for Southern Ocean specific analyses). A multi model comparison of sea-ice extent and concentration, including FESOM-1.4, was discussed in Downes et al. (2015). As reported there, FESOM simulates a reasonable seasonal cycle of sea-ice extent, with a realistic representation of the maximum extent. A notable caveat is a low extent in March, which is shared with all other models in their study. FESOM was reported to have the smallest sea-ice concentration bias of all models in March. Downes et al. (2015) do not compare sea-ice thickness as thickness and concentration correlate positively. Exemplarily, we show sea-ice extent and thickness in Figure S5 in Supporting Information S1. Sea ice extent reaches its maximum in September and its minimum in March, in agreement with remote sensing studies (Comiso & Nishio, 2008). The mean sea ice thickness varies between a minimum of 0.75 m in April and a maximum of 1.06 m in November in the model. The thickest sea ice (>2 m) is in the Weddell Sea, the Bellingshausen and Amundsen Seas, the western Ross Sea, and along the Antarctic coastline. The thinnest ice occurs in the eastern Weddell Sea, and in the Indian and Pacific sectors (Figure S5 in Supporting Information S1), in reasonable agreement with Kurtz and Markus (2012).

The Regulated Ocean Ecosystem Model (Hauck et al., 2013; Schourup-Kristensen et al., 2014; REcoM-2) is the biogeochemical component of the coupled system. It represents the carbonate system, two phytoplankton classes (nanophytoplankton and diatoms), and one zooplankton group representing a fast-growing small zooplankton group (Figure 1a). It resolves the cycling of the nutrients nitrate (DIN), silicic acid (DSi), and iron (DFe). Phytoplankton stoichiometry is allowed to vary with environmental conditions (variable N:C:Chl:Si for diatoms and N:C:Chl for nanophytoplankton). Sinking particles have three sources in the original set-up: aggregation of primary producers, sloppy feeding (which implicitly also includes defecation), and mortality of the zooplankton group. A skill assessment of the biogeochemical model's original version is presented by Schourup-Kristensen et al. (2014). The model version used in this study resembles the version assessed in Schourup-Kristensen et al. (2014) with minor changes as described in the following. Total global net primary production (NPP) is 30.1 Pg C yr^{-1} and EP at 100 m is 5.1 Pg C yr^{-1} (31.6 and 6.1 Pg C yr^{-1}, respectively, in Schourup-Kristensen et al., 2014). The photodamage parameterization by Álvarez et al. (2018) is used and leads to a larger share of diatoms (Figure S6 in Supporting Information S1) in the Southern Ocean compared to Schourup-Kristensen et al. (2014). As a result, the Southern Ocean DIN bias is reduced compared to Schourup-Kristensen et al. (2014) and the silicic acid bias is negative, highlighting the sensitivity of the model to chlorophyll loss process parameterization and parameters. In this study, we

Journal of Geophysical Research: Oceans 10.1029/2021JC017315

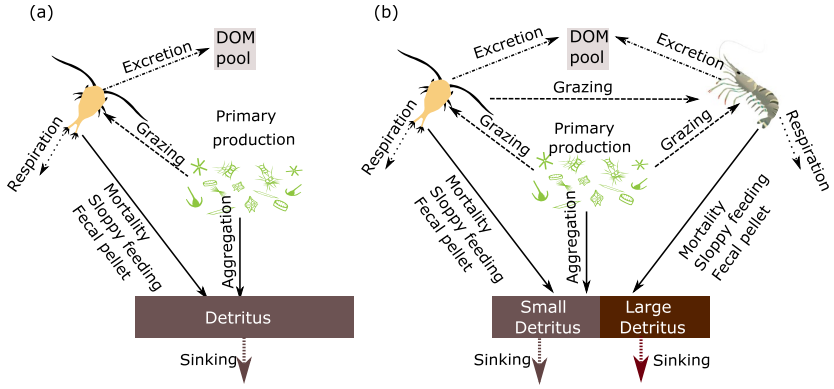

Figure 1. Processes in biogeochemistry model (a) REcoM-2, (b) REcoM-2-M with two zooplankton groups and a second, large detritus class. Both model versions represent primary production by two phytoplankton classes (nanophytoplankton and diatoms) and a small and fast-growing zooplankton group. In both versions, sinking detritus is produced via phytoplankton aggregation and through small zooplankton mortality, and a loss term accounting for sloppy feeding and fecal pellet production. Other loss processes for zooplankton biomass are respiration and excretion of dissolved organic matter. In addition, REcoM-2-M explicitly represents macrozooplankton with losses of sinking particulate organic matter being routed to a large detritus class with a higher sinking speed. The loss through fecal pellets is represented explicitly and macrozooplankton respiration varies in response to the seasonal cycle.

implemented an additional macrozooplankton group and a new detritus group representing large particles (Figure 1b). Also, fecal pellet production was added as an explicit loss term for the new macrozooplankton group (Figure 1b). The set-up of REcoM-2 further differs from previous model descriptions (Hauck et al., 2013; Schourup-Kristensen et al., 2014) by using a temperature-dependent respiration rate with a rate constant of 1% of biomass per day (Le Quéré et al., 2016) for the small zooplankton group, and by considering the effect of diatom nutrient limitation on stickiness and consequently on the aggregation rate (Aumont et al., 2015; Waite et al., 1992, Equation 7).

2.2. Macrozooplankton in FESOM-REcoM

The new macrozooplankton group was parameterized based on the characteristics of Antarctic krill. Nevertheless, we refer to this group as macrozooplankton since it will also cover other niches in the model, as long as these other types (e.g., salps) are not modeled explicitly. Furthermore, not all details of krill are covered here (e.g., life cycle, vertical migration). Macrozooplankton is described by the two-state variables nitrogen (N_{macro}) and carbon (C_{macro}) as shown in differential Equations 1 and 2. Grazing is the single source for macrozooplankton biomass and mortality, excretion, respiration, and fecal pellet production are the loss terms.

$$\underbrace{\frac{dN_{macro}}{dt}}_{\text{nitrogen pool}} = \underbrace{G \cdot \gamma}_{\text{grazing}} - \underbrace{m \cdot N_{macro}^2}_{\text{mortality}} - \underbrace{\epsilon_N \cdot N_{macro}}_{\text{excretion}} - \underbrace{f_N \cdot G}_{\text{fecal pellet}} \tag{1}$$

$$\underbrace{\frac{dC_{macro}}{dt}}_{\text{carbon pool}} = \underbrace{(\sum_i \frac{1}{q_i} \cdot G_i) \cdot \gamma}_{\text{grazing}} - \underbrace{\frac{1}{q} \cdot m \cdot N_{macro}^2}_{\text{mortality}} - \underbrace{\epsilon_C \cdot C_{macro}}_{\text{excretion}} - \underbrace{r \cdot C_{macro}}_{\text{respiration}} - \underbrace{f_C \cdot G_C}_{\text{fecal pellet}} \tag{2}$$

In Equation 1, grazing efficiency (assimilation efficiency) γ determines the fraction of total grazing (G) by macrozooplankton that is converted into macrozooplankton biomass (Equation 3). To mimic predation by higher trophic levels and natural mortality of the macrozooplankton, mortality of the macrozooplankton is described by a quadratic term of the concentration N_{macro} where m is the mortality rate constant ($m \cdot N_{macro}^2$). Nitrogen excretion is determined by the excretion rate constant ϵ_N and is proportional to the N_{macro} biomass. The fecal pellet production rate is described as a function of the total grazing G and the fecal pellet production rate constant (f_N) that determines how much of the grazing fraction is transferred into the larger detritus class nitrogen pool. Equation 2 shows the state variable carbon of the macrozooplankton group. The grazing flux in nitrogen units (G) is converted into

Journal of Geophysical Research: Oceans 10.1029/2021JC017315

Table 1
Chosen Parameter Values for the Representation of Macrozooplankton in REcoM-2-M

Parameter	Symbol	Value (unit)	Reference
Maximum grazing rate	ε	0.1 (d^{-1})	Hofmann and Lascara (2000)
Grazing efficiency	γ	0.8 (dimensionless)	Fach et al. (2002)
Respiration rate constant	r	0.01 (d^{-1})	Hofmann and Lascara (2000)
Mortality rate constant	m	0.003 (d^{-1})	Fach et al. (2002)
N excretion rate constant	ϵ_N	0.02 (d^{-1})	Atkinson et al. (2002)
C excretion rate constant	ϵ_C	0.02 (d^{-1})	Atkinson et al. (2002)
Half saturation constant	σ	0.01 ((mmol N m^{-3})^2)	Meyer et al. (2009)
Initial grazing preference for diatoms	p'_{dia}	1 (dimensionless)	see Section 2.2
Initial grazing preference for nanophy.	p'_{nano}	0.5 (dimensionless)	see Section 2.2
Initial grazing preference for heterotrophs	p'_{zoo}	0.8 (dimensionless)	see Section 2.2
Initial grazing preference for detritus groups	p'_{det}	0.5 (dimensionless)	see Section 2.2
N fecal pellet production rate constant	f_N	0.13 (d^{-1})	see Section 2.2
C fecal pellet production rate constant	f_C	0.295 (d^{-1})	see Section 2.2

carbon units using the respective intracellular N:C ratios (q_i) of each food source (i = diatom, nanophytoplankton, small zooplankton group, detritus classes). The quadratic mortality is converted to carbon using the intracellular macrozooplankton N:C ratio (q). The excretion rate constant (ϵ_C) determines the loss of carbon to the dissolved organic carbon pool and the respiration rate ($r \cdot C_{macro}$) describes the loss of carbon to the dissolved inorganic carbon pool. The fecal pellet production rate constant (f_C) and the grazing rate G together determine the fraction of carbon being lost to the large detritus carbon pool via fecal pellets.

$$G = \varepsilon \cdot \frac{\left(\sum_i p_i \cdot N_i\right)^2}{\sigma + \left(\sum_i p_i \cdot N_i\right)^2} \cdot f_T \cdot N_{macro} \tag{3}$$

$$p_i = \frac{p'_i \cdot N_i}{\sum_i p'_i \cdot N_i} \tag{4}$$

Grazing of the macrozooplankton group is described by the Holling type III ingestion function (Equation 3) on small zooplankton ($i = 1$), diatoms ($i = 2$), nanophytoplankton ($i = 3$), and both detritus classes ($i = 4, 5$) using the relative grazing preferences (p_i) by Fasham et al. (1990) (Equation 4). Since overwintering krill can switch to different food sources and graze on phytodetritus (Meyer, 2012), we implemented grazing on detritus groups by macrozooplankton. The maximum grazing rate (ε) is set to 0.1 d^{-1} (Hofmann & Lascara, 2000) and the half saturation constant (σ) is 0.01 (mmol N m^{-3})^2, based on Meyer et al. (2009). It is generally accepted that diatoms are the main food source for krill, but they also feed on copepods (Schmidt et al., 2014). In this study, the initial grazing preferences (p'_i) are taken as 1, 0.5, 0.8, and 0.5 for diatoms, nanophytoplankton, small zooplankton group and detritus groups respectively. Relative grazing preferences (p_i, i = each food source) are calculated as division of each food source ($p'_i \cdot N_i$) by the total food ($\sum_i p'_i \cdot N_i$). All parameter values for macrozooplankton are summarized in Table 1.

Macrozooplankton grazing varies with temperature. The following parameterization is applied (Butzin & Pörtner, 2016, Equation 5, Figure 2),

$$f_T = \frac{\exp\left(\frac{Q_a}{T_r} - \frac{Q_a}{T}\right)}{1 + \exp\left(\frac{Q_h}{T_h} - \frac{Q_h}{T}\right)} \tag{5}$$

Journal of Geophysical Research: Oceans 10.1029/2021JC017315

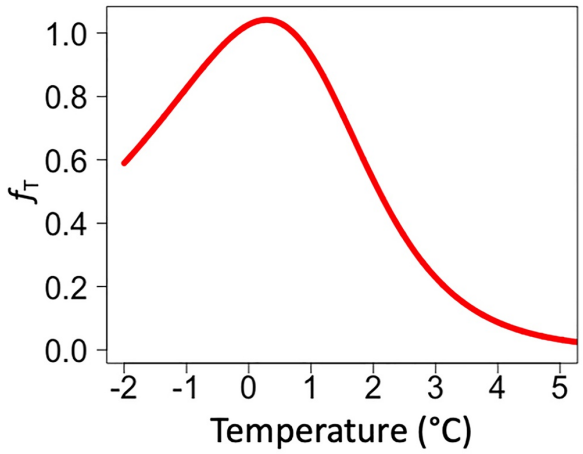

Figure 2. Exponential temperature function (dimensionless) adapted from Butzin and Pörtner (2016) for macrozooplankton grazing (see Equation 5) with an optimum temperature for macrozooplankton growth at 0.5°C (Atkinson et al., 2006).

where T (K) is absolute temperature, T_r and T_h represent the intrinsic optimum temperature for development. Inhibitive processes dominate outside this temperature window. Q_a and Q_h are the temperatures for the uninhibited and inhibited reaction kinetics, respectively (Butzin & Pörtner, 2016). The parameter values were chosen as $T_r = 272.5$ K, $T_h = 274.5$ K, $Q_a = 28{,}145$ K, and $Q_h = 105{,}234$ K to represent the temperature sensitivity of daily growth rates with the maximum growth of krill occurring at 0.5°C as described in Atkinson et al. (2006).

Mortality, sloppy feeding, and fecal pellet production are the processes through which macrozooplankton forms detrital particles. The mortality rate constant m is set to 0.3% per day (Fach et al., 2002) in a quadratic formulation (Equation 1) and $1 - \gamma = 20\%$ of the grazed material is transferred to the detritus pool through sloppy feeding (Fach et al., 2002). Fecal pellet production was set to 29% of grazing flux in carbon units and 13% of grazing flux in nitrogen units to be consistent with the observed high C:N ratio of around 13 in krill fecal pellets (Atkinson et al., 2012). The excretion rate constant of dissolved organic carbon and nitrogen is taken as 2% per day from Atkinson et al. (2002).

The daily respiration rate constant (r) of macrozooplankton in the model depends on the season and grazing activity and a standard respiration rate (R_s, Equation 6, Hofmann & Lascara, 2000).

$$r = R_s \cdot (1 + R_f + R_a) \tag{6}$$

The term respiration activity factor (R_a) accounts for reduced krill respiration rates in winter. R_a is set to −0.5 from Julian day 150 through 250 (southern hemisphere winter) which represents a 50% metabolic reduction. We chose to make respiration rates dependent on Julian day because the metabolic activity of krill is affected by the Antarctic light regime (Meyer, 2012; Teschke et al., 2007), which in the model is tied to Julian Day. The feeding activity factor (R_f) represents the metabolic cost of feeding activity and depends on the daily ratio of grazing flux to carbon biomass of macrozooplankton. It increases linearly from 0 to 1 for daily grazing to biomass ratio between 0% and 10% and remains constant at 1 for ratios above 10%. The standard respiration rate (R_s) is set to 1% per day (Hofmann & Lascara, 2000).

2.3. Two Sinking Particle Classes and Particulate Organic Carbon Production in FESOM-REcoM

To better represent macrozooplankton-related export processes, we implemented a second detritus class which represents large, fast-sinking particles. Mortality, sloppy feeding, and fecal pellet production by the macrozooplankton group are the only sources for the large detritus class in REcoM-2-M (Figure 1b). In the Scotia Sea, sinking rates of krill fecal pellets ranged between 27 and 1,218 m d^{-1} with a median value of 304 m d^{-1} (Atkinson et al., 2012). In REcoM-2-M, a constant sinking rate of 200 m d^{-1} was set for the large detritus. In the control simulation, there is only one detritus class (Figure 1a) with an initial sinking speed of 20 m d^{-1} at the surface which increases linearly with depth until reaching a maximum sinking rate of 170 m d^{-1} at the depth of 5,300 m depth. This detritus class represents smaller particles formed by aggregation of phytoplankton and processes related to the small zooplankton group (mortality and sloppy feeding) in the simulations with two detritus classes.

In this study, we refer to sinking particulate organic carbon (sPOC) as dead material which is transferred into the detritus pool. Processes that lead to sPOC production are an aggregation of phytoplankton, sloppy feeding, mortality of zooplankton, and the fecal pellet production by macrozooplankton in our modeling experiments. Aggregation of phytoplankton is calculated in two steps. First, the aggregation rate constant (a, unit: d^{-1}, Equation 7) is calculated from the specific aggregation rate constants for phytoplankton (a_{pp}) and detritus (a_{pd}). The effect of increased stickiness of diatoms under nutrient limitation (Aumont et al., 2015; Waite et al., 1992) is taken into account by multiplication with (1 - L^D_{lim}) where L^D_{lim} is the nutrient limitation factor which ranges between 0 under

Journal of Geophysical Research: Oceans 10.1029/2021JC017315

Table 2
Processes Included (X) in Model Experiments With Increasing Complexity of Macrozooplankton Representation

Simulation	Macrozooplankton	Large detritus	Detritus grazing	Fecal pellet production
CTRL	–	–	–	–
MACROZOO	X	–	–	–
MACROZOO_2DET	X	X	–	–
MACROZOO_DETGRAZ	X	X	X	–
MACROZOO_ALL	X	X	X	X

strong nutrient limitation, and 1 when nutrients are replete. Second, total aggregation ($sPOC_{phy}^{prod}$) is calculated from the phytoplankton biomass (*PhyC, DiaC*) and the aggregation rate constant (Equation 8).

$$a = a_{pd} \cdot DetN + a_{pp} \cdot PhyN + a_{pp}(1 - L_{\text{lim}}^{D}) \cdot DiaN \tag{7}$$

$$sPOC_{phy}^{prod} = a \cdot PhyC + a \cdot DiaC \tag{8}$$

Another important source for sPOC comes through both zooplankton groups in REcoM-2-M. The sPOC production from sloppy feeding, mortality and fecal pellet production (Equation 9) are described for macrozooplankton in Section 2.2, equations (Equations 1 and 2). Fecal pellet production is only represented explicitly for the macrozooplankton group. The sPOC production from sloppy feeding is calculated by multiplication of the grazing fluxes in carbon units ($\sum_i \frac{1}{q_i} \cdot G_i$) with the one minus grazing efficiency term (γ) for macrozooplankton. The small zooplankton group contributes to sPOC formation by mortality and sloppy feeding, which implicitly includes fecal pellets (Equation 10).

$$sPOC_{zoo}^{prod} = sPOC_{zoo}^{mortality} + sPOC_{zoo}^{sloppyfeeding} + sPOC_{macrozoo}^{fecalpellet} \tag{9}$$

$$sPOC_{zoo}^{sloppyfeeding} = \underbrace{\left(\sum_i \frac{1}{q_i} \cdot G_i\right) \cdot (1 - \gamma)}_{\text{Macrozoo.}} + \underbrace{\left(\sum_i \frac{1}{q_i} \cdot G_{i\_\text{zoo1}}\right) \cdot (1 - \gamma_{\text{zoo1}})}_{\text{Small zoo.}} \tag{10}$$

2.4. Model Setup and Simulations

The global model was forced with the JRA-55-do atmospheric forcing data set version 1.3.1 (Kobayashi et al., 2015) in a 60 years long simulation. Repeated year forcing fields from the year 1961 of surface downwelling short and long-wave radiation, surface rainfall, and snowfall fluxes as well as near-surface (2 m) air temperature, specific humidity, eastward and northward wind components, and sea level pressure were used. Freshwater runoff and the surface salinity field for a weak surface salinity restoration (Sidorenko et al., 2011) are taken from the CORE-II climatology (Griffies et al., 2009). The nutrients dissolved inorganic nitrogen and dissolved silicic acid were initialized with World Ocean Atlas 2013 products (Garcia et al., 2013), and dissolved inorganic carbon (DIC) and alkalinity from GLODAPv2 (Lauvset et al., 2016). We performed global model simulations, but only analyzed the Southern Ocean. The last 5 years of the model simulation were analyzed with respect to nutrient concentrations, net primary production, export production at 100 m, particulate organic carbon production, and ecosystem structure south of 50°S. Export production was calculated by multiplying detritus concentration at 100 m with the sinking speed at 100 m.

We conducted five simulations to analyze the effects of different processes within the newly implemented macrozooplankton group (Table 2). First, the control simulation (CTRL) was conducted with the original setup with only one zooplankton group of REcoM-2. Further, we executed four simulations with the increasing complexity of macrozooplankton representation. These simulations include (a) only the new macrozooplankton group (MACROZOO), (b) a simulation with macrozooplankton and a second detritus pool (MACROZOO_2DET), (c) another including in addition detritus grazing (MACROZOO_DETGRAZ), and (d) a final one including

Journal of Geophysical Research: Oceans 10.1029/2021JC017315

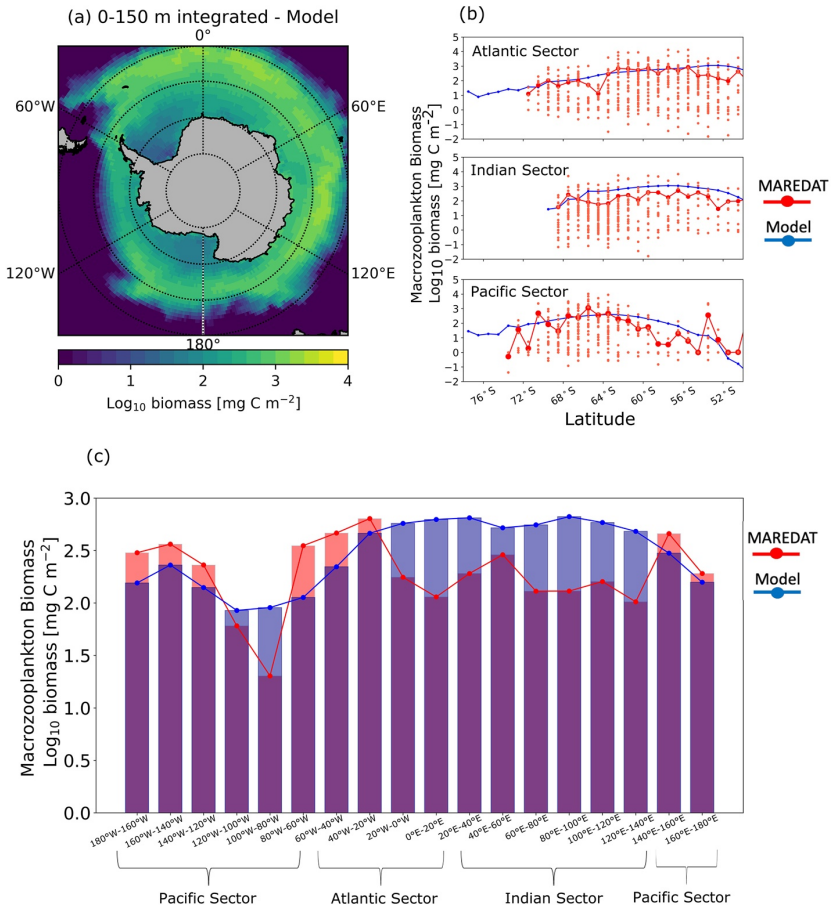

Figure 3. Modeled macrozooplankton biomass, presented as vertically-integrated (0–150 m), and annually averaged log10 biomass [mg C m^{-2}] in the Southern Ocean (a) spatial distribution, (b) Zonal mean of biomass in Atlantic, Indian and Pacific sectors for model (dots with blue line) and MAREDAT (dots with red line, small dots indicate individual data points, and larger dots the mean), (c) Spatial mean of the region within each 20° longitude bin in the Southern Ocean for model and MAREDAT data. The light red areas and light blue areas in the bars show underestimation and overestimation of the model compared to data, respectively.

also fecal pellet production (MACROZOO_ALL). In the results Section 3.1 we focus only on the evaluation of the MACROZOO_ALL simulation, and in Section 3.2 and 3.3, we focus on the comparison of the CTRL and MACROZOO_ALL simulations. In Section 3.4, we analyze the effect of the different processes on NPP, EP, and sPOC production using all simulations.

2.5. Evaluation of Modeled Macrozooplankton Biomass

To evaluate the macrozooplankton biomass results, we used the MAREDAT global macrozooplankton dataset, covering the period from 1926 to 2010 (Moriarty et al., 2013). Since there is no data in the MAREDAT data set for the austral winter months July to September, these months were also excluded for the biomass comparison from the model output. The modeled annual mean (October–June) macrozooplankton biomass from the last five model years 2013–2017 was interpolated to the MAREDAT data grid (1° × 1°). We restricted the comparison to the Southern Ocean south of 50°S. Here, the comparison focuses on two aspects: (a) the spatial mean of macrozooplankton biomass for the model and MAREDAT and (b) the depth-integrated macrozooplankton distribution integrated over the upper 150 m for model and data (Figure 3). Furthermore,

Journal of Geophysical Research: Oceans 10.1029/2021JC017315

the statistical distribution of macrozooplankton biomass where we subsampled the model for MAREDAT data points considering different depth ranges is summarized in Table S1 in Supporting Information S1.

3. Results

3.1. Macrozooplankton Biomass in the Southern Ocean

The order of magnitude of the mean biomass is captured well, although the model mean (2.55 mg C m^{-3}) is lower than the MAREDAT (Moriarty et al., 2013) mean (5.25 mg C m^{-3}, Table S1 in Supporting Information S1). This is caused by some very high biomass numbers in MAREDAT, being reflected in a maximum annual mean of 582.3 mg C m^{-3} which are not captured by the model with a maximum annual mean of 23.5 mg C m^{-3} derived from the subsampled model. This might to some extent reflect a sampling and reporting bias with more observations at locations with high biomass. The integrated modeled macrozooplankton biomass is 2.81 Tg C which is closer to 3.07 Tg C in observations (Table S1 in Supporting Information S1).

When integrating over the whole Southern Ocean, the mean biomass of the modeled macrozooplankton over the upper 150 m is 367.2 mg C m^{-2}. While this would suggest an underestimation of the modeled macrozooplankton biomass as compared to the MAREDAT mean biomass of 495.9 mg C m^{-2}, the sampling bias needs to be taken into account. When subsampling the model according to the data points in MAREDAT including their same depth range, the mean biomass equals 517.5 mg C m^{-2}, which is reasonably close to the MAREDAT numbers. The modeled macrozooplankton biomass decreases with depth. While 98.4% of the modeled biomass is within the upper 150 m, 74.3% is between 0 and 50 m. While there is some available data below 150 m in MAREDAT (max. 120.4 mg C m^{-3}), the model does not reproduce biomass below 150 m. This is expected since the vertical migration of macrozooplankton is not represented.

We further investigate the spatial distribution of macrozooplankton biomass. In MAREDAT, the observations are denser around the Antarctic Peninsula than at other sites in the Southern Ocean. In the upper 150 m, 39% of all observations were obtained between 0°W and 80°W, and 39% of them between 0°W and 120°E, making the Pacific sector the least observed sector of the Southern Ocean. According to the model, the maximum modeled macrozooplankton biomass occurs in the Atlantic and Indian sectors of the Southern Ocean (Figure 3). In the Pacific sector, the model results suggest lower macrozooplankton biomass (Figure 3c). The latitudinal patterns of macrozooplankton biomass distribution are fairly similar between our simulation and MAREDAT. The biomass is relatively constant across latitudes in the Indian sector, increases from south to north in the Atlantic sector, and has a peak around 65°S in the Pacific sector of the Southern Ocean (Figure 3b). The maximum macrozooplankton biomass occurs around the Antarctic Peninsula in MAREDAT and the model reproduces the same order of magnitude. However, the model suggests that the maximum biomass is located in the central Atlantic sector.

Implementing a new zooplankton group reduces the mismatch with the observed chlorophyll and nutrient concentrations. In the CTRL, there is a positive bias (up to 1 mg chl m^{-3}) compared to the satellite chlorophyll concentrations in the coastal areas of the Southern Ocean. In MACROZOO_ALL this positive bias is reduced to 0.3 mg chl m^{-3} (Figure S4 in Supporting Information S1). This is also in agreement with the role of krill grazing on the Southern Ocean ecosystem described by (Smetacek et al., 2004). When CTRL and WOA silicic acid (DSi) concentrations are compared, a negative bias is revealed, especially close to Antarctica. The negative bias is around 12 mmol DSi m^{-3} between 50 and 64°S and 30–100 m depth (Figure S3e in Supporting Information S1). DIN shows positive and negative biases, with a negative DIN bias of up to 8 mmol m^{-3} between 50 and 60°S and 0–150 m depth in the CTRL simulation (Figure S2g in Supporting Information S1). A positive bias for DIN (up to 6 mmol DSi m^{-3}) is present between 60 and 64°S and 100–150 m depth. In MACROZOO_ALL, there is a slight increase in DSi (up to 5 mmol m^{-3}) south of 50°S in the upper 100 m. This spatial pattern shows similarity with the changes in diatom chlorophyll concentrations (Figure S1 in Supporting Information S1), presumably as a result of the decreasing diatom abundance. In MACROZOO_ALL, there is a notable decrease (up to 1 mmol m^{-3}) in nitrate concentration between 60 and 64°S and 100–150 m depth.

Journal of Geophysical Research: Oceans 10.1029/2021JC017315

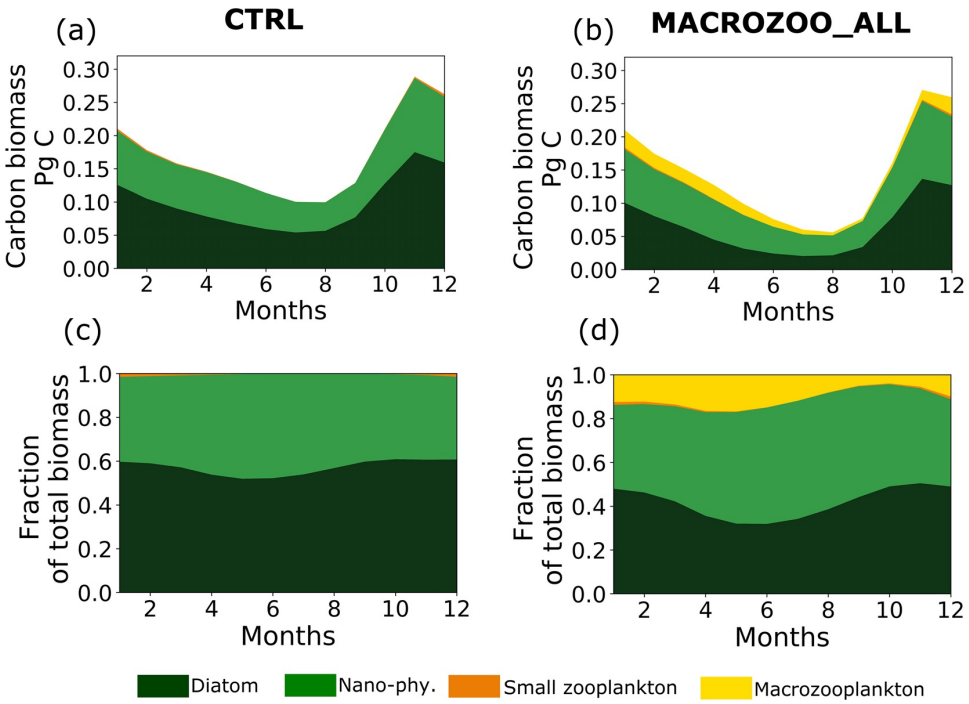

Figure 4. Seasonal cycle of carbon biomass (a and b) and share (c and d) of phytoplankton and zooplankton contribution to the total carbon biomass integrated over the upper 150 m south of 50°S. First column control simulation, second column MACROZOO_ALL.

3.2. Phytoplankton and Zooplankton Community Composition in the Southern Ocean

In the control simulation, the shares of nanophytoplankton, diatoms, and zooplankton of the total carbon biomass amount to 41.6%, 57.8%, and 0.6% of the total carbon biomass south of 50°S, respectively. In MACROZOO_ALL, the fraction of diatoms decreases to 45.9% of total carbon biomass due to increased grazing pressure, while the fraction of nanophytoplankton increases to 44.8%. Small zooplankton remains at 0.6% and macrozooplankton contributes 8.7% to the total carbon biomass. Hence, the total share of grazers increases from 0.6% to 9.3% of the total carbon biomass in the modeled ecosystem.

The total carbon biomass reaches its maximum (0.29 Pg C in CTRL, 0.27 Pg C in MACROZOO_ALL) in November and its minimum between June and August in both simulations. While the grazer biomass reaches its maximum <0.01 Pg C in December in CTRL, the maximum biomass is increased (0.03 Pg C) in MACROZOO_ALL and occurs in December and January (Figures 4a and 4b). Diatoms contribute the largest fraction of the total biomass in both CTRL and MACROZOO_ALL throughout the year. In CTRL, the fractions of diatoms, nanophytoplankton, and the small zooplankton group vary over the year, with values between 52%-61% (diatoms), 38%–48% (nanophytoplankton), and 0.03%–1.4% (zooplankton), respectively. In MACROZOO_ALL, the fraction of diatoms varies at lower levels between 32% and 50%. Nanophytoplankton exhibit a slightly increased variability between 35% and 54%. The new macrozooplankton group contributes between 4% (in October) and 17% (in April-May) to the total biomass (Figures 4c and 4d). While nanophytoplankton prevails between 50°S and 60°S in both simulations, diatoms are the dominant phytoplankton group south of 60°S (Figures 5e and 5f).

While there are some changes in the biomass of phytoplankton groups, as described above, the main characteristics of the seasonal cycle in CTRL, as diagnosed from monthly mean model output, are preserved in the MACROZOO_ALL set-up. In both simulations, the spring peak takes place in November, and the minimum biomass occurs from July to August (Figure 4). The phenology thus follows similar patterns as in the preceding model version with the magnitude of NPP comparable to satellite-derived estimates, and a fast and early

Journal of Geophysical Research: Oceans 10.1029/2021JC017315

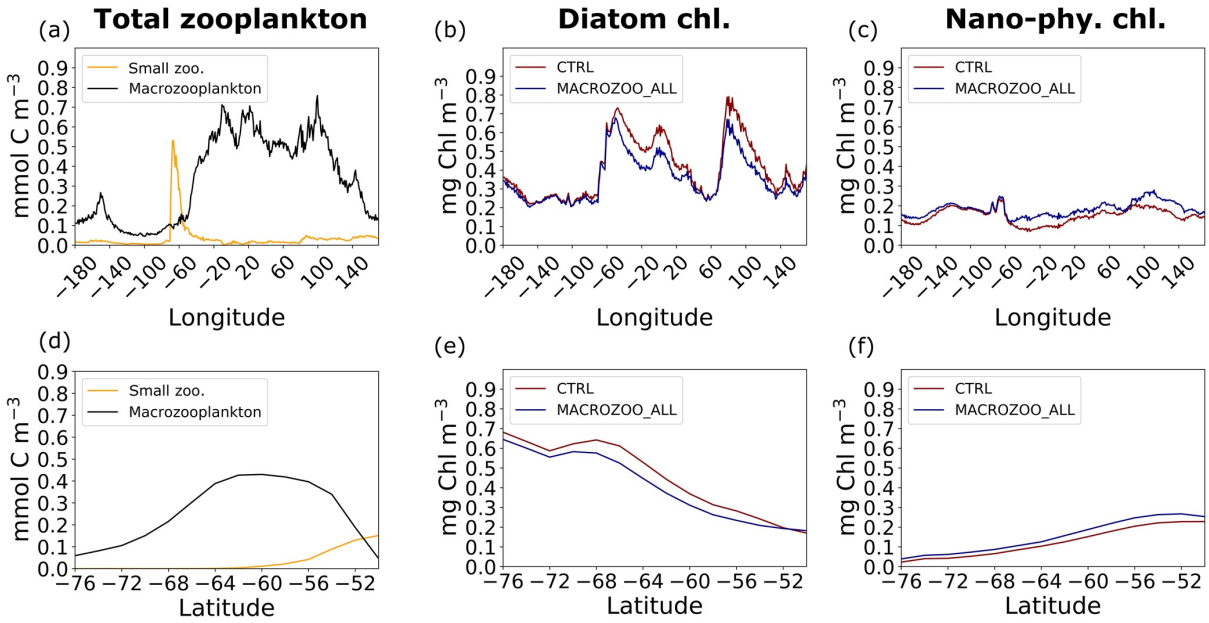

Figure 5. Annual mean surface concentrations of zooplankton biomass and phytoplankton chlorophyll that have then been averaged in the meridional (first row) and zonal (second row) directions. Panels (a) and (d) depict the annual mean zooplankton biomass in MACROZOO_ALL, panels (b) and (e) diatom chlorophyll in control simulation (CTRL) and MACROZOO_ALL, and (c) and (f) nanophytoplankton chlorophyll in CTRL and MACROZOO_ALL.

spring bloom (see analysis in Schourup-Kristensen et al., 2014). One notable difference is a one month shift of spring maximum NPP in the Atlantic, Indian and Pacific sectors and a slightly lower NPP in the Atlantic sector (annual mean is 160 mg C m^{-2} day^{-1} in new simulations) compared to the results in Schourup-Kristensen et al. (2014) that we relate to the parameterization of photodamage used here (Álvarez et al., 2018). A detailed analysis of phytoplankton bloom phenology is beyond the scope of this study and would require higher frequency model output.

Macrozooplankton carbon biomass is higher (0.02–0.025 Pg C) between December and April when sea-ice extent is decreasing (minimum in March 3.1 km^{-2}, Figure S5c in Supporting Information S1). After April, macrozooplankton biomass continues to decrease and reaches minimum values (0.004 Pg C) when the sea-ice extent is reaching maximum (18.6 km^{-2} in September, Figure S5c in Supporting Information S1). In nature, different life stages of macrozooplankton (krill) can use the sea ice as a refuge area or sea-ice algae as a winter food source and increase survival capability (Meyer, 2012). Since we do not represent these mentioned processes, winter macrozooplankton biomass is almost 10 times lower than summer macrozooplankton biomass. The seasonal evolution of macrozooplankton biomass expectedly follows the phytoplankton biomass.

The surface distribution of phytoplankton and zooplankton along longitude and latitude is illustrated in Figure 5. Diatom chlorophyll concentration exhibits a maximum of 0.7 mg chl m^{-3} around 60°W, near the Antarctic Peninsula. It reaches another peak around 100°E (in the Indian sector) and is generally lower in the Pacific sector (0.3–0.4 mg chl m^{-3}, Figure 5b). The surface zooplankton concentrations follow a similar pattern in the east-west direction. The small zooplankton group increases in abundance going northwards (Figure 5d) and peaks around 60°W (0.5 mmol C m^{-3}, Figure 5a). The macrozooplankton carbon concentration reaches a plateau of 0.7 mmol C m^{-3} between 20°W (in the Atlantic sector) and 100°E (in the Indian sector) and it is the dominant grazer group throughout most of the Southern Ocean (Figures 5a and 5d). The new grazing pressure slightly decreases diatom chlorophyll concentration (by <0.1 mg chl m^{-3}) and increases nano-phytoplankton chlorophyll concentration (by <0.1 mg chl m^{-3}) between 60°W and 100°E (Figures 5b–5f).

Journal of Geophysical Research: Oceans 10.1029/2021JC017315

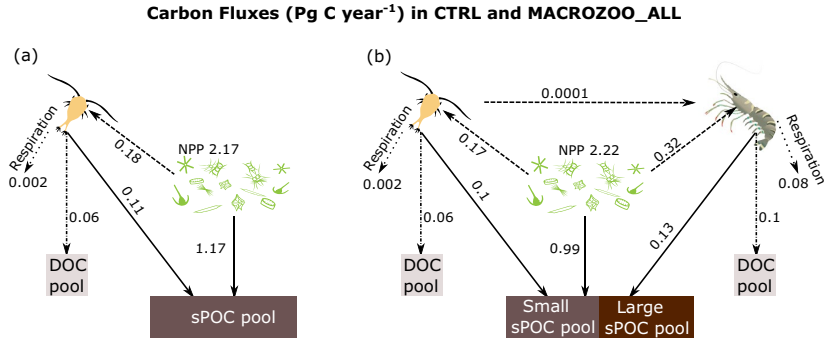

Figure 6. Fluxes between model compartments in (left) CTRL and (right) MACROZOO_ALL: sPOC production via phytoplankton aggregation, mortality, sloppy feeding and fecal pellets of zooplankton groups (solid line), grazing flux to zooplankton (dashed line), DOC production (dashed-dotted line), respiration of zooplanktons (dotted line). DOC: dissolved organic carbon, sPOC: sinking particulate organic carbon, NPP: net primary production.

3.3. Carbon Transfer Pathways in FESOM-REcoM in the Southern Ocean

Carbon fluxes between different ecosystem compartments are presented in Figure 6. Total NPP increased slightly from 2.17 to 2.22 Pg C yr^{-1} in the MACROZOO_ALL simulation compared to CTRL (Figure 6). The grazing flux from primary producers to zooplankton groups is more than doubled with 0.49 Pg C yr^{-1} (22.1% of NPP) in MACROZOO_ALL compared to 0.18 Pg C yr^{-1} (8.3% of total NPP) in CTRL. The contribution of the total zooplankton to total particle formation also doubled from 0.11 Pg C yr^{-1} (8.6% of total particle flux formation) in CTRL to 0.23 Pg C yr^{-1} (18.9%) in MACROZOO_ALL. DOC-excretion by zooplankton increased from 0.06 Pg C yr^{-1} in CTRL to 0.16 Pg C yr^{-1} in MACROZOO_ALL (with 0.10 Pg C yr^{-1} from macrozooplankton). Respiration by both zooplankton groups transfer <0.01 and 0.08 Pg C yr^{-1}, respectively, to the dissolved inorganic carbon pool. In total, macrozooplankton contributes 65% to the total zooplankton grazing flux, 10% to sPOC formation, 63% to DOC production, and 97% to total zooplankton respiration (Figure 6).

The sPOC production by different groups is shown in Figure 7a. In CTRL, the main contribution to sPOC production is from primary producers as a result of aggregation. It is dominated by diatoms (varying from <0.01 in July/August to 0.18 Pg C $month^{-1}$ in November) with a smaller contribution of nanophytoplankton (varying from <0.01 in July to 0.12 Pg C $month^{-1}$ in November). Zooplankton-related sPOC production occurs mostly between November and April and it ranges between 2×10^{-4} to 0.03 Pg C $month^{-1}$ (Figure 7a). In MACROZOO_ALL, phytoplankton aggregation is still the dominant process. In contrast to the control simulation, nanophytoplankton and diatoms now contribute in similar shares to sPOC production via aggregation (diatoms: <0.01 to 0.15 Pg C $month^{-1}$, nanophytoplankton: <0.01 to 0.13 Pg C $month^{-1}$) in MACROZOO_ALL. The sPOC production by the small zooplankton varies between <0.01 and 0.03 Pg C $month^{-1}$ and macrozooplankton sPOC production ranges between <0.01 and 0.02 Pg C $month^{-1}$ (Figure 7b).

Over the course of the year, the fraction of diatom and nanophytoplankton aggregation in sPOC formation pathways peaks in June and July (98.4%) in CTRL. In MACROZOO_ALL, aggregation shows higher contributions in spring/summer with a maximum of 91.6% in November. The contribution of zooplankton (sloppy feeding, mortality, fecal pellets) to sPOC production increases from 1.5%–13.0% in CTRL to 11.8%–39.0% in MACROZOO_ALL. While the zooplankton contribution is lowest (1.5%–5.0%) from May to November in CTRL (Figure 7c), in MACROZOO_ALL it shows a higher contribution throughout the year and has the largest share after the spring/summer phytoplankton bloom (Figure 7d). The relative contribution of macrozooplankton is lowest in November (6%) and highest in April (30%), while the small zooplankton contributes 2%–13% (Figure 7d).

Journal of Geophysical Research: Oceans 10.1029/2021JC017315

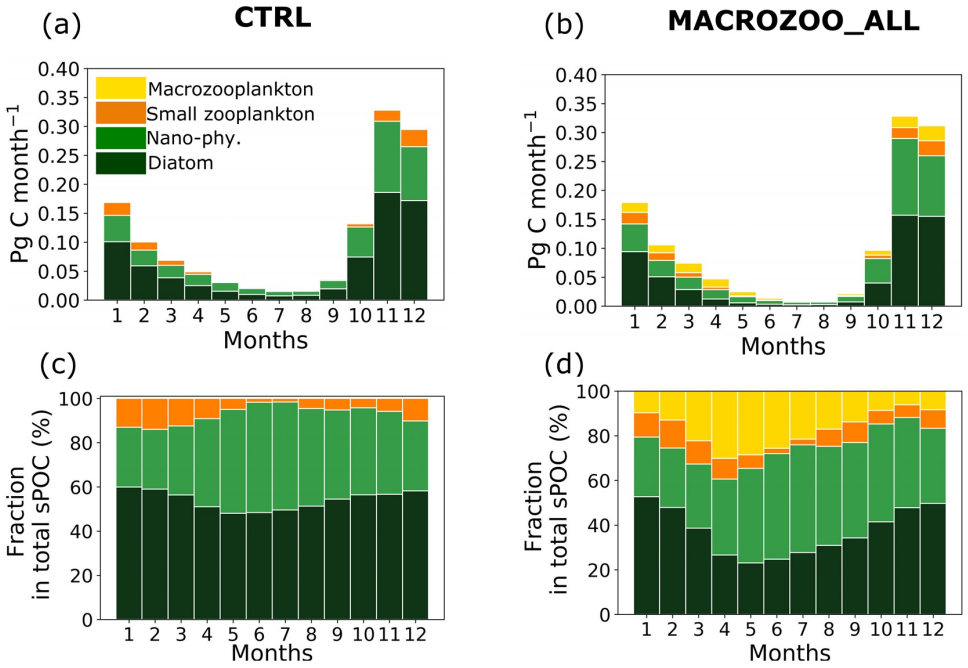

Figure 7. Seasonal cycle of sinking particulate organic carbon (sPOC) production south of 50°S by phyto- and zooplankton groups in absolute and relative terms for both simulations. The sPOC production in CTRL and MACROZOO_ALL (a, b) and fractions of different groups in CTRL and MACROZOO_ALL (c, d). Left column (a, c) shows results in CTRL, and right column (b, d) shows MACROZOO_ALL simulation.

3.4. Particulate Organic Matter Export in the Southern Ocean

Implementation of the macrozooplankton group into the ecosystem model affects the particulate nitrate and carbon export to the deep ocean, and this effect increases with depth (Figure 8). The total amount of exported carbon and nitrogen hardly changes across the 100 m depth level with 0.82 Pg C yr^{-1} and 0.18 Pg N yr^{-1} in CTRL and 0.81 Pg C yr^{-1} and 0.17 Pg N yr^{-1} in MACROZOO_ALL. Depth profiles of exported carbon and nitrogen exhibit similar patterns in both simulations. EP reaches its maximum around 90 m and decreases in deeper layers (Figures 8a and 8b). Carbon export in MACROZOO_ALL increases in almost all depth layers, but especially below 200 m (Figure 8c). This increase reaches 0.05 Pg C yr^{-1} at 1,000 m. In contrast, the exported nitrogen mostly decreases in the upper 200 m and increases by 0.01 PgC yr^{-1} below 200 m in MACROZOO_ALL (Figure 8d).

In addition, we calculated the p-ratio (sPOC production/NPP), s-ratio (EP/sPOC production), and their product e-ratio (EP/NPP) to analyze the export more closely (Laufkötter et al., 2016). The p-ratio describes the efficiency of the particle formation in the ecosystem and the s-ratio is the fraction of particles that escape remineralization at the surface. A higher s-ratio indicates that a larger proportion of formed particles sinks through the 100 m horizon, that is, a smaller amount of particles is remineralized. The s-ratio slightly increases (from 0.67 to 0.70) due to the higher sinking rate of the large detritus class. The p-ratio and e-ratio decrease from 0.58 to 0.55 and 0.39 to 0.38, respectively compared to CTRL. The change of the p-ratio and e-ratio is a result of an increase in NPP in MACROZOO_ALL.

In regions where macrozooplankton is abundant, carbon and nitrogen export across 1,000 m depth almost double in the MACROZOO_ALL simulation (Figures 9a and 9b). While in the CTRL carbon export across 1,000 m mostly varies between 2 and 8 g C m^{-2} yr^{-1}, it can reach values up to 15 g C m^{-2} yr^{-1} in MACROZOO_ALL. Similarly, nitrogen export across 1,000 m reaches peak values of 2.6 g C m^{-2} yr^{-1} in MACROZOO_ALL, 73% higher than the 1.5 g C m^{-2} yr^{-1} in CTRL. These higher values occur in places with high macrozooplankton concentrations at the surface. After implementing macrozooplankton, the exported material becomes richer in terms

Journal of Geophysical Research: Oceans 10.1029/2021JC017315

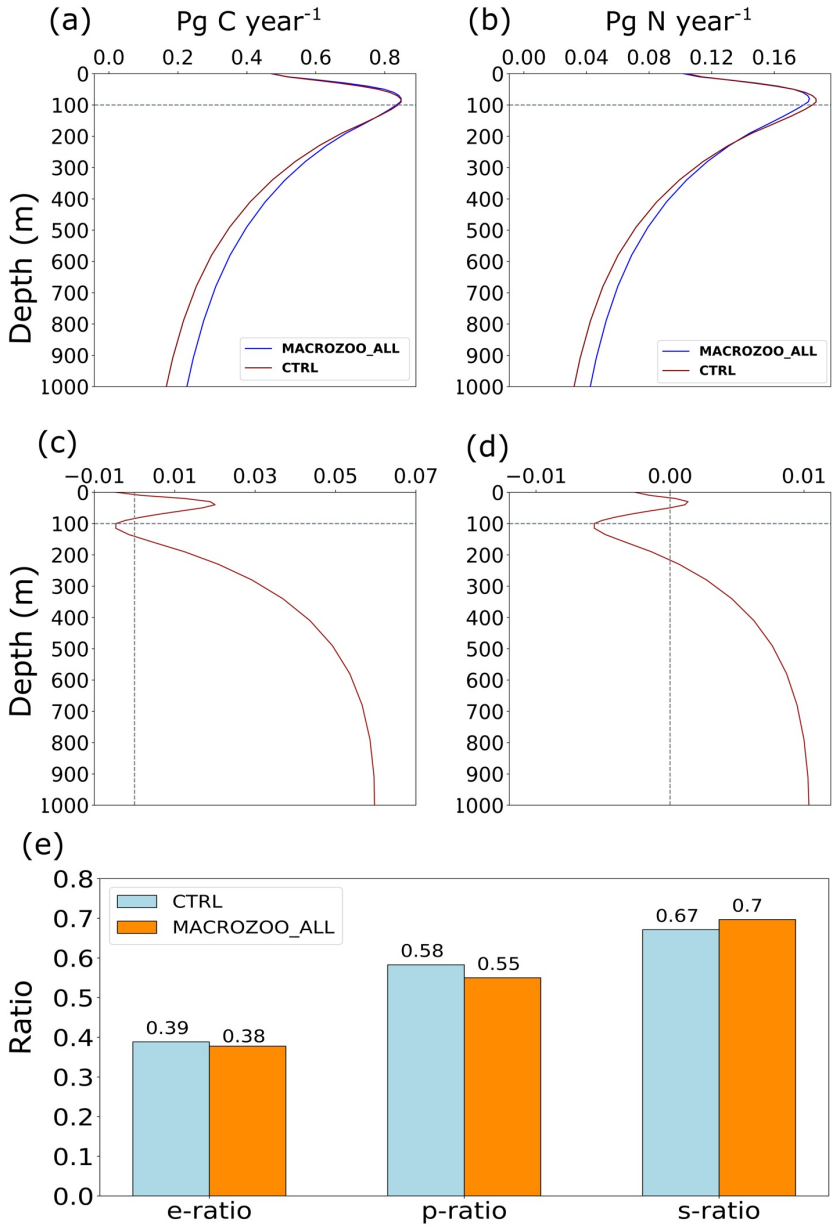

Figure 8. Annual export fluxes of particulate organic carbon (POC) and nitrogen (PON) south of 50°S in CTRL (red) and MACROZOO_ALL (blue) (a, b), difference between MACROZOO_ALL and CTRL POC and PON export fluxes (c, d), and annual mean of e-, p- and s-ratios south of 50°S in both simulations (e).

of carbon, and C:N ratios increase up to 5.5 (Figure 9c). It is directly related to the carbon to nitrogen ratio of the large detritus class which varies between 6.0 (minimum) and 6.7 (maximum) in different depth levels (Figure S3 in Supporting Information S1).In addition, the transfer efficiency (EP_{1000}/EP_{100}) relating the sequestration flux at 1,000 m to the export flux (Passow & Carlson, 2012) is three times higher at places with higher macrozooplankton concentration compared to the CTRL simulation, due to the high sinking rates of particles and the carbon-enrichment of macrozooplankton fecal pellets (Figure 9d).

Journal of Geophysical Research: Oceans 10.1029/2021JC017315

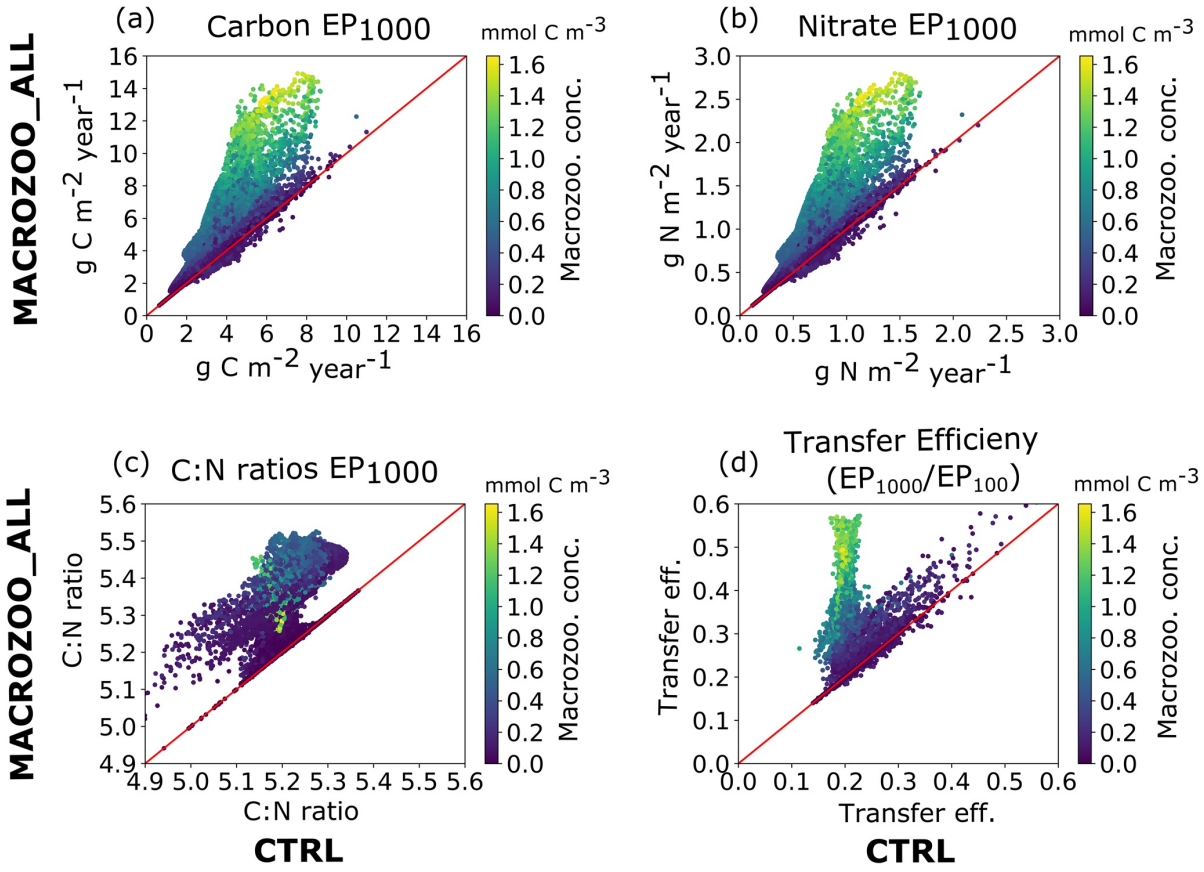

Figure 9. Point-wise comparison of annual mean carbon and nitrogen export at 1,000 m, (c)N ratio of exported material and transfer efficiency between CTRL (*x*-axis) and MACROZOO_ALL (*y*-axis) south of 50°S. Each dot represents one model grid point. Annual export of C and N at 1,000 m (a, b), C:N ratios of exported material (c) and transfer efficiency (EP_{1000}/EP_{100}) (d). The red line represents the one-to-one line in the plots. The color shading indicates the surface macrozooplankton concentration.

Increases in the transfer efficiency show spatial differences. In MACROZOO_ALL, the highest transfer efficiency (more than 50%) is located in the Atlantic and Indian sectors of the Southern Ocean (Figures 10a and 10b) where high macrozooplankton biomass (Figures 3a) occurs. This is due to the macrozooplankton-related larger particle class. Also, the difference between carbon and nitrogen transfer efficiencies (Figure 10f) is higher (up to 0.05) which indicates carbon-enrichment of macrozooplankton fecal pellets. In CTRL, the maximum transfer efficiency is located in the Pacific sector (up to 25%, Figure 10a). Differences between carbon and nitrogen transfer efficiencies are positive, with values up to 0.02 (Figure 10c).

3.5. Disentangling Processes Contributing to Changes in Carbon Pathways

In this section, we analyze the effects of different aspects of the macrozooplankton representation. In Table 3, annual total NPP, EP, and sPOC formation are presented for the various simulations. All simulations with macrozooplankton have in common that there is a 2%–6% increase in total NPP and a 1%–17% decrease in EP at 100 m in comparison to the CTRL simulation (Table 3). Total sinking particle formation decreases by 4.6%–9% in the macrozooplankton simulations, while the contribution of the zooplankton groups to sPOC formation increases from 8.5% (CTRL) to 14%–19% (macrozooplankton simulations, Table 3). In all simulations with the macrozooplankton group, diatom chlorophyll concentrations decrease (Figure 5), and consequently, the contribution of diatoms to sPOC formation decreases from 57% in CTRL to 47% in the simulations with

Journal of Geophysical Research: Oceans 10.1029/2021JC017315

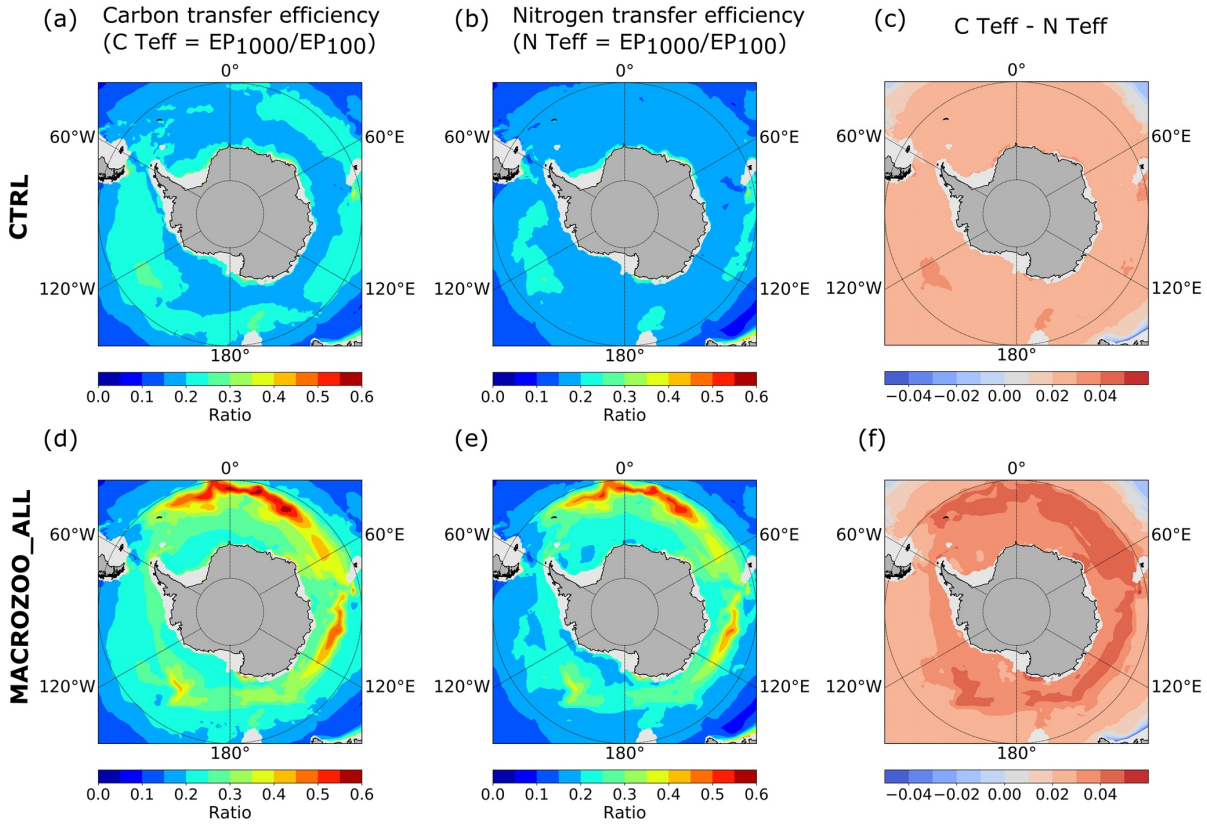

Figure 10. Spatial distributions of (a, d) carbon transfer efficiency (C Teff = EP_{1000}/EP_{100}), (b, e) nitrogen transfer efficiency (N Teff = EP_{1000}/EP_{100}) and (c, f) difference between C Teff and N Teff in CTRL (first row) and MACROZOO_ALL (second row). EP_{1000}: export flux at 1,000 m. EP_{100}: export flux at 100 m.

macrozooplankton. The new macrozooplankton group helps to reduce a probably overly large role of diatom aggregation that was found in the model without macrozooplankton. When we implement only the bare new macrozooplankton group (MACROZOO) to the model, NPP increases by 0.13 Pg C yr^{-1}, as nutrients are kept in the surface layer via excretion by macrozooplankton. The new large detritus class for the macrozooplankton group in the model (MACROZOO_2DET) causes a 35% increase in EP_{1000} compared to MACROZOO. After implementing particle grazing by the zooplankton groups (MACROZOO_DETGRAZ), NPP increases 0.01 Pg C yr^{-1} compared to MACROZOO_2DET. EP_{100} decreases in the simulations in MACROZOO, MACROZOO_2DET, and MACROZOO_DETGRAZ as the grazed biomass also builds up macrozooplankton biomass and

Table 3
Spatially-Integrated Net Primary Production (NPP), Carbon Export Flux at 100 m (EP_{100}) and 1,000 m (EP_{1000}), Total Particle Formation (Total sPOC), Total Phytoplankton Aggregation (Total agg.) and Total Particle Formation by the Zooplankton Groups (sPOC zoo.) South of 50°S in Different Simulations

Simulation	NPP	EP_{100}	EP_{1000}	Total sPOC	Total agg.	sPOC zoo.
CTRL	2.17	0.82	0.16	1.28	1.17	0.11
MACROZOO	2.30	0.77	0.14	1.19	0.99	0.2
MACROZOO_2DET	2.28	0.77	0.19	1.17	0.96	0.21
MACROZOO_DETGRAZ	2.29	0.77	0.19	1.18	0.97	0.21
MACROZOO_ALL	2.22	0.81	0.22	1.22	0.99	0.23

Note. All fluxes are in units Pg C yr^{-1}.

Journal of Geophysical Research: Oceans 10.1029/2021JC017315

is redistributed via excretion and respiration. When representing fecal pellets with a high C:N ratio explicitly for the macrozooplankton group, macrozooplankton sPOC production and hence export production increase and compensate for the EP decrease due to decreased particle formation. NPP still increases due to the fast recycling of nutrients by the zooplankton group in MACROZOO_ALL, but to a smaller amount than in MACROZOO as part of this effect is compensated by the additional nutrient loss via fecal pellets. The export flux at 1,000 m increases by 0.06 Pg C yr^{-1} when all processes are included (MACROZOO_ALL). This is a pertinent feature in all simulations with the large detritus class (MACROZOO_2DET, MACROZOO_DETGRAZ). The carbon transfer efficiency (EP_{1000}/EP_{100}) south of 50°S increases from 19% (CTRL, MACROZOO) to 25%–27% in the simulations with the large detritus class.

4. Discussion

In this modeling study, we analyze the effect of implementing a macrozooplankton functional type on biogeochemical processes with a focus on the biological carbon pump in the Southern Ocean. Based on our results, annual macrozooplankton sPOC production amounts to more than 10% of total sPOC production in the Southern Ocean (south of 50°S), and carbon transfer efficiency (EP_{1000}/EP_{100}) reaches up to 50% in the areas with high surface macrozooplankton density (Figure 9). Additionally, having macrozooplankton represented in the model enhances the recycling of nutrients in the surface layers, thus increasing NPP.

Our results indicate that macrozooplankton plays an important role in particulate organic carbon production and export efficiency. The seasonal contribution of macrozooplankton to sPOC production (11.8%–39.0%, Figure 7) matches the range observed in field studies (Turner, 2015, highly variable, mostly <40%). In the MACROZOO_ALL simulation, 15.3% of total carbon export at 100 m (0.12 Pg C yr^{-1}, Figure 8) originates from macrozooplankton-related processes in the Southern Ocean. South of 60°S, the modeled total macrozooplankton carbon export is 0.29 Pg C yr^{-1}, which is at the upper end of the reported range from satellite-based estimates (Belcher et al., 2019, 0.09 to 0.29 Pg C yr^{-1}). In the model, macrozooplankton contributes 0.042 Pg C yr^{-1} or 14.3% to the POC flux at 100 m south of 60°S, in agreement with the estimate of 0.039 Pg C yr^{-1} on average, corresponding to 12.5%–43.3% of POC flux by Belcher et al. (2019). REcoM now captures the typical shift from a dominance of phytodetrital aggregates in spring to zooplankton fecal pellets later in the year which was reported for a subantarctic site (Ebersbach & Trull, 2008; Laurenceau-Cornec et al., 2015; Rembauville et al., 2015, Figure 7d).

A pertinent feature of REcoM-2 is its low zooplankton biomass and zooplankton contribution to POC production in the Southern Ocean, in comparison to other biogeochemical models such as BEC and PISCES (Laufkötter et al., 2016). After implementing the macrozooplankton group, the zooplankton share of modeled total biomass increases from 0.6% to 9.3% in the upper 150 m along with the complexity of zooplankton representation (particle grazing, fecal pellet production). This is the first step to a more realistic description of particle formation and destruction processes.

Our estimated macrozooplankton biomass in the upper ocean is in the same range as in the global macrozooplankton dataset MAREDAT. The model simulates maximum macrozooplankton biomass in the Atlantic and Indian sectors of the Southern Ocean and lowers biomass in the Pacific sector, roughly following the chlorophyll distribution (Figure 3). This distribution pattern generally matches observations of Antarctic krill biomass (Atkinson et al., 2004; Siegel, 2016). The modeled biomass maximum occurs in the central Atlantic sector rather than near the Antarctic Peninsula as in MAREDAT, which may be explained by the food availability for the macrozooplankton group in the model. The comparison is hampered by the much higher density of observations near the Antarctic Peninsula. Since we do not include swarm forming and vertical migration behavior of macrozooplankton the model captures the mean biomass by design rather than the patches of very high biomass densities in MAREDAT (Figure 3).

The presence of macrozooplankton affects the biomass of primary producers (Figure 4) and, thus, the chlorophyll concentrations (Figure 5) in the model simulations. There is a modest shift from diatoms to nanophytoplankton, but diatoms remain the dominant phytoplankton PFT. Annual mean diatom chlorophyll at the surface decreases by 10% from 0.40 to 0.36 mg chl m^{-3} and nanophytoplankton chlorophyll increases by 20% from 0.15 to 0.18 mg chl m^{-3}. However, the implementation of macrozooplankton does not lead to a drastic reduction in summer

Journal of Geophysical Research: Oceans 10.1029/2021JC017315

(November to January) chlorophyll concentrations in the Pacific sector of the Southern Ocean as in Le Quéré et al. (2016). This discrepancy can be explained by differences in the latitudinal macrozooplankton biomass distribution between the two models due to different temperature functions (Le Quéré et al., 2016). The maximum annual mean macrozooplankton biomass at the surface occurs closer to the Antarctic continent (between 54°S and 64°S) in the FESOM-REcoM simulations (Figure 3). Since macrozooplankton is parameterized to mimic the temperature tolerance of Antarctic krill in our study, we do not intend to represent macrozooplankton biomass in the warmer regions. In the simulations with macrozooplankton, the model bias of observational nutrient concentrations (Garcia et al., 2018) was slightly reduced in different depth levels in the Southern Ocean (Figure S2 in Supporting Information S1). One reason for this change is a shift in phytoplankton composition (decrease in diatom and increase in nanophytoplankton biomass). Another reason is the recycling of nitrogen and iron by macrozooplankton via excretion, thus retaining nutrients in the surface layer. As the excretion of iron is modeled via a fixed Fe:N ratio, the magnitude of the nutrient recycling effect and the importance of krill in the iron cycling might be underestimated (Tovar-Sanchez et al., 2007).

Our results highlight the important role of macrozooplankton in the carbon and nutrient cycles of the Southern Ocean. The model further supports that macrozooplankton fecal pellet production is an important component of the export flux of the Antarctic biological carbon pump in the Southern Ocean (Belcher et al., 2019; Cavan et al., 2019). Representations of zooplankton loss terms and their contribution to sinking particles are considerably different in ocean biogeochemical models (Laufkötter et al., 2016). The representation of carbon-rich fecal pellets and fast-sinking large particles in our model are crucial macrozooplankton characteristics that lead to a high transfer efficiency of carbon. In agreement with Passow and Carlson (2012), our model results show that macrozooplankton increase carbon-rich particle sinking across 1,000 m.

This particular and important role of polar macrozooplankton may, however, change in the future. Climate change and fisheries could impact krill abundance negatively (Atkinson et al., 2019; Brooks et al., 2018; Klein et al., 2018). Because of the projected decline of krill, the ratio of phytodetrital aggregates to fecal pellets could increase in the future (Cavan et al., 2019) and the efficient particulate organic carbon transfer via macrozooplankton activity could decrease. This scenario is similar to our control model simulation. In such a case, carbon sequestration flux below 1,000 m could substantially decrease in the future.

Our results also suggest that macrozooplankton stimulates net primary production. This feature is in agreement with the reported role of krill in the Southern Ocean (Coello-Camba et al., 2017; Smetacek, 2008). Krill supports phytoplankton growth by releasing nutrients via excretion, sloppy feeding, and egestion (Lehette et al., 2012). This effect might be even larger when considering varying Fe:N ratios (Tovar-Sanchez et al., 2007). Mass migration of krill swarms could also mix nutrients and stimulate primary production (Cavan et al., 2019), although our model does not include this particular feature (migration). Thus, the reported effect on NPP may be underestimated.

In our model, macrozooplankton is parameterized based on specific characteristics of Antarctic krill. However, salps could replace krill in case of reported and projected declines in krill biomass (Atkinson et al., 2004, 2019; Huang et al., 2011; Pakhomov & Hunt, 2017). One of the main differences between krill and salps is the feeding strategy. While krill prefers filter-feeding on diatoms and smaller zooplankton (Smetacek et al., 2004), salps are non-selective filter-feeders (Henschke et al., 2016). This difference could substantially affect the modeled and real phytoplankton composition in the Southern Ocean and may have a direct impact on the use of macronutrients (Plum et al., 2020). Besides, microphagous feeding of salps might pack nanophytoplankton to larger particles and thus create food items for zooplankton (Iversen et al., 2017). This could have an impact on the spatial distribution of zooplankton in the (modeled) ecosystem.

Furthermore, a shift from krill to salp dominance could impact the POC export fluxes. Since salps can form ”swarms” (due to budding) and produce fast-sinking pellets, they can partially fill the ecological niche of krill (Cavan et al., 2019). However, it remains unresolved whether POC export would increase if salps partially replace krill, or not. Although POC flux is thought to be high during high salp abundance, fragmentation can reduce their sinking speed and contribution to carbon export considerably (Henschke et al., 2016; Iversen et al., 2017). Thus, additional modeling work is needed to resolve the impacts of a potential shift from krill to salps.

Journal of Geophysical Research: Oceans 10.1029/2021JC017315

Our model takes into account the key characteristics of Antarctic macrozooplankton. While we are confident that the representation of macrozooplankton is solid and captures first-order effects for Southern Ocean biogeochemistry, second-order processes are not taken into account here. For example, a more advanced relationship between the macrozooplankton and sea ice could improve the model results. First, it might improve the seasonal development of macrozooplankton biomass since winter sea ice extent is important for recruitment success and population size (Siegel & Loeb, 1995). Second, implementation of sea-ice algae as an additional food source for the macrozooplankton group (Meyer, 2012; Meyer et al., 2017; Schmidt et al., 2014) could affect the spatial and temporal distribution of macrozooplankton biomass. Also, unrepresented life stages and life-cycle strategies such as molting and resting stages could fundamentally affect nutrient cycles (Everett et al., 2017). In addition, modeling active carbon transport via zooplankton vertical migration is important for carbon export estimates (Archibald et al., 2019). Further steps to represent vertical migration could amplify the role of macrozooplankton in the modeled carbon cycle.

5. Conclusion

In summary, representing macrozooplankton as a plankton functional type and including large rapidly-sinking particles in a biogeochemical model has a strong impact on major carbon pathways in the modeled Southern Ocean. These carbon-rich particles increase carbon transfer to greater depths, especially below the twilight zone. Concurrently, macrozooplankton (krill) play an important role as "gardeners," as the excretion of micro- and macronutrients enhances their recycling in the surface layer. However, the projected decline of macrozooplankton biomass or a shift from a krill- to a salp-dominated ecosystem could weaken the sequestration flux and change the recycling of nutrients. Thus, representing components of the planktonic community and their impacts on carbon cycling is important to improve future projections of carbon cycling.

Data Availability Statement

MAREDAT is available on https://doi.org/10.1594/PANGAEA.777398 and WOA18 products are available on https://www.nodc.noaa.gov/OC5/woa18/woa18data.html. The authors acknowledge open access to the data sets "Global distributions of epipelagic macrozooplankton abundance and biomass—Gridded data product (NetCDF)—Contribution to the MAREDAT World Ocean Atlas of Plankton Functional Types" and World Ocean Atlas 2018 nutrient products. The model results can be downloaded from https://doi.pangaea.de/10.1594/PANGAEA.935006.

Acknowledgments
The authors thank the editor Dr. Nadia Pinardi, reviewer Dr. Mark Hague and one anonymous reviewer for their valuable comments and suggestions. This research was supported under the Initiative and Networking Fund of the Helmholtz Association (Helmholtz Young Investigator Group Marine Carbon and Ecosystem Feedbacks in the Earth System [MarESys], grant number VH-NG-1301). Open access funding enabled and organized by Projekt DEAL.

References

Álvarez, E., Thoms, S., & Völker, C. (2018). Chlorophyll to carbon ratio derived from a global ecosystem model with photodamage. *Global Biogeochemical Cycles*, *32*(5), 799–816. https://doi.org/10.1029/2017gb005850

Anderson, T. R., Hessen, D. O., Mitra, A., Mayor, D. J., & Yool, A. (2013). Sensitivity of secondary production and export flux to choice of trophic transfer formulation in marine ecosystem models. *Journal of Marine Systems*, *125*, 41–53. https://doi.org/10.1016/j.jmarsys.2012.09.008

Archibald, K. M., Siegel, D. A., & Doney, S. C. (2019). Modeling the impact of zooplankton diel vertical migration on the carbon export flux of the biological pump. *Global Biogeochemical Cycles*, *33*(2), 181–199. https://doi.org/10.1029/2018GB005983

Arrigo, K. R., Worthen, D. L., & Robinson, D. H. (2003). A coupled ocean-ecosystem model of the Ross Sea: 2. Iron regulation of phytoplankton taxonomic variability and primary production. *Journal of Geophysical Research*, *108*(C7), 3231. https://doi.org/10.1029/2001JC000856

Arteaga, L., Haëntjens, N., Boss, E., Johnson, K. S., & Sarmiento, J. L. (2018). Assessment of export efficiency equations in the Southern Ocean applied to satellite-based net primary production. *Journal of Geophysical Research: Oceans*, *123*(4), 2945–2964. https://doi.org/10.1002/2018JC013787

Atkinson, A., Hill, S. L., Pakhomov, E. A., Siegel, V., Reiss, C. S., Loeb, V. J., et al. (2019). Krill (*Euphausia superba*) distribution contracts southward during rapid regional warming. *Nature Climate Change*, *9*(2), 142–147. https://doi.org/10.1038/s41558-018-0370-z

Atkinson, A., Meyer, B., Stübing, D., Hagen, W., Schmidt, K., & Bathmann, U. V. (2002). Feeding and energy budgets of Antarctic krill *Euphausia superba* at the onset of winter-II. Juveniles and adults. *Limnology & Oceanography*, *47*(4), 953–966. https://doi.org/10.4319/lo.2002.47.4.0953

Atkinson, A., Schmidt, K., Fielding, S., Kawaguchi, S., & Geissler, P. A. (2012). Variable food absorption by Antarctic krill: Relationships between diet, egestion rate and the composition and sinking rates of their fecal pellets. *Deep-Sea Research Part II Topical Studies in Oceanography*, *59–60*, 147–158. https://doi.org/10.1016/j.dsr2.2011.06.008

Atkinson, A., Shreeve, R. S., Hirst, A. G., Rothery, P., Tarling, G. A., Pond, D. W., et al. (2006). Natural growth rates in Antarctic krill (*Euphausia superba*): II. Predictive models based on food, temperature, body length, sex, and maturity stage. *Limnology & Oceanography*, *51*(2), 973–987. https://doi.org/10.4319/lo.2006.51.2.0973

Journal of Geophysical Research: Oceans 10.1029/2021JC017315

Atkinson, A., Siegel, V., Pakhomov, E., & Rothery, P. (2004). Long-term decline in krill stock and increase in salps within the Southern Ocean. *Nature*, *432*(7013), 100–103. https://doi.org/10.1038/nature02996

Atkinson, A., Siegel, V., Pakhomov, E. A., Jessopp, M. J., & Loeb, V. (2009). A re-appraisal of the total biomass and annual production of Antarctic krill. *Deep-Sea Research Part I Oceanographic Research Papers*, *56*(5), 727–740. https://doi.org/10.1016/j.dsr.2008.12.007

Aumont, O., Ethé, C., Tagliabue, A., Bopp, L., & Gehlen, M. (2015). PISCES-v2: An ocean biogeochemical model for carbon and ecosystem studies. *Geoscientific Model Development*, *8*(8), 2465–2513. https://doi.org/10.5194/gmd-8-2465-2015

Belcher, A., Henson, S. A., Manno, C., Hill, S. L., Atkinson, A., Thorpe, S. E., et al. (2019). Krill faecal pellets drive hidden pulses of particulate organic carbon in the marginal ice zone. *Nature Communications*, *10*(1), 1–8. https://doi.org/10.1038/s41467-019-08847-1

Belcher, A., Tarling, G. A., Manno, C., Atkinson, A., Ward, P., Skaret, G., et al. (2017). The potential role of Antarctic krill faecal pellets in efficient carbon export at the marginal ice zone of the South Orkney Islands in spring. *Polar Biology*, *40*(10), 2001–2013. https://doi.org/10.1007/s00300-017-2118-z

Boyd, P. W., Claustre, H., Levy, M., Siegel, D. A., & Weber, T. (2019). Multi-faceted particle pumps drive carbon sequestration in the ocean. *Nature*, *568*(7752), 327–335. https://doi.org/10.1038/s41586-019-1098-2

Brooks, C. M., Ainley, D. G., Abrams, P. A., Dayton, P. K., Hofman, R. J., Jacquet, J., & Siniff, D. B. (2018). Watch over Antarctic waters. *Nature*, *558*(7709), 177–180. https://doi.org/10.1038/d41586-018-05372-x

Butzin, M., & Pörtner, H. O. (2016). Thermal growth potential of Atlantic cod by the end of the 21st century. *Global Change Biology*, *22*(12), 4162–4168. https://doi.org/10.1111/gcb.13375

Cavan, E. L., Belcher, A., Atkinson, A., Hill, S. L., Kawaguchi, S., McCormack, S., et al. (2019). The importance of Antarctic krill in biogeochemical cycles. *Nature Communications*, *10*(1), 1–13. https://doi.org/10.1038/s41467-019-12668-7

Clarke, A., Quetin, L. B., & Ross, R. M. (1988). Laboratory and field estimates of the rate of faecal pellet production by Antarctic krill, *Euphausia superba*. *Marine Biology*, *98*(4), 557–563. https://doi.org/10.1007/BF00391547

Coello-Camba, A., Llabrés, M., Duarte, C. M., & Agustí, S. (2017). Zooplankton excretion metabolites stimulate Southern Ocean phytoplankton growth. *Polar Biology*, *40*(10), 2035–2045. https://doi.org/10.1007/s00300-017-2123-2

Comiso, J. C., & Nishio, F. (2008). Trends in the sea ice cover using enhanced and compatible AMSR-E, SSM/I, and SMMR data. *Journal of Geophysical Research*, *113*(C2). Retrieved from https://agupubs.onlinelibrary.wiley.com/doi/abs/10.1029/2007JC004257

Dagg, M. J., Urban-Rich, J., & Peterson, J. O. (2003). The potential contribution of fecal pellets from large copepods to the flux of biogenic silica and particulate organic carbon in the Antarctic Polar Front region near 170°W. *Deep-Sea Research Part II Topical Studies in Oceanography*, *50*(3–4), 675–691. https://doi.org/10.1016/S0967-0645(02)00590-8

Downes, S., Farneti, R., Uotila, P., Griffies, S. M., Marsland, S. J., Bailey, D., et al. (2015). An assessment of Southern Ocean water masses and sea ice during 1988–2007 in a suite of interannual CORE-II simulations. *Ocean Modelling*, *94*, 67–94. https://doi.org/10.1016/j.ocemod.2015.07.022

Downes, S., Spence, P., & Hogg, A. (2018). Understanding variability of the Southern Ocean overturning circulation in CORE-II models. *Ocean Modelling*, *123*, 98–109. https://doi.org/10.1016/j.ocemod.2018.01.005

Ebersbach, F., & Trull, T. W. (2008). Sinking particle properties from polyacrylamide gels during the KErguelen Ocean and Plateau compared Study (KEOPS): Zooplankton control of carbon export in an area of persistent natural iron inputs in the Southern Ocean. *Limnology & Oceanography*, *53*(1), 212–224. https://doi.org/10.4319/lo.2008.53.1.0212

Everett, J. D., Baird, M. E., Buchanan, P., Bulman, C., Davies, C., Downie, R., et al. (2017). Modeling what we sample and sampling what we model: Challenges for zooplankton model assessment. *Frontiers in Marine Science*, *4*, 77. Retrieved from https://www.frontiersin.org/article/10.3389/fmars.2017.00077

Fach, B. A., Hofmann, E. E., & Murphy, E. J. (2002). Modeling studies of antarctic krill *Euphausia superba* survival during transport across the Scotia Sea. *Marine Ecology Progress Series*, *231*, 187–203. https://doi.org/10.3354/meps231187

Farneti, R., Downes, S. M., Griffies, S. M., Marsland, S. J., Behrens, E., Bentsen, M., et al. (2015). An assessment of Antarctic Circumpolar Current and Southern Ocean meridional overturning circulation during 1958–2007 in a suite of interannual CORE-II simulations. *Ocean Modelling*, *93*, 84–120. https://doi.org/10.1016/j.ocemod.2015.07.009

Fasham, M. J., Ducklow, H. W., & McKelvie, S. M. (1990). A nitrogen-based model of plankton dynamics in the oceanic mixed layer. *Journal of Marine Research*, *48*(3), 591–639. https://doi.org/10.1357/002224090784984678

Frölicher, T. L., Rodgers, K., Stock, C. A., & Cheung, W. W. (2016). Sources of uncertainties in 21st century projections of potential ocean ecosystem stressors. *Global Biogeochemical Cycles*, *30*, 22–1243. https://doi.org/10.1002/2015GB005338

Garcia, H., Locarnini, R., Boyer, T. P., Antonov, J. I., Baranova, O. K., Zweng, M. M., et al. (2013). World Ocean Atlas 2013 volume 4: Nutrients (phosphate, nitrate, silicate). *NOAA Atlas NESDIS*, *76*, 396.

Garcia, H., Weathers, K., Paver, C., Smolyar, I., Boyer, T., Locarnini, R., et al. (2018). World Ocean Atlas 2018. Volume 4: Dissolved inorganic nutrients (phosphate, nitrate and nitrate+nitrite, silicate). *NOAA Atlas NESDIS*, *84*, 35.

Griffies, S. M., Biastoch, A., Böning, C., Bryan, F., Danabasoglu, G., Chassignet, E. P., et al. (2009). Coordinated ocean-ice reference experiments (cores). *Ocean Modelling*, *26*(1), 1–46. https://doi.org/10.1016/j.ocemod.2008.08.007

Griffies, S. M., Yin, J., Durack, P. J., Goddard, P., Bates, S. C., Behrens, E., et al. (2014). An assessment of global and regional sea level for years 1993–2007 in a suite of interannual CORE-II simulations. *Ocean Modelling*, *78*, 35–89. https://doi.org/10.1016/j.ocemod.2014.03.004

Halfter, S., Cavan, E. L., Swadling, K. M., Eriksen, R. S., & Boyd, P. W. (2020). The role of zooplankton in establishing carbon export regimes in the Southern Ocean—A comparison of two representative case studies in the subantarctic region. *Frontiers in Marine Science*, *7*, 1–8. https://doi.org/10.3389/fmars.2020.567917

Hauck, J., Völker, C., Wang, T., Hoppema, M., Losch, M., & Wolf-Gladrow, D. A. (2013). Seasonally different carbon flux changes in the Southern Ocean in response to the southern annular mode. *Global Biogeochemical Cycles*, *27*(4), 1236–1245. https://doi.org/10.1002/2013GB004600

Henschke, N., Everett, J. D., Richardson, A. J., & Suthers, I. M. (2016). Rethinking the role of salps in the ocean. *Trends in Ecology & Evolution*, *31*(9), 720–733. https://doi.org/10.1016/j.tree.2016.06.007

Hense, I., Timmermann, R., Beckmann, A., & Bathmann, U. V. (2003). Regional ecosystem dynamics in the ACC: Simulations with a three-dimensional ocean-plankton model. *Journal of Marine Systems*, *42*(1–2), 31–51. https://doi.org/10.1016/S0924-7963(03)00063-0

Henson, S. A., Sanders, R., & Madsen, E. (2012). Global patterns in efficiency of particulate organic carbon export and transfer to the deep ocean. *Global Biogeochemical Cycles*, *26*(1), 1. https://doi.org/10.1029/2011GB004099

Hofmann, E. E., & Lascara, C. M. (2000). Modeling the growth dynamics of Antarctic krill *Euphausia superba*. *Marine Ecology Progress Series*, *194*, 219–231. https://doi.org/10.3354/meps194219

Honjo, S. (2004). Particle export and the biological pump in the Southern Ocean. *Antarctic Science*, *16*(4), 501–516. https://doi.org/10.1017/S0954102004002287

Journal of Geophysical Research: Oceans 10.1029/2021JC017315

Huang, T., Sun, L., Stark, J., Wang, Y., Cheng, Z., Yang, Q., & Sun, S. (2011). Relative changes in krill abundance inferred from antarctic fur seal. *PLoS One*, *6*(11), 11–14. https://doi.org/10.1371/journal.pone.0027331

Iversen, M. H., Pakhomov, E. A., Hunt, B. P., van der Jagt, H., Wolf-Gladrow, D., & Klaas, C. (2017). Sinkers or floaters? Contribution from salp pellets to the export flux during a large bloom event in the Southern Ocean. *Deep-Sea Research Part II Topical Studies in Oceanography*, *138*, 116–125. https://doi.org/10.1016/j.dsr2.2016.12.004

Klein, E. S., Hill, S. L., Hinke, J. T., Phillips, T., & Watters, G. M. (2018). Impacts of rising sea temperature on krill increase risks for predators in the Scotia Sea. *PLoS One*, *13*(1), 1–21. https://doi.org/10.1371/journal.pone.0191011

Kobayashi, S., Ota, Y., Harada, Y., Ebita, A., Moriya, M., Onoda, H., et al. (2015). The JRA-55 reanalysis: General specifications and basic characteristics. *Journal of the Meteorological Society of Japan*, *93*(1), 5–48. https://doi.org/10.2151/jmsj.2015-001

Kurtz, N. T., & Markus, T. (2012). Satellite observations of Antarctic sea ice thickness and volume. *Journal of Geophysical Research*, *117*(C8). https://doi.org/10.1029/2012jc008141

Lancelot, C., Hannon, E., Becquevort, S., Veth, C., & De Baar, H. J. (2000). Modeling phytoplankton blooms and carbon export production in the Southern Ocean: Dominant controls by light and iron in the Atlantic sector in Austral spring 1992. *Deep-Sea Research Part I Oceanographic Research Papers*, *47*(9), 1621–1662. https://doi.org/10.1016/S0967-0637(00)00005-4

Laufkötter, C., Vogt, M., Gruber, N., Aumont, O., Bopp, L., Doney, S. C., et al. (2016). Projected decreases in future marine export production: The role of the carbon flux through the upper ocean ecosystem. *Biogeosciences*, *13*(13), 4023–4047. https://doi.org/10.5194/bg-13-4023-2016

Laurenceau-Cornec, E. C., Trull, T. W., Davies, D. M., Bray, S. G., Doran, J., Planchon, F., et al. (2015). The relative importance of phytoplankton aggregates and zooplankton fecal pellets to carbon export: Insights from free-drifting sediment trap deployments in naturally iron-fertilised waters near the Kerguelen Plateau. *Biogeosciences*, *12*(4), 1007–1027. https://doi.org/10.5194/bg-12-1007-2015

Lauvset, S. K., Key, R. M., Olsen, A., Van Heuven, S., Velo, A., Lin, X., et al. (2016). A new global interior ocean mapped climatology: The 1° 11° GLODAP version 2. *Earth System Science Data*, *8*(2), 325–340. https://doi.org/10.5194/essd-8-325-2016

Lehette, P., Tovar-Sánchez, A., Duarte, C. M., & Hernández-León, S. (2012). Krill excretion and its effect on primary production. *Marine Ecology Progress Series*, *459*, 29–38. https://doi.org/10.3354/meps09746

Le Quéré, C., Buitenhuis, E. T., Moriarty, R., Alvain, S., Aumont, O., Bopp, L., et al. (2016). Role of zooplankton dynamics for Southern Ocean phytoplankton biomass and global biogeochemical cycles. *Biogeosciences*, *13*(14), 4111–4133. https://doi.org/10.5194/bg-13-4111-2016

Maiti, K., Charette, M. A., Buesseler, K. O., & Kahru, M. (2013). An inverse relationship between production and export efficiency in the Southern Ocean. *Geophysical Research Letters*, *40*(8), 1557–1561. https://doi.org/10.1002/grl.50219

Meyer, B. (2012). The overwintering of Antarctic krill, *Euphausia superba*, from an ecophysiological perspective. *Polar Biology*, *35*(1), 15–37. https://doi.org/10.1007/s00300-011-1120-0

Meyer, B., Freier, U., Grimm, V., Groeneveld, J., Hunt, B. P., Kerwath, S., et al. (2017). The winter pack-ice zone provides a sheltered but food-poor habitat for larval Antarctic krill. *Nature Ecology and Evolution*, *1*(12), 1853–1861. https://doi.org/10.1038/s41559-017-0368-3

Meyer, B., Fuentes, V., Guerra, C., Schmidt, K., Atkinson, A., Spahic, S., et al. (2009). Physiology, growth, and development of larval krill *Euphausia superba* in autumn and winter in the Lazarev Sea, Antarctica. *Limnology & Oceanography*, *54*(5), 1595–1614. https://doi.org/10.4319/lo.2009.54.5.1595

Moriarty, R., Buitenhuis, E. T., Le Quéré, C., & Gosselin, M.-P. (2013). Distribution of known macrozooplankton abundance and biomass in the global ocean. *Earth System Science Data*, *5*(2), 241–257. https://doi.org/10.5194/essd-5-241-2013

Nicol, S., Constable, A. J., & Pauly, T. (2000). Estimates of circumpolar abundance of Antarctic krill based on recent acoustic density measurements. *CCAMLR Science*, *7*, 87–99.

Pakhomov, E. A., & Hunt, B. P. (2017). Trans-Atlantic variability in ecology of the pelagic tunicate *Salpa thompsoni* near the Antarctic Polar. *Front. Deep-Sea Research Part II: Topical Studies in Oceanography*, *138*(March), 126–140. https://doi.org/10.1016/j.dsr2.2017.03.001

Passow, U., & Carlson, C. (2012). The biological pump in a high CO_2 world. *Marine Ecology Progress Series*, *470*(2), 249–271. https://doi.org/10.3354/meps09985

Plum, C., Hillebrand, H., & Moorthi, S. (2020). Krill vs salps: Dominance shift from krill to salps is associated with higher dissolved N:P ratios. *Scientific Reports*, *10*(1), 5911. https://doi.org/10.1038/s41598-020-62829-8

Rembauville, M., Blain, S., Armand, L., Quéguiner, B., & Salter, I. (2015). Export fluxes in a naturally iron-fertilized area of the Southern Ocean—Part 2: Importance of diatom resting spores and faecal pellets for export. *Biogeosciences*, *12*(11), 3171–3195. https://doi.org/10.5194/bg-12-3171-2015

Schlitzer, R. (2002). Carbon export fluxes in the Southern Ocean: Results from inverse modeling and comparison with satellite-based estimates. *Deep-Sea Research Part II Topical Studies in Oceanography*, *49*(9–10), 1623–1644. https://doi.org/10.1016/S0967-0645(02)00004-8

Schmidt, K., Atkinson, A., Pond, D. W., & Irel, L. C. (2014). Feeding and overwintering of Antarctic krill across its major habitats: The role of sea ice cover, water depth, and phytoplankton abundance. *Limnology & Oceanography*, *59*(1), 17–36. https://doi.org/10.4319/lo.2014.59.1.0017

Schourup-Kristensen, V., Sidorenko, D., Wolf-Gladrow, D. A., & Völker, C. (2014). A skill assessment of the biogeochemical model REcoM2 coupled to the Finite Element Sea Ice–Ocean Model (FESOM 1.3). *Geoscientific Model Development*, *7*(6), 2769–2802. https://doi.org/10.5194/gmd-7-2769-2014

Séférian, R., Berthet, S., Yool, A., Palmiéri, J., Bopp, L., Tagliabue, A., et al. (2020). Tracking Improvement in Simulated Marine Biogeochemistry Between CMIP5 and CMIP6. *Current Climate Change Reports*, *6*(3), 95–119. https://doi.org/10.1007/s40641-020-00160-0

Sidorenko, D., Wang, Q., Danilov, S., & Schröter, J. (2011). FESOM under coordinated ocean-ice reference experiment forcing. *Ocean Dynamics*, *61*(7), 881–890. https://doi.org/10.1007/s10236-011-0406-7

Siegel, V., Kawaguchi, S., Ward, P., Litvinov, F., Sushin, V., Loeb, V., & Watkins, J. (2004). Krill demography and large-scale distribution in the southwest Atlantic during January/February 2000. Deep-Sea Research Part II. *Topical Studies in Oceanography*, *51*(12–13 SPEC.ISS), 1253–1273. https://doi.org/10.1016/s0967-0645(04)00078-5

Siegel, V., & Loeb, V. (1995). Recruitment of Antarctic krill *Euphausia superba* and possible causes for its variability. *Marine Ecology Progress Series*, *123*(1–3), 45–56. https://doi.org/10.3354/meps123045

Siegel, V., & Watkins, J. L. (2016). Distribution, Biomass and Demography of Antarctic Krill *Euphausia superba*. In V. Siegel (Ed.). *Biology and ecology of the Antarctic krill*. Springer. https://doi.org/10.1007/978-3-319-29279-3

Smetacek, V. (2008). Are declining Antarctic krill stocks a result of global warming or of the decimation of whales? In *Impacts of global warming on polar ecosystems* (pp. 45–83). Fundacion BBVA. Retrieved from https://www.fbbva.es/wp-content/uploads/2017/05/dat/02SMETACEK-SEPARATA.pdf

Smetacek, V., Assmy, P., & Henjes, J. (2004). The role of grazing in structuring Southern Ocean pelagic ecosystems and biogeochemical cycles. *Antarctic Science*, *16*(4), 541–558. https://doi.org/10.1017/S0954102004002317

Journal of Geophysical Research: Oceans 10.1029/2021JC017315

Steinberg, D. K., & Landry, M. R. (2017). Zooplankton and the ocean carbon cycle. *Annual Review of Marine Science*, *9*(1), 413–444. https://doi.org/10.1146/annurev-marine-010814-015924

Stock, C. A., Dunne, J. P., Fan, S., Ginoux, P., John, J., Krasting, J. P., et al. (2020). Ocean biogeochemistry in GFDL's Earth System Model 4.1 and its response to increasing atmospheric CO_2. *Journal of Advances in Modeling Earth Systems*, *12*(10). https://doi.org/10.1029/2019MS002043

Stock, C. A., Dunne, J. P., & John, J. G. (2014). Global-scale carbon and energy flows through the marine planktonic food web: An analysis with a coupled physical–biological model. *Progress in Oceanography*, *120*, 1–28. https://doi.org/10.1016/j.pocean.2013.07.001

Teschke, M., Kawaguchi, S., & Meyer, B. (2007). Simulated light regimes affect feeding and metabolism of Antarctic krill, *Euphausia superba*. *Limnology & Oceanography*, *52*(3), 1046–1054. Retrieved from https://aslopubs.onlinelibrary.wiley.com/doi/abs/10.4319/lo.2007.52.3.1046

Tovar-Sanchez, A., Duarte, C. M., Hernández-León, S., & Sañudo-Wilhelmy, S. A. (2007). Krill as a central node for iron cycling in the Southern Ocean. *Geophysical Research Letters*, *34*(11), 1–4. https://doi.org/10.1029/2006GL029096

Turner, J. T. (2002). Zooplankton fecal pellets, marine snow and sinking phytoplankton blooms. *Aquatic Microbial Ecology*, *27*, 57–102. https://doi.org/10.3354/Ame027057

Turner, J. T. (2015). Zooplankton fecal pellets, marine snow, phytodetritus and the ocean's biological pump. *Progress in Oceanography*, *130*, 205–248. https://doi.org/10.1016/j.pocean.2014.08.005

Volk, T., & Hoffert, M. I. (1985). Ocean carbon pumps: Analysis of relative strengths and efficiencies in ocean-driven atmospheric CO_2 changes. In *The carbon cycle and atmospheric CO_2: Natural variations Archean to present* (pp. 99–110). American Geophysical Union (AGU). https://doi.org/10.1029/GM032p0099

Waite, A. M., Thompson, P. A., & Harrison, P. J. (1992). Does energy control the sinking rates of marine diatoms? *Limnology & Oceanography*, *37*(3), 468–477. https://doi.org/10.4319/lo.1992.37.3.0468

Wang, Q., Danilov, S., Sidorenko, D., Timmermann, R., Wekerle, C., Wang, X., et al. (2014). The finite element sea ice-ocean model (FESOM) v.1.4: Formulation of an ocean general circulation model. *Geoscientific Model Development*, *7*(2), 663–693. https://doi.org/10.5194/gmd-7-663-2014

JOURNAL OF GEOPHYSICAL RESEARCH

Modeling the Impact of Macrozooplankton on Carbon Export Production in the Southern Ocean

Onur Karakuş[1], Christoph Völker[1], Morten Iversen[1], Wilhelm Hagen[2,3],

Dieter Wolf Gladrow[1], Bettina Fach[4], Judith Hauck[1]

[1]Alfred-Wegener-Insititut Helmholtz-Zentrum für Polar- und Meeresforschung, Am Handelshafen 12, 27570 Bremerhaven, Germany

[2]University of Bremen, BreMarE, Marine Zoology, P.O. Box 330440, 28334 Bremen, Germany

[3]University of Bremen, MARUM Center of Environmental Sciences, P.O. Box 330440, 28334 Bremen, Germany

[4]Middle East Technical University, Institute of Marine Sciences, P.O.Box 28, 33731, Erdemli-Mersin, Turkey

Contents of this file

1. Fig. S1: Phytoplankton chlorophyll and total zooplankton biomass in zonal mean-depth space.

2. Fig. S2: Biases in nutrient concentrations and effect of macrozooplankton on nutrients in zonal mean-depth space.

3. Fig. S3: Detritus C:N ratios for the CTRL and MACROZOO_ALL simulations.

4. Fig. S4: Annual mean chlorophyll concentrations.

5. Fig. S5: Sea ice cover and thickness in the Southern Ocean in MACROZOO_ALL simulation

6. Fig. S6: Contribution of diatoms to NPP in the Southern Ocean.

7. Table S1: Macrozooplankton biomass (mg C m^{-3}) in the MAREDAT data and in the model south of 50°S in different depth ranges.

Introduction The supplementary material contains six figures and one table: 1) Phytoplankton chlorophyll and total zooplankton biomass in zonal mean-depth space, 2) Biases in nutrient concentrations and effect of macrozooplankton on nutrients in zonal mean-depth space, 3) Detritus C:N ratios for the CTRL and MACROZOO_ALL simulations, 4) Surface chlorophyll concentration in wo simulations, 5) Sea ice conditions in the Southern Ocean in the model, 6)Contribution of diatom to the NPP, and 4) Macrozooplankton biomass in the MAREDAT data and in the model south of 50°S in different depth ranges.

Text for the Figures S1, S2 and S3

Figure S1 shows the changes in phytoplankton chlorophyll and zooplankton biomass in latitude-depth space due to the implementation of macrozooplankton (MACROZOO_ALL - CTRL). The mean zonal concentration of total zooplankton increases by 0.2 to 0.5 mmol C m^{-3} especially between the latitudes 50°S and 62°S (Fig S1h) and 0 to 60 m depth. The new grazing pressure by macrozooplankton decreases the diatom chlorophyll concentrations by up to 0.2 mg chl m^{-3} compared to the control run with the largest effects between 56 and 68°S and 30 to 90 m depth (Fig. S1f). In contrast, nanophytoplankton chlorophyll concentrations increase slightly by up to 0.05 mg chl m^{-3} in comparison to the control run (Fig. S1e) with the largest effects between 50 and 60°S and 0 to 30 m depth.

Figure S2 shows the analysis on the macronutrients nitrate and silicic acid in latitude-depth space.

The new macrozooplankton and the fast sinking detritus class affect carbon to nitrogen ratios of total detritus (Fig. S3). In the MACROZOO_ALL simulation, the carbon to nitrogen ratio of the detritus group slightly increases in the upper 160 m. The median

values of C:N ratio stays almost similar in CTRL and MACROZOO_ALL and it varies between 5.3 to 5.4 in MACROZOO_ALL (Fig. S3a). The slight increase in MACROZOO_ALL is a result of the higher carbon to nitrogen ratio of the larger detritus class, which varies between 6.0 (minimum) and 6.7 (maximum) in different depth levels, while the small detritus group's C:N ratio is between 5.3 to 5.4 (Fig. S3b).

Figure S4 shows annual mean of surface surface chlorophyll concentrations for the satellite product OC-CCI (Sathyendranath et al., 2018) and model simulations.

Figure S5 shows seasonal sea ice properties in the Southern Ocean. In our model, the minimum sea-ice extent is 3.1 km^{-2} in March and the sea ice thickness is 0.83 m in the Southern Ocean. The maximum sea-ice extent is 18.6 km^{-2}. In September, average ice thickness reaches 0.93 m.

Figure S6 shows the contribution of diatom to the total NPP. In the original model version, diatom contribution was similar to Alvain, Moulin, Dandonneau, and Loisel (2008). In this version, it is in the higher edge and close to estimases by Hirata et al. (2011). However, strong silicic acid bias suggests that diatom is too high close to continent.

Text for the Table S1

In Table S1, we show the statistical distribution of macrozooplankton biomass in MAREDAT and model.

References

Alvain, S., Moulin, C., Dandonneau, Y., & Loisel, H. (2008). Seasonal distribution and succession of dominant phytoplankton groups in the global ocean: A satellite view. *Global Biogeochemical Cycles*, *22*(3). Retrieved from https://agupubs.onlinelibrary.wiley.com/doi/abs/10.1029/2007GB003154 doi: https://doi.org/10.1029/2007GB003154

Garcia, Weathers, K., Paver, C., Smolyar, I., Boyer, T., Locarnini, R., ... Reagan, J. (2018). World Ocean Atlas 2018. Volume 4: Dissolved Inorganic Nutrients (phosphate, nitrate and nitrate+nitrite, silicate). *NOAA Atlas NESDIS 84*, *84*(July), 35.

Hirata, T., Hardman-Mountford, N. J., Brewin, R. J. W., Aiken, J., Barlow, R., Suzuki, K., ... Yamanaka, Y. (2011). Synoptic relationships between surface Chlorophyll-a and diagnostic pigments specific to phytoplankton functional types. *Biogeosciences*, *8*(2), 311–327. Retrieved from `https://bg.copernicus.org/articles/8/311/2011/` doi: 10.5194/bg-8-311-2011

Sathyendranath, S., M., G., R.J.W., B., Brockmann, C., Brotas, V., Chuprin, A., ... Zibordi, G. (2018). Esa ocean colour climate change initiative (ocean colour cci): Version 3.1. *Data Centre for Environmental Data Analysis*. doi: 10.5285/9c334fbe6d424a708cf3c4cf0c6a53f5

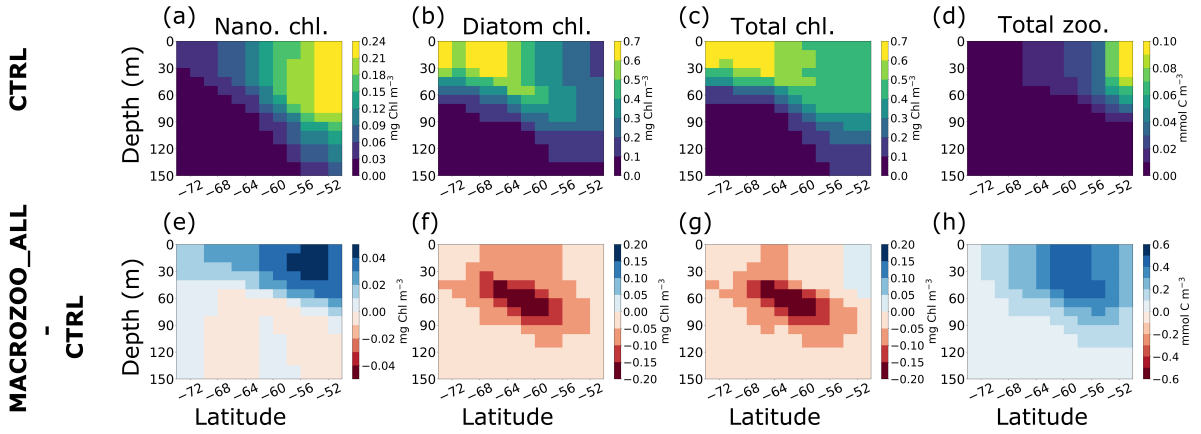

Figure S1. Phytoplankton chlorophyll and total zooplankton biomass in zonal mean-depth space. The first row shows the annual mean concentrations in the CTRL simulation and the second row depicts the difference between MACROZOO_ALL and CTRL. (a, e) Nanophytoplankton chlorophyll (mg chl m^{-3}), (b, f) diatom chlorophyll (mg chl m^{-3}), (c, g) total chlorophyll (mg chl m^{-3}), (d, h) total zooplankton carbon biomass (mmol C m^{-3}).

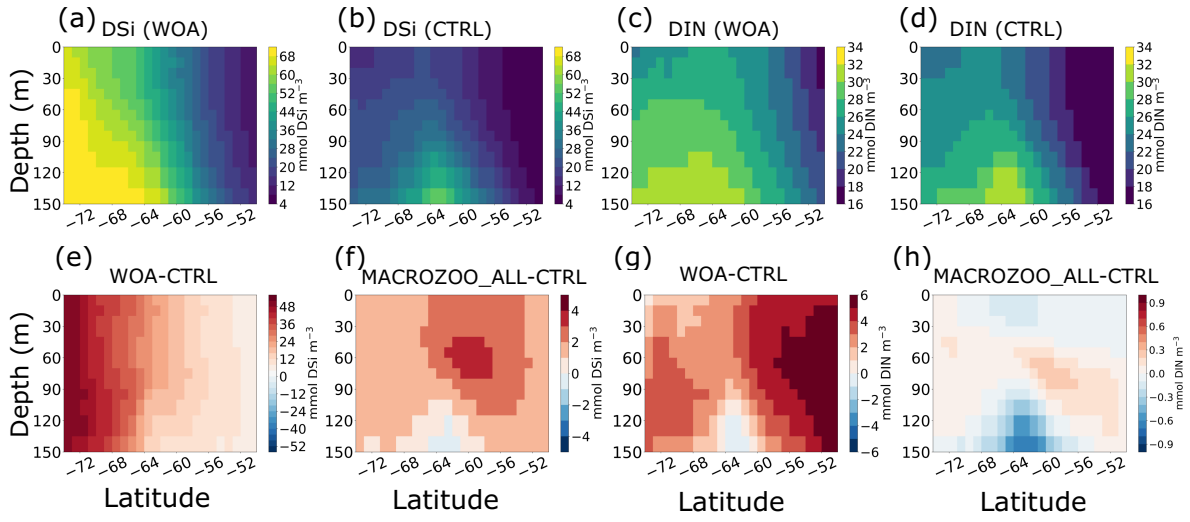

Figure S2. Biases in nutrient concentrations and effect of macrozooplankton on nutrients in zonal mean-depth space. Shown are the annual means of silicic acid (DSI) and nitrate (DIN) (mmol m^{-3}), from (a, c) World Ocean Atlas 2018 (Garcia et al., 2018), (b, d) the CTRL simulation, and the differences between (e, g) WOA18 and CTRL, and (f, h) MACROZOO_ALL and CTRL.

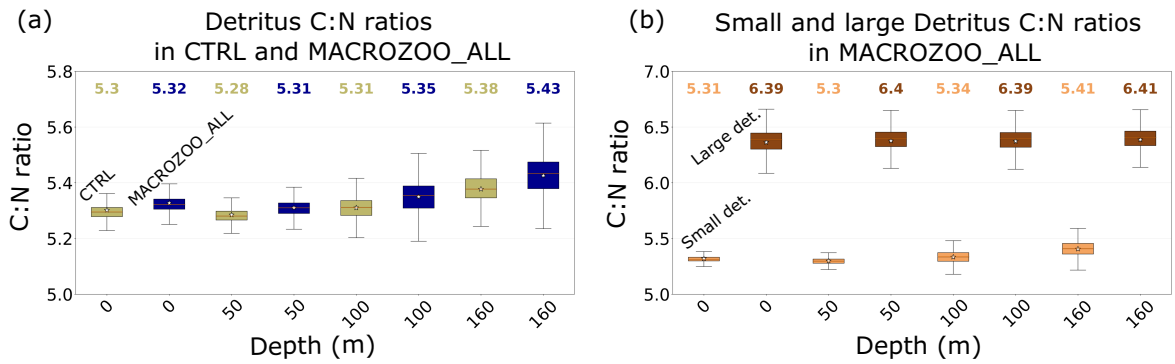

Figure S3. Detritus C:N ratios for (a) total detritus in the CTRL and MACROZOO _ALL simulations, and (b) for small detritus (light brown) and large detritus (dark brown) in MACROZOO_ALL.

Table S1. Macrozooplankton biomass (mg C m^{-3}) in the MAREDAT data and in the model south of 50°S in different depth ranges. Last column is the integrated value (Tg C) for the model and MAREDAT.

	Min	**Max**	**Mean**	**Median**	**Integrated biomass**
MAREDAT south of 50°S	0	582.30	5.25	0.08	3.07
Depth range 0-50 m	0	582.30	7.84	0.15	1.05
Depth range 50-150 m	0	531.30	5.55	0.19	1.50
Depth range 150-350 m	0	78.80	1.50	0	0.25
Depth range >350 m	0	120.40	1.08	0	0.27
Model south of 50°S	<0.01	23.50	2.55	0.49	2.81
Depth range 0-50 m	<0.01	23.50	6.40	5.45	2.16
Depth range 50-150 m	<0.01	15.30	1.14	0.37	0.63
Depth range 150-350 m	<0.01	0.70	0.03	<0.01	<0.01
Depth range >350 m	<0.01	0.06	< 0.01	<0.01	<0.01

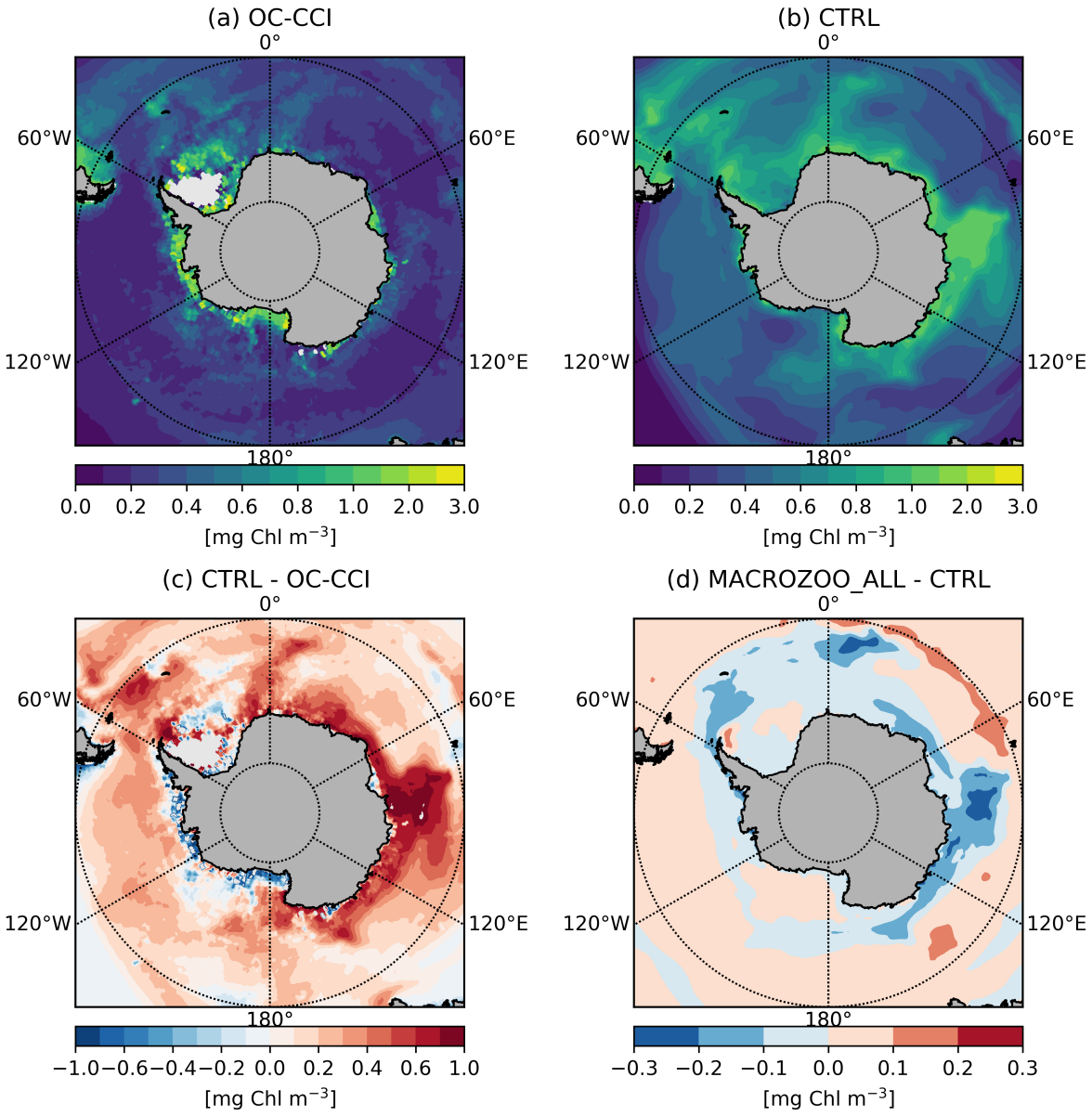

Figure S4. Annual mean of surface surface chlorophyll concentrations for (a) satellite product OC-CCI, (b) CTRL, (c) CTRL minus satellite product and (d) MACROZOO_ALL minus CTRL

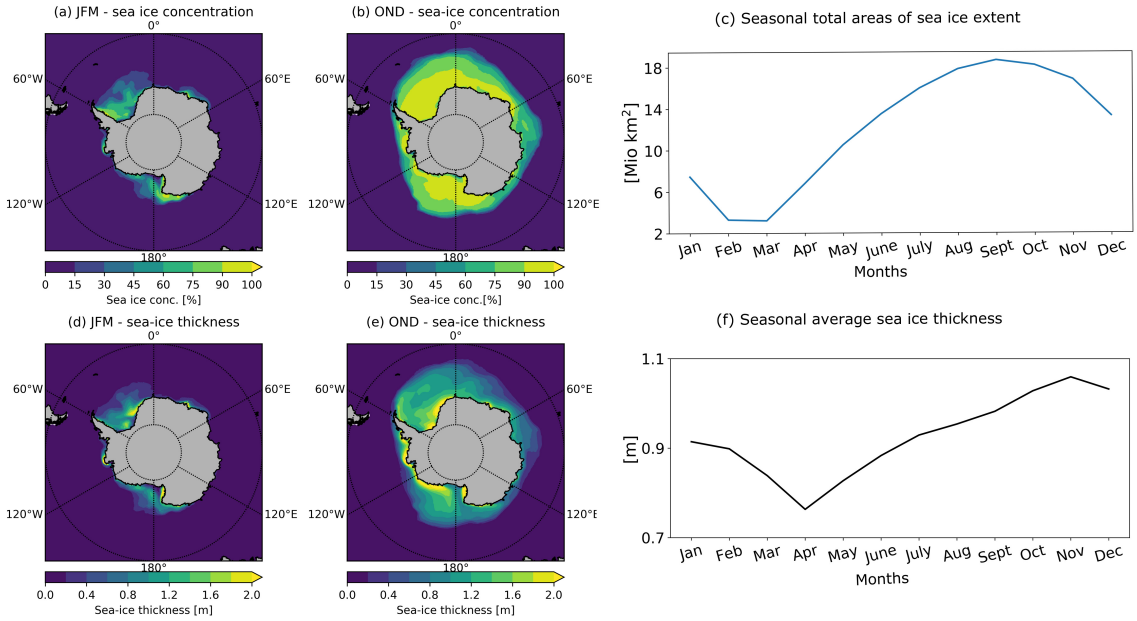

Figure S5. Sea ice concentration and thickness in the Southern Ocean: (a,b) Mean sea-ice concentration in January, February, March (JFM) and October, November, December (OND), (c) seasonal total area of sea ice extent. The total sea ice area is calculated as the area with a sea ice concentration higher than 15%. (d,e) Mean sea ice thickness in January, February, March (JFM) and October, November, December (OND) (f) Seasonal average sea ice thickness. It is calculated when sea-ice concentration is higher than 15%.

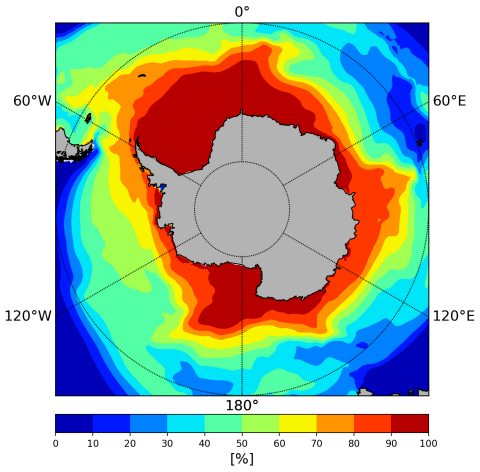

Figure S6. Contribution of diatoms to NPP in the model.

3

PUBLICATION II

THE ROLE OF ZOOPLANKTON GRAZING AND NUTRIENT RECYCLING FOR GLOBAL OCEAN BIOGEOCHEMISTRY AND PHYTOPLANKTON PHENOLOGY

in review at JGR:Biogeosciences

THE ROLE OF ZOOPLANKTON GRAZING AND NUTRIENT RECYCLING FOR GLOBAL OCEAN BIOGEOCHEMISTRY AND PHYTOPLANKTON PHENOLOGY

Onur Karakuş[1], Christoph Völker[1], Morten Iversen[1,2], Wilhelm Hagen[2,3], Judith Hauck[1]

[1] Alfred-Wegener-Institut, Helmholtz-Zentrum für Polar- und Meeresforschung, Am Handelshafen 12, 27570 Bremerhaven, Germany

[2] MARUM and University of Bremen, Leobener Strasse 8, 28359 Bremen, Germany

[3] Universität Bremen, FB2, Leobener Strasse, 28359 Bremen, Germany

ABSTRACT

Zooplankton plays a notable role in ocean biogeochemical cycles. However, it is often simulated as one generic group and top closure term in ocean biogeochemical models. This study presents the description of three zooplankton functional types (zPFTs, micro-, meso- and macrozooplankton) in the ocean biogeochemical model FESOM-REcoM. In the presented model, microzooplankton is a fast-growing herbivore group, mesozooplankton is another major consumer of phytoplankton, and macrozooplankton is a slow-growing group with a low temperature optimum. Meso- and macrozooplankton produce fast-sinking fecal pellets. With three zPFTs, the annual mean zooplankton biomass increases threefold to 210 Tg C. The new food web structure leads to a 25% increase in net primary production and a 10% decrease in export production globally. Consequently, the export ratio decreases from 17% to 12% in the model. The description of three zPFTs reduces model mismatches with observed dissolved inorganic nitrogen and chlorophyll concentrations in the South Pacific and the Arctic Ocean, respectively. Representation of three zPFTs also strongly affects phytoplankton phenology: Fast nutrient recycling by zooplankton sustains higher chlorophyll concentrations in summer and autumn. Additional zooplankton grazing delays the start of the phytoplankton bloom by three weeks and controls the magnitude of the bloom peak in the Southern Ocean. As a result, the system switches from a light-controlled Sverdrup system to a dilution-controlled Behrenfeld system. Overall, the results suggest that representation of multiple zPFTs is important to capture underlying processes that may shape the response of ecosystems and ecosystem services to on-going and future environmental change in model projections.

INTRODUCTION

Marine zooplankton forms an important component of the ocean ecosystem. It serves as a link between primary producers and higher trophic levels (*Steinberg and Landry*, 2017). Although zooplankton consists of a large variety of taxa from unicellular flagellates to multicellular organisms like copepods, it can be classified into five different size classes; nano (2-20 μm, e.g., flagellates), micro (20-200 μm, e.g., ciliates), meso (0.2-20 mm, e.g., copepods), macro (2-20 cm, e.g., krill) and mega (0.2-2 m, e.g., jellyfish; *Sieburth et al.*, 1978). These different size classes of zooplankton have distinct functions in the ecosystem. For example, microzooplankton consume almost 60% of the daily primary production as major grazers of phytoplankton (*Landry and Calbet*, 2004; *Calbet*, 2008), while mesozooplankton and macrozooplankton produce fast sinking particulate matter as fecal pellets, which can contribute the highest share to carbon flux (*Turner*, 2002, 2015). These groups also prefer different prey. While meso- and macrozooplankton prefer larger prey items such as diatoms and smaller zooplankton, microzooplankton prefer smaller organisms such as smaller phytoplankton (*Hansen et al.*, 1994; *Calbet and Landry*, 1999;

Schmidt et al., 2014). Additionally, meso- and macrozooplankton release nutrients via sloppy feeding and excretion (*Saba et al.*, 2009; *Cavan et al.*, 2019). Zooplankton can therefore stimulate phytoplankton growth (*Coello-Camba et al.*, 2017b) and meso- and microzooplankton nutrient regeneration can support 11-25% of primary and bacterial production (*Hernández-León et al.*, 2008; *Verity*, 1985).

The first ocean ecosystem models represented zooplankton with just one model state variable (*Frost*, 1987) and this is still common in the majority of ocean biogeochemical models used for projections of the global carbon cycle and marine primary productivity (*Séférian et al.*, 2020). A minority of models uses multiple zooplankton functional types, such as COBALTv2 (small, medium and large zooplankton; *Stock et al.*, 2020), PLANKTOM-11 (proto-, meso-, macrozooplankton and jellyfish; *Wright et al.*, 2020), PISCESv2 (micro- and mesozooplankton; *Aumont et al.*, 2015), MEDUSA (micro- and mesozooplankton; *Yool et al.*, 2013). Yet the effect of representing multiple zooplankton functional types in biogeochemical models has hardly been studied and documented, and the question remains whether this additional complexity adds sufficient improvement to a model state to justify its computational cost and the added uncertainty due to more parameters (*Anderson*, 2005). Pioneering studies, such as (*Le Quéré et al.*, 2016) showed the pivotal role of a slow-growing macrozooplankton functional type to obtain a realistic north-south chlorophyll ratio in a biogeochemical model. Also, the implementation of micro- and mesozooplankton functional types improved the formation of sinking particles, grazing and nutrient recycling by zooplankton in the same model (*Buitenhuis et al.*, 2006, 2010). Recently, (*Wright et al.*, 2020) showed that predation pressure of jellyfish changed the macrozooplankton biomass and distribution due to competition in a three-dimensional ocean biogeochemical model.

While model development on representing zooplankton types and processes is underway, the level of complexity covered by different models spans a wide range. The number of zooplankton functional types and their traits (parameters, processes) still represent major differences among models and cause for uncertainty in model results (*Laufkötter et al.*, 2016). For example, differences in zooplankton feeding preferences, mortality, and ingestion rates can result in three times higher or lower zooplankton and phytoplankton biomass in modeled plankton food webs (*Mitra et al.*, 2014). Also, prey-ratio based predation schemes such as a type III or active switching formulations improve the phytoplankton succession and increase phytoplankton diversity in a global model (*Prowe et al.*, 2012). Similarly, the choice of different grazing formulations (Michelis-Menten, Blackman, or Ivlev) can cause three times higher surface diatom concentrations in a global biogeochemical model (*Anderson et al.*, 2013). Furthermore, diel vertical migration (grazing refuge) to escape predation for zooplankton can impact the model results. Diel vertical migration is generally not included, since biogeochemical models are limited in the complexity of represented processes, but first parameterizations were recently suggested. For example, *Archibald et al.* (2019) showed that parametrizing zooplankton diel vertical migration increases the modeled global export flux by 14% in the global ocean. Also, *Chenillat et al.* (2021) indicated that different grazing refuge formulations cause large changes in plankton diversity, structure, and ecosystem functioning in a regional modeling study.

One under-exploited aspect to assess the model performance with respect to zooplankton processes is the phytoplankton bloom phenology. To first order, models can reproduce major bloom properties and their timing (phenology) since growth rates of phytoplankton depend on abiotic factors (*Sverdrup*, 1953; *Behrenfeld and Boss*, 2018). However, top-down mechanisms can also control phytoplankton bloom initiation due to ecosystem imbalances (*Behrenfeld et al.*, 2013) and bloom termination due to overgrazing (*Banse*, 1992, 2002). Hence, phytoplankton phenology is directly connected with predator-prey relationships and the parametrization of several grazers in the system. Timing of grazing losses and predator-prey decoupling is vital

to capture the phytoplankton bloom timing (*Kiorboe*, 1997; *Banse*, 2013; *Behrenfeld et al.*, 2013). Pioneering studies by *Frost* (1991, 1993) and *Banse* (1994) showed that grazers often control phytoplankton stock and production in the open ocean. Recently, *Hashioka et al.* (2013) and *Nissen and Vogt* (2021) have discussed the early phytoplankton bloom peak compared to the satellite products in biogeochemical models, which could be caused by too weak zooplankton grazing in the Southern Ocean. Therefore, a better understanding of ecosystem functioning and phenology structures requires complex and well-defined grazing processes in the models. Phytoplankton phenology contains more information than only the mean state and can be used to evaluate how well a model represents the response of phytoplankton growth and loss (e.g. grazing, respiration) rates to processes such as deepening and shoaling of the mixed layer depth (MLD), changes in light availability, and nutrient variations over the year.

Here, we present a new version of REcoM-2 with three zooplankton functional types (herbivorous microzooplankton, omnivorous mesozooplankton, and omnivorous macrozooplankton) and compare this to a previous version with one herbivorous zooplankton group. To analyze the impact of zooplankton functional types, we discuss the changes in the mean states (phytoplankton and zooplankton biomass, productivity, nutrient fields), and attribute these differences to nutrient excretion and grazing by zooplankton. We then exemplarily analyze the effect of zooplankton representation on the phytoplankton bloom phenology in the Southern Ocean within a global ocean biogeochemical model.

MATERIALS AND METHODS

Ocean Biogeochemical Model

We use a three-dimensional ocean biogeochemical model, namely the Regulated Ecosystem Model (REcoM-2; *Hauck et al.*, 2013; *Schourup-Kristensen et al.*, 2014) coupled to the Finite Element Sea-Ice Ocean Model FESOM-1.4 (*Wang et al.*, 2014). Originally, REcoM-2 has two phytoplankton classes (small phytoplankton and diatoms) and one zooplankton group. It represents the carbonate system and resolves the cycling of the nutrients nitrate, silicic acid and iron. Phytoplankton stoichiometry varies with environmental conditions (variable N:C:Chl:Si for diatoms and N:C:Chl for small phytoplankton, *Geider et al.*, 1998) and the sinking of particles is simulated explicitly. For representing the global ocean, we use the CORE-II mesh, roughly comparable to a global 1x1° resolution. It has a higher resolution (20 km - 70 km) in dynamical areas and coarser resolution in less dynamic (100 km -120 km), e.g., subtropical areas (*Sidorenko et al.*, 2011).

Zooplankton and Sinking Particles in the Model

In addition to the original version of REcoM-2 (with one zooplankton group), we already implemented a polar macrozooplankton group (parametrized as Antarctic Krill) and a fast-sinking detritus class (*Karakuş et al.*, 2021). In this study, we go one step further and separate the herbivore group into the microzooplankton and mesozooplankton groups. The complete set of zooplankton equations and parameter values are provided in the supplementary text. Here, we describe the main differences of zooplankton groups, grazing structure, and sinking particles in the two model versions.

In our zooplankton functional types set-up, microzooplankton ($<$200 μm) is parameterized as a fast-growing herbivore group which is closely coupled to the growth of phytoplankton groups. They are the main grazers of phytoplankton in tropical and subtropical regions (60% of

daily primary production) and their grazing usually exceeds that of mesozooplankton (*Landry and Calbet*, 2004; *Calbet*, 2008). This is represented in a high grazing rate of 0.42 (d^{-1}) at 0°C with a Q_{10} value of 1.48 taken from a data compilation by *Le Quéré et al.* (2016). The assimilation efficiency is set to 0.8 which is higher than for mesozooplankton and macrozooplankton (*Le Quéré et al.*, 2016). The unassimilated part represents mini pellet production (*Gowing and Silver*, 1985) and all the sinking particles from this group go to the slow-sinking detritus class (Table 3.1). Microzooplankton has a feeding preference on small phytoplankton rather than on diatoms (Fig. 3.1, Z1, *Froneman and Perissinotto*, 1996; *Le Quéré et al.*, 2005). The respiration rate of microzooplankton is temperature-dependent using the Q_{10} value of 2.36 and a rate of 0.01 d^{-1} at 0°C is taken from *Le Quéré et al.* (2016). The production of dissolved organic material (DOM) by nitrogen and carbon excretion is assigned daily rate constants of 0.05 d^{-1} which is the same as for phytoplankton C and N excretion rates. The microzooplankton group is parametrized as prey for the mesozooplankton and macrozooplankton groups (*Calbet*, 2008).

The mesozooplankton group is another major consumer of phytoplankton (10% of daily primary production) in the global ocean (*Calbet*, 2008). Also, it produces large fast-sinking fecal pellets (*Turner*, 2002). We take these two main roles into account for the parametrization of this functional group. Mesozooplankton grazing rate is slower than that of microzooplankton and it is set to 0.31 d^{-1} at 0°C with a Q_{10} value of 1.27 (*Le Quéré et al.*, 2016). Mesozooplankton produces large sinking particles (fecal pellets) and prefers feeding on large phytoplankton (diatoms in REcoM) and microzooplankton rather than on small phytoplankton (*Mullin*, 1963; *Calbet and Landry*, 1999; *Le Quéré et al.*, 2005). It also grazes on both simulated detritus groups. Different from microzooplankton, a part of the grazed material is lost and routed to detritus ('sloppy feeding'). Sloppy feeding is set to 20% of the grazing flux (*Steinberg and Landry*, 2017) initially and it increases with increasing food concentration as described in *Roy et al.* (1989); *Montagnes and Fenton* (2012). The assimilation efficiency of ingested carbon and nitrogen is set to 68% and 75% for nitrogen and carbon respectively to mimic the higher C:N ratio in fecal pellets (*Morales*, 1987). All the sinking particles from mesozooplankton go to the fast-sinking detritus class (Table 3.1). The respiration rate of mesozooplankton is temperature-dependent using a Q_{10} value of 2.34 and a rate 0.028 d^{-1} at 0°C is taken from *Le Quéré et al.* (2016). The DOC and DON excretion rate constants are set higher than for microzooplankton with 0.1 d^{-1}, in line with an estimate based on (*Hernández-León et al.*, 2008) of 12% between 50°N and 50°S.

The macrozooplankton group is parametrized as krill (*Karakuş et al.*, 2021) and mainly represents the polar macrozooplankton in the model with a maximum grazing rate at a temperature optimum of 0.5°C. Sloppy feeding was set to 20% for macrozooplankton and this group produces large fecal pellets with a high C:N ratio. The sinking particles from the macrozooplankton group were assigned to the fast-sinking detritus class (Table 1). Macrozooplankton grazes on phytoplankton, zooplankton, and both detritus groups and has a lower grazing preference for small phytoplankton than for diatoms and other zooplankton groups. DOC and DON excretion rate constants were set to 0.02 d^{-1} (*Atkinson et al.*, 2002). Differently from the other zooplankton groups, the respiration rate of the macrozooplankton group is down-regulated during winter and at low food availability (*Hofmann and Lascara*, 2000).

Simulations

We conduct two simulations to analyze the impact of the representation of zooplankton in the model. One simulation is carried out with REcoM-2 (with one zooplankton group) and the other simulation with REcoM-3ZOO (with three zooplankton functional types). The global model is forced with the JRA-55-do atmospheric forcing data set version 1.3.1 (*Kobayashi et al.*, 2015) in sixty years long simulations. Repeated year forcing fields from the year 1961

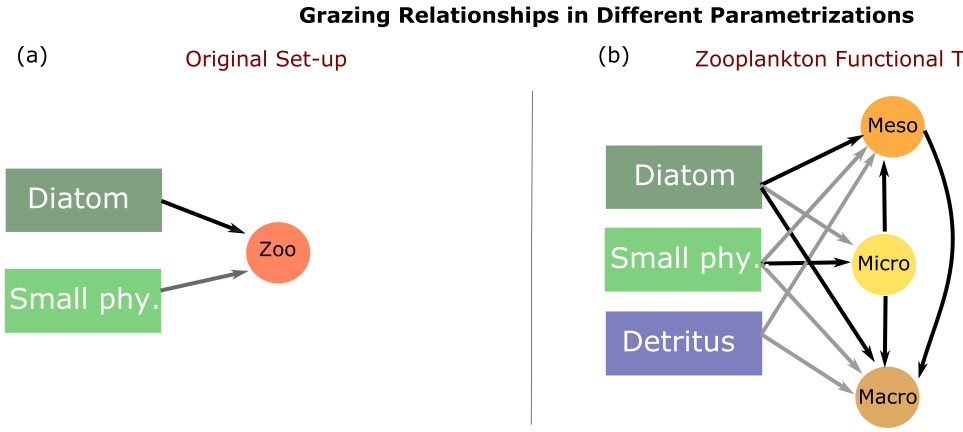

FIGURE 3.1: Grazing relations in the two model versions: (a) Original REcoM-2, (b) Zooplankton functional types set-up. The colors of the arrows indicate the initial relative preferences (parameter values can be found in the supplementary text), black shows the preferred food source for the zooplankton functional type. Multiple black lines indicate an equal grazing preference. **Micro**: microzooplankton feeds on diatoms, and small phytoplankton. **Meso**: mesozooplankton feeds on diatom, small phytoplankton, detritus and microzooplankton. **Macro**: macrozooplankton feeds on diatoms, small phytoplankton, detritus, microzooplankton, and mesozooplankton.

	Grazing on					**Particle Formation**	
zPFTs	Diatom	Small phy.	Particles	Microzoo.	Mesozoo.	Slow-sinking sPOC	Fast-sinking sPOC
Microzoo.	X	X	–	–	–	X	–
Mesozoo.	X	X	X	X	–	–	X
Macrozoo.	X	X	X	X	X	–	X

TABLE 3.1: Specifics of zooplankton functional types (zPFTs): Grazing on various food sources and routing of sinking particles into slow and fast sinking detritus classes in the model.

of surface rainfall, and snowfall fluxes, as well as near-surface (2 m) air temperature, specific humidity, surface downwelling short- and long-wave radiation, eastward and northward wind components, and sea level pressure for the years 1958-2017, are used. Freshwater runoff and the surface salinity field for a weak surface salinity restoring (*Sidorenko et al.*, 2011) are taken from the CORE-II climatology (*Griffies et al.*, 2009). The nutrients dissolved silicic acid (DSi) and dissolved inorganic nitrogen (DIN)are initialized with World Ocean Atlas 2013 products (*Garcia et al.*, 2013), and alkalinity and dissolved inorganic carbon (DIC) from GLODAPv2 (*Lauvset et al.*, 2016).

The global nutrients, chlorophyll concentrations, and zooplankton biomass are analyzed for the surface annual mean over the last five years of the model simulation by using monthly model output. Daily output from the last five years of the chlorophyll and phytoplankton biomass is used to assess the impact of zooplankton processes on phytoplankton phenology.

Bloom Phenology Evaluation and Skill Assesment

In this study, we use two different methods to assess the surface phytoplankton bloom phenology. The first method uses the surface phytoplankton carbon biomass (P_C, mmol C m^{-3})

and its accumulation rate (r, d^{-1}) as a metric (*Llort et al.*, 2015) and the second one uses the surface chlorophyll concentration with a given threshold (*Siegel et al.*, 2002).

In the first method, we decompose the bloom phenology into onset, climax, and apex as described in *Llort et al.* (2015). The net biomass accumulation rate (r, d^{-1}) was used to define these three events (Eq.3.1).

$$r = \frac{1}{P_C}.\frac{dP_C}{dt} \tag{3.1}$$

The bloom onset is the day when total biomass (P_C, mmol C m^{-3}) starts to increase. On this day, biomass is at its minimum, the net accumulation rate (r, d^{-1}) equals zero and the temporal derivative (dr/dt) is greater than zero. On the climax day, the bloom accumulation rate is maximum and its time derivative equals zero. Finally, the bloom apex is defined as the day when total phytoplankton biomass (P_C, mmol C m^{-3}) reaches its maximum, the net accumulation rate (r, d^{-1}) is zero and its time derivative (dr/dt) is negative.

In the second method, we identify the bloom start, peak, and end days by using surface chlorophyll concentrations (*Siegel et al.*, 2002). For comparison with satellite products, we disregard model output during times when no observations are available (May-August). The first day when chlorophyll concentration is higher than the threshold value is the bloom start day (BSD), the day when chlorophyll concentration reaches a maximum is bloom peak day and finally, the day when chlorophyll concentration is below the threshold is the bloom end day (BED). However, we should acknowledge that even though this method is used widely (*Henson et al.*, 2009; *Racault et al.*, 2012; *Soppa et al.*, 2016), the result depends on the chosen threshold value (*Racault et al.*, 2012). In this study, we use a threshold value of 5% above the median as in *Soppa et al.* (2016).

A Taylor diagram (*Taylor*, 2001) was used to assess the performance of the two model versions. We used the OC-CCI satellite surface chlorophyll concentration product (*Sathyendranath et al.*, 2019), the remotely sensed net primary production data set VGPM (*Behrenfeld and Falkowski*, 1997), CPBM (*Westberry et al.*, 2008) and World Ocean Atlas nutrient fields (*Garcia et al.*, 2018) to assess the global macronutrient and chlorophyll concentration results of the model simulations at the surface (Fig. 3.3). To assess the Southern Ocean bloom phenology, the surface chlorophyll satellite product (2003-2013) of *Johnson et al.* (2013) was used.

Analysis on zooplankton grazing and nutrient excretion

We focus on two main processes: the grazing loss of phytoplankton due to zooplankton grazing and the total nutrient recycling by all zooplankton groups in a biogeochemical model. The total grazing loss of phytoplankton (Eq. 3.2, $Phy_{grzloss}$, d^{-1}) is calculated by dividing the total zooplankton grazing rate ($\sum_i G_i$, i =each zooplankton, mmol C m^{-3} d^{-1}) through the total phytoplankton biomass concentration (P_C, mmol C m^{-3}). The total DON excretion by zooplankton (Eq. 3.3, Zoo_{excr}, mmol N m^{-3} d^{-1}) is calculated as the sum of the product of total zooplankton biomass (Z_N, mmol N m^{-3}) times the excretion rate constants of each zooplankton group (ϵ_{Z_i}). Iron excretion is directly converted from DON excretion as the model assumes a constant N:Fe ratio of 0.033 (mmol/μmol).

$$Phy_{grzloss} = \frac{\sum_i G_i}{P_C} \tag{3.2}$$

$$Zoo_{excr} = \sum_i Z_{N_i} \cdot \epsilon_{Z_i} \tag{3.3}$$

RESULTS

Global Ecosystem Properties in the REcoM-3ZOO model

In REcoM-3ZOO, microzooplankton has the highest biomass integrated over the top 200 m (160 Tg C) among the zooplankton groups, followed by mesozooplankton (30 Tg C) and macrozooplankton (20 Tg C). We observe a significant increase and improvement in total zooplankton biomass representation in REcoM-3ZOO (Table 3.2). Modeled micro- and macrozooplankton biomasses are in the observational range, and microzooplankton is the major grazer in the model as in the real world, although the fraction of primary production grazed is with 22% of the annual net primary production lower than the 60% by *Calbet and Landry* (2004) (Table 3.2). Modeled mesozooplankton biomass is relatively low in the model, but its contribution to grazing is well represented with about 10% of global net primary production (NPP), which is similar to the estimate of 12% by *Calbet* (2001).

In both versions, small phytoplankton group biomass is higher than the diatom biomass. While small phytoplankton amounts to 66% of total phytoplankton biomass in REcoM-2, this share increases to 72% in REcoM-3ZOO. The share of diatoms (28%) is still within the reported range of 20% - 60% (*Buitenhuis et al.*, 2013). The slight decrease (50 Tg C) in diatom biomass is a result of increased grazing pressure on diatoms after parametrizing meso- and macrozooplankton functional types.

A major difference in the new version of the model is the zooplankton fraction of total modeled plankton biomass. While in the original version zooplankton biomass contributes only 5% to plankton biomass, in REcoM-3ZOO this share increases to 15% in the upper 200 m. The ratio of total zooplankton biomass to total phytoplankton biomass (ZtoP ratio) is 0.05 in REcoM-2 and 0.15 in REcoM-3ZOO. Previous quantifications of the ZtoP ratio show large differences depending on the seasons and the structure of the ecosystem models. For example, it is 0.83 in the global plankton functional type (PFT) model PLANKTOM10 and was 0.53 in the previous version PLANKTOM6 (*Le Quéré et al.*, 2016). The ZtoP ratio in REcoM-3ZOO averaged over the upper 200 m, varies between a minimum of 0.15 and a maximum of 0.63. Observational studies reported a ratio of heterotrophic to autotrophic biomass between 0.05-3.2 in the coastal ocean and 0.17-10.2 in the open ocean (*Gasol et al.*, 1997). While the observational range is large, we consider the increase of the ZtoP ratio as an improvement in the model.

Standing stocks of organic carbon and nutrients are transferred up the food chain to zooplankton in a model formulation with three zooplankton functional types. Zooplankton partitions the carbon and nutrients initially bound by primary production between zooplankton growth, export and recycled production. This leads to a different model state with more recycling-fuelled NPP at the expense of less export: The global annual mean NPP increases by 7.7 Pg C y^{-1} (25 %) to 38 Pg C y^{-1} in the REcoM-3ZOO simulation. It now falls into the range of satellite-based observations (35-70 Pg C y^{-1}, *Carr et al.*, 2006) and agrees well with the recent estimate of 38.8 Pg C y^{-1} to 42.1 Pg C y^{-1} (*Kulk et al.*, 2020). In addition, the ratio of EP to NPP decreases from 17% to 12% illustrating the altered carbon pathways in the model.

In REcoM-3ZOO, the small phytoplankton is spread across the global ocean, while the diatom functional type mainly dominates in high latitudes and in the equatorial Pacific (Fig. 3.2) due to the growth limitation by silicic acid (*Smetacek*, 1998). The distribution of the zooplankton functional types shows distinct spatial patterns. While microzooplankton is widely spread in the global ocean, in line with *Buitenhuis et al.* (2010), mesozooplankton is mainly present in subpolar areas and in the equatorial Pacific in accord with observational data compilations (*Moriarty and O'Brien*, 2013). The macrozooplankton group is mainly represented in the polar regions, in agreement with the reported global macrozooplankton dataset (*Moriarty et al.*, 2013).

	REcoM-2	REcoM-3ZOO	Data - Previous studies
Rates (Pg C yr^{-1})			
NPP	30.3	38	47.3 (*Behrenfeld and Falkowski*, 1997)*
			35-70 (*Carr et al.*, 2006; *Kulk et al.*, 2020)*
			51 - 65 (*Buitenhuis et al.*, 2013)^{o}
EP at 100 m	5.2	4.7	9-10 (*Schlitzer*, 2004; *Lee*, 2001)*
			5.8–13.0 (*Dunne et al.*, 2007)*
			5 (*Henson et al.*, 2011)$^{+}$
			6 (*Siegel et al.*, 2014)*
Integrated phytoplankton biomass over the upper 200 m (Tg C)			
Small-phy.	730	830	—
Diatom	380	330	13-750 (*Leblanc et al.*, 2012)$^{+}$
Integrated zooplankton biomass over the upper 200 m (Tg C)			
Microzoo.	—	160	100-370 (*Buitenhuis et al.*, 2010)$^{+}$
Mesozoo.	60	30	210-340 (*Moriarty and O'Brien*, 2013)$^{+}$
Macrozoo.	—	20	10-640 (*Moriarty et al.*, 2013)$^{+}$

* Remote sensing, $^{+}$ Observations, ^{o} Models

TABLE 3.2: Global annual total values for net primary production (NPP), export production (EP) at 100 m and plankton functional types biomass from observations and previous studies, REcoM-2 and REcoM-3ZOO. Model results are averaged over the last five years.

Comparison of the Global Nutrient and Chlorophyll Concentrations in REcoM-2 and REcoM-3ZOO

The overall differences in how well REcoM-2 and REcoM-3ZOO agree with climatological data for chlorophyll, net primary production and nutrients, are quantified statistically in a Taylor diagram (*Taylor*, 2001). The differences in correlation coefficients with observational data sets are less than 0.1 between the two simulations (Fig. 3.3). The correlation coefficients are slightly lower (0.35, 0.67) for annual mean chlorophyll and net primary production and slightly higher (0.89, 0.83) for DIN and silicic acid concentrations in REcoM-3ZOO. In addition, the normalized standard deviation is closer to the observations and root mean square error smaller for annual mean chlorophyll concentrations in REcoM-3ZOO. Both model versions generally produce similar spatial patterns of surface nutrient and chlorophyll concentrations (Figs. 3.4, 3.5). A notable exception is the South Pacific, where a strong change in surface DIN and iron concentrations occurs.

Observed surface annual mean DIN and silicic acid concentrations are higher in the high latitudes and Equatorial Pacific compared to the rest of the ocean (Fig. 3.4). Both model versions also produce a similar spatial distribution of nutrients compared to WOA18 products (*Garcia et al.*, 2018). However, while REcoM-2 has a strong positive bias in surface DIN concentrations in the South Pacific (20°S-40°S), the bias decreases significantly in REcoM-3ZOO. The mean DIN concentration decreases from 7 mmol m^{-3} in REcoM-2 to 2.2 mmol m^{-3} in REcoM-3ZOO and gets closer to observations (0.8 mmol m^{-3}) in the South Pacific. We find that this is related to the more complex ecosystem interactions, which include different pathways of nutrient recycling by zooplankton. In addition, the mean DIN concentrations decrease in northern and southern high latitudes. In the northern high latitudes, the mean surface DIN

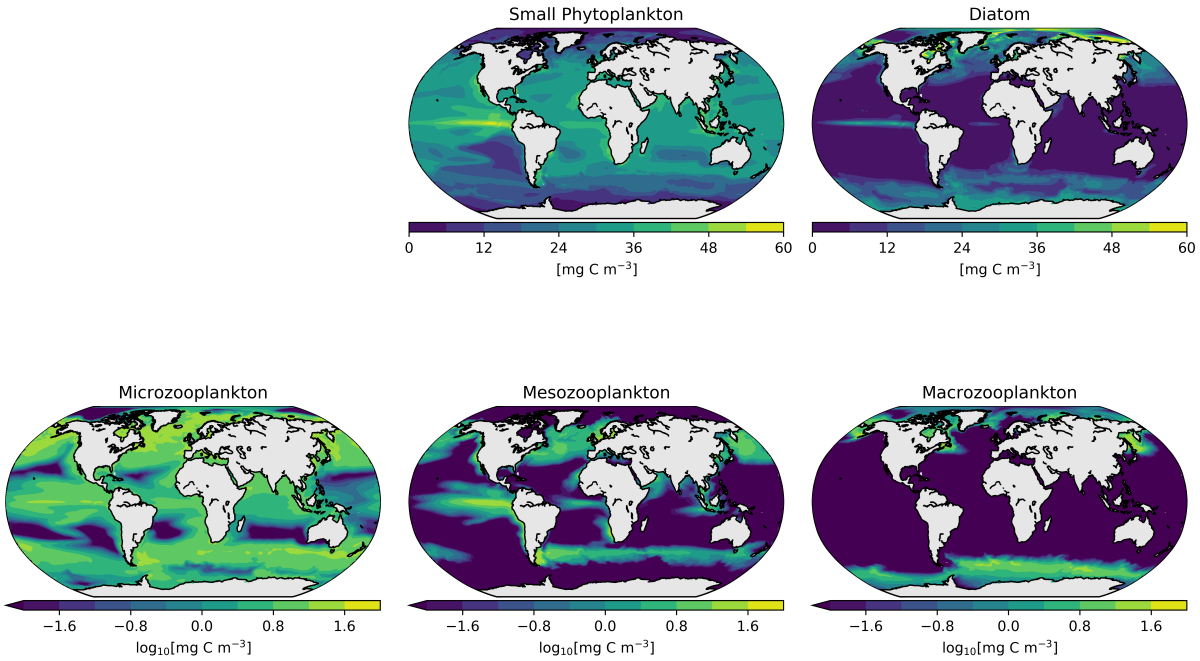

FIGURE 3.2: Annual mean surface carbon biomasses for plankton functional types in the REcoM-3ZOO model. Phytoplankton functional types: small phytoplankton and diatoms (mg C m^{-3}). Zooplankton functional types: micro- meso and macrozooplankton are shown in logarithmic scale (log$_{10}$[mg C m^{-3}]). Model results are averaged for the last five years of the simulations.

concentrations (4.1 mmol m^{-3} in REcoM-2 and 3.5 mmol m^{-3} in REcoM-3ZOO) are lower than the observations (5.6 mmol m^{-3}). In the southern high latitudes, mean DIN concentrations also slightly decrease from 19.9 mmol m^{-3} in REcoM-2 to 19 mmol m^{-3} in REcoM-3ZOO. Both model versions underestimate the surface mean silicic acid concentrations in the high latitudes. This bias is ameliorated in REcoM-3ZOO with a DSi concentration increase by 20% to 15 mmol m^{-3} south of 50°S getting closer to observations (31.6 mmol m^{-3})). The annual mean iron concentration increases in REcoM-3ZOO by 20-25% in high latitudes and by 270% (from 0.04 μmol m^{-3} to 0.14 μmol m^{-3}) in the South Pacific compared to REcoM-2. This is an important feature, since it directly affects surface chlorophyll concentrations due to the iron limitation.

The new zooplankton formulation affects the surface mean chlorophyll concentrations directly by grazing pressure and indirectly by altered nutrient availability. The spatial distributions of surface chlorophyll of both simulations resemble each other with the highest chlorophyll concentrations in high latitudes and the equatorial Pacific (Fig. 3.5). In REcoM-3ZOO, a previously apparent strong positive bias in the North Atlantic and the Arctic chlorophyll disappears. In these regions, the annual mean chlorophyll concentrations decrease from 1.2 mg m^{-3} to 0.94 mg m^{-3}, in better agreement with the remotely sensed 0.9 mg m^{-3} (Figs. 3.5, 3.6). South of 50°S, the mean chlorophyll concentration remains similar with 0.55 mg m^{-3} in REcoM-2 and 0.57 mg m^{-3} in REcoM-3ZOO, close to satellite observations (0.63 mg m^{-3}, *Johnson et al.*, 2013). In the Atlantic and Indian sectors of the Southern Ocean increase of chlorophyll can reach up to 0.58 mg m^{-3} in REcoM-3ZOO, Newly distributed iron and nitrate concentrations in the South Pacific provide a noticeable improvement in the mean surface chlorophyll concentrations. The mean value increases in South Pacific from 0.05 mg m^{-3} in REcoM-2 to 0.12 mg m^{-3} in REcoM-3ZOO and matches better with satellite observations of 0.1 mg m^{-3} (*Sathyendranath et al.*, 2019).

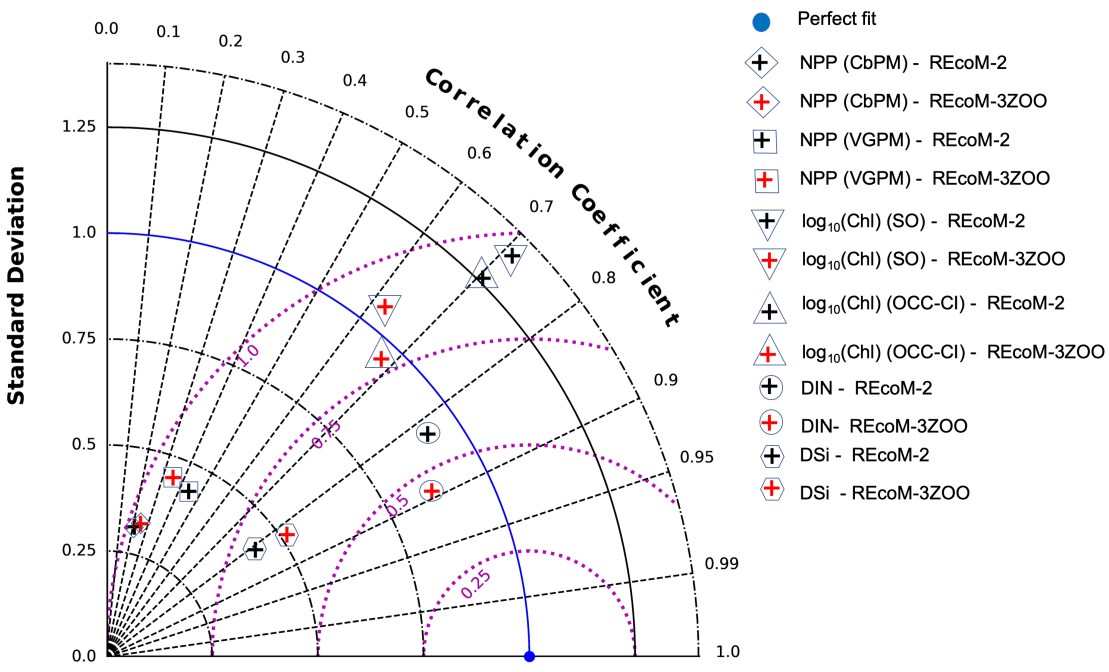

FIGURE 3.3: Normalized Taylor diagram comparing the distributions of surface concentration in annual mean chlorophyll ($\log_{10}$(Chl), mg m^{-3}), dissolved inorganic nitrogen (DIN, mmol m^{-3}), silicic acid (DSi, mmol m^{-3}) and net primary production (NPP, mg C m^{-2}) for REcoM-2 (in black) and REcoM-3ZOO (in red) with observations. Pink dotted lines show the axes for the root mean square error (RMSE). Surface chlorophyll observations are taken from OC-CCI (*Sathyendranath et al.*, 2019) for global and from *Johnson et al.* (2013) for the Southern Ocean (SO) comparison. World Ocean Atlas 2018 products (*Garcia et al.*, 2018) are used for nutrient observations. Net primary production observations are taken from the VGPM *Behrenfeld and Falkowski* (1997) and CBPM *Westberry et al.* (2008) data sets. The blue dot shows the perfect fit.

Grazing and Nutrient Recycling by Zooplankton

Figure 3.6 shows the zonally and annually averaged and depth-integrated zooplankton biomass in the model and a comparison with data compilations. We use three MAREDAT data compilations for microzooplankton (*Buitenhuis et al.*, 2010), mesozooplankton (*Moriarty and O'Brien*, 2013) and macrozooplankton biomass *Moriarty et al.* (2013). In REcoM-3ZOO, the zonal average of zooplankton biomass follows a similar distribution as apparent in the MAREDAT dataset (Fig. 3.6). While microzooplankton and mesozooplankton prevail from north to south with maxima in the subpolar and equatorial regions, macrozooplankton is primarily present in the higher latitudes. The total zooplankton biomass is higher in REcoM-3ZOO compared to REcoM-2. While total zooplankton biomass increases throughout all latitudes, the strongest increase occurs poleward of 30°N and 30°S (Fig. 3.6). Maxima in annually-averaged and depth-integrated total zooplankton biomass can reach up to 2000 mg C m^{-2} in MAREDAT in the high latitudes. In REcoM-3ZOO, the maximum of total zooplankton biomass increases from 783 mg C m^{-2} in REcoM-2 to 2877 mg C m^{-2}. The zonally-averaged total zooplankton biomass is almost 0 mg C m^{-2} poleward of 60°N and 60°S in REcoM-2. It further increases to 1339 mg C m^{-2} north of 60°N and 577 mg C m^{-2} south of 60°S.

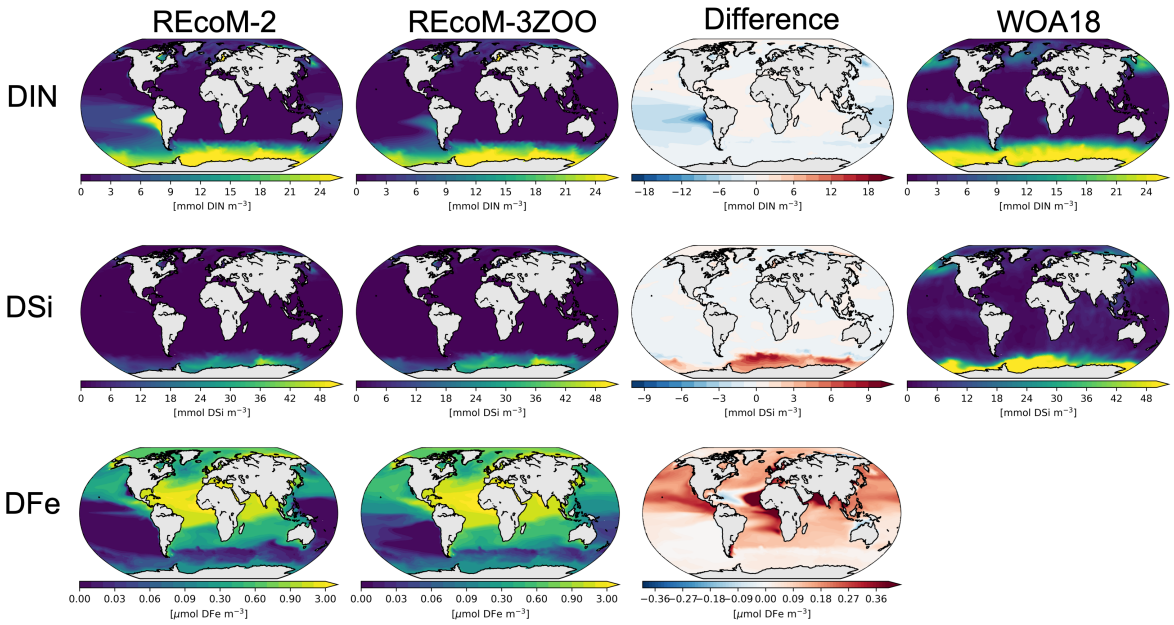

FIGURE 3.4: Annual mean surface nutrient concentrations (DIN, DSi, DFe) in REcoM-2, REcoM-3ZOO, difference (REcoM-3ZOO minus REcoM-2) and WOA18 (*Garcia et al.*, 2018). Model results are averaged over the last five years of the simulation.

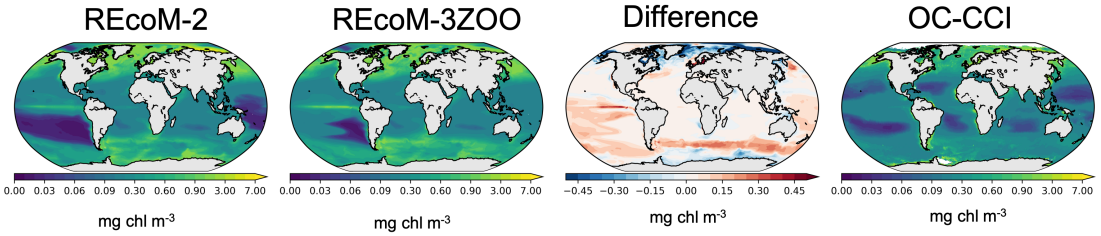

FIGURE 3.5: Annual mean surface chlorophyll concentrations in REcoM-2, REcoM-3ZOO, their difference (REcoM-3ZOO minus REcoM-2) and OC-CCI satellite product (*Sathyendranath et al.*, 2019). Model results are averaged over the last five years of the simulation.

These changes in zooplankton biomass and distribution affect grazing patterns and the fast recycling of nutrients by zooplankton excretion. Consequently, they impact the nutrient fields presented in section 3.2. We observe a distinct latitudinal pattern with an increased grazing loss of phytoplankton in the extra-tropics and a reduced grazing loss in the tropics in the new parametrization in REcoM-3ZOO (Fig. 3.7). In REcoM-2, the highest annual mean grazing-related phytoplankton loss in the global ocean occurs between 20°N and 20°S, which is a result of the temperature-dependence of grazing. The gradient between phytoplankton loss rates in high latitudes and in the tropics is smaller in REcoM-3ZOO compared to REcoM-2, as a result of the parametrization of zooplankton functional types with different parameter values of excretion and grazing and temperature dependencies. In REcoM-3ZOO, the spatial peak of the grazing loss of phytoplankton occurs between 40°N and 60°N (Fig. 3.7, Table 3.3). In the subtropics (20°-40°N, 20°-40°S), the zooplankton-related grazing loss of phytoplankton remains similar in both simulations (0.033-0.021 d^{-1} in REcoM-2, 0.037-0.020 d^{-1} in REcoM-3ZOO). In the northern temperate (40°-60°N) and high latitudes (60°-90°N), the grazing loss of phytoplankton increases by 26% and 120%, respectively in REcoM-3ZOO. Consequently, this decreases the mean surface chlorophyll concentrations by 32% and satellite-based

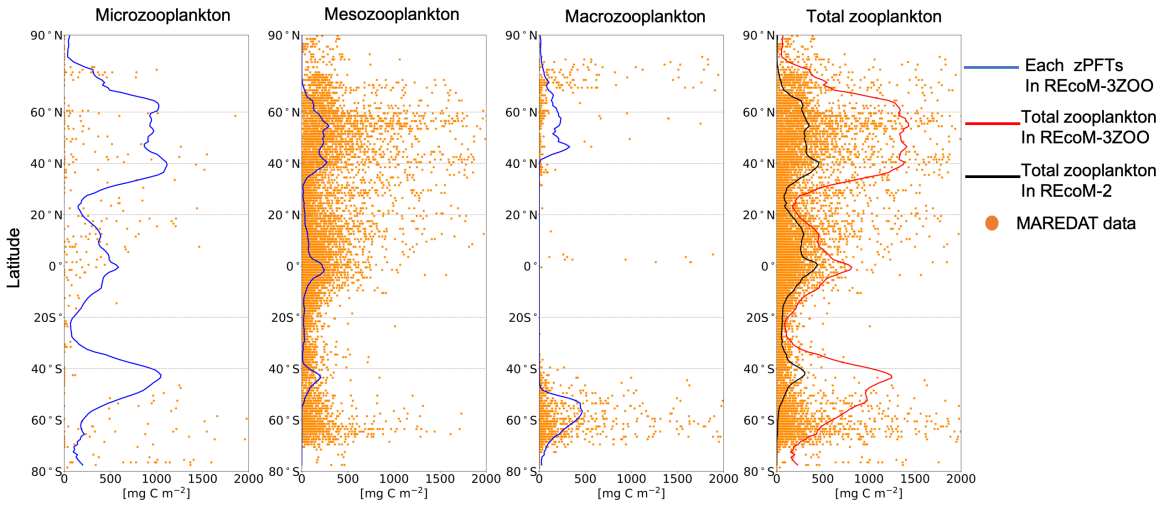

FIGURE 3.6: Zonally and annually averaged and depth-integrated zooplankton biomass (micro-, meso-, and macrozooplankton, total zooplankton) in REcoM-2 (black line) and REcoM-3ZOO (blue line) compared to annually averaged and depth-integrated gridded MAREDAT observations (orange dots, *Buitenhuis et al.*, 2010; *Moriarty and O'Brien*, 2013; *Moriarty et al.*, 2013).

(1.02 mg chl m^{-3}) and model-based (0.91 mg chl m^{-3}) estimates come to close agreement. In the southern hemisphere temperate and high latitudes (40°-60°S, 60°-90°S), a similar increase in grazing loss rates occurs, ranging between 100% (40°-60°S), and 1800% south of 60°S where grazing rates were previously very small. Despite this strong grazing loss, we see a 20% increase in mean chlorophyll concentrations (40°-60°S), which we relate to the nutrient excretion of zooplankton.

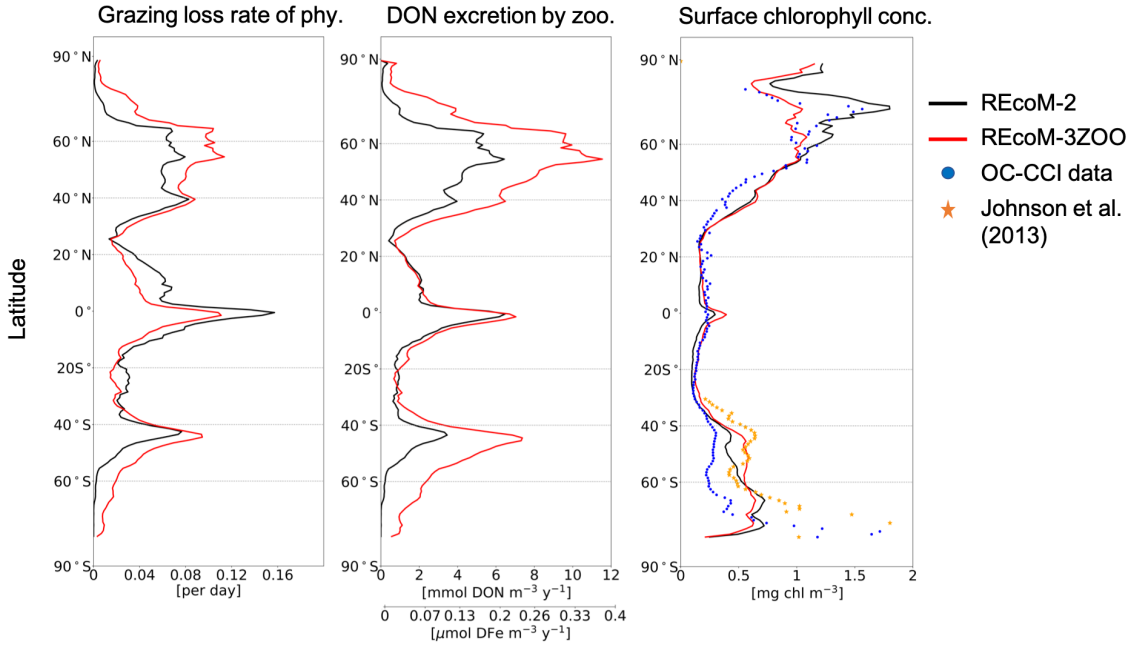

FIGURE 3.7: Annual mean surface grazing loss of phytoplankton, zooplankton excretion of dissolved organic nitrogen (DON) and chlorophyll concentrations in REcoM-2 (black) and REcoM-3ZOO (red). Surface chlorophyll concentrations from satellite products are shown as blue dots (*Sathyendranath et al.*, 2019) and orange stars (*Johnson et al.*, 2013).

DON and with it DFe excretion intensifies throughout the ocean (Fig. 3.7) with a notably larger increase outside the tropics (poleward of about 30°N and S). Local exceptions occur in the equatorial Pacific and some coastal regions (e.g., off the coast of Australia, Fig. 3.8). The increase of excretion rates is expected since the rates are directly coupled to the total zooplankton biomass in the model. DON and DFe excretion rates have identical spatial patterns as the DFe excretion rate is calculated by multiplication of the DON excretion rate with a fixed Fe:N ratio in the model. While the annual mean DON excretion by zooplankton is 1.61 mmol m^{-3} y^{-1} in REcoM-2 between 40°S and 60°S, it is 5.55 mmol m^{-3} y^{-1} in REcoM-3ZOO. An increase of DFe excretion occurs in the same region, between 40°S and 60°S. The zooplankton DFe excretion is 0.05 μmol m^{-3} y^{-1} in REcoM-2, and increases to 0.16 μmol m^{-3} y^{-1} (Fig. 3.3).

In summary, we relate the reduced chlorophyll bias in the North Atlantic and the Arctic to higher grazing-related phytoplankton loss terms. Considering the role of iron limitation in the Southern Ocean, we conclude that here the nutrient recycling through zooplankton has a stronger effect on mean chlorophyll concentrations than grazing. The increase in nutrients and chlorophyll in the Equatorial Pacific (Figs. 3.4, 3.5) and in the Southern Ocean (iron) are co-located with regions of strongest change in nutrient excretion.

Competing Effects of Phytoplankton Grazing Loss and Nutrient Excretion by Zooplankton

Grazing loss of phytoplankton and nutrient excretion by zooplankton show spatial patterns in the model that are directly coupled with zooplankton biomass. In REcoM-2, the annual mean grazing loss of phytoplankton is 0.22 d^{-1} in the Equatorial Pacific, around 0.07 d^{-1} in the North Atlantic and coastal regions, and $<$0.01 d^{-1} in south of 50°S (Fig. 3.8). While both processes play only a minor role in the high latitudes in REcoM-2, they become an important component for the ecosystem dynamics in REcoM-3ZOO (Fig. 3.8). The annual mean grazing loss of phytoplankton increases by 28% (from 0.07 d^{-1} to 0.09 d^{-1}) in the North Atlantic, and by more than 100% (from $<$0.01 d^{-1} to 0.02 d^{-1}) in the Southern Ocean.One exceptional region is the Equatorial Pacific where the average grazing loss of phytoplankton decreases by 50% (from 0.3 d^{-1} to 0.15 d^{-1}, Fig. 3.8) due to different temperature dependencies of grazing in both model versions.The nutrient excretion by zooplankton increases throughout the global ocean since total zooplankton biomass increased in REcoM-3ZOO (Fig. 3.6), but the magnitude is largest in temperate and high latitudes (poleward of 40°N/S). The annual mean of DON excretion increases by 86% (from 4.2 to 7.8 mmol DON m^{-3} y^{-1}) in the North Atlantic and by more than 100% (from 0.39 to 2.66 mmol DON m^{-3} y^{-1}) in the Southern Ocean, respectively.

Overall, a reinforcement or decline of the same patterns in grazing and nutrient excretion with similar seasonal patterns occurs north of 50°S (Fig. S1). However, a substantial change in zooplankton-related processes appears south of 50°S in the simulation with REcoM-3ZOO. The grazing loss of phytoplankton reaches 0.2 d^{-1} in spring and summer, whereas it was barely existent in REcoM-2. A similar effect can be observed in DON excretion (followed by iron excretion), reaching up to 3 mmol DON m^{-3} per month in November. Zooplankton nutrient excretion between January and April increases the chlorophyll concentrations in the Southern Ocean in the same period (Fig. 3.11), but we have so far not investigated the direct effect on phytoplankton phenology. In REcoM-3ZOO,

Although we use the same ingestion function for zooplankton in both model versions, temperature dependencies and the parameter values differ. In the original version REcoM-2, the grazing rate constant of zooplankton is 2.4 d^{-1} at 15°C that increases up to 5 d^{-1} at 30°C and the assimilation efficiency is 0.4 (the remaining 60% of grazing are routed to fecal pellet production and sloppy feeding). This parametrization causes firstly a very high grazing rate in warm equatorial regions and consequently a strong annual grazing loss rate of

	Grazing loss rate		DON excretion by zoo.		DFe excretion by zoo.		Surface chlorophyll conc.		
Region	REcoM-2	REcoM-3ZOO	REcoM-2	REcoM-3ZOO	REcoM-2	REcoM-3ZOO	REcoM-2	REcoM-3ZOO	Satellite
60° - 90°N	0.02	0.04	1.55	4.02	0.05	0.13	1.34	0.91	1.02
40° - 60°N	0.07	0.08	4.44	8.13	0.14	0.27	0.81	0.81	0.7
20° - 40°N	0.03	0.03	1.39	2.32	0.05	0.08	0.27	0.29	0.23
20°N - 20°S	0.06	0.04	2.34	2.63	0.08	0.09	0.16	0.20	0.2
20° - 40°S	0.02	0.02	0.92	1.33	0.03	0.04	0.16	0.20	0.16
40° - 60°S	0.03	0.05	1.61	4.80	0.05	0.16	0.43	0.54	0.27 (0.52)
60° - 90°S	< 0.01	0.01	0.11	1.76	< 0.01	0.05	0.65	0.6	0.3 (0.83)

TABLE 3.3: Annual mean phytoplankton grazing loss rate (d^{-1}), DON (mmol DON m^{-3} y^{-1}) and DFe (μmol DFe m^{-3} y^{-1}) excretion by zooplankton, surface chlorophyll concentrations (mg chl m^{-3}) in REcoM-2 (reference) and REcoM-3ZOO averaged over the last five years of the simulation in seven latitudinal bands. The last column shows the satellite-based estimates of surface chlorophyll concentrations from OC-CCI (*Sathyendranath et al.*, 2019) and in parentheses from *Johnson et al.* (2013).

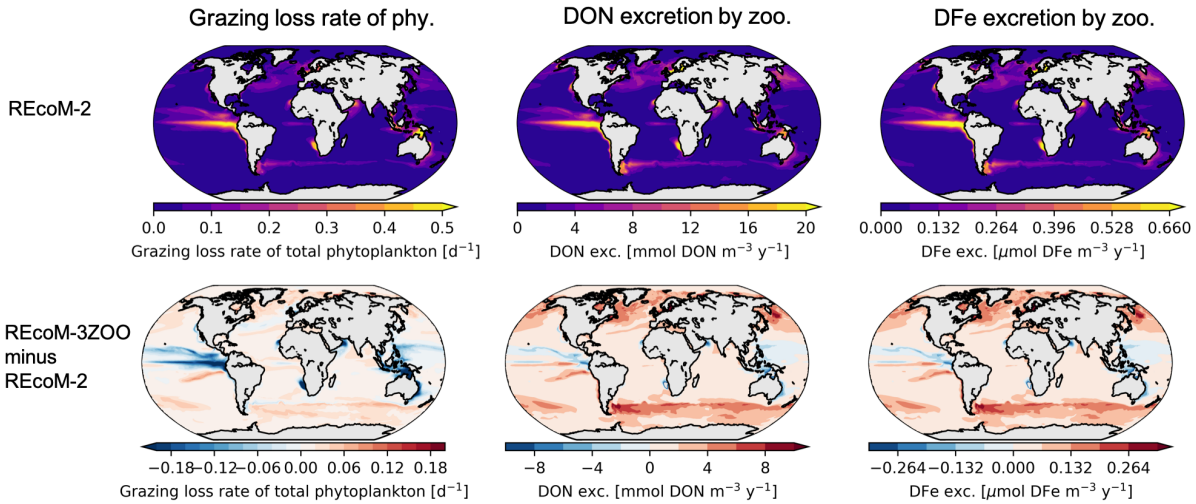

FIGURE 3.8: Annual mean phytoplankton loss rate due to zooplankton grazing (d^{-1}), DON (mmol m^{-3} y^{-1}) and DFe (μmol m^{-3} y^{-1}) excretion by zooplankton in REcoM-2 (reference) and the change in REcoM-3ZOO (REcoM-3ZOO minus REcoM-2). The model results are averaged over the last five years of the simulations.

phytoplankton (Table 3.3, Fig. 3.7). Secondly, this leads to low zooplankton biomass in the cold polar regions and therefore causes grazing loss rates for phytoplankton and nutrient excretion by zooplankton to be very low (Table 3.3, Fig. 3.7). In REcoM-3ZOO, parametrizing three zooplankton functional types gives the flexibility to choose different assimilation efficiencies and temperature dependencies of grazing. For example, the microzooplankton temperature-dependent grazing rate is higher than for mesozooplankton. The initial assimilation efficiency of the mesozooplankton group is 0.8 and decreases with increasing prey abundance. Also, polar slow-growing macrozooplankton which is parametrized as krill (*Karakuş et al.*, 2021) is represented in this version. This new parameterization allows us to improve the spatial distribution of zooplankton biomass and related processes in high latitudes (Fig. 3.8). Figure 3.9 shows the point-wise comparison of zooplankton biomass, nutrient excretion and grazing rates as well as grazing loss of phytoplankton with annual mean surface temperature. The maximum of zooplankton biomass is three times higher in REcoM-3ZOO and the strongest increase occurs at temperatures below 14°C. Grazing and nutrient excretion follow the change in biomass. The magnitude of DON excretion and grazing by zooplankton is similar in both model versions at temperatures above 14°C, and increases at colder temperatures in REcoM-3ZOO. The average of grazing loss of phytoplankton increases by 100% (from 0.02 to 0.04 d^{-1}) and by 40% (from 0.05 to 0.07 d^{-1}) poleward of 40°S and 40°N in REcoM-3ZOO, respectively. However, it is up to three times lower between 40°S and 40°N in REcoM-3ZOO as a result of the new parametrization. Our results demonstrate that a high zooplankton biomass does not directly imply a high grazing loss of phytoplankton in biogeochemical models. The loss term results from an interplay of temperature dependency, chosen parameter values for grazing and excretion rates, and food web structure in the model.

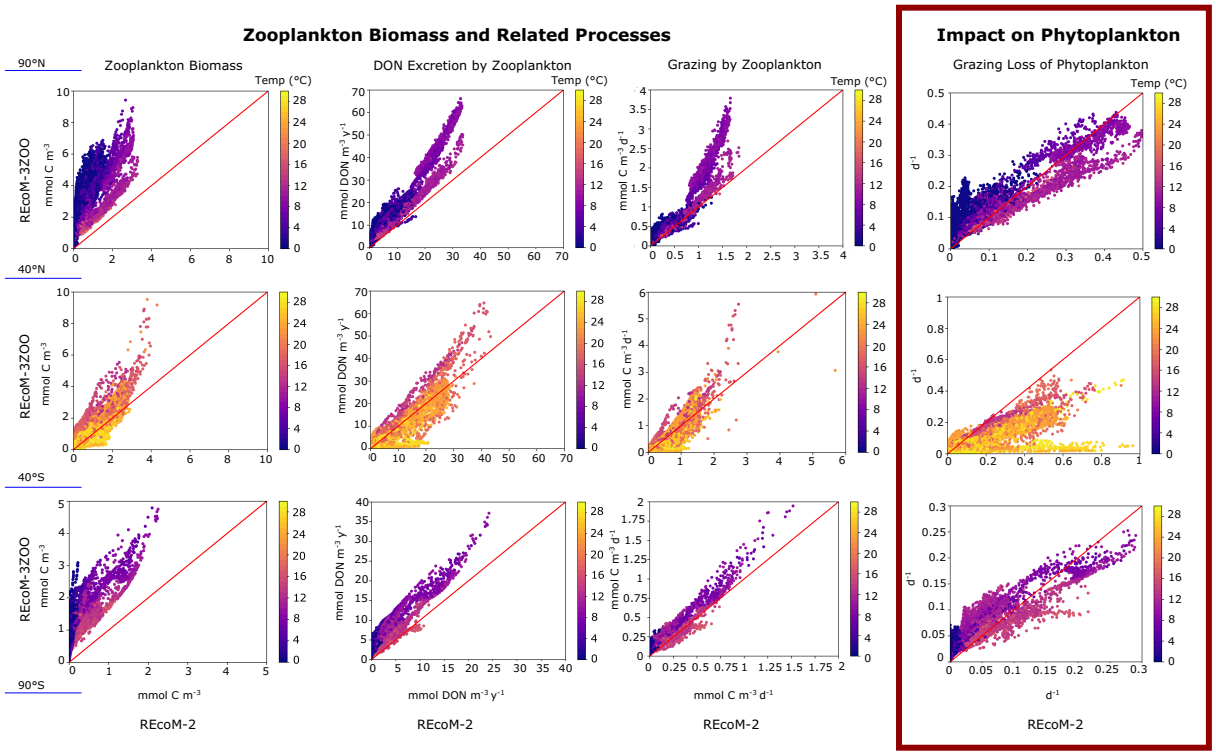

FIGURE 3.9: Point-wise comparison of annual mean surface zooplankton biomass (mmol C m^{-3}), DON excretion by zooplankton (mmol m^{-3} y^{-1}), grazing by zooplankton (mmol C m^{-3} d^{-1}) and grazing loss of phytoplankton (d^{-1}) between REcoM-2 (x-axis) and REcoM-3ZOO (y-axis) in three regions from north to south (90°-40°N, 40°N-40°S and 40°-90°S). Each dot represents one surface model grid point. The red line represents the one-to-one line in the plots. The color shading indicates the annual mean surface temperature. Note the different y-axis ranges.

Impact of Zooplankton Grazing on Southern Ocean Phytoplankton Bloom Phenology

Phytoplankton bloom start and peak days occur later in the year in the whole Southern Ocean south of 50°S in REcoM-3ZOO (Fig. S3). However, the magnitude of the effect is larger in regions where high zooplankton biomass causes larger grazing loss of phytoplankton. In this section, we focus on a specific region in the Southern Ocean (subpolar Atlantic sector of the Southern Ocean, 50°-60°S and 20°E-60°W) to analyze the impact of the zooplankton parametrization on phytoplankton phenology. We specifically chose this region since it is located in an area of substantial change in zooplankton processes from REcoM-2 to REcoM-3ZOO.

Carbon accumulation rate-based analysis: As we showed in the previous sections, the ecosystem structure of the two model versions differs. Therefore, we describe the bloom phenology separately in each model version rather than comparing the two simulations directly.

In REcoM-2, the onset of the phytoplankton bloom (the day when the biomass accumulation rate becomes positive) happens in the last week of July, i.e. after the winter solstice and when deepening of the mixed layer occurs (Fig. 3.10a and c). The maximum carbon accumulation rate of the phytoplankton biomass (climax) occurs in the last week of October when the mixed layer depth (MLD) is roughly halfway between its deepest and shallowest state and can be related to light availability. Maximum phytoplankton biomass (apex) falls into the first week of November with only eleven days between climax and apex. Phytoplankton reaches its maximum biomass shortly after the carbon accumulation rate is at its maximum. Phytoplankton loss rates due to

grazing are very low compared to other loss rates (Fig. 3.10c and e). We interpret this as a sign of a too weak representation of zooplankton grazing in REcoM-2. Both phytoplankton groups, small phytoplankton and diatoms, are iron limited, but the limitation is stronger for diatoms (Fig. 3.10g).

In REcoM-3ZOO, the phytoplankton bloom onset happens in the last week of July as in REcoM-2. The climax, however, now occurs in the first week of October, before significant shoaling of the MLD sets in (Fig. 3.10b and d). This can be explained by the dilution of zooplankton when MLD is at its maximum (*Behrenfeld et al.*, 2013) and is supported by the fact that phytoplankton losses due to zooplankton grazing are now an important component of mortality losses (Fig. 3.10f). Total zooplankton grazing contributes up to 39% to spring and summer phytoplankton loss rates. The time that passes between climax and apex is 29 days because phytoplankton biomass accumulation is delayed by stronger grazing pressure. In REcoM-3ZOO, iron limitation is lower than in the original version of the model (Fig. 3.10h).

The results of the two simulations illustrate the sensitivity of the phytoplankton bloom phenology to modeled ecosystem structure and processes in the biogeochemical model. Both model versions can produce the main properties of phytoplankton growth (e.g., high rates in spring) depending on abiotic factors (light, temperature etc.). However, a detailed analysis reveals differences. Shifts in the timing of the climax between the model versions, for example, show that the representation of zooplankton processes can lead to a different system state, in which carbon accumulation is driven by grazer dilution rather than by light limitation (bottom-up control).

Chlorophyll-based analysis and comparison with satellite data: In REcoM-2, the bloom start day (BSD) occurs in August (day 237) and bloom peak is in November (day 306, Fig. 3.11). We see a sharp decrease in chlorophyll concentration after the peak, and the bloom terminates in the beginning of January (day 6). The mean chlorophyll concentration is 0.26 mg chl m^{-3} between January and May.

The bloom start day occurs in September (day 258) in REcoM-3ZOO, which is three weeks later than in REcoM-2, whereas the peak day remains unchanged (day 306 in both simulations, Figure 3.11). The peak of chlorophyll occurs as a plateau and lasts two weeks longer in the simulation with three zooplankton groups (until day 322). Also, the shift in the bloom start day and the increase in summer chlorophyll concentrations (due to the fast recycling of nutrients) move the bloom end day by three weeks (to day 27). The calculated bloom duration (time between BSD and BED) is similar in REcoM-3ZOO. We caution that this should not be interpreted as no change of the bloom duration in REcoM-3ZOO, as the result of the threshold method is strongly dependent on the chosen threshold value. In REcoM-3ZOO simulations, the chlorophyll concentrations after the BED are very close to the threshold (until May). The mean chlorophyll concentration is 0.42 mg chl m^{-3} between January and May which is almost two times higher than in REcoM-2.

In each year of the satellite observations, chlorophyll concentrations reach the 5% threshold value after mid-September (bloom start), reach peak chlorophyll between October and December (up to 200% of the annual median) and slowly decline from 100% to 0% until mid-March (Fig. 3.11b). In the average over ten years, the satellite-derived bloom starts in October (day 291) and ends in February (day 33, marked green BSD and BED, Fig. 3.11b). Even though there are certain limitations to using the satellite products (missing areas, clouds, interannual variability) for comparison, the start of bloom occurs consistently after mid-September and the end of bloom consistently until mid-March in all years. With the more complex parametrization of zooplankton in REcoM-3ZOO, the phenology indicators compare better with the satellite-derived indicators than in REcoM-2. Specifically, the very early bloom start date in August in

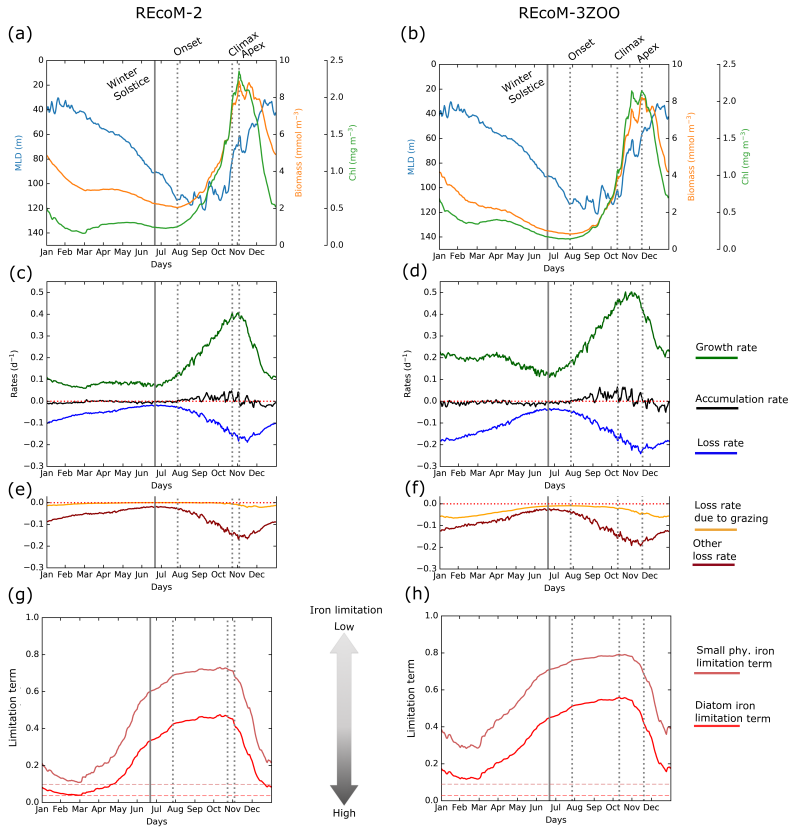

FIGURE 3.10: Seasonal cycles of mixed layer depth (MLD), surface chlorophyll, phytoplankton biomass, growth and loss rates in REcoM-2 (left) and REcoM-3ZOO (right). (a, b) Mixed layer depth (blue), phytoplankton biomass (orange) and chlorophyll (green). (c, d) Growth rate (green), net accumulation rate (black), and loss rates (blue) of phytoplankton. (e, f) Decomposition of phytoplankton loss rates into loss rate due to grazing (orange) and other loss rates (aggregation, respiration, excretion; dark red). (g,h) Iron limitation term affecting phytoplankton growth and horizontal lines show the minimum of the limitation term in REcoM-2 for both phytoplankton groups. Bloom onset, climax, and apex days are indicated as vertical dashed lines. The seasonal cycle was calculated as the average over the last five years of the simulation, from daily model output.

REcoM-2 is delayed to mid-September, and also the bloom end date shifts from early January in REcoM-2 to the end of January in REcoM-3ZOO (Fig. 3.11b).

Role of zooplankton functional types in REcoM-3ZOO: Our results indicate that zooplankton grazing delays the bloom initiation and controls the peak of the bloom. Macrozooplankton grazing is an important component of phytoplankton loss rate throughout the year (Fig. S2). Despite exerting the highest grazing pressure of all zooplankton groups between the winter solstice and bloom onset, the day of bloom onset remains the same in the two model versions (Fig. 3.10). Micro- and mesozooplankton biomass and consequently grazing follow the seasonal cycle of phytoplankton very closely. Therefore, their contributions to phytoplankton loss rates are higher, especially in spring and summer (Fig. S2). Both, but especially the more abundant microzooplankton, control the spring and summer chlorophyll concentrations and phytoplankton biomass in the model.

We identify two distinct roles of zooplankton in the simulated phytoplankton phenology. Firstly, zooplankton affects the duration of the period between climax and apex. Zooplankton grazing prolongs this phase by controlling the magnitude of the spring peak of biomass and

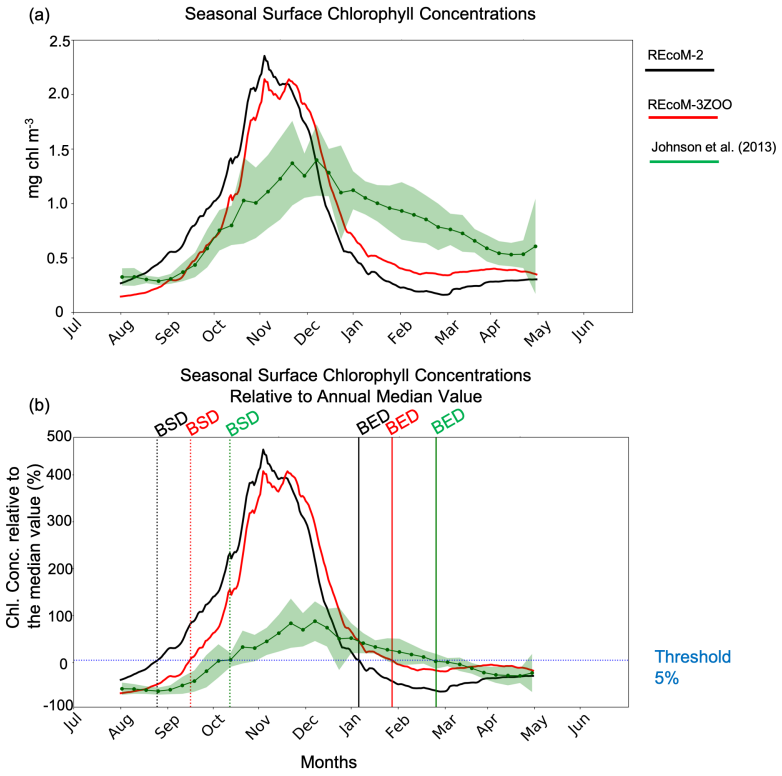

FIGURE 3.11: Comparison of the seasonal cycle of phytoplankton chlorophyll concentrations in two simulations and in a satellite product (2003-2012, *Johnson et al.*, 2013). The seasonal cycle was calculated as the average over the last five years of the simulations, from the daily model output. (a) Seasonal surface chlorophyll concentrations, (b) seasonal surface chlorophyll concentrations relative to the annual median value. The horizontal blue line represents the 5% threshold. The vertical dashed lines are the mean bloom start days (BSD) in REcoM-2 (black), REcoM-3ZOO (red) and in the satellite product (green). Bloom end days (BED) are shown with the solid lines with the same color code.

chlorophyll concentrations (Fig. 3.10a). Secondly, zooplankton prolongs the growing season (apex occurs later) and sustains higher chlorophyll concentrations in summer and autumn (after apex) due to fast nutrient recycling (Fig. 3.11a).

The role of zooplankton in nutrient recycling

Zooplankton grazing is known to be an important phytoplankton loss term that can exert a dominant control over phytoplankton dynamics (Prowe et al., 2012). However, zooplankton does not only affect phytoplankton biomass by grazing, but also by recycling of nutrients such as iron and nitrogen (*Tovar-Sanchez et al.*, 2007; *Alcaraz et al.*, 2010). A portion of the assimilated organic carbon and nitrogen by zooplankton is released as dissolved organic material (*Møller*, 2007; *Saba et al.*, 2009) and comprises an important share of total DOM release (7-80%, *Carlson and Hansell*, 2015). In our simulation, the added nutrient recycling leads to an increase of global net primary production by 25% (Table 3.2). Representing a more complex and realistic grazing and nutrient recycling by zooplankton decreases the biases in nutrient and chlorophyll concentrations (Fig. 3.4, 3.5) Our analysis emphasizes that zooplankton nutrient recycling increases summer chlorophyll concentrations in the Southern Ocean (Fig. 3.11a) and affects

bloom phenology (discussed in section 3). Therefore, our results emphasize the importance of a mechanistic representation of the zooplankton compartment in ocean biogeochemical models.

Zooplankton herbivory partitions the primary production between zooplankton growth, export, and recycled production. Although the global NPP increases substantially by 7.7 Pg C y^{-1} (25%) to 38 Pg C y^{-1} due to nutrient recycling by zooplankton after the parametrization of zooplankton functional types, the total export decreases by 0.5 Pg C y^{-1} (10%) to 4.7 Pg C y^{-1}. Consequently, the export ratio of the modeled ecosystem decreases. This suggests that more carbon and nutrients are retained in the euphotic zone after a more realistic food web representation.

Pathways for nutrient recycling by zooplankton are sloppy feeding, excretory release, and leaching from fecal pellets (*Carlson and Hansell*, 2015). The relative contributions of these different processes and the biological availability of recycled nutrients vary largely, depending on zooplankton body mass and temperature (*Ikeda*, 2014), food quality (*Saba et al.*, 2009), prey size (*Møller*, 2007) or species (*Böckmann et al.*, 2021). In this study, we only consider the effect of total zooplankton biomass and indirectly of temperature (since temperature affects zooplankton grazing and consequently biomass) on nutrient excretion rates. While our results clearly suggest that the zooplankton compartment is more than a top closure term in biogeochemical models, we are only starting to resolve the relevant processes. Further work is required to represent the role of zooplankton for nutrient recycling based on mechanistic process understanding such as effects of food type and quality, prey size, and different species.

In our simulations, micronutrient (iron) recycling emerged as a determining process in the Southern Ocean (Fig. 3.10h). The increased iron availability fuels the phytoplankton growth throughout the year (Fig. 3.10d). In particular, total chlorophyll concentrations between January and May increase due to the weakening of iron limitation in the Southern Ocean (Fig. 3.10b). This finding is supported by the experimentally quantified large iron release by krill (*Tovar-Sanchez et al.*, 2007) and observations of a rapid recycling of particulate iron by copepods (*Laglera et al.*, 2017). In our model, we only consider iron as a limiting micronutrient and the direct iron excretion or leaching fluxes from fecal pellets are converted from nitrogen excretion with a fixed Fe:N ratio. However, a recent study by *Richon and Tagliabue* (2021) showed that micronutrient recycling does not occur in fixed stoichiometric ratios and is further affected by food quality and food quantity. Given its role in sustaining primary production (Fig. 3.5), a more detailed parametrization of zooplankton micronutrient recycling as in *Richon and Tagliabue* (2021) would be well justified.

The role of zooplankton processes in bloom phenology

The Critical Depth Hypothesis proposes that spring phytoplankton blooms are initiated as a consequence of mixed layer depth shoaling and thus triggered by an increase in light availability (*Sverdrup*, 1953). However, *Behrenfeld* (2010) argued that this theory is not sufficient to explain phytoplankton seasonal dynamics. Specifically, the authors proposed in their 'Dilution–Recoupling Hypothesis' that a bloom is initiated when growth rates are larger than loss rates and that a dilution of grazers during maximum winter mixed layer depth reduces grazing pressure to an extent that triggers the start of the spring bloom. Our two numerical experiments are a good example of the importance of the ecosystem structure on phytoplankton bloom dynamics. In the set-up with only one zooplankton group, the start of the spring bloom in the Southern Ocean depends on the increased light availability associated with the shoaling of the mixed layer depth (Sverdrup's 'Critical Depth Hypothesis', Fig. 3.10). In contrast, in the three zooplankton set-up, the spring bloom is initialized when the mixed layer depth is at its maximum (Behrenfeld's 'Dilution–Recoupling Hypothesis').

The carbon accumulation rate-based analysis illustrates that nutrient recycling by zooplankton is an important driver for phytoplankton growth rate in the Southern Ocean (Fig. 3.10b). The growth rate of phytoplankton is higher throughout the year in REcoM-3ZOO compared to REcoM-2 due to the weakening of iron limitation (Fig. 3.10g, h). While summer chlorophyll concentrations increase for both phytoplankton groups due to alleviated iron limitation, winter chlorophyll concentrations decrease due to the enhanced grazing pressure. The magnitude of the spring peak in productivity increases for small phytoplankton and decreases for diatoms due to the higher grazing pressure. These results are in agreement with the key role of zooplankton grazing for determining Southern Ocean phytoplankton biomass (*Le Quéré et al.*, 2016) and phytoplankton composition (*Smetacek et al.*, 2004).

Plankton functional type models generally estimate that the bloom peak occurs earlier than in satellite-based estimates in the Southern Ocean (*Hashioka et al.*, 2013; *Nissen and Vogt*, 2021). In this context, our model results and comparison with satellite data (Fig. 3.11) indicate that early spring blooms could be linked to the weak zooplankton grazing in biogeochemical models. Higher winter grazing rates by zooplankton (Fig. 3.10f) delay the bloom start day by 21 days in our model (Fig. 3.11). Our analysis illustrates that the choice of method on phytoplankton bloom phenology indicators can lead to different conclusions. While the chlorophyll-based threshold method (*Siegel et al.*, 2002) indicates a delay of the bloom start due to grazing, the carbon accumulation rate based analysis vLlort2015 suggests that the bloom onset is unchanged, but grazing prolongs the duration between climax and apex (Fig. 3.10b). Both methods, however, agree on a prolongation of the bloom by zooplankton grazing. Our findings support the previous conclusions by *Prowe et al.* (2012) and *Sailley et al.* (2013) that marine ecosystem models are highly sensitive to zooplankton parametrization.

The spring bloom terminates due to exhaustion of surface nutrients or overgrazing by heterotrophs (*Banse*, 1992, 2002). In the one-zooplankton set-up, we can observe the exhaustion of surface nutrients in early summer, since there is low grazing pressure on phytoplankton. This causes a bloom termination at the beginning of January. When we have three zooplankton types in the system, bloom termination occurs later. Fast nutrient recycling in the system increases summer chlorophyll concentrations, and at the same time zooplankton grazing prevents overuse of the nutrients by phytoplankton. Therefore, chlorophyll concentrations stay close to the threshold value (Fig. 3.11) until the end of May, which is a further indicator of a longer bloom duration.

Implications for biogeochemical modeling

Representation of zooplankton is one of the grand challenges of biogeochemical modeling. This is because the performance of the zooplankton compartment in models is difficult to assess against field observations since the temporal and spatial resolution of the observations does not resemble the models (*Everett et al.*, 2017). Furthermore, its computational cost, uncertainties in parameter estimations, and difficulties of representation of subscale processes such as swarming and vertical migration cause underrepresentation of the zooplankton in the model (*Anderson*, 2005). As a result, the representation of zooplankton groups varies broadly among the models. In the most simplistic models, zooplankton processes are represented implicitly (*Dunne et al.*, 2013), or with only one explicit group (*Ilyina et al.*, 2013). Recently, some models use two or more zooplankton functional groups to represent processes such as grazing, sinking particle formation and nutrient recycling better (*Yool et al.*, 2013; *Aumont et al.*, 2015; *Le Quéré et al.*, 2016; *Stock et al.*, 2020). It is undisputed that realistic parameter choice is the foundation of setting up a useful plankton functional type model (*Anderson*, 2005). In contrast, an unresolved open question in the ocean biogeochemical modeling community is how much complexity should

be represented in a model and whether the added value justifies the additional computational costs (*Anderson*, 2005; *Le Quéré*, 2006; *Friedrichs et al.*, 2007; *Kriest et al.*, 2010; *Kwiatkowski et al.*, 2014). On the one hand, a comparison of twelve models with different numbers of PFTs showed that models with more multiple plankton functional types are more suitable for simulating ecosystems in different environments ('portability') than simpler models (*Friedrichs et al.*, 2007). On the other hand, results from *Kwiatkowski et al.* (2014) and *Kriest et al.* (2010) suggest that lower biological complexity implies less biases in comparison to global nutrient or oxygen data sets. However, *Xiao and Friedrichs* (2014) found that simple models with only a single zooplankton size class may reproduce observed data fields by using unrealistic parameters. In agreement with these authors, we show that our implementation of multiple zooplankton functional groups provides the needed flexibility to choose parameters realistically and leads to reduced model-data mismatch with respect to to global patterns of nutrients and chlorophyll, (i.e., similar metrics as used in *Kwiatkowski et al.* (2014) and *Kriest et al.* (2010)). With the advent of the MAREDAT data compilations (*Buitenhuis et al.*, 2010; *Moriarty and O'Brien*, 2013; *Moriarty et al.*, 2013), three zooplankton groups can now be reasonably simulated. In addition, we demonstrate that metrics that go beyond global nutrient and chlorophyll patterns, such as regional phytoplankton phenology can add additional insights and provide support for a representation of multiple zooplankton functional types. Correctly representing these processes is important for robust projections of how marine ecosystem changes respond to environmental change. For the next step-change in plankton functional type modeling, robust observation-based constraints on process rates are needed. This holds true for the zooplankton processes that are traditionally considered (nutrient excretion, sloppy feeding, fecal pellet production, etc.), but also extends beyond these, for example for diel vertical migration, food quality, life cycle (*Steinberg and Landry*, 2017).

Our results confirm that model results are sensitive to the zooplankton parameterization as shown previously (*Prowe et al.*, 2012; *Mitra et al.*, 2014; *Laufkötter et al.*, 2016). Going beyond these previous studies, we show that high zooplankton biomass can lead to either an increase in phytoplankton concentration due to nutrient recycling or a decrease due to high grazing pressure. In addition, the increase of zooplankton biomass does not directly translate into more grazing loss of phytoplankton in the model (e.g., between 20°N and 20°S, Figs. 3.6, 3.7). Temperature dependencies of grazing parameters of zooplankton play an important role in determining the grazing loss of phytoplankton (Fig. 3.9). This result clearly emphasizes the importance of using robust data-driven process formulations and temperature dependencies to capture the delicate balance between zooplankton processes that enhance or reduce phytoplankton growth and biomass in the models. Therefore, it will be important to get more observations for evaluating the underlying processes.

Implementing multiple zooplankton functional types in biogeochemical models provides the flexibility to assign different parameter values for different zooplankton groups (*Séférian et al.*, 2020). When the zooplankton compartment is represented by only one group, grazing and nutrient recycling by zooplankton are not adequately represented on the global scale (Fig. 3.7). When parameterizing multiple zooplankton functional types, these processes are better captured, with more realistic ecosystem interactions. We demonstrated that increasing the complexity and zooplankton process representation in FESOM-RecoM not only increases understanding of the interactions of the ecosystem, but also practically provides better agreement with observations. This can be a gradual change such as a decrease of the positive bias in DIN concentration in the subtropical Pacific and a reduction of the surface chlorophyll concentration bias in the Arctic (Fig. 3.5), but also a substantial change and a better agreement with observations as seen in the seasonal cycle of phytoplankton chlorophyll in the Southern Ocean (Fig. 3.11).

While models capture the mean surface chlorophyll concentrations within reasonable bounds, the processes behind similar results can be very different. Our case study on the Southern Ocean phytoplankton bloom phenology also illustrates such a case. The annual mean surface chlorophyll concentrations are similar in two different simulations except for the Arctic (Fig. 3.5). However, the seasonal cycle of chlorophyll concentrations differs between the two simulations (Fig. 3.11). Our results emphasize that phytoplankton bloom phenology is sensitive to the representation of zooplankton grazing and nutrient recycling.

Zooplankton is generally treated as a top closure term in ocean biogeochemical models (*Edwards and Yool*, 2000), which causes underestimation of predation of potential competitors among zooplankton (*Mitra*, 2009). In REcoM-3ZOO, this ecological interaction is represented to some extent with predation of meso- and macrozooplankton on microzooplankton. However, the mortality terms for macrozooplankton (and mesozooplankton in temperate regions) are still the top closure terms. REcoM-2 and REcoM-3ZOO do not account for the interaction between zooplankton and larger predators such as fish, birds and mammals. In both model versions, we mimic the predation by higher trophic levels with the mortality term of the zooplankton groups, which remains an unavoidable simplification.

CONCLUSION

In conclusion, representing new zooplankton functional types in an ocean biogeochemical model has a strong impact on the seasonal dynamics of phytoplankton, food web structure, and elemental cycles. Our results highlight the importance of zooplankton micronutrient recycling for global primary production and bloom duration and end date in the Southern Ocean. In addition, zooplankton grazing controls the bloom start day, thus supporting the Dilution-Recoupling hypothesis (*Behrenfeld*, 2010) and the magnitude of the spring peak. To represent the main functions of nutrient recycling, grazing, and sinking particulate organic carbon production (fecal pellets) by zooplankton in the global ocean, it is essential that biogeochemical models represent more than one zooplankton group.

BIBLIOGRAPHY

Alcaraz, M., R. Almeda, A. Calbet, E. Saiz, C. M. Duarte, S. Lasternas, S. Agustí, R. Santiago, J. Movilla, and A. Alonso (2010), The role of arctic zooplankton in biogeochemical cycles: respiration and excretion of ammonia and phosphate during summer, *Polar Biology*, *33*(12), 1719–1731, doi:10.1007/s00300-010-0789-9.

Anderson, T. R. (2005), Plankton functional type modelling: running before we can walk?, *Journal of Plankton Research*, *27*(11), 1073-1081, doi:10.1093/plankt/fbi076.

Anderson, T. R., D. O. Hessen, A. Mitra, D. J. Mayor, and A. Yool (2013), Sensitivity of secondary production and export flux to choice of trophic transfer formulation in marine ecosystem models, *Journal of Marine Systems*, *125*, 41–53, doi:10.1016/j.jmarsys.2012.09.008.

Archibald, K. M., D. A. Siegel, and S. C. Doney (2019), Modeling the Impact of Zooplankton Diel Vertical Migration on the Carbon Export Flux of the Biological Pump, *Global Biogeochemical Cycles*, *33*(2), 181–199, doi:10.1029/2018GB005983.

Atkinson, A., B. Meyer, D. Stuübing, W. Hagen, K. Schmidt, and U. V. Bathmann (2002), Feeding and energy budgets of Antarctic krill *Euphausia superba* at the onset of winter-II. Juveniles and adults, *Limnology and Oceanography*, *47*(4), 953–966, doi:10.4319/lo.2002.47.4.0953.

Atkinson, A., R. S. Shreeve, A. G. Hirst, P. Rothery, G. A. Tarling, D. W. Pond, R. E. Korb, E. J. Murphy, and J. L. Watkins (2006), Natural growth rates in Antarctic krill (*Euphausia superba*): II. Predictive models based on food, temperature, body length, sex, and maturity stage, *Limnology and Oceanography*, *51*(2), 973–987, doi:10.4319/lo.2006.51.2.0973.

Atkinson, A., K. Schmidt, S. Fielding, S. Kawaguchi, and P. A. Geissler (2012), Variable food absorption by Antarctic krill: Relationships between diet, egestion rate and the composition and sinking rates of their fecal pellets, *Deep-Sea Research Part II: Topical Studies in Oceanography*, *59-60*(January), 147–158, doi:10.1016/j.dsr2.2011.06.008.

Aumont, O., C. Ethé, A. Tagliabue, L. Bopp, and M. Gehlen (2015), PISCES-v2: An ocean biogeochemical model for carbon and ecosystem studies, *Geoscientific Model Development*, *8*(8), 2465–2513, doi:10.5194/gmd-8-2465-2015.

Banse, K. (1992), Grazing, temporal changes of phytoplankton concentrations, and the microbial loop in the open sea, doi:10.1007/978-1-4899-0762-2_22.

Banse, K. (1994), Grazing and Zooplankton Production as Key Controls of Phytoplankton Production in the Open Ocean, *Oceanography*, *7*(1), 13–20, doi:10.5670/oceanog.1994.10.

Banse, K. (2002), Steemann Nielsen and the zooplankton, *Hydrobiologia*, *480*, 15–28, doi:10.1023/A:1021220714899.

Banse, K. (2013), Reflections about chance in my career, and on the top-down regulated world, *Annual Review of Marine Science*, *5*, 1–19, doi:10.1146/annurev-marine-121211-172359.

Behrenfeld, M. J. (2010), Abandoning Sverdrup's critical depth hypothesis on phytoplankton blooms, *Ecology*, *91*(4), 977–989, doi:10.1890/09-1207.1.

Behrenfeld, M. J., and E. S. Boss (2018), Student's tutorial on bloom hypotheses in the context of phytoplankton annual cycles, *Global Change Biology*, *24*(1), 55-77, doi:10.1111/gcb.13858.

Behrenfeld, M. J., and P. G. Falkowski (1997), Photosynthetic rates derived from satellite-based chlorophyll concentration, *Limnology and Oceanography*, *42*(1), 1-20, doi:10.4319/lo.1997.42.1.0001.

Behrenfeld, M. J., S. C. Doney, I. Lima, E. S. Boss, and D. A. Siegel (2013), Annual cycles of ecological disturbance and recovery underlying the subarctic Atlantic spring plankton bloom, *Global Biogeochemical Cycles*, *27*(2), 526–540, doi:10.1002/gbc.20050.

Böckmann, S., F. Koch, B. Meyer, F. Pausch, M. Iversen, R. Driscoll, L. M. Laglera, C. Hassler, and S. Trimborn (2021), Salp fecal pellets release more bioavailable iron to Southern Ocean phytoplankton than krill fecal pellets, *Current Biology*, *31*(13), 2737–2746.e3, doi:10.1016/j.cub.2021.02.033.

Buitenhuis, E., C. Le Quéré, O. Aumont, G. Beaugrand, A. Bunker, A. Hirst, T. Ikeda, T. O'Brien, S. Piontkovski, and D. Straile (2006), Biogeochemical fluxes through mesozooplankton, *Global Biogeochemical Cycles*, *20*(2), doi:10.1029/2005GB002511.

Buitenhuis, E., R. B. Rivkin, S. Séailley, and C. Le Quéré (2010), Biogeochemical fluxes through microzooplankton, *Global Biogeochemical Cycles*, *24*(4), doi:10.1029/2009GB003601.

Buitenhuis, E., T. Hashioka, and C. L. Quéré (2013), Combined constraints on global ocean primary production using observations and models, *Global Biogeochemical Cycles*, *27*(3), 847-858, doi:10.1002/gbc.20074.

Butzin, M., and H. O. Pörtner (2016), Thermal growth potential of Atlantic cod by the end of the 21st century, *Global Change Biology*, *22*(12), 4162–4168, doi:10.1111/gcb.13375.

Calbet, A. (2001), Mesozooplankton grazing effect on primary production: A global comparative analysis in marine ecosystems, *Limnology and Oceanography*, *46*(7), 1824-1830, doi:10.4319/lo.2001.46.7.1824.

Calbet, A. (2008), The trophic roles of microzooplankton in marine systems, *ICES Journal of Marine Science*, *65*(3), 325-331, doi:10.1093/icesjms/fsn013.

Calbet, A., and M. R. Landry (1999), Mesozooplankton influences on the microbial food web: Direct and indirect trophic interactions in the oligotrophic open ocean, *Limnology and Oceanography*, *44*(6), 1370-1380, doi:10.4319/lo.1999.44.6.1370.

Calbet, A., and M. R. Landry (2004), Phytoplankton growth, microzooplankton grazing, and carbon cycling in marine systems, *Limnology and Oceanography*, *49*(1), 51-57, doi:10.4319/lo.2004.49.1.0051.

Carlson, C. A., and D. A. Hansell (2015), Chapter 3 - DOM Sources, Sinks, Reactivity, and Budgets, in *Biogeochemistry of Marine Dissolved Organic Matter (Second Edition)*, edited by D. A. Hansell and C. A. Carlson, second edition ed., pp. 65–126, Academic Press, Boston, doi:10.1016/B978-0-12-405940-5.00003-0.

Carr, M.-E., M. A. Friedrichs, M. Schmeltz, M. Noguchi Aita, D. Antoine, K. R. Arrigo, I. Asanuma, O. Aumont, R. Barber, M. Behrenfeld, R. Bidigare, E. T. Buitenhuis, J. Campbell, A. Ciotti, H. Dierssen, M. Dowell, J. Dunne, W. Esaias, B. Gentili, W. Gregg, S. Groom, N. Hoepffner, J. Ishizaka, T. Kameda, C. Le Quéré, S. Lohrenz, J. Marra, F. Mélin, K. Moore, A. Morel, T. E. Reddy, J. Ryan, M. Scardi, T. Smyth, K. Turpie, G. Tilstone, K. Waters, and Y. Yamanaka (2006), A comparison of global estimates of marine primary production from ocean color, *Deep Sea Research Part II: Topical Studies in Oceanography*, *53*(5), 741-770, doi:10.1016/j.dsr2.2006.01.028, the US JGOFS Synthesis and Modeling Project: Phase III.

Cavan, E. L., A. Belcher, A. Atkinson, S. L. Hill, S. Kawaguchi, S. McCormack, B. Meyer, S. Nicol, L. Ratnarajah, K. Schmidt, D. K. Steinberg, G. A. Tarling, and P. W. Boyd (2019), The importance of Antarctic krill in biogeochemical cycles, *Nature Communications*, *10*(1), 1–13, doi:10.1038/s41467-019-12668-7.

Chenillat, F., P. Rivière, and M. D. Ohman (2021), On the sensitivity of plankton ecosystem models to the formulation of zooplankton grazing, *Plos One*, *16*(5), e0252033, doi:10.1371/journal.pone.0252033.

Coello-Camba, A., M. Llabrés, C. M. Duarte, and S. Agustí (2017a), Zooplankton excretion metabolites stimulate southern ocean phytoplankton growth, *Polar Biology*, *40*(10), 2035–2045, doi:10.1007/s00300-017-2123-2.

Coello-Camba, A., M. Llabrés, C. M. Duarte, and S. Agustí (2017b), Zooplankton excretion metabolites stimulate Southern Ocean phytoplankton growth, *Polar Biology*, *40*(10), 2035–2045, doi:10.1007/s00300-017-2123-2.

Dunne, J. P., J. L. Sarmiento, and A. Gnanadesikan (2007), A synthesis of global particle export from the surface ocean and cycling through the ocean interior and on the seafloor, *Global Biogeochemical Cycles*, *21*(4), doi:10.1029/2006GB002907.

Dunne, J. P., J. G. John, E. Shevliakova, R. J. Stouffer, J. P. Krasting, S. L. Malyshev, P. C. D. Milly, L. T. Sentman, A. J. Adcroft, W. Cooke, K. A. Dunne, S. M. Griffies, R. W. Hallberg, M. J. Harrison, H. Levy, A. T. Wittenberg, P. J. Phillips, and N. Zadeh (2013), GFDL's ESM2 Global Coupled Climate–Carbon Earth System Models. Part II: Carbon System Formulation and Baseline Simulation Characteristics, *Journal of Climate*, *26*(7), 2247 - 2267, doi:10.1175/JCLI-D-12-00150.1.

Edwards, A. M., and A. Yool (2000), The role of higher predation in plankton population models, *Journal of Plankton Research*, *22*(6), 1085-1112, doi:10.1093/plankt/22.6.1085.

Everett, J. D., M. E. Baird, P. Buchanan, C. Bulman, C. Davies, R. Downie, C. Griffiths, R. Heneghan, R. J. Kloser, L. Laiolo, A. Lara-Lopez, H. Lozano-Montes, R. J. Matear, F. McEnnulty, B. Robson, W. Rochester, J. Skerratt, J. A. Smith, J. Strzelecki, I. M. Suthers, K. M. Swadling, P. van Ruth, and A. J. Richardson (2017), Modeling what we sample and sampling what we model: Challenges for zooplankton model assessment, *Frontiers in Marine Science*, *4*, 77, doi:10.3389/fmars.2017.00077.

Fach, B. A., E. E. Hofmann, and E. J. Murphy (2002), Modeling studies of Antarctic Krill *Euphausia superba* survival during transport across the Scotia Sea, *Marine Ecology Progress Series*, *231*, 187–203, doi:10.3354/meps231187.

Fasham, M. J., H. W. Ducklow, and S. M. McKelvie (1990), A nitrogen-based model of plankton dynamics in the oceanic mixed layer, *Journal of Marine Research*, *48*(3), 591–639, doi:10.1357/002224090784984678.

Friedrichs, M. A. M., J. A. Dusenberry, L. A. Anderson, R. A. Armstrong, F. Chai, J. R. Christian, S. C. Doney, J. Dunne, M. Fujii, R. Hood, D. J. McGillicuddy Jr., J. K. Moore, M. Schartau, Y. H. Spitz, and J. D. Wiggert (2007), Assessment of skill and portability in regional marine biogeochemical models: Role of multiple planktonic groups, *Journal of Geophysical Research: Oceans*, *112*(C8), doi:10.1029/2006JC003852.

Froneman, P., and R. Perissinotto (1996), Microzooplankton grazing in the southern ocean: Implications for the carbon cycle, *Marine Ecology*, *17*(1-3), 99-115, doi:10.1111/j.1439-0485.1996.tb00493.x.

Frost, B. W. (1987), Grazing control of phytoplankton stock in the open subarctic Pacific Ocean: a model assessing the role of mesozooplankton, particularly the large calanoid copepods Neocalanus spp, *Marine Ecology Progress Series*, *39*(1), 49–68.

Frost, B. W. (1991), The role of grazing in nutrient-rich areas of the open sea, *Limnology and Oceanography*, *36*(8), 1616–1630, doi:10.4319/lo.1991.36.8.1616.

Frost, B. W. (1993), A modelling study of processes regulating plankton standing stock and production in the open subarctic Pacific Ocean, *Progress in Oceanography*, *32*(1-4), 17–56, doi:10.1016/0079-6611(93)90008-2.

Garcia, R. Locarnini, T. P. Boyer, J. I. Antonov, O. K. Baranova, M. M. Zweng, J. R. Reagan, and D. R. Johnson (2013), World Ocean Atlas 2013 Volume 4 : Nutrients (phosphate , nitrate , silicate), *NOAA Atlas NESDIS 76*, *4*(September), 396.

Garcia, K. Weathers, C. Paver, I. Smolyar, T. Boyer, R. Locarnini, M. Zweng, A. Mishonov, O. Baranova, D. Seidov, and J. Reagan (2018), World Ocean Atlas 2018. Volume 4: Dissolved Inorganic Nutrients (phosphate, nitrate and nitrate+nitrite, silicate), *NOAA Atlas NESDIS 84*, *84*(July), 35.

Gasol, J. M., P. A. Del Giorgio, and C. M. Duarte (1997), Biomass distribution in marine planktonic communities, *Limnology and Oceanography*, *42*(6), 1353–1363, doi:10.4319/lo.1997.42.6.1353.

Geider, R. J., H. L. MacIntyre, and T. M. Kana (1998), A dynamic regulatory model of phytoplanktonic acclimation to light, nutrients, and temperature, *Limnology and Oceanography*, *43*(4), 679-694, doi:10.4319/lo.1998.43.4.0679.

Gowing, M. M., and M. W. Silver (1985), Minipellets: A new and abundant size class of marine fecal pellets, *Journal of Marine Research*, *43*(2), 395-418, doi:doi:10.1357/002224085788438676.

Griffies, S. M., A. Biastoch, C. Böning, F. Bryan, G. Danabasoglu, E. P. Chassignet, M. H. England, R. Gerdes, H. Haak, R. W. Hallberg, W. Hazeleger, J. Jungclaus, W. G. Large, G. Madec, A. Pirani, B. L. Samuels, M. Scheinert, A. S. Gupta, C. A. Severijns, H. L. Simmons, A. M. Treguier, M. Winton, S. Yeager, and J. Yin (2009), Coordinated Ocean-ice Reference Experiments (COREs), *Ocean Modelling*, *26*(1), 1-46, doi:10.1016/j.ocemod.2008.08.007.

Hansen, B., P. K. Bjornsen, and P. J. Hansen (1994), The size ratio between planktonic predators and their prey, *Limnology and Oceanography*, *39*(2), 395-403, doi:10.4319/lo.1994.39.2.0395.

Hashioka, T., M. Vogt, Y. Yamanaka, C. Le Quéré, E. T. Buitenhuis, M. N. Aita, S. Alvain, L. Bopp, T. Hirata, I. Lima, S. Sailley, and S. C. Doney (2013), Phytoplankton competition during the spring bloom in four plankton functional type models, *Biogeosciences*, *10*(11), 6833–6850, doi:10.5194/bg-10-6833-2013.

Hauck, J., C. Völker, T. Wang, M. Hoppema, M. Losch, and D. A. Wolf-Gladrow (2013), Seasonally different carbon flux changes in the Southern Ocean in response to the southern annular mode, *Global Biogeochemical Cycles*, *27*(4), 1236–1245, doi:10.1002/2013GB004600.

Henson, S. A., J. P. Dunne, and J. L. Sarmiento (2009), Decadal variability in North Atlantic phytoplankton blooms, *Journal of Geophysical Research: Oceans*, *114*(4), 1–11, doi:10.1029/2008JC005139.

Henson, S. A., R. Sanders, E. Madsen, P. J. Morris, F. Le Moigne, and G. D. Quartly (2011), A reduced estimate of the strength of the ocean's biological carbon pump, *Geophysical Research Letters*, *38*(4), doi:10.1029/2011GL046735.

Hernández-León, S., C. Fraga, and T. Ikeda (2008), A global estimation of mesozooplankton ammonium excretion in the open ocean, *Journal of Plankton Research*, *30*(5), 577-585, doi:10.1093/plankt/fbn021.

Hofmann, E. E., and C. M. Lascara (2000), Modeling the growth dynamics of Antarctic krill *Euphausia superba*, *Marine Ecology Progress Series*, *194*, 219–231, doi:10.3354/meps194219.

Hood, R. R., E. A. Laws, R. A. Armstrong, N. R. Bates, C. W. Brown, C. A. Carlson, F. Chai, S. C. Doney, P. G. Falkowski, R. A. Feely, M. A. Friedrichs, M. R. Landry, J. Keith Moore, D. M. Nelson, T. L. Richardson, B. Salihoglu, M. Schartau, D. A. Toole, and J. D. Wiggert (2006), Pelagic functional group modeling: Progress, challenges and prospects, *Deep-Sea Research Part II: Topical Studies in Oceanography*, *53*(5-7), 459–512, doi:10.1016/j.dsr2.2006.01.025.

Ikeda, T. (2014), Respiration and ammonia excretion by marine metazooplankton taxa: synthesis toward a global-bathymetric model, *Marine Biology*, *161*(12), 2753–2766, doi:10.1007/s00227-014-2540-5.

Ilyina, T., K. D. Six, J. Segschneider, E. Maier-Reimer, H. Li, and I. Núñez-Riboni (2013), Global ocean biogeochemistry model HAMOCC: Model architecture and performance as component of the MPI-Earth system model in different CMIP5 experimental realizations, *Journal of Advances in Modeling Earth Systems*, *5*(2), 287-315, doi:10.1029/2012MS000178.

Johnson, R., P. G. Strutton, S. W. Wright, A. McMinn, and K. M. Meiners (2013), Three improved satellite chlorophyll algorithms for the Southern Ocean, *Journal of Geophysical Research: Oceans*, *118*(7), 3694-3703, doi:10.1002/jgrc.20270.

Karakuş, O., C. Völker, M. Iversen, W. Hagen, D. Wolf-Gladrow, B. Fach, and J. Hauck (2021), Modeling the Impact of Macrozooplankton on Carbon Export Production in the Southern Ocean, *Journal of Geophysical Research: Oceans*, *126*(12), doi:10.1029/2021JC017315.

Kiorboe, T. (1997), Population regulation and role of mesozooplankton in shaping marine pelagic food webs, *Hydrobiologia*, *363*, 13–27, doi:10.1023/A:1003173721751.

Kobayashi, S., Y. Ota, Y. Harada, A. Ebita, M. Moriya, H. Onoda, K. Onogi, H. Kamahori, C. Kobayashi, H. Endo, K. Miyaoka, and T. Kiyotoshi (2015), The JRA-55 reanalysis: General specifications and basic characteristics, *Journal of the Meteorological Society of Japan*, *93*(1), 5–48, doi:10.2151/jmsj.2015-001.

Kriest, I., S. Khatiwala, and A. Oschlies (2010), Towards an assessment of simple global marine biogeochemical models of different complexity, *Progress in Oceanography*, *86*(3), 337-360, doi:10.1016/j.pocean.2010.05.002.

Kulk, G., T. Platt, J. Dingle, T. Jackson, B. F. Jönsson, H. A. Bouman, M. Babin, R. J. W. Brewin, M. Doblin, M. Estrada, F. G. Figueiras, K. Furuya, N. González-Benítez, H. G. Gudfinnsson, K. Gudmundsson, B. Huang, T. Isada, . Kovač, V. A. Lutz, E. Marañón, M. Raman, K. Richardson, P. D. Rozema, W. H. v. d. Poll, V. Segura, G. H. Tilstone, J. Uitz, V. v. Dongen-Vogels, T. Yoshikawa, and S. Sathyendranath (2020), Primary production, an index of climate change in the ocean: Satellite-based estimates over two decades, *Remote Sensing*, *12*(5), doi:10.3390/rs12050826.

Kwiatkowski, L., A. Yool, J. I. Allen, T. R. Anderson, R. Barciela, E. T. Buitenhuis, M. Butenschön, C. Enright, P. R. Halloran, C. Le Quéré, L. De Mora, M. F. Racault, B. Sinha, I. J. Totterdell, and P. M. Cox (2014), IMarNet: An ocean biogeochemistry model intercomparison project within a common physical ocean modelling framework, *Biogeosciences*, *11*(24), 7291–7304, doi:10.5194/bg-11-7291-2014.

Laglera, L. M., A. Tovar-Sánchez, M. Iversen, H. González, H. Naik, G. Mangesh, P. Assmy, C. Klaas, M. Mazzocchi, M. Montresor, S. Naqvi, V. Smetacek, and D. Wolf-Gladrow (2017), Iron partitioning during LOHAFEX: Copepod grazing as a major driver for iron recycling in the Southern Ocean, *Marine Chemistry*, *196*, 148-161, doi:10.1016/j.marchem.2017.08.011.

Landry, M. R., and A. Calbet (2004), Microzooplankton production in the oceans, *ICES Journal of Marine Science*, *61*(4), 501-507, doi:10.1016/j.icesjms.2004.03.011.

Laufkötter, C., M. Vogt, N. Gruber, O. Aumont, L. Bopp, S. C. Doney, J. P. Dunne, J. Hauck, J. G. John, I. D. Lima, R. Seferian, and C. Völker (2016), Projected decreases in future marine export production: The role of the carbon flux through the upper ocean ecosystem, *Biogeosciences*, *13*(13), 4023–4047, doi:10.5194/bg-13-4023-2016.

Lauvset, S. K., R. M. Key, A. Olsen, S. Van Heuven, A. Velo, X. Lin, C. Schirnick, A. Kozyr, T. Tanhua, M. Hoppema, S. Jutterström, R. Steinfeldt, E. Jeansson, M. Ishii, F. F. Perez, T. Suzuki, and S. Watelet (2016), A new global interior ocean mapped climatology: The 1° x 1° GLODAP version 2, *Earth System Science Data*, *8*(2), 325–340, doi:10.5194/essd-8-325-2016.

Le Quéré, C., E. T. Buitenhuis, R. Moriarty, S. Alvain, O. Aumont, L. Bopp, S. Chollet, C. Enright, D. J. Franklin, R. J. Geider, S. P. Harrison, A. G. Hirst, S. Larsen, L. Legendre, T. Platt, I. C. Prentice, R. B. Rivkin, S. Sailley, S. Sathyendranath, N. Stephens, M. Vogt, and S. M. Vallina (2016), Role of zooplankton dynamics for Southern Ocean phytoplankton biomass and global biogeochemical cycles, *Biogeosciences*, *13*(14), 4111–4133, doi:10.5194/bg-13-4111-2016.

Le Quéré, C. (2006), Reply to Horizons Article 'Plankton functional type modelling: running before we can walk' Anderson (2005): I. Abrupt changes in marine ecosystems?, *Journal of Plankton Research*, *28*(9), 871-872, doi:10.1093/plankt/fbl014.

Le Quéré, C., S. P. Harrison, I. Colin Prentice, E. T. Buitenhuis, O. Aumont, L. Bopp, H. Claustre, L. Cotrim Da Cunha, R. Geider, X. Giraud, C. Klaas, K. E. Kohfeld, L. Legendre, M. Manizza, T. Platt, R. B. Rivkin, S. Sathyendranath, J. Uitz, A. J. Watson, and D. Wolf-Gladrow (2005), Ecosystem dynamics based on plankton functional types for global ocean biogeochemistry models, *Global Change Biology*, *11*(11), 2016-2040, doi:10.1111/j.1365-2486.2005.1004.x.

Leblanc, K., J. Arístegui, L. Armand, P. Assmy, B. Beker, A. Bode, E. Breton, V. Cornet, J. Gibson, M.-P. Gosselin, E. Kopczynska, H. Marshall, J. Peloquin, S. Piontkovski, A. J. Poulton, B. Quéguiner, R. Schiebel, R. Shipe, J. Stefels, M. A. van Leeuwe, M. Varela, C. Widdicombe, and M. Yallop (2012), A global diatom database – abundance, biovolume and biomass in the world ocean, *Earth System Science Data*, *4*(1), 149–165, doi:10.5194/essd-4-149-2012.

Lee, K. (2001), Global net community production estimated from the annual cycle of surface water total dissolved inorganic carbon, *Limnology and Oceanography*, *46*(6), 1287-1297, doi:10.4319/lo.2001.46.6.1287.

Llort, J., M. Lévy, J.-B. Sallée, and A. Tagliabue (2015), Onset, intensification, and decline of phytoplankton blooms in the Southern Ocean, *ICES Journal of Marine Science*, *72*(6), 1971-1984, doi:10.1093/icesjms/fsv053.

Meyer, B., V. Fuentes, C. Guerra, K. Schmidt, A. Atkinson, S. Spahic, B. Cisewski, U. Freier, A. Olariaga, and U. Bathmann (2009), Physiology, growth, and development of larval krill *Euphausia superba* in autumn and winter in the Lazarev Sea, Antarctica, *Limnology and Oceanography*, *54*(5), 1595–1614, doi:10.4319/lo.2009.54.5.1595.

Mitra, A. (2009), Are closure terms appropriate or necessary descriptors of zooplankton loss in nutrient-phytoplankton-zooplankton type models?, *Ecological Modelling*, *220*(5), 611–620, doi:10.1016/j.ecolmodel.2008.12.008.

Mitra, A., C. Castellani, W. C. Gentleman, S. H. Jónasdóttir, K. J. Flynn, A. Bode, C. Halsband, P. Kuhn, P. Licandro, M. D. Agersted, A. Calbet, P. K. Lindeque, R. Koppelmann, E. F. Møller, A. Gislason, T. G. Nielsen, and M. St. John (2014), Bridging the gap between marine biogeochemical and fisheries sciences; configuring the zooplankton link, *Progress in Oceanography*, *129*(PB), 176–199, doi:10.1016/j.pocean.2014.04.025.

Møller, E. F. (2007), Production of dissolved organic carbon by sloppy feeding in the copepods Acartia tonsa, Centropages typicus, and Temora longicornis, *Limnology and Oceanography*, *52*(1), 79–84, doi:10.4319/lo.2007.52.1.0079.

Montagnes, D. J., and A. Fenton (2012), Prey-abundance affects zooplankton assimilation efficiency and the outcome of biogeochemical models, *Ecological Modelling*, *243*, 1-7, doi: 10.1016/j.ecolmodel.2012.05.006.

Morales, C. (1987), Carbon and nitrogen content of copepod faecal pellets: effect of food concentration and feeding behavior, *Marine Ecology Progress Series*, *36*, 107–114, doi:10.3354/mepso36107.

Moriarty, R., and T. D. O'Brien (2013), Distribution of mesozooplankton biomass in the global ocean, *Earth System Science Data*, *5*(1), 45–55, doi:10.5194/essd-5-45-2013.

Moriarty, R., E. T. Buitenhuis, and C. Le Quéré (2013), Distribution of known macrozooplankton abundance and biomass in the global ocean, *Earth System Science Data*, *5*(2), 241–257, doi: 10.5194/essd-5-241-2013.

Mullin, M. M. (1963), Some factors affecting the feeding of marine copepods of the genus calanus, *Limnology and Oceanography*, *8*(2), 239-250, doi:10.4319/lo.1963.8.2.0239.

Nissen, C., and M. Vogt (2021), Factors controlling the competition between *Phaeocystis* and diatoms in the Southern Ocean and implications for carbon export fluxes, *Biogeosciences*, *18*(1), 251–283, doi:10.5194/bg-18-251-2021.

Prowe, A., M. Pahlow, S. Dutkiewicz, M. Follows, and A. Oschlies (2012), Top-down control of marine phytoplankton diversity in a global ecosystem model, *Progress in Oceanography*, *101*(1), 1–13, doi:10.1016/j.pocean.2011.11.016.

Racault, M. F., C. Le Quéré, E. Buitenhuis, S. Sathyendranath, and T. Platt (2012), Phytoplankton phenology in the global ocean, *Ecological Indicators*, *14*(1), 152–163, doi:10.1016/j.ecolind.2011.07.010.

Richon, C., and A. Tagliabue (2021), Biogeochemical feedbacks associated with the response of micronutrient recycling by zooplankton to climate change, *Global Change Biology*, *27*(19), 4758-4770, doi:10.1111/gcb.15789.

Roy, S., R. P. Harris, and S. A. Poulet (1989), Inefficient feeding by Calanus helgolandicus and Temora longicornis on Coscinodiscus wailesii : quantitative estimation using chlorophyll-type pigments and effects on dissolved free amino acids, *Marine Ecology Progress Series*, *52*, 145–153. doi:10.3354/mepso52145.

Saba, G. K., D. K. Steinberg, and D. A. Bronk (2009), Effects of diet on release of dissolved organic and inorganic nutrients by the copepod Acartia tonsa, *Marine Ecology Progress Series*, *386*, 147–161, doi:10.3354/mepso8070.

Sailley, S., M. Vogt, S. Doney, M. Aita, L. Bopp, E. Buitenhuis, T. Hashioka, I. Lima, C. Le Quéré, and Y. Yamanaka (2013), Comparing food web structures and dynamics across a suite of global marine ecosystem models, *Ecological Modelling*, *261-262*, 43-57, doi:10.1016/j.ecolmodel.2013.04.006.

Sathyendranath, S., R. J. Brewin, C. Brockmann, V. Brotas, B. Calton, A. Chuprin, P. Cipollini, A. B. Couto, J. Dingle, R. Doerffer, C. Donlon, M. Dowell, A. Farman, M. Grant, S. Groom, A. Horseman, T. Jackson, H. Krasemann, S. Lavender, V. Martinez-Vicente, C. Mazeran, F. Mélin, T. S. Moore, D. Müller, P. Regner, S. Roy, C. J. Steele, F. Steinmetz, J. Swinton, M. Taberner, A. Thompson, A. Valente, M. Zühlke, V. E. Brando, H. Feng, G. Feldman, B. A. Franz, R. Frouin, R. W. Gould, S. B. Hooker, M. Kahru, S. Kratzer, B. G. Mitchell, F. E.

Muller-Karger, H. M. Sosik, K. J. Voss, J. Werdell, and T. Platt (2019), An Ocean-Colour Time Series for Use in Climate Studies: The Experience of the Ocean-Colour Climate Change Initiative (OC-CCI), *Sensors*, *19*(19), doi:10.3390/s19194285.

Schlitzer, R. (2004), Export production in the Equatorial and North Pacific derived from dissolved oxygen, nutrient and carbon data, *Journal of Oceanography*, *60*(1), 53–62, doi:10.1023/B:JOCE.0000038318.38916.e6.

Schmidt, K., A. Atkinson, D. W. Pond, and L. C. Irel (2014), Feeding and overwintering of Antarctic Krill across its major habitats: The role of sea ice cover, water depth, and phytoplankton abundance, *Limnology and Oceanography*, *59*(1), 17–36, doi:10.4319/lo.2014.59.1.0017.

Schmoker, C., S. Hernández-León, and A. Calbet (2013), Microzooplankton grazing in the oceans: impacts, data variability, knowledge gaps and future directions, *Journal of Plankton Research*, *35*(4), 691-706, doi:10.1093/plankt/fbt023.

Schourup-Kristensen, V., D. Sidorenko, D. A. Wolf-Gladrow, and C. Völker (2014), A skill assessment of the biogeochemical model REcoM2 coupled to the Finite Element Sea Ice–Ocean Model (FESOM 1.3), *Geoscientific Model Development*, *7*(6), 2769–2802, doi:10.5194/gmd-7-2769-2014.

Séférian, R., S. Berthet, A. Yool, J. Palmiéri, L. Bopp, A. Tagliabue, L. Kwiatkowski, O. Aumont, J. Christian, J. Dunne, M. Gehlen, T. Ilyina, J. G. John, H. Li, M. C. Long, J. Y. Luo, H. Nakano, A. Romanou, J. Schwinger, C. Stock, Y. Santana-Falcón, Y. Takano, J. Tjiputra, H. Tsujino, M. Watanabe, T. Wu, F. Wu, and A. Yamamoto (2020), Tracking Improvement in Simulated Marine Biogeochemistry Between CMIP5 and CMIP6, *Current Climate Change Reports*, *6*(3), 95–119, doi:10.1007/s40641-020-00160-0.

Sidorenko, D., Q. Wang, S. Danilov, and J. Schröter (2011), FESOM under coordinated ocean-ice reference experiment forcing, *Ocean Dynamics*, *61*(7), 881–890, doi:10.1007/s10236-011-0406-7.

Sieburth, J. M., V. Smetacek, and J. Lenz (1978), Pelagic ecosystem structure: Heterotrophic compartments of the plankton and their relationship to plankton size fractions, *Limnology and Oceanography*, *23*(6), 1256-1263, doi:10.4319/lo.1978.23.6.1256.

Siegel, D. A., S. C. Doney, and J. A. Yoder (2002), The North Atlantic Spring Phytoplankton Bloom and Sverdrup's Critical Depth Hypothesis, *Science*, *296*(5568), 730–733, doi:10.1126/science.1069174.

Siegel, D. A., K. O. Buesseler, S. C. Doney, S. F. Sailley, M. J. Behrenfeld, and P. W. Boyd (2014), Global assessment of ocean carbon export by combining satellite observations and food-web models, *Global Biogeochemical Cycles*, *28*(3), 181-196, doi:10.1002/2013GB004743.

Smetacek, V. (1998), Diatoms and the silicate factor, *Nature*, *391*(6664), 224–225, doi:10.1038/34528.

Smetacek, V., P. Assmy, and J. Henjes (2004), The role of grazing in structuring Southern Ocean pelagic ecosystems and biogeochemical cycles, *Antarctic Science*, *16*(4), 541–558, doi:10.1017/S0954102004002317.

Soppa, M. A., C. Völker, and A. Bracher (2016), Diatom phenology in the Southern Ocean: Mean patterns, trends and the role of climate oscillations, *Remote Sensing*, *8*(5), 1–17, doi:10.3390/rs8050420.

Steinberg, D. K., and M. R. Landry (2017), Zooplankton and the Ocean Carbon Cycle, *Annual Review of Marine Science*, *9*(1), 413–444, doi:10.1146/annurev-marine-010814-015924.

Stock, C. A., J. P. Dunne, S. Fan, P. Ginoux, J. John, J. P. Krasting, C. Laufkötter, F. Paulot, and N. Zadeh (2020), Ocean Biogeochemistry in GFDL's Earth System Model 4.1 and Its Response to Increasing Atmospheric CO_2, *Journal of Advances in Modeling Earth Systems*, *12*(10), doi:10.1029/2019MS002043.

Sverdrup, H. U. (1953), On Conditions for the Vernal Blooming of Phytoplankton, *ICES Journal of Marine Science*, *18*(3), 287-295, doi:10.1093/icesjms/18.3.287.

Taylor, K. E. (2001), Summarizing multiple aspects of model performance in a single diagram, *Journal of Geophysical Research: Atmospheres*, *106*(D7), 7183-7192, doi:10.1029/2000JD900719.

Tovar-Sanchez, A., C. M. Duarte, S. Hernández-León, and S. A. Sañudo-Wilhelmy (2007), Krill as a central node for iron cycling in the southern ocean, *Geophysical Research Letters*, *34*(11), doi:10.1029/2006GL029096.

Turner, J. T. (2002), Zooplankton fecal pellets, mrine snow and sinking phytoplankton blooms., *Aquatic Microbial Ecology*, *27*, 57–102, doi:10.3354/Ame027057.

Turner, J. T. (2015), Zooplankton fecal pellets, marine snow, phytodetritus and the ocean's biological pump, *Progress in Oceanography*, *130*, 205–248, doi:10.1016/j.pocean.2014.08.005.

Verity, P. G. (1985), Grazing, respiration, excretion, and growth rates of tintinnids, *Limnology and Oceanography*, *30*(6), 1268-1282, doi:10.4319/lo.1985.30.6.1268.

Wang, Q., S. Danilov, D. Sidorenko, R. Timmermann, C. Wekerle, X. Wang, T. Jung, and J. Schröter (2014), The Finite Element Sea Ice-Ocean Model (FESOM) v.1.4: formulation of an ocean general circulation model, *Geoscientific Model Development*, *7*(2), 663–693, doi:10.5194/gmd-7-663-2014.

Ward, B. A., S. Dutkiewicz, O. Jahn, and M. J. Follows (2012), A size-structured food-web model for the global ocean, *Limnology and Oceanography*, *57*(6), 1877-1891, doi:10.4319/lo.2012.57.6.1877.

Westberry, T., M. J. Behrenfeld, D. A. Siegel, and E. Boss (2008), Carbon-based primary productivity modeling with vertically resolved photoacclimation, *Global Biogeochemical Cycles*, *22*(2), doi:10.1029/2007GB003078.

Wright, R. M., C. Le Quéré, E. Buitenhuis, S. Pitois, and M. Gibbons (2020), Unique role of jellyfish in the plankton ecosystem revealed using a global ocean biogeochemical model, *Biogeosciences Discussions*, pp. 1–43, doi:10.5194/bg-2020-136.

Xiao, Y., and M. A. M. Friedrichs (2014), Using biogeochemical data assimilation to assess the relative skill of multiple ecosystem models in the mid-atlantic bight: effects of increasing the complexity of the planktonic food web, *Biogeosciences*, *11*(11), 3015–3030, doi:10.5194/bg-11-3015-2014.

Yool, A., E. E. Popova, and T. R. Anderson (2013), MEDUSA-2.0: an intermediate complexity biogeochemical model of the marine carbon cycle for climate change and ocean acidification studies, *Geoscientific Model Development*, *6*(5), 1767–1811, doi:10.5194/gmd-6-1767-2013.

SUPPLEMENTAL MATERIAL

Contents of this file

1. Implementation of zooplankton functional types in REcoM.
2. Figure 3.S1: Temperature functions for micro- and mesozooplankton and prey dependent grazing efficiency for the mesozooplankton group.
3. Figure 3.S2: Temperature function for the macrozooplankton group.
4. Table 3.S4: Microzooplankton and mesozooplankton parameters in REcoM-3ZOO.
5. Table 3.S5: Macrozooplankton parameters in REcoM-3ZOO.

INTRODUCTION

This Appendix presents a full description of zooplankton groups in the REcoM-3ZOO model, a global marine biogeochemical model with two phytoplankton classes. In the model, there are three zooplankton functional types (zPFTs) which are parametrized as micro-, meso- and macrozooplankton.

MICRO- AND MESOZOOPLANKTON BIOMASS

In this section, we describe microzooplankton and mesozooplankton. The temporal evolution of zooplankton concentrations Z_i (i = micro, meso) in REcoM-3ZOO are described as follows:

$$\underbrace{\frac{dN_{Z_i}}{dt}}_{\text{nitrogen pool}} = \underbrace{G_{Z_i} \cdot \gamma_{Z_i}}_{\text{grazing}} - \underbrace{\epsilon^N_{Z_i} \cdot N_{Z_i}}_{\text{excretion}} - \underbrace{m_{Z_i} \cdot N^2_{Z_i}}_{\text{mortality}} - \underbrace{f_{N_{Z_i}} \cdot G_{Z_i}}_{\text{fecal pellet}} \tag{3.4}$$

$$\underbrace{\frac{dC_{Z_i}}{dt}}_{\text{carbon pool}} = \underbrace{(\sum_{i,j} \frac{1}{q_j} \cdot G^j_{Z_i}) \cdot \gamma_{Z_i}}_{\text{grazing}} - \underbrace{\frac{1}{q_{Z_i}} \cdot m_{Z_i} \cdot N^2_{Z_i}}_{\text{mortality}} - \underbrace{\epsilon^C_{Z_i} \cdot C_{Z_i}}_{\text{excretion}} - \underbrace{r^0_{Z_i} \cdot c^T_{Z_i} \cdot C_{Z_i}}_{\text{respiration}} - \underbrace{f_{C_{Z_i}} \cdot G_{C_{Z_i}}}_{\text{fecal pellet}} \tag{3.5}$$

In Equation 3.4, the grazing efficiency (assimilation efficiency) γ determines the fraction of the total grazing (G_{Z_i}, Eq. 3.7) by the zooplankton groups (micro- or mesozooplankton) that are converted into their biomass. Excretion by zooplankton is determined by the excretion rate constant $\epsilon^C_{Z_i}$ and is proportional to the biomass N_{Z_i}. The mortality of the zooplankton groups is described by a quadratic term of the concentration N_{Z_i} and the mortality rate constant ($m_{Z_i} \cdot N^2_{Z_i}$). The fecal pellet production rate is described as a function of the total grazing G_{Z_i} and the fecal pellet production rate constant ($f_{N_{Z_i}}$) that determines how much of the grazing flux is transferred into the detritus nitrogen pool. Since the fecal pellet production is not defined for microzooplankton, the parameter $f_{N_{Z_i}}$ is assigned 0 (Table 3.S4).

Equation 3.5 describes the sources and sinks of the zooplankton carbon pool. Zooplankton grazing of each food source ($G^j_{Z_i}$, j= each food source) is converted to carbon units by using the respective intracellular N:C ratios (q_j) of each food source. The quadratic mortality is converted to carbon by using the intracellular $N : C$ ratio of zooplankton (q_{Z_i}). The excretion rate constant ($\epsilon^C_{Z_i}$) determines dissolved organic carbon excretion. The respiration rate is calculated from a respiration rate constant at 0°C ($r^0_{Z_i}$) and increases with temperature. The temperature

dependence is an exponential function (f(T), Eq. 3.6) where x (c_{Z_i} for respiration) is a base that determines the slope of the increase with temperature (T, °C). The fecal pellet production rate constant ($f_{C_{Z_i}}$) and the grazing rate in carbon units $G_{C_{Z_i}}$ together determine the fecal pellet production rate. Since the fecal pellet production is not defined for microzooplankton, the parameter $f_{C_{Z_i}}$ is assigned 0 (Table 3.S4).

$$f(T) = x^T \tag{3.6}$$

$$G_{Z_i} = \varepsilon^0_{Z_i} \cdot \frac{(\sum_k p_k \cdot N_k)^2}{\sigma^2_{Z_i} + (\sum_k p_k \cdot N_k)^2} \cdot b^T_{Z_i} \cdot N_{Z_i}. \tag{3.7}$$

The grazing rate of each group (G_{Z_i}) is the product of the grazing rate constant at 0° ($\varepsilon^0_{Z_i}$), the Holling Type III ingestion formula (total food $\sum_k p_k \cdot N_k$ and half saturation constant σ_{Z_i}), each zooplankton group's nitrogen biomass(N_{Z_i}) and a temperature function. The temperature dependence is an exponential function (Eq. 3.6) where x (b_{Z_i} for grazing) is a base that determines the slope of the increase with temperature (T, °C).

The relative grazing preferences (p_k) are calculated for each group following *Fasham et al.* (1990). The term p'_k determines the initial grazing preferences of zooplankton to different food sources (e.g., for microzooplankton k=small phytoplankton, diatom, Table 3.S4).

$$p_k = \frac{p'_k \cdot N_k}{\sum_i p'_k \cdot N_k} \tag{3.8}$$

The initial grazing efficiency of the mesozooplankton group (γ_{meso}) is 0.8 at P=0 and decreases with increasing prey abundance (Eq. 3.9, Fig. 3.S2c, *Montagnes and Fenton*, 2012).

$$\gamma_{meso} = 0.3 + \frac{1}{(0.2 * P + 2)} \tag{3.9}$$

Table 3.S4 lists all the parameter values for the microzooplankton and mesozooplankton groups.

MACROZOOPLANKTON BIOMASS

The macrozooplankton group is parameterized based on the characteristics of Antarctic krill and is described in *Karakuş et al.* (2021). It is also defined by the two-state variables nitrogen (N_{macro}) and carbon (C_{macro}) as shown in differential equations 3.10 and 3.11. For simplicity, *macro* subscript is left out from parameter symbols in the equations 3.10 and 3.11. Grazing is the single source for macrozooplankton biomass and mortality, excretion, respiration, and fecal pellet production are the loss terms.

$$\underbrace{\frac{dN_{macro}}{dt}}_{\text{nitrogen pool}} = \underbrace{G \cdot \gamma}_{\text{grazing}} - \underbrace{m \cdot N^2_{macro}}_{\text{mortality}} - \underbrace{\epsilon^N \cdot N_{macro}}_{\text{excretion}} - \underbrace{f_N \cdot G}_{\text{fecal pellet}} \tag{3.10}$$

$$\underbrace{\frac{dC_{macro}}{dt}}_{\text{carbon pool}} = \underbrace{(\sum_{i,j} \frac{1}{q_j} \cdot G^j) \cdot \gamma}_{\text{grazing}} - \underbrace{\frac{1}{q} \cdot m \cdot N^2_{macro}}_{\text{mortality}} - \underbrace{\epsilon^C \cdot C_{macro}}_{\text{excretion}} - \underbrace{r \cdot C_{macro}}_{\text{respiration}} - \underbrace{f_C \cdot G_C}_{\text{fecal pellet}} \tag{3.11}$$

Grazing of the macrozooplankton group is also described by the Holling type III ingestion function (Eq. 3.12) on microzooplankton, mesozooplankton, diatom, small phytoplankton, and

both detritus classes using the relative grazing preferences (Eq. 3.8) by *Fasham et al.* (1990). The grazing rate of each group (G) is the product of the maximum grazing rate constant (ε), the Holling Type III ingestion formula (total food $\sum_k p_k \cdot N_k$ and half saturation constant σ), macrozooplankton nitrogen biomass (N_{macro}) and a temperature function (f_{Temp}).

$$G = \varepsilon \cdot \frac{(\sum_k p_k \cdot N_k)^2}{\sigma^2 + (\sum_k p_k \cdot N_k)^2} \cdot f_{Temp} \cdot N_{macro} \tag{3.12}$$

Macrozooplankton grazing varies with temperature. The following parameterization is applied (Eq. 3.13 *Butzin and Pörtner*, 2016),

$$f_{Temp}(T) = \frac{\exp(\frac{Q_a}{T_r} - \frac{Q_a}{T})}{1 + \exp(\frac{Q_h}{T_h} - \frac{Q_h}{T})} \tag{3.13}$$

where T (K) is absolute temperature, two parameters T_r and T_h represent the intrinsic optimum temperatures for development. Inhibitive processes dominate outside this temperature window. Q_a and Q_h are the temperatures for the uninhibited and inhibited reaction kinetics, respectively (*Butzin and Pörtner*, 2016). The parameter values were chosen as $T_r = 272.5$ K, $T_h = 274.5$ K, $Q_a = 28145$ K, and $Q_h = 105234$ K to represent the temperature sensitivity of daily growth rates with the maximum growth of krill occurring at 0.5°C as described in *Atkinson et al.* (2006).

The grazing efficiency (assimilation efficiency) γ determines the fraction of total grazing (G, Eq. 3.12) by macrozooplankton that is converted into macrozooplankton biomass (Eqs. 3.10, 3.11). The mortality rate constant m is set to 0.3% per day (*Fach et al.*, 2002) in a quadratic formulation (Eq. 3.10). Fecal pellet production rate constants (f_C and f_N) were set to 29% and 13% to be consistent with the observed high C:N ratio of around 13 in krill fecal pellets (*Atkinson et al.*, 2012). The excretion rate constant (ϵ^C) of dissolved organic carbon and nitrogen is taken as 2% per day from *Atkinson et al.* (2002). The daily respiration rate constant (r) of macrozooplankton in the model depends on the season and grazing activity and a standard respiration rate (R_s, Eq. 3.14, *Hofmann and Lascara*, 2000). The term respiration activity factor (R_a) accounts for reduced krill respiration rates in winter. R_a is set to -0.5 from Julian day 150 through 250 (southern hemisphere winter) which represents a 50% metabolic reduction. The feeding activity factor (R_f) represents the metabolic cost of feeding activity and depends on the daily ratio of grazing flux to carbon biomass of macrozooplankton. It increases linearly from 0 to 1 for a daily grazing to biomass ratio between 0 and 10%, and remains constant at 1 for ratios above 10%. The standard respiration rate (R_s) is set to 1% per day (*Hofmann and Lascara*, 2000).

$$r = R_s \cdot (1 + R_f + R_a) \tag{3.14}$$

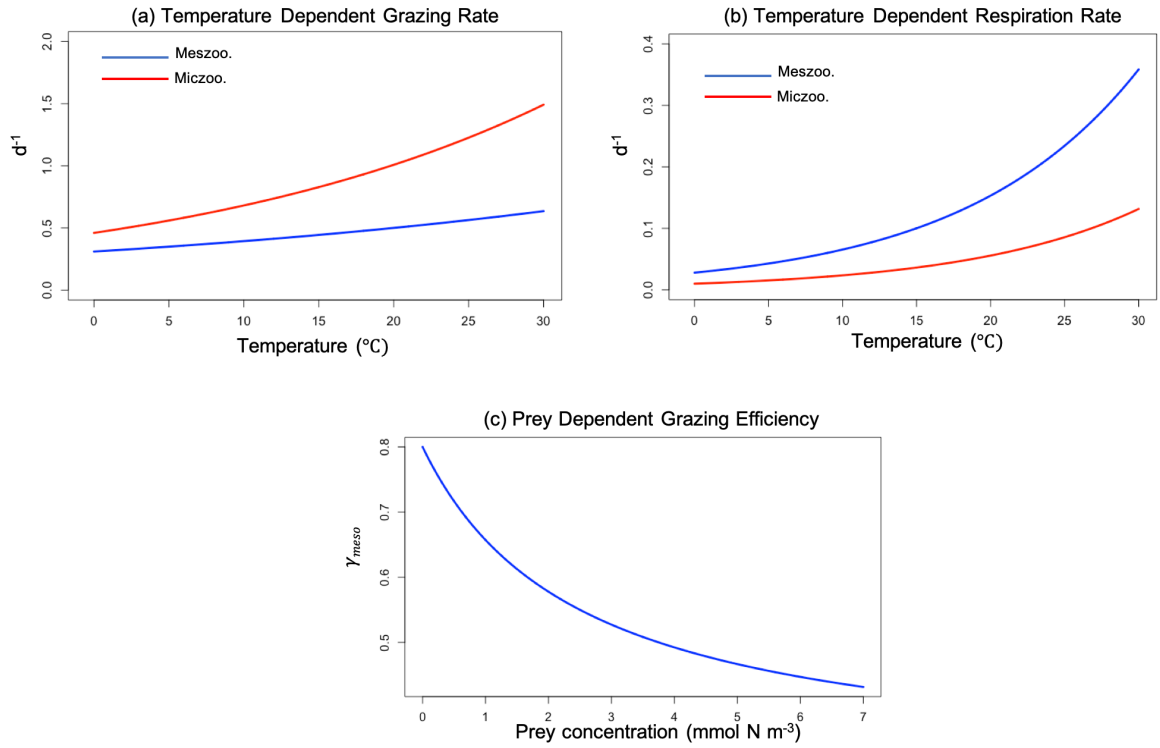

FIGURE 3.S1: Temperature functions for micro and mesozooplankton, prey dependent grazing efficiency for the mesozooplankton group: (a) Temperature-dependent grazing rate microzooplankton (red) and mesozooplankton (blue), (b) temperature-dependent respiration rate microzooplankton (red) and mesozooplankton(blue) (c) Varying grazing efficiency for the mesozooplankton group.

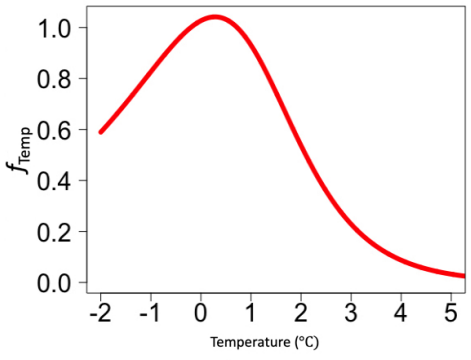

FIGURE 3.S2: Exponential temperature function (dimensionless) adapted from *Butzin and Pörtner* (2016) for macrozooplankton grazing (see Eq. 3.13) with an optimum temperature for macrozooplankton growth at 0.5°C (*Atkinson et al.*, 2006).

Parameter (Unit)	Symbol	Micro.	Meso.	Reference
Maximum grazing rate constant at 0 °C (d^{-1})	$\varepsilon^0_{Z_i}$	0.46	0.31	*Le Quéré et al.* (2016)
Grazing efficiency (dimensionless)	γ_{Z_i}	0.8	0.8*	*Le Quéré et al.* (2016)
Grazing temp. dep.	b_{Z_i}	1.04	1.0242	*Le Quéré et al.* (2016)
Half saturation constant (mmol N m^{-3})	σ_{Z_i}	0.8	0.3	*Yool et al.* (2013)
Respiration rate constant o°C (d^{-1})	$r^0_{Z_i}$	0.01	0.028	*Le Quéré et al.* (2016)
Respiration temp. dep.	c_{Z_i}	1.0887	1.0897	*Le Quéré et al.* (2016)
Mortality rate constant ((mmol N m^{-3})$^{-1}$ d^{-1})	m_{Z_i}	0.01	0.04	*Le Quéré et al.* (2016)
N excretion rate constant (d^{-1})	$\epsilon^N_{Z_i}$	0.05	0.1	—
C excretion rate constant (d^{-1})	$\epsilon^C_{Z_i}$	0.05	0.1	—
Initial grazing preference on diatom	p'_d	0.5	1	—
Initial grazing preference on small-phy.	p'_n	1	0.5	—
Initial grazing preference on microzoo.	p'_h	—	1	—
Initial grazing preference on detritus groups	p'_{de}	—	0.5	—
N fecal pellet production rate constant (d^{-1})	f_{N_i}	0	0.25	—
C fecal pellet production rate constant (d^{-1})	f_{C_i}	0	0.32	—

* It decreases with increasing prey abundance Eq. 3.9.

TABLE 3.S4: Microzooplankton and mesozooplankton parameters in REcoM-3ZOO. All temperature dependent rate constants (grazing and respiration) are given for 0°C.

Parameter (Unit)	Symbol	Value	Reference
Maximum grazing rate constant (d^{-1})	ε	0.1	*Hofmann and Lascara* (2000)
Grazing efficiency (dimensionless)	γ	0.8	*Fach et al.* (2002)
Half saturation constant (mmol N m^{-3})	σ	0.12	*Meyer et al.* (2009)
Respiration rate constant (d^{-1})	r	0.01	*Hofmann and Lascara* (2000)
Mortality rate constant ((mmol N $m^{-3})^{-1}$ d^{-1})	m	0.003	*Fach et al.* (2002)
N excretion rate constant (d^{-1})	ϵ^N	0.02	*Atkinson et al.* (2002)
C excretion rate constant (d^{-1})	ϵ^C	0.02	*Atkinson et al.* (2002)
Initial grazing preference on diatom	p'_d	1	—
Initial grazing preference on small-phy.	p'_n	0.5	—
Initial grazing preference on zooplankton	p'_h	0.8	—
Initial grazing preference on detritus groups	p'_{de}	0.5	—
N fecal pellet production rate constant (d^{-1})	f_N	0.13	—
C fecal pellet production rate constant (d^{-1})	f_C	0.295	—

TABLE 3.S5: Macrozooplankton parameters in REcoM-3ZOO

4

PUBLICATION III

THE ROLE OF BALLASTING, SEAWATER VISCOSITY AND OXYGEN FOR CARBON EXPORT AND TRANSFER EFFICIENCIES IN THE GLOBAL OCEAN

to be submitted to Global Biogeochemical Cycles

THE ROLE OF BALLASTING, SEAWATER VISCOSITY AND OXYGEN FOR CARBON EXPORT AND TRANSFER EFFICIENCIES IN THE GLOBAL OCEAN

Onur Karakuş[1], Cara Nissen[1], Wilhelm Hagen[3], Morten Iversen[1,2], Christoph Völker[1], Özgür Gürses[1], Judith Hauck[1]

[1] Alfred-Wegener-Institut, Helmholtz-Zentrum für Polar- und Meeresforschung, Am Handelshafen 12, 27570 Bremerhaven, Germany

[2] MARUM and University of Bremen, Leobener Strasse 8, 28359 Bremen, Germany

[3] University of Bremen, BreMarE and MARUM, P.O. Box 33 04 40, 28334 Bremen, Germany

ABSTRACT

The flux of particulate organic carbon (POC) from the euphotic zone to the deep ocean plays an essential role in the global carbon cycle. The efficiency of this flux is evaluated generally by the metrics 'export efficiency' and 'transfer efficiency.' While export efficiency summarizes both the particulate organic carbon formation and its sinking from the euphotic zone, transfer efficiency illustrates the carbon sequestration efficiency of the system. Only limited observations of both metrics are available, and there is thus considerable interest in using biogeochemical models to analyze large-scale patterns. This study aims to assess the global spatial distribution of export and transfer efficiencies. In particular, we analyze the impact of ballast minerals, seawater viscosity, and oxygen-dependent remineralization, which are often not considered in biogeochemical models, on carbon export and transfer efficiencies. Therefore, we implemented a new sinking routine describing the effects of the processes mentioned above on the sinking speeds and remineralization rates of the particulate organic matter into the ocean biogeochemical model REcoM. The globally integrated POC flux across the euphotic zone varies between 4.7 and 5 Pg C yr^{-1} depending on the inclusion of the processes in the model. Our results show that the global mean export efficiency across the euphotic depth stays similar (13.7±0.2%) whether or not the effects of seawater viscosity, mineral ballasting, and oxygen-dependent remineralization were included in the model. However, the global mean carbon transfer efficiency is more sensitive and varies between 25% and 32% in the different simulations. Our results highlight that ballast minerals increase aggregate settling velocity and were more efficient in increasing transfer efficiency than both seawater viscosity and decreased remineralization due to oxygen limitations. In the model, high export efficiency only co-occurred with high transfer efficiency when zooplankton fecal pellets had a substantial contribution to the export flux.

INTRODUCTION

The ocean's biological carbon pump (BCP) describes the flux of dissolved and particulate organic carbon from the euphotic to the mesopelagic zone and from there to the deep ocean, the bathypelagic zone (*Volk and Hoffert*, 1985). It plays a significant role in the global carbon cycle, as without it, the atmospheric CO_2 concentration would be 200 ppm higher than the actual concentrations (*Parekh et al.*, 2006). Net primary production (NPP) by marine phytoplankton accounts for half of the global net primary production (*Field et al.*, 1998) and forms the base of BCP. A part of this organic material is transferred to secondary producers that graze on phytoplankton and is assimilated into their biomass (*Steinberg and Landry*, 2017). Another portion of carbon rains out from the euphotic zone (*Boyd et al.*, 2019), and only a fraction of

biogenic carbon (less than 20%) reaches the deep ocean (>1000 m *Passow and Carlson*, 2012; *Omand et al.*, 2020). The amount of carbon reaching the deep ocean depends on multiple factors, such as the remineralization of particles by bacteria (*Iversen and Ploug*, 2010; *Buchan et al.*, 2014; *Belcher et al.*, 2016) plankton composition (*Turner*, 2015; *Cavan et al.*, 2015), fragmentation of particles by zooplankton (*Giering et al.*, 2020) and density of the particles (*Klaas and Archer*, 2002; *Iversen and Robert*, 2015). The density of particles increases due to different minerals such as calcium carbonate, opal, and lithogenic material, which consequently enhances the sinking speed of particles and reduces the time for remineralization (*Armstrong et al.*, 2001b; *Klaas and Archer*, 2002). The strength of the BCP is often measured as the fraction of carbon reaching the mesopelagic and deep ocean, and it can be assessed using two metrics: export and transfer efficiencies (*Buesseler et al.*, 2020).

The first metric, 'export efficiency (e-ratio)' is defined as the ratio between the export flux and primary production and represents the fraction of NPP that is exported out of the euphotic zone. Many studies tried to explain patterns of export efficiency as a function of physical and biological boundary conditions with partially contradictory results. Previous studies suggested a negative relationship between e-ratio and sea surface temperature (*Laws et al.*, 2000, 2011) or a positive relationship between the e-ratio and net primary production (*Dunne et al.*, 2005; *Henson et al.*, 2011). The global pattern was explained by empirical equations that depend on SST and chlorophyll concentrations (e.g., *Dunne et al.*, 2005) or on sea surface temperature (SST) and NPP (e.g., *Laws et al.*, 2011; *Henson et al.*, 2011). In contrast, *Siegel et al.* (2014) illustrated that the fraction of microphytoplankton biovolume anomaly can explain the patterns of the e-ratio in the global ocean, with a high fraction of microphytoplankton being associated with high e-ratios. Other exceptions in the relations between NPP, SST, and e-ratio were reported on a regional scale. For example, *Maiti et al.* (2013) found that the e-ratio is negatively correlated with NPP in the high southern latitudes, and the relation with SST is weak. Furthermore, recent studies found that opal (silica)-induced ballasting is a key process that may determine carbon export and e-ratio in the Southern Ocean (*Britten et al.*, 2017; *Arteaga et al.*, 2018). *Henson et al.* (2019) described that the high export efficiency is rather related to the low abundance of macrozooplankton and bacteria or high mesozooplankton biomass than to the phytoplankton community composition. Besides the observational and experimental studies, biogeochemical models are used to analyze the global pattern and the drivers of the e-ratio. Previously, *Laufkötter et al.* (2016) showed that e-ratio at a fixed depth horizon of 100 m differs strongly between four three-dimensional ocean biogeochemical models (REcoM-2 (*Hauck et al.*, 2013), BEC (*Moore et al.*, 2013), TOPAZ (*Dunne et al.*, 2013), and PISCES (*Aumont and Bopp*, 2006)) due to the different parametrizations of plankton functional types and processes among the models. In addition, *Henson et al.* (2015) used the ocean biogeochemical model MEDUSA to investigate larger-scale patterns of the e-ratio at a fixed 100 m depth horizon. Models generally predict high (15-25%) e-ratio in the high latitudes and low e-ratio towards the equator (*Henson et al.*, 2015; *Laufkötter et al.*, 2016). Recent findings show that the modeled e-ratio is sensitive to the chosen depth horizon, and the global e-ratio varies between 12 and 14.6% dependent on the choice of different depth horizons (euphotic depth, mixed layer depth, or fixed 100 m, *Palevsky and Doney* (2018)). These different choices of depth horizons are not only a technical detail, but may decide whether processes are clearly separated from each other or not. For example, evaluating export at the base of euphotic depth separates the processes that produce particulate organic carbon from the region below where the remineralization happens and are often used in observational studies (e.g., *Buesseler and Boyd*, 2009; *Siegel et al.*, 2016; *Palevsky and Doney*, 2018).

The second metric, 'transfer efficiency (T_{eff})' is the ratio between the sequestration flux (i.e., the flux at 1000 m, or sometimes at 2000 m) and the export flux at a reference depth

(e.g., euphotic depth, fixed 100 m) and it provides information about the carbon sequestration efficiency of the system (*Buesseler et al.*, 2020). Here, the 'sequestration flux' defines the sinking of biogenic carbon to the deep ocean (>1000 m, *Lampitt et al.*, 2008; *Passow and Carlson*, 2012). The T_{eff} varies spatially, but different patterns were proposed. *Henson et al.* (2012) found high T_{eff} in low latitudes (>20%) and low T_{eff} (<5%) in the Southern Ocean, based on Th-based export observations of transfer efficiency. In contrast, *Weber et al.* (2016) deduced low T_{eff} in the subtropics (5%) and high T_{eff} (25%) in the high latitudes from deep ocean nutrient concentrations and an ocean inverse model. Possible explanations for this difference are collection biases of sediment traps or analytical errors associated with the Th-based export observations (*Weber et al.*, 2016). Similar to the export ratio, T_{eff} also depends on ballast minerals (*Weber et al.*, 2016), temperature due to its enhancing effect on remineralization (*Iversen and Ploug*, 2013) and oxygen (*Devol and Hartnett*, 2001). The relative importance of all these factors is an area of intense research. For example, *Marsay et al.* (2015) illustrated that a warmer mesopelagic zone could cause a decrease in the transfer efficiency and consequently reduce carbon (CO_2) storage in the ocean. *Henson et al.* (2012) emphasized that ecosystem structure is the key factor that controls the T_{eff}. Although biogeochemical models are rarely used to analyze the transfer efficiency, *Maerz et al.* (2020) showed a high transfer efficiency of particulate organic carbon in high latitudes, the Equatorial Pacific, and the Indian Ocean after detailed parametrization of marine aggregates in a global ocean biogeochemical model. *Cram et al.* (2018) found a strong influence of temperature and particle size on T_{eff} by using a one-dimensional particle model, and *Laufkötter et al.* (2017) illustrated the strong effect of the influence of oxygen-dependent remineralization on the T_{eff} in the Tropical Pacific.

Mirroring the current state of research on carbon export fluxes, export efficiency, and transfer efficiency from field studies, simulations of these properties in the biogeochemical models are associated with high uncertainty. Currently, Earth System Models do not agree on the magnitude and the direction of the evolution of export flux by 2100 (*Henson et al.*, 2022). The authors assessed potentially important processes (e.g., zooplankton vertical migration, particle stickiness) for the export fluxes that are currently not represented in the models. According to this assessment, omitting the seawater viscosity (*Taucher et al.*, 2014) effect on particle sinking likely causes a positive bias in present-day export estimates, while omitting mineral ballasting (*Wilson et al.*, 2012; *Le Moigne et al.*, 2014) is expected to lead to a negative bias. Further, not considered oxygen-dependent remineralization (*Devol and Hartnett*, 2001; *Laufkötter et al.*, 2017) would also lead to a positive bias of present-day estimates of export flux. In summary, ten out of nineteen models that were analysed and compared by Henson et al. 2020 include oxygen-dependent, but only five include ballast minerals, and only one model accounts for seawater viscosity.

This paper revisits the spatial patterns and physical and biological drivers of export and transfer efficiencies in the global ocean by using a biogeochemical model. To this end, we use for the first time a modified version of the one-dimensional particle model that is proposed by *Cram et al.* (2018) in a three-dimensional ocean biogeochemical model to answer the following questions: (1) To what extent are the e-ratio and T_{eff} affected by the parametrization of mineral ballasting, seawater viscosity, and oxygen-dependent remineralization?, (2) Is high export efficiency an indicator of high transfer efficiency?.

MATERIALS AND METHODS

Description of the Ocean Biogeochemical Model FESOM-REcoM

In this study, we use the global ocean general circulation model FESOM-1.4 (*Wang et al.*, 2014) coupled to the biogeochemical model REcoM-3ZOO (see *Publication II*) that builds on the previous version REcoM-2 (*Schourup-Kristensen et al.*, 2014; *Hauck et al.*, 2013; *Karakuş et al.*, 2021). FESOM-1.4 uses a finite element method to solve primitive equations on an unstructured mesh which allows for high resolution in areas that are more dynamic than others (*Sidorenko et al.*, 2011; *Wang et al.*, 2014). The version of REcoM-3ZOO used here consists of two phytoplankton classes (small phytoplankton and diatoms) and three zooplankton functional types (micro-, meso- and macrozooplankton, see *Publication II*). REcoM-3ZOO is a medium complexity ocean biogeochemical model resolving carbonate chemistry and the cycling of the nutrients dissolved inorganic nitrogen, silicic acid, and iron. REcoM-3ZOO applies varying cellular stoichiometry for diatoms (N:C:Chl:Si) and small phytoplankton (N:C:Chl) after *Geider et al.* (1998). In the current version of REcoM-2, sinking particulate organic carbon (sPOC) is divided into two pools: one slow-sinking and one fast-sinking detritus group (for a more detailed description see *Karakuş et al.*, 2021).

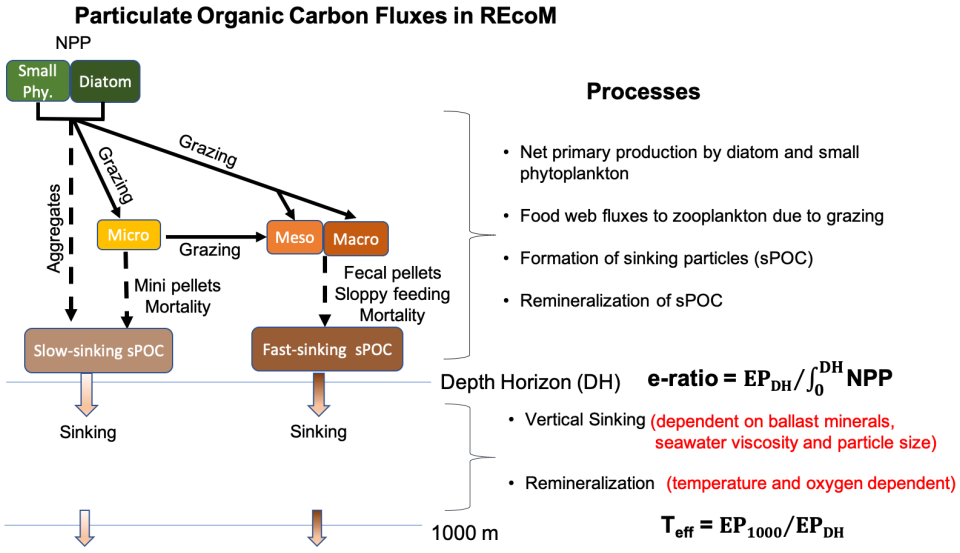

FIGURE 4.1: Particulate organic carbon fluxes and related processes in the ocean biogeochemical model REcoM-3ZOO. Two phytoplankton groups (small phytoplankton and diatoms) are responsible for net primary production (NPP), and three zooplankton groups (micro-, meso- and macrozooplankton) graze on the phytoplankton groups. Phytoplankton aggregation, microzooplankton mini pellet production, and the mortality from microzooplankton compose the slow-sinking particulate organic carbon (POC) pool. Fecal pellets, mortality, and sloppy feeding from the meso- and macrozooplankton groups form the fast-sinking particulate organic carbon pool.

Particulate organic carbon (POC), which is produced by the primary production of phytoplankton, is redistributed among model compartments of zooplankton and sinking particulate organic carbon (Fig. 4.1). In the version of REcoM that we use in this study, three zooplankton functional types graze on phytoplankton groups, representing the food web fluxes. Sinking

particles are represented by two detritus classes. The slow-sinking detritus class is fuelled by phytoplankton aggregation, microzooplankton mortality, and microzooplankton mini pellet production. Fecal pellets, sloppy feeding, and mortality of the meso- and macrozooplankton are the sources of fast-sinking detritus particles. The sPOC is remineralized as a function of temperature and oxygen, and remineralization products are transferred to the dissolved organic carbon pool. The following section describes how the model parametrizes sinking speed and remineralization as a function of particle density, seawater viscosity, temperature, and oxygen.

The New Parametrization of Sinking Speed and Remineralization of the Particles

In the previous versions of REcoM, the slow-sinking particles had an initial sinking speed of 20 m d^{-1} at the surface, which increased linearly with depth (*Hauck et al.*, 2013; *Schourup-Kristensen et al.*, 2014; *Karakuş et al.*, 2021), and the fast-sinking particles had a constant sinking speed of 200 m d^{-1} (*Karakuş et al.*, 2021). In the new version of the particle sinking routine, we use a parametrization that allows for spatio-temporal variability in sinking speeds due to the effect of seawater viscosity (*Taucher et al.*, 2014), and ballast minerals (*Iversen and Ploug*, 2010). Further, remineralization of sPOC depends on oxygen concentration (*Devol and Hartnett*, 2001) in addition to the temperature dependence already present in previous versions. These processes are implemented using a modified version of the particle sinking model by *Cram et al.* (2018) into REcoM. In the modified version, we consider the particle sinking speed as a function of seawater viscosity and the density difference between the particle and the water. However, we do not apply the effect of particle size as described in *Cram et al.* (2018). The effect of the particle sizes is implemented by the depth scaling factor, which increases the sinking speed with depth because the particles with large size and high sinking speed reach the deep ocean (*Kriest and Oschlies*, 2008). The new parametrization for calculating particle sinking speeds is applied to both slow and fast sinking particles (Eq. 4.1). Particle sinking speed (w_{sink}) depends on a reference particle sinking speed (w_{ref}), the difference between the particle and the water densities ($\Delta\rho$), seawater viscosity (μ) and a depth scaling ($ds \cdot Z(k)$):

$$w_{sink} = w_{ref} \cdot \frac{\Delta\rho}{\Delta\rho_{ref}} \cdot \frac{\mu_{ref}}{\mu} + ds \cdot Z(k) \tag{4.1}$$

The reference particle sinking speeds are 10 m d^{-1} (w_{ref_1}, Table 4.S1) and 200 m d^{-1} (w_{ref_2}, Table 4.S1) for slow and fast sinking particles, respectively. The 5-year mean of sinking speeds and the profiles of sinking speeds in four subregions are shown in the Figures 4.S4 and 4.S5 in the suplementary text. The density scaling ($\frac{\Delta\rho}{\Delta\rho_{ref}}$) is defined as the ratio of the density difference ($\Delta\rho$) between the particle ($\rho_{particle}$, see supplementary Eq. 1) and the seawater to a reference density difference ($\Delta\rho_{ref}$) which is accordingly calculated from a reference particle density (ρ_{ref}, Table 4.S1) and the reference water density (ρ_{swref}, Table 4.S1). If the sinking particles are composed mainly of particulate organic carbon and nitrogen, the ratio is <1, and the density scaling factor acts to reduce the sinking speed. In contrast, if the fraction of ballasting agents (opal and calcite) in the particle is high, the ratio exceeds 1, and the density scaling factor acts to enhance the sinking speed (ballasting). The viscosity scaling ($\frac{\mu_{ref}}{\mu}$) is derived as the ratio of a reference seawater viscosity (μ_{ref}, Table 4.S1) to the in-situ seawater viscosity (μ, see supplementary Eq. 2). Viscosity can either increase the sinking speed at warm temperatures or decrease the sinking speed at colder temperatures (supplementary Fig. 4.S2f). The last term, depth scaling ($ds \cdot Z_k$, Table 4.S1), is introduced to represent the linear increase of the sinking speed of a particle with depth, and this term is only applied to the slow sinking particles. A maximum sinking velocity of 250 m d^{-1} was used for both sPOC classes to ensure numerical

stability. The remineralization rate of particles is dependent on both temperature (*Lopez-Urrutia and Moran*, 2007) and oxygen concentrations (*Devol and Hartnett*, 2001) to mimic the bacterial metabolism (Eq. 4.2):

$$r_{rate} = r_{ref} \cdot \exp\left(-4500 \cdot \left(\frac{1}{T} - \frac{1}{T_{ref}}\right)\right) \cdot \frac{[O_2]}{k_{O_2} + [O_2]} \tag{4.2}$$

The remineralization rate (r_{rate}) of the particles is a product of a reference remineralization rate (r_{ref}), the Arrhenius temperature function, and oxygen concentration. The remineralization rate increases exponentially with increasing temperature. The last term describes the sensitivity of the remineralization rate to oxygen levels, i.e., the remineralization rate is lower when oxygen concentration is low and follows Michaelis-Menten kinetics (*Cram et al.*, 2018).

The parameter list of the new sinking routine (see supplementary Table 4.S1) and an evaluation of the particle flux through comparison with the data set of *Mouw et al.* (2016, see supplementary Fig. 4.S6) are provided in the supplementary text.

Model Simulations

We conducted four simulations to analyze the effects of different processes on carbon export and transfer efficiencies with the newly implemented sinking routine (Table 4.1). First, the reference simulation (REF) accounts for all processes described in the previous section, namely ballast minerals, seawater viscosity, and temperature and oxygen-dependent remineralization. Further, we aim to quantify the impact of each process with three sensitivity simulations in which one process is switched off per simulation. In particular, these simulations exclude (a) the particle density effect on sinking speed (NO_DENSITY), (b) the seawater viscosity effect on sinking speed (NO_VISCOSITY), and (c) the oxygen-dependent but not temperature-dependent particle remineralization (NO_OXYGEN).

	Particle sinking speed		**Particle remineralization**	
Simulation	Ballast Minerals	Seawater Viscosity	Temperature	Oxygen
REF	Yes	Yes	Yes	Yes
NO_DENSITY	—	Yes	Yes	Yes
NO_VISCOSITY	Yes	—	Yes	Yes
NO_OXYGEN	Yes	Yes	Yes	—

TABLE 4.1: Overview of model simulations performed for this study. Simulations differ in the parametrization of particle sinking speed and organic matter remineralization. The active processes in each experiment are indicated. See text for details.

In all simulations, the global model was forced with the JRA-55-do atmospheric data set version 1.3.1 (*Kobayashi et al.*, 2015). Repeated year forcing fields from the year 1961 of surface down-welling short and long-wave radiation, surface rainfall, and snowfall fluxes as well as near-surface (2 m) air temperature, specific humidity, eastward and northward wind components, and sea level pressure were used. Freshwater runoff and the surface salinity field for a weak surface salinity restoration (*Sidorenko et al.*, 2011) are taken from the CORE-II climatology (*Griffies et al.*, 2009). The nutrients dissolved inorganic nitrogen and dissolved silicic acid were initialized with World Ocean Atlas 2013 products (*Garcia et al.*, 2013), and dissolved inorganic carbon (DIC) and alkalinity from GLODAPv2 (*Lauvset et al.*, 2016). We performed 60 year-long simulations and analyzed the last five years of the model runs. As we revealed in

our earlier study (*Karakuş et al.*, 2021), this simulation time is long enough for the upper ocean ecosystem to be in a quasi-steady state.

Analysis on Particle Export and Transfer Efficiencies

We use the simulation REF to analyze and compare the integrated global values and spatial distribution of the e-ratio and T_{eff} with current literature. This simulation will also be used to assess the effect of temperature and plankton composition on e-ratio and T_{eff}. The additional three simulations (NO_DENSITY, NO_VISCOSITY, NO_OXYGEN) will be used to separate the effects of temperature, ballast minerals, and oxygen-dependent remineralization on export and transfer efficiencies.

The export efficiency or 'e-ratio' (Eq. 4.3) defines the ratio between particulate organic carbon export flux at the depth horizon (EP_{DH}) and integrated NPP between the surface and the depth horizon:

$$e-ratio = \frac{\int_0^{DH} NPP}{EP_{DH}} \tag{4.3}$$

The transfer efficiency (T_{eff}, Eq. 4.4) is defined as the ratio between the POC flux at 1000 m (EP_{1000}) and at the chosen depth horizon (EP_{DH}) :

$$T_{eff} = \frac{EP_{1000}}{EP_{DH}} \tag{4.4}$$

While the e-ratio comprises both the particulate organic carbon formation and its sinking across the depth horizon, the T_{eff} describes the efficiency of particulate organic carbon flux to the deep ocean.

The integrated global modeled POC flux, NPP and e-ratio vary depending on the choice of depth horizon (*Palevsky and Doney*, 2018). We calculated global POC flux, NPP, and their ratio at different depth horizons (DH), where we considered seasonally varying euphotic depth, annual mean euphotic depth, seasonally varying MLD, annual maximum MLD, fixed 100 m, and 190 m, as described in Table 4.2. We will further use the monthly calculated euphotic depth (Table 4.2, the first row) in this study because the base of euphotic depth separates the processes that produce particulate organic carbon from the region below where the remineralization happens. However, the effect of different depth choices will be discussed in the following section.

Following *Henson et al.* (2019), we divide the global ocean into different regimes according to the annual mean values of primary production and export efficiency. All regions above the median of primary production are regions of **high productivity** and vice versa (Fig. 4.2). Similarly, regions with an e-ratio above the median of the e-ratio are classified as regions of **high export efficiency** and vice versa. After applying this criterion, the four subregions are low productivity, high export efficiency (LPHE), low productivity and low export efficiency (LPLE), high productivity and high export efficiency (HPHE), and high productivity and high export efficiency (HPHE).

RESULTS

Globally-Integrated Net Primary Production and Particulate Organic Carbon Fluxes

To determine how different choices of depth horizon influence globally-integrated net primary production and carbon export fluxes, we calculate the modeled global annual mean NPP, POC flux, and e-ratio using seven depth horizon choices (Table 4.2). The modeled global NPP is on

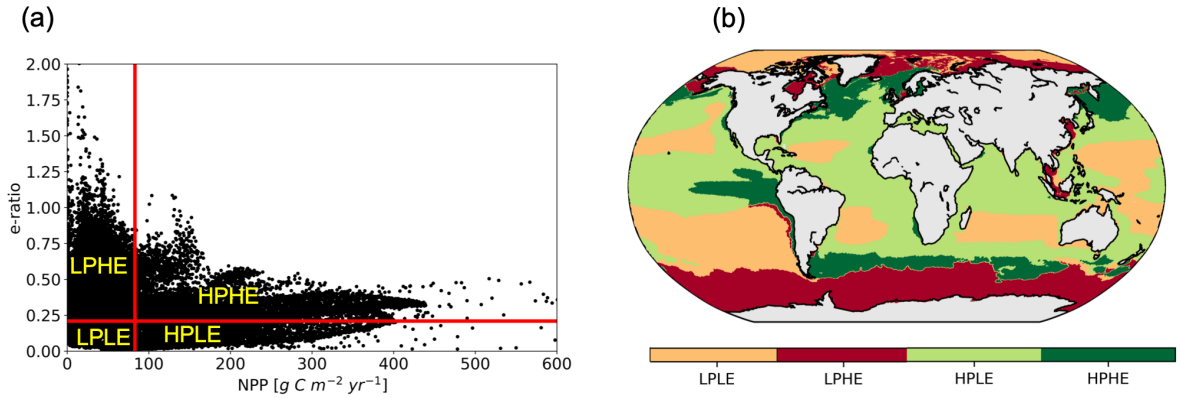

FIGURE 4.2: (a) 5-year mean export efficiency (e-ratio) plotted against net primary productivity (NPP) . The horizontal solid red line indicates the median export efficiency which is used as the threshold for high and low export efficiency regimes; the vertical solid red line indicates the median NPP, which is used as the threshold for high and low NPP regimes (see Methods). (b) Map showing the spatial distribution of the four regimes in the reference simulation (REF). Low NPP/low e-ratio is shown in orange, low NPP/high e-ratio is shown in dark red, high NPP/low e-ratio is shown in light green, and high NPP/high e-ratio is shown in dark green.

the low side of observational estimates (35-70 Pg C yr^{-1}) (*Carr et al.*, 2006; *Kulk et al.*, 2020), yielding rates ranging from (28.1 to 35.9 Pg C yr^{-1}) depending on the choice of depth horizon. Similarly, the global POC flux across different depth horizons is on the low end of observational estimates (4-13 Pg C yr^{-1}) (*Henson et al.*, 2011; *Dunne et al.*, 2007), producing rates ranging from 3.4 to 5.1 Pg C yr^{-1} across the suite of depth horizons.

Globally-integrated net primary production and carbon export fluxes are sensitive to the choice of depth horizons in our model. The integrated NPP within the euphotic zone is 34.8 Pg C yr^{-1}, and global POC flux across the euphotic depth is 4.8 Pg C yr^{-1} (Table 4.2). We use these values as the reference values for the comparison throughout the manuscript. The globally integrated POC flux estimates are up to 21% lower than the reference value when the annual mean or maximum MLD is used as the depth horizon. Similarly, a fixed depth level (100 m or 190 m) yields lower estimates (Table 4.2). One exception occurs when we use monthly MLD as a depth horizon. In this case, global POC flux is 6% higher than for the choice of the euphotic depth. The MLD-related depth horizons do not cover the entire productive surface layer of the model, and hence the NPP is always lower when integrating over the MLD (25.3-32.9 Pg C yr^{-1}) than over the euphotic zone.

These results are in line with *Palevsky and Doney* (2018) who showed that global POC flux rates vary by 30% and global e-ratios by 21% across different depth horizon choices within a single biogeochemical model. The global e-ratio is 13.7% across the euphotic depth in REcoM-3ZOO. It varies between 9.5 and 20.1% for other depth horizon choices (Table 4.2). Especially the global e-ratio across monthly MLD (20%) is higher compared to the e-ratio across the euphotic depth, because of the shallower MLD. When we use a fixed 190 m as depth horizon, the global e-ratio is lower (9.5%). This indicates that 190 m is typically below the euphotic zone and remineralization of particles has already reduced the sPOC flux.

Small phytoplankton and diatoms contribute with 79% and 31% to the total NPP in the euphotic zone in FESOM-REcoM-3ZOO (Fig. 4.1). In the model, the microzooplankton group is the main consumer of phytoplankton, and it grazes 21.7% of the annual primary production. This is lower than the estimated 60% of consumption by (*Calbet and Landry*, 2004). The slow-

Depth Horizon	Depth Horizon Definition	Integrated NPP from surface to depth horizon (Pg C yr^{-1})	Global POC flux across depth horizon (Pg C yr^{-1})	Global e-ratio (%)
Euphotic Zone	Monthly calculated Euphotic depth where PAR $<= 0.01 \cdot PAR_{surf}$	34.8	4.8	13.7
Annual mean euphotic zone	Annual mean of euphotic depth, determined for each grid point	34.8	4.8	13.7
Mixed Layer Depth (MLD)	MLD from the model, monthly output for each grid point	25.3	5.1	20.1
Annual mean MLD	Annual mean of MLD from the model, determined for each grid point	28.1	3.8	13.5
Annual maximum MLD	MLD from the model, maximum value in a year for each grid point	32.9	4.1	12.5
100 m	constant for each grid point	35.9	4.3	12
190 m	constant for each grid point	35.9	3.4	9.5

TABLE 4.2: Depth horizons used to define global net primary production (NPP), particulate organic carbon (POC) export, and e-ratio.

sinking particulate organic carbon pool constitutes 67.3% of the total sinking particles and is dominated by phytoplankton aggregates (64.1% of the slow-sinking particles). The fast-sinking particles are formed by mesozooplankton and macrozooplankton processes and make up 32.7% of the total sinking particles. The slow-sinking and fast-sinking particles contribute 3 and 1.8 Pg C yr^{-1}, respectively, to the particulate organic carbon flux out of the euphotic zone. However, the main difference between slow- and fast-sinking particles is the amount of carbon that reaches the depth of 1000 m. While 55.5% of the fast-sinking particles that sink out of the euphotic zone reach 1000 m, only 16.6% of the slow-sinking particles reach that level. This is consistent with the role of zooplankton fecal pellets for carbon export (*Henson et al.*, 2019; *Turner*, 2015).

Global Spatial Patterns of Net Primary Production, Export Production, Export Efficiency and Transfer Efficiency

The spatial distribution of the modeled annual mean of net primary production is similar to distributions presented by *Behrenfeld and Falkowski* (1997), with higher production in the high latitudes and Equatorial Pacific and lower in subtropical gyres (Fig. 4.4a). The spatial distribution of modeled export across the euphotic depth shows high export in the high

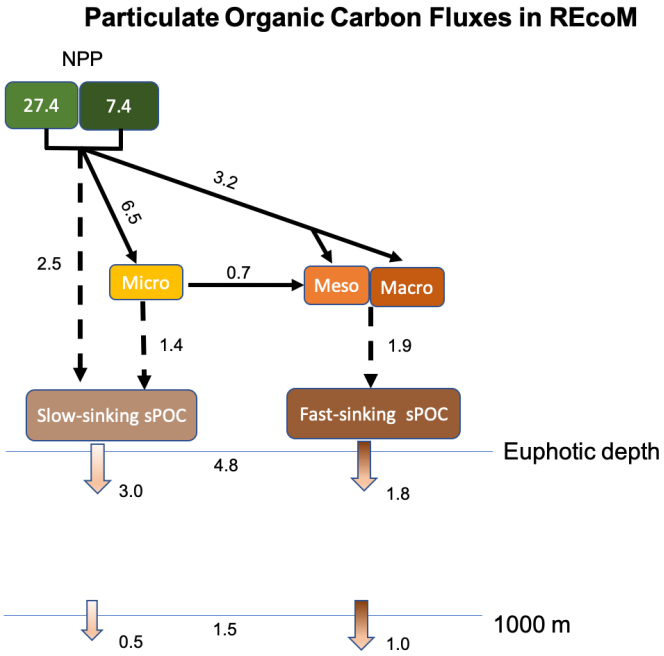

FIGURE 4.3: Annually integrated routing of particulate organic carbon fluxes (Pg C yr^{-1}) between the model compartments.

latitudes and Equatorial upwelling regions, and is thus similar to the spatial distribution of carbon export estimates from satellite-derived products or other models (*Henson et al.*, 2011; *Laufkötter et al.*, 2016).

The simulated e-ratio and T_{eff} are higher in the high latitudes and the equatorial Pacific, which mirrors the distribution of the net primary production. North of 40°N, the spatial means of e-ratio and T_{eff} are 0.25 and 0.20, respectively. In the low latitudes (40°N-40°S), the spatial averages of the e-ratio and the T_{eff} are 0.07 and 0.29, respectively, and these values are lower than in both northern and southern high latitudes. While the southern high latitudes show a particularly high average e-ratio (0.29) compared to northern high latitudes and low latitudes, the average T_{eff} of 0.21 is similar to the northern high latitudes. Our results show a similar latitudinal gradient for the export efficiency as in data compiled by *Henson et al.* (2019) suggesting a low export ratio in the low latitudes and a high export ratio in the high latitudes. The latitudinal gradient of the transfer efficiency is similar to the satellite-based estimates and in-situ observations of *Henson et al.* (2012) that show higher transfer efficiency in the low latitudes. The spatial distribution of the transfer efficiency is similar to previous modeling studies by *Cram et al.* (2018) and *Maerz et al.* (2020), despite the fact that our values are higher compared to the previous studies.

Drivers of e-ratio and T_{eff}

The spatial variability in the e-ratio (as described above) implies that there are different drivers at work. In this context, the effect of several factors, such as NPP, temperature, ballast minerals, silicic acid concentrations, and macrozooplankton and bacteria abundance, have been discussed in the literature (e.g., *Laws et al.*, 2011; *Britten et al.*, 2017; *Arteaga et al.*, 2018; *Henson et al.*, 2019). In our model, temperature and NPP could explain the variability of e-ratio in the low

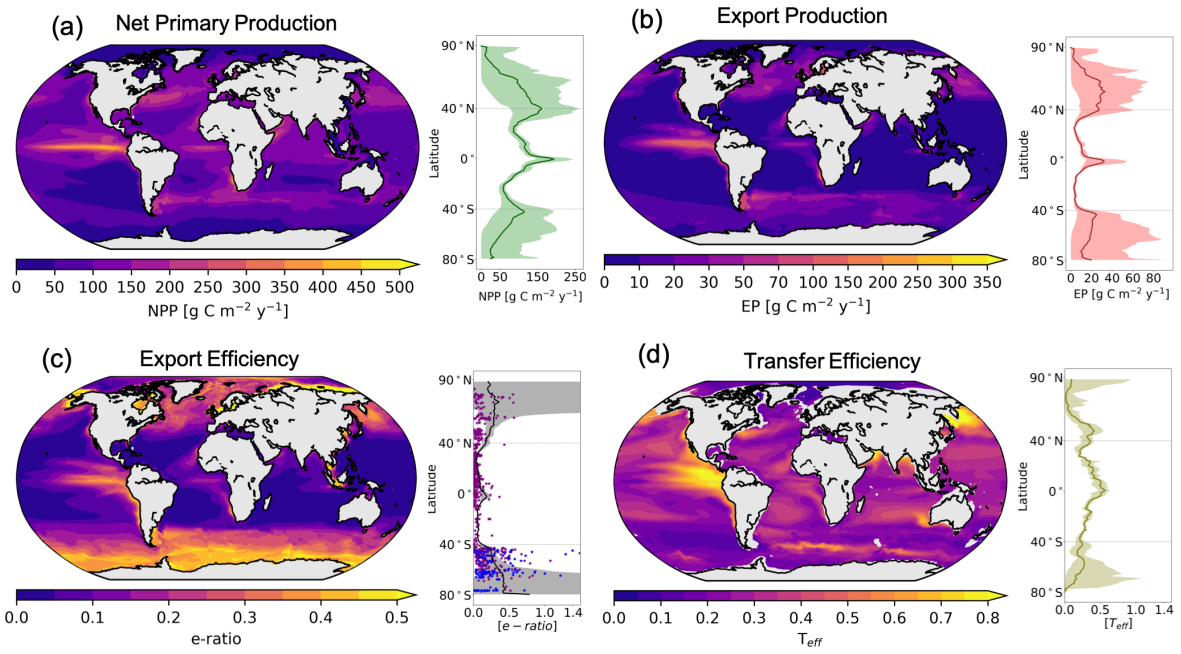

FIGURE 4.4: Net primary production, export flux of particulate organic carbon at the euphotic depth, e-ratio, and T_{eff} averaged over the last five years of the simulation. The zonal averages of each field are shown on the right side of the maps. The shaded areas represent the minimum and maximum as derived from monthly output. The figure showing the zonal average of the export efficiency in panel c includes observational data (blue dots from *Maiti et al.* (2013) and purple dots from *Henson et al.* (2019)).

latitudes to some extent (see supplementary Fig. 4.S9). However, the large variability in the model cannot be explained by the empirical equation of *Laws et al.* (2011, Fig. 4.5), especially in the high latitudes' low primary production and high export efficiency regions. The suggested empirical equations for the Southern Ocean by *Britten et al.* (2017) and *Arteaga et al.* (2018) explain better the inverse relation between NPP and e-ratio (see supplementary Fig. 4.S9). Especially the equation including silicic acid concentration (*Britten et al.*, 2017), agrees well with the model in the southern high latitudes (see supplementary Fig. 4.S9). However, they still do not account for the plankton composition explicitly. Therefore, we discuss the effect of plankton composition on export and transfer efficiencies in the four subregions.

In our model, different factors affect the magnitude of export and transfer efficiencies of carbon in different productivity and export regimes. Our analysis illustrates that the export efficiency is more sensitive to the sea surface temperature than the plankton composition in the LPLE region (Fig. 4.6a). The export efficiency is lower than 21% (the median of export efficiency over all grid points where each grid point is a 5-year mean) as a result of the criteria we used for the subdivision of the ocean (see Methods). However, the export efficiency becomes as low as 1% in the areas with high sea surface temperatures (Fig. 4.6a). This indicates the control of remineralization on export efficiency. In this region, the transfer efficiency of carbon is mostly lower than 25% (the median of transfer efficiency over all grid points where each grid point is a 5-year mean), and there is no apparent effect of SST or plankton composition. However, we note that carbon transfer efficiency becomes as low as 5% in locations where the contribution from small phytoplankton to the total NPP is below 20% (Fig. 4.6c).

The LPHE regions are located in the high latitudes in our model (Fig. 4.2b), and the main contributor to total NPP is diatoms (57%) in this region. Our analysis shows that the export ratio exceeds 42% in the locations where diatoms' contribution to total NPP reaches up to >

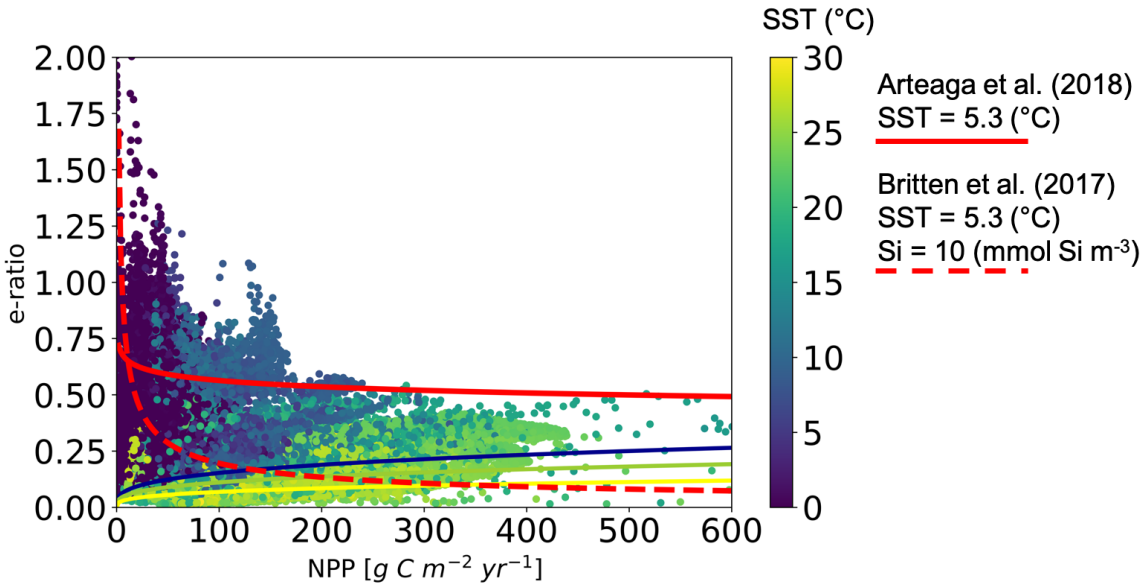

FIGURE 4.5: The modeled e-ratio versus net primary production (NPP), with points colored by sea surface temperature (SST, °C).Also, the relationship between NPP and e-ratio was calculated using the empirical equation from *Laws et al.* (2011) at 5.3°C, 18 °C, 30 °C. Two red lines show the results from the empirical equations suggested by *Arteaga et al.* (2018) and *Britten et al.* (2017). SST was chosen 5.3°C for both equations and silicic acid concentration was chosen 10 mmol Si m^{-3} for the equation from *Britten et al.* (2017).

60% (4.6b). In the LPHE region, the transfer efficiency of carbon can exceed 25%, and processes related to zooplankton (meso- and macrozooplankton) play a determining role in pushing the system to a maximum (∼50%) transfer efficiency (Fig. 4.6d).

In the HPLE regions, NPP is dominated by small phytoplankton (Fig. 4.7a). There is no particular relation between plankton composition and export and transfer efficiencies within this region (Fig. 4.7c). The low export efficiency can be related to the high remineralization rates due to the high SST (Fig. 4.7a) since this region is mainly located in the low latitudes. However, SST variability cannot explain the patterns within this regime. In this region, the transfer efficiency of carbon is generally higher than 25% and can exceed 50% (Fig. 4.7a).

The HPHE regions are characterized by high diatom and large zooplankton biomass. Diatoms make up on average 47% of the total NPP in this region. Our analysis shows that the export ratio exceeds 42% in the locations where the contribution of diatoms to total NPP exceeds 60% (4.7b). In the HPHE region, the transfer efficiency of carbon is generally higher than 25%, and large zooplankton-related processes enhance the transfer efficiency of carbon (to 80%, Fig. 4.7d).

In general, our model results indicate that high export efficiency regimes (>21%, LPHE and HPHE) generally have high transfer efficiency (>25%) of carbon. Diatoms reach the highest contribution to total NPP in these regions, and large zooplankton drives the high transfer efficiency. Low export efficiency regimes (<21%, LPLE and HPLE) do not directly indicate low transfer efficiency of carbon. In these regions, temperature plays a decisive role in the magnitude of export efficiency.

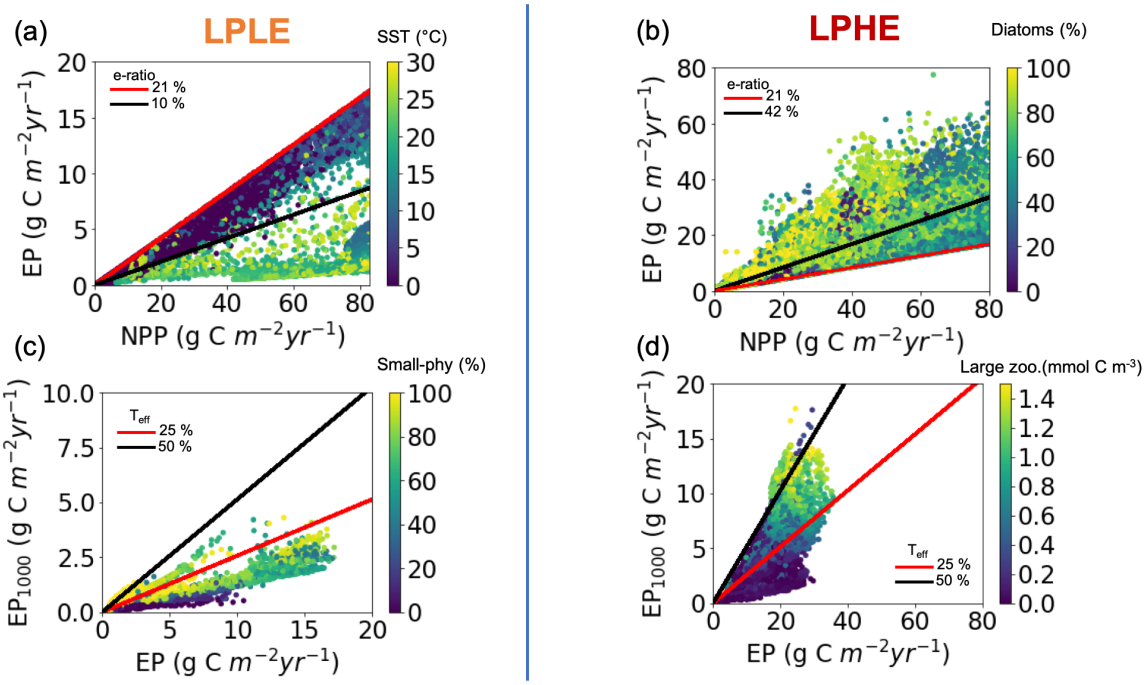

FIGURE 4.6: Relationship between (a, b) export flux at the euphotic depth (EP, g C m^{-2} yr^{-1}) to net primary production (NPP, g C m^{-2} yr^{-1}) and between (c, d) export flux at 1000 m (EP_{1000}, g C m^{-2} yr^{-1}) to export flux at the euphotic depth in the low productivity low export regime (LPLE, a and c) and in the low productivity high export regime (LPHE, b and d) in the REF simulation. Panel (a) is colored by sea surface temperature (SST, °C), (b) is colored by the relative contribution of diatoms to total NPP, (c) is colored by the relative contribution of small phytoplankton to total NPP, (d) is colored by mean surface large zooplankton (meso- and macrozooplankton) concentration.

Sensitivities of e-ratio and T_{eff} to Ballast Minerals, Seawater Viscosity and Oxygen-dependent Remineralization

Our results suggest that the export and transfer efficiencies are most sensitive to the ballast minerals (Fig 4.8b, f), which are produced by diatoms and small phytoplankton and increase particle density. The effect of particle density enhances the export efficiency in the Southern Ocean (by up to 0.05), which hosts a high share of diatom biomass and consequently opal in the sinking particles. Seawater viscosity has a minor effect on the export efficiency. It slightly decreases the export efficiency in high latitudes. Similarly, oxygen-dependent remineralization has a minor effect on the export efficiency compared to particle density (Fig. 4.8). The impact of these processes on export efficiency is by far outweighed by their effects on carbon transfer efficiency. Similar to the export efficiency, the strongest impact (increases by 0.5) comes from the effect of particle density on the particle sinking speed. This is expected since the effect of particle density is the highest increasing or decreasing factor for the sinking speed of particles in the sinking routine (see supplementary Figure 4.S2). While the effect of seawater viscosity is relatively small throughout the global ocean, oxygen-dependent remineralization notably affects the transfer efficiency in oxygen minimum zones (Equatorial Pacific and Indian Oceans), which coincides with previous findings of *Laufkötter et al.* (2017).

The general particle flux profile remains the same across all simulations over the regions of LPLE, LPHE, HPLE and HPHE (Fig. 4.9). The POC flux reaches a maximum at or above the euphotic depth and decreases with depth (Fig. 4.2a,b,c,d). In the LPLE region, ballast minerals enhance the particle flux below 200 m (by up to 40%), and reduce the flux by up to 40% above

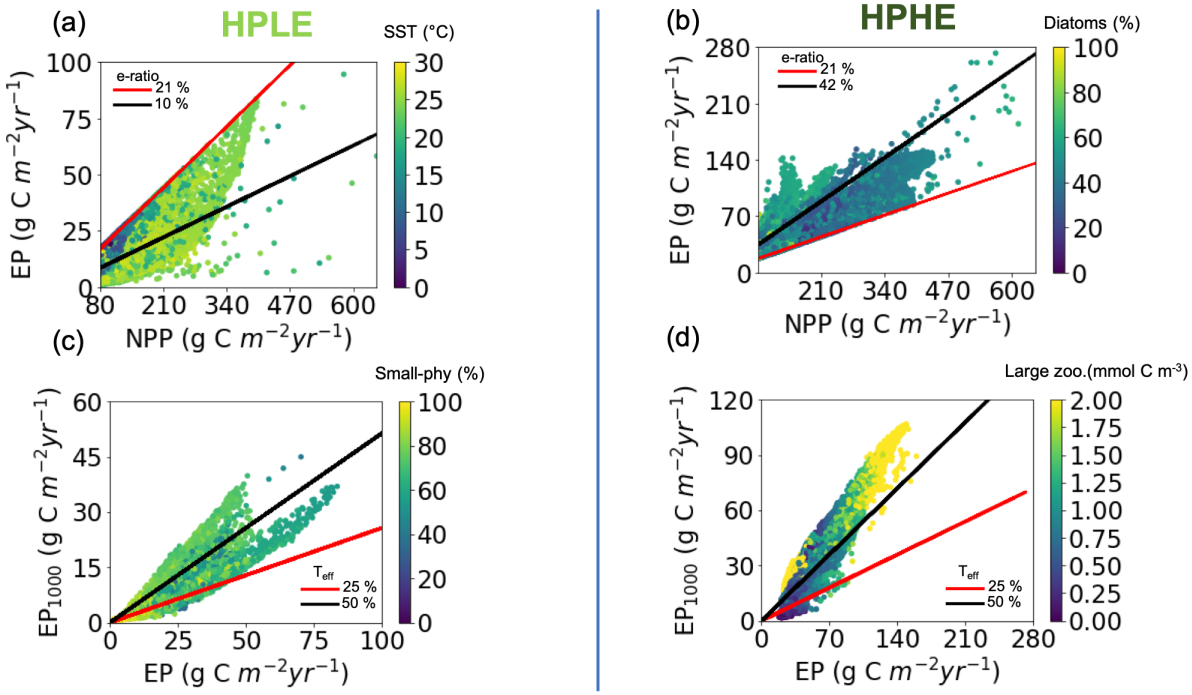

FIGURE 4.7: Relationship between (a, b) export flux at the euphotic depth (EP, g C m^{-2} yr^{-1}) to net primary production (NPP, g C m^{-2} yr^{-1}) and between (c, d) export flux at 1000 m (EP_{1000}, g C m^{-2} yr^{-1}) to export flux at the euphotic depth in the high productivity low export regime (HPLE, a and c) and in the high productivity high export regime (HPHE, b and d) in the REF simulation. Panel (a) is colored by sea surface temperature (SST, °C), (b) is colored by the relative contribution of diatoms to total NPP, (c) is colored by the relative contribution of small phytoplankton to total NPP, (d) is colored by mean surface large zooplankton (meso- and macrozooplankton) concentration.

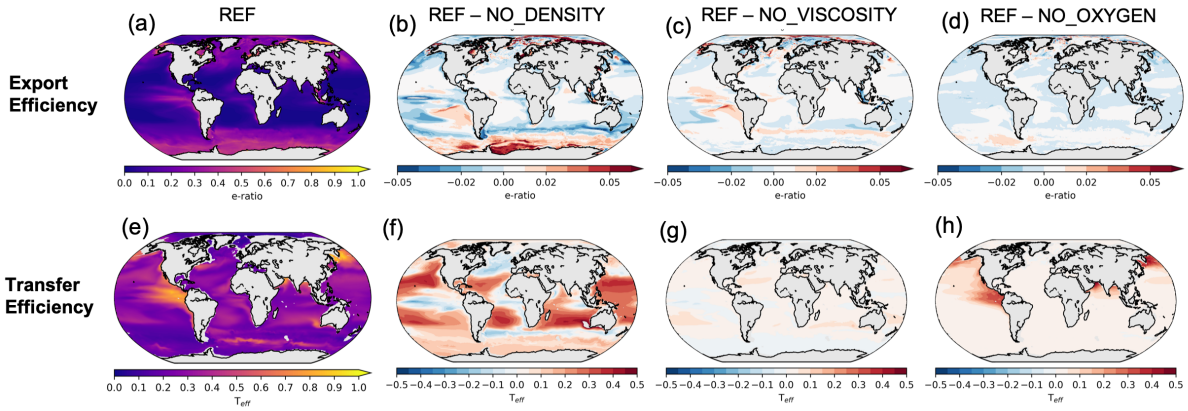

FIGURE 4.8: The 5-year mean of export and transfer efficiencies in the baseline simulation REF (first column) compared to the simulations NO_DENSITY, NO_VISCOSITY, and NO_OXYGEN. Note that the scales for the export and transfer efficiencies are different.

200 m. This indicates that ballast minerals play an important role in carrying the particles from the surface layer to the mesopelagic. Similarly, the ballast minerals affect the particle flux in the same way in the LPHE region. The high concentrations of small phytoplankton (consequently $CaCO_3$ in sinking particles, LPLE) and diatoms (consequently opal in sinking particles, LPHE) could explain these features. In these two regions, the effect of seawater viscosity and oxygen-dependent remineralization on the sinking profile is smaller than the

effect of ballast minerals. In the HPLE region, the effect of seawater viscosity on particle organic carbon flux is prominent, and it enhances the particle sinking flux by up to 18% throughout the water column (Fig. 4.2g). In addition, oxygen-dependent remineralization enhances the POC flux (by up to 20%) below 200 m in HPLE (Fig. 4.2g). In HPHE, the effect of the processes is smaller than in the other regions. The most visible impact comes from the oxygen-dependent remineralization, and this process increases the POC flux (by up to 20%) below 200 m.

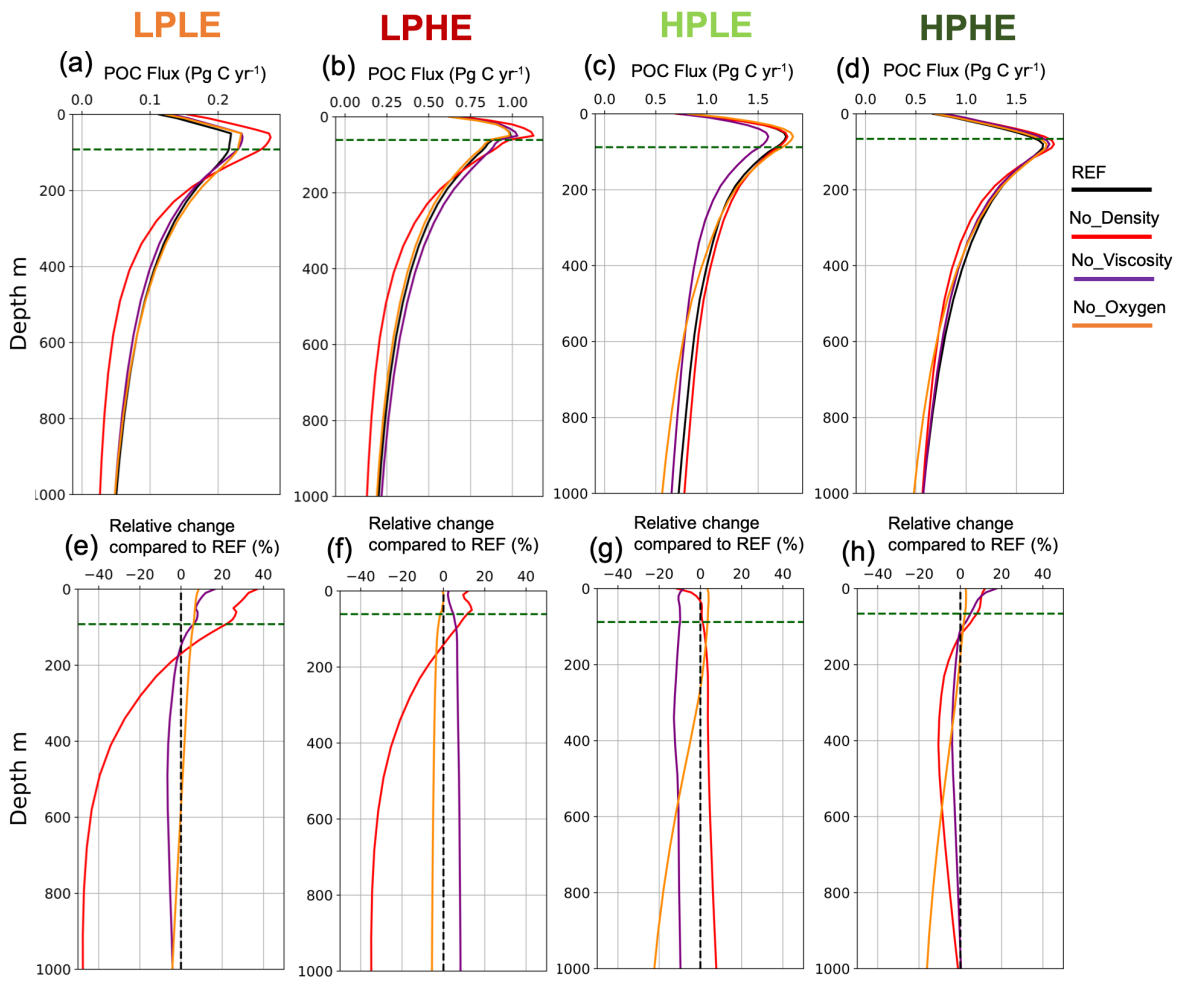

FIGURE 4.9: Profiles of POC flux in four productivity and export efficiency regimes LPLE (low productivity, low export efficiency), LPHE (low productivity, high export efficiency), HPLE (high productivity, low export efficiency), and HPHE (high productivity, high export efficiency) in all four simulations. Second row: the relative change of the fluxes in these simulations compared to the baseline simulation REF (black). The horizontal green dashed lines represent the euphotic depth level.

Figure 4.10 summarizes the spatial mean of export and transfer efficiencies in four subregions and for all four simulations. In the LPLE region, the shares of diatoms, small-phytoplankton, microzooplankton, and large zooplankton (meso- and macrozooplankton) in total plankton biomass are 87%, 7%, 5%, and 0.3%, respectively (Fig. 4.10). The mean export ratio remains unchanged at 6% in NO_DENSITY, NO_VISCOSITY and NO_OXYGEN compared to REF in this region. However, the mean transfer efficiency is sensitive to neglecting the ballast minerals,

seawater viscosity, and oxygen-dependent remineralization in the model. Especially when the effect of particle density is neglected (NO_DENSITY), the transfer efficiency is 0.03 in the LPLE region, which is almost nine times smaller than in all other simulations. In the LPHE region, the shares of diatoms, small-phytoplankton, microzooplankton, and large zooplankton (meso- and macrozooplankton) in total plankton biomass are 44%, 33%, 13%, and 8%, respectively. In this region, the mean export ratio decreases (by 0.02) slightly in NO_DENSITY but remains unchanged in NO_VISCOSITY and NO_OXYGEN compared to REF. The transfer efficiency is lowest (0.1) in NO_DENSITY and highest in NO_VISCOSITY, which indicates the determining role of ballast minerals on the transfer of carbon to the deep ocean. In the HPLE region, the transfer efficiency is sensitive to mineral ballasting and oxygen-dependent remineralization. Thus, the transfer efficiency in HPLE decreases from 0.28 in REF to 0.19 in NO_DENSITY and 0.23 in NO_OXYGEN. Similarly, in the HPHE region, carbon transfer efficiency decreases from 0.35 (REF) to 0.26 (NO_OXYGEN). Although we see the effect of seawater viscosity in the flux profiles (Fig. 4.1), its impact is relatively minor (maximum decrease of 0.2 in LPLE, maximum increase of 0.1 in LPHE) on the average values compared to the impact of the other processes (Fig. 4.10).

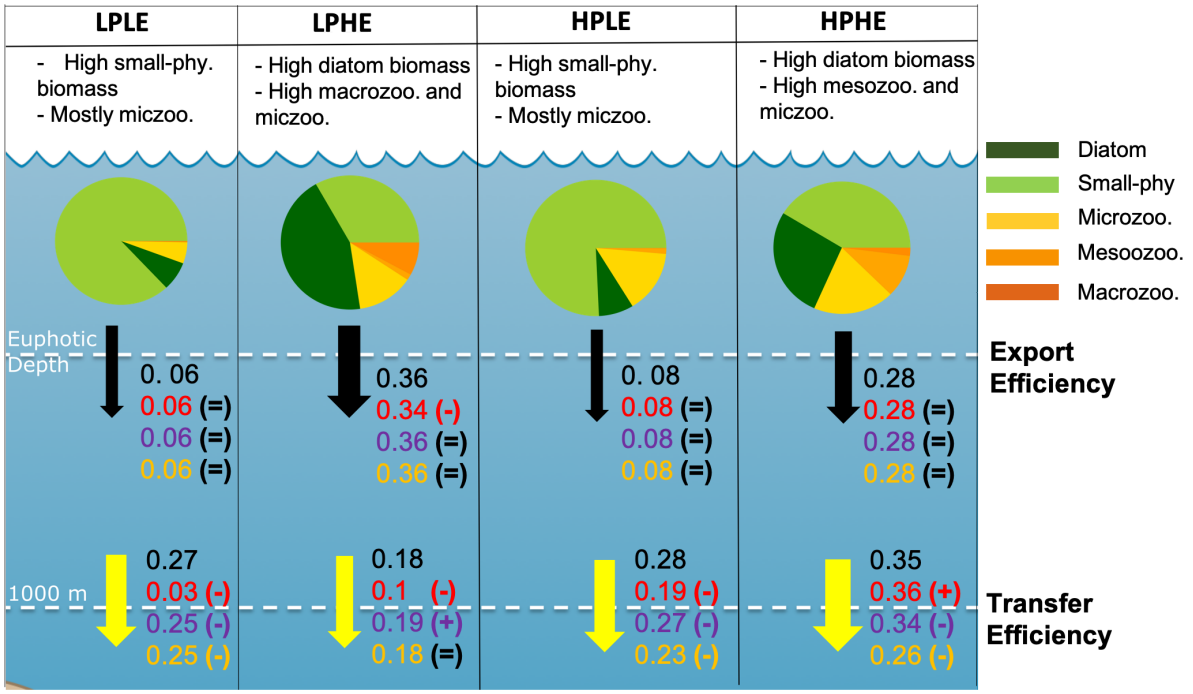

FIGURE 4.10: Summary of the spatial mean of export and transfer efficiencies in four subregions and in all four simulations: The shares of diatoms (dark green), small phytoplankton (light green), microzooplankton (yellow), mesozooplankton (orange), and macrozooplankton (dark orange) in the total biomass of plankton functional types in the euphotic zone are illustrated in the pie chart in four subregions in the reference (REF) simulation by using the 5-year average. The black and yellow arrows represent export and transfer efficiencies, respectively. The numbers next to the arrows indicate the mean export and transfer efficiencies in the simulations REF (black), NO_DENSITY (red), NO_VISCOSITY (purple), and NO_OXYGEN (orange). The signs in the parenthesis show the direction of changes. The plus, minus, and equal signs indicate an increase, decrease, and no change.

Our results suggest that ballast minerals, seawater viscosity, and oxygen-dependent remineralization are more critical for transfer efficiency than export efficiency. The results indicate that export through the euphotic depth is more related to food web processes (net primary

production, grazing) in the euphotic layer and independent of the ballast minerals, seawater viscosity, and oxygen-dependent remineralization. Therefore, the global distribution of LPHE, LPLE, LPHE, and HPHE regions do not show significant differences among the different simulations (see Fig. 4.S3). Thus, we applied similar criteria for defining new regions according to export and transfer efficiencies distribution. All regions above (below) the median of export efficiency (0.21) are regions of **high (low) export efficiency**. Similarly, regions with a transfer efficiency above (below) the median of the transfer efficiency (0.25) are classified as regions of **high (low) transfer efficiency**. After applying this criterion, the four subregions are low export efficiency and low transfer efficiency (LELT), low export efficiency and high transfer efficiency (LEHT), high export efficiency and low transfer efficiency (HELT), and high productivity high export efficiency (HEHT) as seen in Figure 4.11. When we classify the global ocean in terms of export and transfer efficiencies and compare the different simulations, we note that accounting for particle density leads to an expansion of the regions defined as low export efficiency and high transfer efficiency (LEHT) in the subtropical gyres (compare Fig. 4.11a and b). The low export efficiency and low transfer efficiency (LELT) is located mainly in the Southern Pacific Ocean. Within high export efficiency regimes (high latitudes and Equatorial Pacific), we find high transfer efficiencies, which we relate to large zooplankton abundance (Figures 4.6d, 4.7d). Large zooplankton fecal pellets drive the high transfer efficiency of carbon (dark purple areas, Fig. 4.11), which is parallel to the spatial distribution of the high contribution of fast-sinking particles to the total particles (see supplementary Figure 4.S1b).

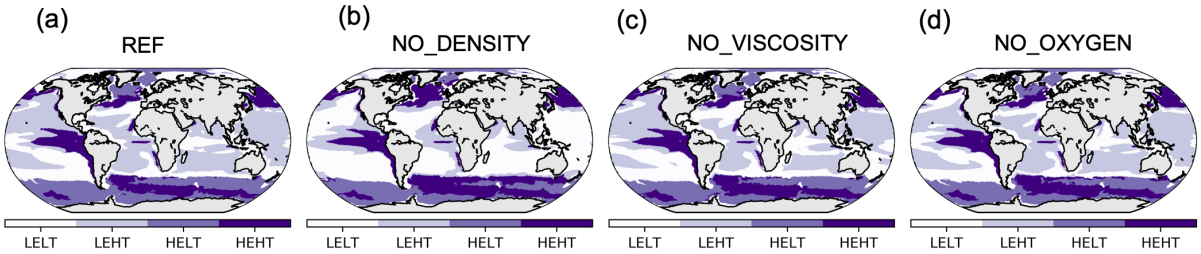

FIGURE 4.11: Regimes are classified according to their export and transfer efficiencies. To define the different regimes, we applied the threshold method described in Methods to 5-year mean export and transfer efficiency fields. The regimes are marked as low export efficiency and low transfer efficiency (LELT, white), low export efficiency and high transfer efficiency (LEHT, light purple), high export efficiency and low transfer efficiency (HELT, purple), and high export efficiency and high transfer efficiency (HPHT, dark purple). One map is shown per simulation: REF, NO_DENSITY, NO_VISCOSITY, and NO_OXYGEN

DISCUSSION

Export efficiency

The inverse relationship between NPP and the e-ratio was previously observed for the Southern Ocean (*Maiti et al.*, 2013; *Britten et al.*, 2017; *Arteaga et al.*, 2018) and globally (*Henson et al.*, 2019). In our model, a similar relationship is found in the global ocean (Fig. 4.5). However, the inverse relationship is more prominent in the high latitudes (see supplementary Figure 4.S9). The empirical models that are suggested in the literature (*Laws et al.*, 2011; *Britten et al.*, 2017; *Arteaga et al.*, 2018; *Henson et al.*, 2019) are derived from databases of satellites and in situ measurements which are sparsely distributed both temporally and spatially. Here, we used a

medium complexity ocean biogeochemical model to investigate whether these patterns also hold on a larger scale.

Previously, *Henson et al.* (2019) suggested a classification of the global ocean according to the magnitude of productivity and export efficiency. The authors showed that almost all data points that exhibit LPHE characteristics are located at high latitudes and LPLE characteristics in subtropical gyres, HPLE characteristics at the low latitudes, and HPHE characteristics in the South, Equatorial, and North Atlantic. In this study, we extrapolated these temporal and spatial snapshots of the characteristics of the global ocean by using mean modeled NPP and export efficiency patterns. Our results show a similar spatial distribution (Fig. 4.2) as shown in *Henson et al.* (2019), except for the Equatorial Pacific, which is classified as HPHE in our model and was classified as HPLE by *Henson et al.* (2019).

Observations show that high export events can be related to the plankton composition, i.e., the dominance of large cells and diatoms that control the high export events (*Boyd and Newton*, 1999; *Buesseler*, 1998). In addition, fast-sinking zooplankton fecal pellets could dominate the export flux (*Turner*, 2015). *Henson et al.* (2019) illustrated for the first time the link between e-ratio and plankton community composition on the global scale by using micro-, nano- and picoplankton data (*Uitz et al.*, 2010), bacteria abundance (*Buitenhuis et al.*, 2012), and mesozooplankton and macrozooplankton biomass (*Moriarty and O'Brien*, 2013; *Moriarty et al.*, 2013). The authors showed that while a high share of microplankton in the plankton community and high mesozooplankton and macrozooplankton biomass could enhance export efficiency, a high share of picoplankton could decrease the export efficiency. Our model does not differentiate between larger and smaller phytoplankton cells. However, we indirectly see the effect of phytoplankton composition since they affect the density of sinking particulate matter. Especially, we see that the high export efficiency regions are dominated by high primary production by diatoms and related meso - and macrozooplankton biomass.

Transfer Efficiency

In contrast to export efficiency, there are relatively limited data for transfer efficiency, and this makes it difficult to detect large-scale spatial variability (*Weber et al.*, 2016). Previous studies provide spatial patterns by using an ocean inverse model (*Weber et al.*, 2016) and biogeochemical model (*Maerz et al.*, 2020) of transfer efficiency in the global ocean. Both studies illustrated high transfer efficiency in the high latitudes and lower transfer efficiency in the low latitudes (except for Equatorial Pacific). Their results partly contradict previous findings showing high transfer efficiency (>20%) in low latitudes and low transfer efficiency (<5%) in high latitudes (*Henson et al.*, 2012). It was discussed that this could be a result of the collection biases of bottom-moored sediment traps and/or analytical errors associated with the Th-based export observations used (*Weber et al.*, 2016). Our results indicate a similar latitudinal gradient (Fig. 4.4d) as described in *Henson et al.* (2012). However, there are two exceptions for the high latitudes: (1) the effect of seasonality and (2) large zooplankton abundance. Firstly, the transfer efficiency reaches a maximum of 1 depending on the season (Fig. 4.4d, zonal mean) in the high southern latitudes, which we do not see a similar seasonal effect in the low latitudes. Secondly, high transfer efficiency is more related to fast sinking particles (i.e., large zooplankton abundance) in high latitudes (Fig. 4.6d).

As noted before, the magnitude of the transfer efficiency is more sensitive to the ballast minerals, seawater viscosity, and oxygen-dependent remineralization than the export efficiency (Fig. 4.8). Similar results were provided by *Maerz et al.* (2020) after the implementation of microaggregates, which impact sinking velocity, and led to a threefold increase in the mean transfer efficiency in the Antarctic zone. This region falls into the LPHE region in our study,

and we show that omitting ballast minerals results in a 44% lower transfer efficiency in this region (Fig. 4.10). *Maerz et al.* (2020) do not report a significant impact of ballast minerals on the mean transfer efficiency in the low latitudes. However, we show that the missing ballast minerals affect transfer efficiency in the low latitudes (e.g., LPLE, HPLE). Here, we need to note that it is related to the spatial distribution of small-phytoplankton which includes calcifiers in our model. In addition, oxygen-dependent remineralization plays a role in the magnitude of the transfer efficiency in the regions HPLE and HPHE, where oxygen minimum zones are located, in agreement with *Laufkötter et al.* (2017). Omitting oxygen-dependent remineralization decreases the transfer efficiency of carbon in these regions since low oxygen concentration decreases the reference remineralization rate.

The transfer efficiency of carbon in the LPLE regions (in subtropical gyres, Fig. 4.2) is highly sensitive to the representation of mineral ballasting (Fig. 4.8f). In all three simulations that include mineral ballasting (REF, NO_VISCOSITY, and NO_OXYGEN), the subtropical gyres are characterized as having low export efficiency ($<$21%) and high transfer efficiency ($>$25%). When the ballasting minerals are excluded from the model, these regions have low export efficiency ($<$21%) and low transfer efficiency ($<$25%). One previous study showed that the transfer efficiency of carbon is greatest in the subtropical gyres because of little remineralization due to ballasting by calcium carbonate (*Francois et al.*, 2002). This spatial feature is captured when the ballast minerals are included in the model (Figures 4.10, 4.11).

Observations from deep ocean sediment traps have shown strong correlations between organic carbon fluxes and ballast minerals, and this was associated with the effect of ballast minerals on the particle sinking speed and/or protection of the organic matter from remineralization (*Klaas and Archer*, 2002; *Armstrong et al.*, 2001b; *Francois et al.*, 2002). *Iversen and Robert* (2015) showed that ballast minerals enhance the sinking speed of particles. Here, we quantify its role in export and transfer efficiencies by using the global ocean biogeochemical model. Our results show that ballast minerals can lead to substantial regional variability of sinking speed and change the global mean transfer efficiency. However, the impact of ballast minerals is not uniform in the global ocean (*Wilson et al.*, 2012), for instance, ballast composition had little or no effect on particle settling velocity in the Mediterranean Sea (*Lee et al.*, 2009). Therefore, our results need more understanding from sediment trap studies.

Limitations and Implications

Our description of spatial patterns and drivers of the export and transfer efficiencies goes well beyond previous studies that developed empirical equations or analyzed observations. We are confident that our model captures the spatial distribution and relation between NPP and e-ratio reasonably well. Nevertheless, we acknowledge that additional work (i.e., comparison with other models, missing processes) may lead to a more complete picture. In this study, we test the effect of ballast minerals, seawater viscosity, and oxygen-dependent remineralization on carbon transfer efficiency by using outputs of a single biogeochemical model. Therefore, the results could be affected by the structure and the parametrization of the model. For instance, the version of REcoM-3ZOO used in this study explicitly divides the spectrum of sinking particles into two pools: slow-sinking and fast-sinking particles (see model description in Methods). This separation gives a strong geographical separation between two sinking particle pools. For example, the model results suggest that slow-sinking particles can, in some locations, make up 100% of total sinking particles (see supplementary Figure 4.S1). Although a single type of sinking particle can drive the entire export flux in some regions and seasons (*Markussen et al.*, 2020), the bulk of sinking particles usually consists of many different sources such as fecal pellets and marine snow (*Turner*, 2015; *Laurenceau-Cornec et al.*, 2015). Similarly, the

fast-sinking particles dominate the euphotic zone only in the regions with high meso- and macrozooplankton biomass, which directly causes a high carbon transfer efficiency. The transfer efficiency of carbon is relatively higher in our model compared to *Henson et al.* (2012) and *Weber et al.* (2016). This is partly related to the high sinking velocity of fast-sinking particles in the model. Therefore, further tests of different reference sinking speeds might be tested. In addition, the evaluation of particle fluxes was performed in a 60-years long simulation. In addition, longer simulations should be performed to evaluate the effects on deep ocean nutrient concentrations.

The motivation of this study was to analyze and quantify the possible effect of missing ballast minerals, seawater viscosity, and oxygen-dependent remineralization on carbon export. *Henson et al.* (2022) assess the predicted influence of omitting specific mechanisms on modeled present-day carbon export estimates. In our model, the effect of ballasting, seawater viscosity, and oxygen-dependent remineralization hardly affect the total integrated POC flux across the euphotic depth (4.7-5 Pg C yr^{-1} in four simulations). The impacts of all three processes could increase or decrease the POC flux depending on the region (see supplementary Fig. 4.S8). According to the summary of *Henson et al.* (2022), not considering mineral ballasting from the models likely causes a negative bias, or the size of the effect is unknown on the global scale. We find that the globally integrated export flux across the euphotic depth decreases by 4% from 5 in NO_DENSITY when to 4.8 in REF accounting for mineral ballasting. It shows that most particles are transferred below the euphotic zone due to the enhancing effect of ballasting on sinking speed. Consequently, the POC flux across the euphotic depth decreases. *Henson et al.* (2022) also mention that omitting seawater viscosity could cause a positive bias in present-day estimates. However, our results show that omitting seawater viscosity causes a negative bias and the globally integrated POC flux decreases by 2.1% (4.7 Pg C yr^{-1} in NO_VISCOSITY and 4.8 Pg C yr^{-1} in REF). Our results differ from the previous findings by *Taucher et al.* (2014) which show that including seawater viscosity decreases export flux at 130 m by 2.8%. This discrepancy might result from the depth choice since we use, in contrast to *Taucher et al.* (2014), a monthly calculated euphotic depth in our analysis. However, both studies confirm that the effects of seawater viscosity on particle sinking speed are unlikely to affect modern-day export estimates significantly (*Henson et al.*, 2022). In our parametrization, we assumed that the particle sinking speed is higher in warm water than in cold water. However, it should be noted that the effect of temperature on particle sinking speed is not clear. Previously, *Bach et al.* (2012) reported that a warming of 9°C leads to an increase in sinking speeds by 40%. While intuitively higher water viscosity at colder temperatures should decrease the sinking speeds, *Iversen and Ploug* (2013) could not confirm such a relationship in their experiments. Finally, we considered oxygen-dependent remineralization, and when this process is omitted, the globally integrated export flux increases by 2.1% (from 4.8 Pg C yr^{-1} in REF to 4.9 Pg C yr^{-1} NO_OXYGEN). This finding is consistent with the summary of *Henson et al.* (2022) which shows that omitting oxygen-dependent remineralization likely causes a positive bias in export flux estimates. Our results contribute to the research community's ongoing interest in estimating the possible effect of missing processes on carbon export in biogeochemical models.

CONCLUSION

In conclusion, the modified version of the particle sinking routine (*Cram et al.*, 2018) provides well-defined effects of mineral ballasting, seawater viscosity, and oxygen-dependent remineralization in REcoM-3ZOO. Thus, the new model version was used as a testbed to analyze the model's potential impacts of missing processes in particulate organic carbon flux. Our results illustrate that the effect of parametrization of mineral ballasting, seawater viscosity,

and oxygen-dependent remineralization on the e-ratio is small in REcoM-3ZOO. These three processes hardly change the estimates of export fluxes across the euphotic depth. However, they play a critical role in the transfer efficiency of carbon. Especially, our results highlight the importance of ballast minerals on particle sinking speed and, consequently, transfer efficiency. Furthermore, large zooplankton play a critical role in carbon transfer efficiency. In the model, high export efficiency is not directly an indicator of high transfer efficiency. Rather, high transfer efficiency is related to high large zooplankton abundance in the high export efficiency regions.

BIBLIOGRAPHY

Armstrong, R. A., C. Lee, J. I. Hedges, S. Honjo, and S. G. Wakeham (2001), A new, mechanistic model for organic carbon fluxes in the ocean based on the quantitative association of POC with ballast minerals, *Deep Sea Research Part II: Topical Studies in Oceanography*, *49*(1), 219-236, doi:10.1016/S0967-0645(01)00101-1.

Arteaga, L., N. Haëntjens, E. Boss, K. S. Johnson, and J. L. Sarmiento (2018), Assessment of Export Efficiency Equations in the Southern Ocean Applied to Satellite-Based Net Primary Production, *Journal of Geophysical Research: Oceans*, *123*(4), 2945-2964, doi:10.1002/2018JC013787.

Aumont, O., and L. Bopp (2006), Globalizing results from ocean in situ iron fertilization studies, *Global Biogeochemical Cycles*, *20*(2), GB2017, doi:10.1029/2005GB002591.

Bach, L. T., U. Riebesell, S. Sett, S. Febiri, P. Rzepka, and K. G. Schulz (2012), An approach for particle sinking velocity measurements in the 3–400 μm size range and considerations on the effect of temperature on sinking rates, *Marine Biology*, *159*(8), 1853–1864, doi:10.1007/s00227-012-1945-2.

Behrenfeld, M. J., and P. G. Falkowski (1997), Photosynthetic rates derived from satellite-based chlorophyll concentration, *Limnology and Oceanography*, *42*(1), 1-20, doi:10.4319/lo.1997.42.1.0001.

Belcher, A., M. Iversen, C. Manno, S. A. Henson, G. A. Tarling, and R. Sanders (2016), The role of particle associated microbes in remineralization of fecal pellets in the upper mesopelagic of the Scotia Sea, Antarctica, *Limnology and Oceanography*, *61*(3), 1049-1064, doi:10.1002/lno.10269.

Boyd, P., and P. Newton (1999), Does planktonic community structure determine downward particulate organic carbon flux in different oceanic provinces?, *Deep Sea Research Part I: Oceanographic Research Papers*, *46*(1), 63-91, doi:10.1016/S0967-0637(98)00066-1.

Boyd, P., H. Claustre, M. Levy, D. A. Siegel, and T. Weber (2019), Multi-faceted particle pumps drive carbon sequestration in the ocean, *Nature*, *568*(7752), 327–335, doi:10.1038/s41586-019-1098-2.

Britten, G. L., L. Wakamatsu, and F. W. Primeau (2017), The temperature-ballast hypothesis explains carbon export efficiency observations in the Southern Ocean, *Geophysical Research Letters*, *44*(4), 1831-1838, doi:10.1002/2016GL072378.

Buchan, A., G. R. LeCleir, C. A. Gulvik, and J. González (2014), Master recyclers: features and functions of bacteria associated with phytoplankton blooms, *Nature Reviews Microbiology*, *12*(10), 686–698, doi:10.1038/nrmicro3326.

Buesseler, K. O. (1998), The decoupling of production and particulate export in the surface ocean, *Global Biogeochemical Cycles*, *12*(2), 297-310, doi:10.1029/97GB03366.

Buesseler, K. O., and P. W. Boyd (2009), Shedding light on processes that control particle export and flux attenuation in the twilight zone of the open ocean, *Limnology and Oceanography*, *54*(4), 1210-1232, doi:10.4319/lo.2009.54.4.1210.

Buesseler, K. O., P. W. Boyd, E. E. Black, and D. A. Siegel (2020), Metrics that matter for assessing the ocean biological carbon pump, *Proceedings of the National Academy of Sciences*, *117*(18), 9679-9687, doi:10.1073/pnas.1918114117.

Buitenhuis, E., W. K. W. Li, M. W. Lomas, D. M. Karl, M. R. Landry, and S. Jacquet (2012), Picoheterotroph (Bacteria and Archaea) biomass distribution in the global ocean, *Earth System Science Data*, *4*(1), 101–106, doi:10.5194/essd-4-101-2012.

Calbet, A., and M. R. Landry (2004), Phytoplankton growth, microzooplankton grazing, and carbon cycling in marine systems, *Limnology and Oceanography*, *49*(1), 51-57, doi:10.4319/lo.2004.49.1.0051.

Carr, M.-E., M. A. Friedrichs, M. Schmeltz, M. Noguchi Aita, D. Antoine, K. R. Arrigo, I. Asanuma, O. Aumont, R. Barber, M. Behrenfeld, R. Bidigare, E. T. Buitenhuis, J. Campbell, A. Ciotti, H. Dierssen, M. Dowell, J. Dunne, W. Esaias, B. Gentili, W. Gregg, S. Groom, N. Hoepffner, J. Ishizaka, T. Kameda, C. Le Quéré, S. Lohrenz, J. Marra, F. Mélin, K. Moore, A. Morel, T. E. Reddy, J. Ryan, M. Scardi, T. Smyth, K. Turpie, G. Tilstone, K. Waters, and Y. Yamanaka (2006), A comparison of global estimates of marine primary production from ocean color, *Deep Sea Research Part II: Topical Studies in Oceanography*, *53*(5), 741-770, doi:10.1016/j.dsr2.2006.01.028.

Cavan, E. L., F. A. C. Le Moigne, A. J. Poulton, G. A. Tarling, P. Ward, C. J. Daniels, G. M. Fragoso, and R. J. Sanders (2015), Attenuation of particulate organic carbon flux in the Scotia Sea, Southern Ocean, is controlled by zooplankton fecal pellets, *Geophysical Research Letters*, *42*(3), 821-830, doi:10.1002/2014GL062744.

Cram, J. A., T. Weber, S. W. Leung, A. M. P. McDonnell, J.-H. Liang, and C. Deutsch (2018), The Role of Particle Size, Ballast, Temperature, and Oxygen in the Sinking Flux to the Deep Sea, *Global Biogeochemical Cycles*, *32*(5), 858-876, doi:10.1029/2017GB005710.

Devol, A. H., and H. E. Hartnett (2001), Role of the oxygen-deficient zone in transfer of organic carbon to the deep ocean, *Limnology and Oceanography*, *46*(7), 1684-1690, doi:10.4319/lo.2001.46.7.1684.

Dunne, J. P., R. A. Armstrong, A. Gnanadesikan, and J. L. Sarmiento (2005), Empirical and mechanistic models for the particle export ratio, *Global Biogeochemical Cycles*, *19*(4), GB4026, doi:10.1029/2004GB002390.

Dunne, J. P., J. L. Sarmiento, and A. Gnanadesikan (2007), A synthesis of global particle export from the surface ocean and cycling through the ocean interior and on the seafloor, *Global Biogeochemical Cycles*, *21*(4), doi:10.1029/2006GB002907.

Dunne, J. P., J. G. John, E. Shevliakova, R. J. Stouffer, J. P. Krasting, S. L. Malyshev, P. C. D. Milly, L. T. Sentman, A. J. Adcroft, W. Cooke, K. A. Dunne, S. M. Griffies, R. W. Hallberg, M. J. Harrison, H. Levy, A. T. Wittenberg, P. J. Phillips, and N. Zadeh (2013), GFDL's ESM2 Global Coupled Climate–Carbon Earth System Models. Part II: Carbon System Formulation

and Baseline Simulation Characteristics, *Journal of Climate*, *26*(7), 2247 - 2267, doi:10.1175/JCLI-D-12-00150.1.

Field, C. B., M. J. Behrenfeld, J. T. Randerson, and P. Falkowski (1998), Primary Production of the Biosphere: Integrating Terrestrial and Oceanic Components, *Science*, *281*(5374), 237-240, doi:10.1126/science.281.5374.237.

Francois, R., S. Honjo, R. Krishfield, and S. Manganini (2002), Factors controlling the flux of organic carbon to the bathypelagic zone of the ocean, *Global Biogeochemical Cycles*, *16*(4), 34-1-34-20, doi:10.1029/2001GB001722.

Garcia, R. Locarnini, T. P. Boyer, J. I. Antonov, O. K. Baranova, M. M. Zweng, J. R. Reagan, and D. R. Johnson (2013), World Ocean Atlas 2013 Volume 4 : Nutrients (phosphate , nitrate , silicate), *NOAA Atlas NESDIS 76*, *4*(September), 396.

Geider, R. J., H. L. Maclntyre, and T. M. Kana (1998), A dynamic regulatory model of phytoplanktonic acclimation to light, nutrients, and temperature, *Limnology and Oceanography*, *43*(4), 679-694, doi:10.4319/lo.1998.43.4.0679.

Giering, S. L. C., E. L. Cavan, S. L. Basedow, N. Briggs, A. B. Burd, L. J. Darroch, L. Guidi, J.-O. Irisson, M. H. Iversen, R. Kiko, D. Lindsay, C. R. Marcolin, A. M. P. McDonnell, K. O. Möller, U. Passow, S. Thomalla, T. W. Trull, and A. M. Waite (2020), Sinking Organic Particles in the Ocean—Flux Estimates From *in situ* Optical Devices, *Frontiers in Marine Science*, *6*, doi:10.3389/fmars.2019.00834.

Griffies, S. M., A. Biastoch, C. Böning, F. Bryan, G. Danabasoglu, E. P. Chassignet, M. H. England, R. Gerdes, H. Haak, R. W. Hallberg, W. Hazeleger, J. Jungclaus, W. G. Large, G. Madec, A. Pirani, B. L. Samuels, M. Scheinert, A. S. Gupta, C. A. Severijns, H. L. Simmons, A. M. Treguier, M. Winton, S. Yeager, and J. Yin (2009), Coordinated ocean-ice reference experiments (cores), *Ocean Modelling*, *26*(1), 1-46, doi:10.1016/j.ocemod.2008.08.007.

Hauck, J., C. Völker, T. Wang, M. Hoppema, M. Losch, and D. A. Wolf-Gladrow (2013), Seasonally different carbon flux changes in the Southern Ocean in response to the southern annular mode, *Global Biogeochemical Cycles*, *27*(4), 1236–1245, doi:10.1002/2013GB004600.

Henson, S., R. Sanders, E. Madsen, P. J. Morris, F. Le Moigne, and G. D. Quartly (2011), A reduced estimate of the strength of the ocean's biological carbon pump, *Geophysical Research Letters*, *38*(4), L04606, doi:10.1029/2011GL046735.

Henson, S., R. Sanders, and E. Madsen (2012), Global patterns in efficiency of particulate organic carbon export and transfer to the deep ocean, *Global Biogeochemical Cycles*, *26*(1), GB1028, doi:10.1029/2011GB004099.

Henson, S., A. Yool, and R. Sanders (2015), Variability in efficiency of particulate organic carbon export: A model study, *Global Biogeochemical Cycles*, *29*(1), 33-45, doi:10.1002/2014GB004965.

Henson, S., F. Le Moigne, and S. Giering (2019), Drivers of Carbon Export Efficiency in the Global Ocean, *Global Biogeochemical Cycles*, *33*(7), 891-903, doi:10.1029/2018GB006158.

Henson, S., C. Laufkötter, S. Leung, S. L. C. Giering, H. I. Palevsky, and E. L. Cavan (2022), Uncertain response of ocean biological carbon export in a changing world, *Nature Geoscience*, doi:10.1038/s41561-022-00927-0.

Iversen, M. H., and H. Ploug (2010), Ballast minerals and the sinking carbon flux in the ocean: carbon-specific respiration rates and sinking velocity of marine snow aggregates, *Biogeosciences*, *7*(9), 2613–2624, doi:10.5194/bg-7-2613-2010.

Iversen, M. H., and H. Ploug (2013), Temperature effects on carbon-specific respiration rate and sinking velocity of diatom aggregates - potential implications for deep ocean export processes, *Biogeosciences*, *10*(6), 4073–4085, doi:10.5194/bg-10-4073-2013.

Iversen, M. H., and M. L. Robert (2015), Ballasting effects of smectite on aggregate formation and export from a natural plankton community, *Marine Chemistry*, *175*, 18-27, doi:10.1016/j.marchem.2015.04.009.

Karakuş, O., C. Völker, M. Iversen, W. Hagen, D. Wolf-Gladrow, B. Fach, and J. Hauck (2021), Modeling the Impact of Macrozooplankton on Carbon Export Production in the Southern Ocean, *Journal of Geophysical Research: Oceans*, *126*(12), e2021JC017315, doi:10.1029/2021JC017315.

Klaas, C., and D. E. Archer (2002), Association of sinking organic matter with various types of mineral ballast in the deep sea: Implications for the rain ratio, *Global Biogeochemical Cycles*, *16*(4), 1116, doi:10.1029/2001GB001765.

Kobayashi, S., Y. Ota, Y. Harada, A. Ebita, M. Moriya, H. Onoda, K. Onogi, H. Kamahori, C. Kobayashi, H. Endo, K. Miyaoka, and T. Kiyotoshi (2015), The JRA-55 reanalysis: General specifications and basic characteristics, *Journal of the Meteorological Society of Japan*, *93*(1), 5–48, doi:10.2151/jmsj.2015-001.

Kriest, I., and A. Oschlies (2008), On the treatment of particulate organic matter sinking in large-scale models of marine biogeochemical cycles, *Biogeosciences*, *5*(1), 55–72, doi:10.5194/bg-5-55-2008.

Kulk, G., T. Platt, J. Dingle, T. Jackson, B. F. Jönsson, H. A. Bouman, M. Babin, R. J. W. Brewin, M. Doblin, M. Estrada, F. G. Figueiras, K. Furuya, N. González-Benítez, H. G. Gudfinnsson, K. Gudmundsson, B. Huang, T. Isada, Z. Kovac, V. A. Lutz, E. Marañón, M. Raman, K. Richardson, P. D. Rozema, W. H. v. d. Poll, V. Segura, G. H. Tilstone, J. Uitz, V. v. Dongen-Vogels, T. Yoshikawa, and S. Sathyendranath (2020), Primary Production, an Index of Climate Change in the Ocean: Satellite-Based Estimates over Two Decades, *Remote Sensing*, *12*(5), doi:10.3390/rs12050826.

Lampitt, R., E. Achterberg, T. Anderson, J. Hughes, M. Iglesias-Rodriguez, B. Kelly-Gerreyn, M. Lucas, E. Popova, R. Sanders, J. Shepherd, D. Smythe-Wright, and A. Yool (2008), Ocean fertilization: a potential means of geoengineering?, *Philosophical Transactions of the Royal Society A: Mathematical, Physical and Engineering Sciences*, *366*(1882), 3919-3945, doi:10.1098/rsta.2008.0139.

Laufkötter, C., M. Vogt, N. Gruber, O. Aumont, L. Bopp, S. C. Doney, J. P. Dunne, J. Hauck, J. G. John, I. D. Lima, R. Seferian, and C. Völker (2016), Projected decreases in future marine export production: The role of the carbon flux through the upper ocean ecosystem, *Biogeosciences*, *13*(13), 4023–4047, doi:10.5194/bg-13-4023-2016.

Laufkötter, C., J. G. John, C. A. Stock, and J. P. Dunne (2017), Temperature and oxygen dependence of the remineralization of organic matter, *Global Biogeochemical Cycles*, *31*(7), 1038-1050, doi:10.1002/2017GB005643.

Laurenceau-Cornec, E. C., T. W. Trull, D. M. Davies, S. G. Bray, J. Doran, F. Planchon, F. Carlotti, M.-P. Jouandet, A.-J. Cavagna, A. M. Waite, and S. Blain (2015), The relative importance of phytoplankton aggregates and zooplankton fecal pellets to carbon export: insights from free-drifting sediment trap deployments in naturally iron-fertilised waters near the Kerguelen Plateau, *Biogeosciences*, *12*(4), 1007–1027, doi:10.5194/bg-12-1007-2015.

Lauvset, S. K., R. M. Key, A. Olsen, S. Van Heuven, A. Velo, X. Lin, C. Schirnick, A. Kozyr, T. Tanhua, M. Hoppema, S. Jutterström, R. Steinfeldt, E. Jeansson, M. Ishii, F. F. Perez, T. Suzuki, and S. Watelet (2016), A new global interior ocean mapped climatology: The 1° x 1° GLODAP version 2, *Earth System Science Data*, *8*(2), 325–340, doi:10.5194/essd-8-325-2016.

Laws, E. A., P. G. Falkowski, W. O. Smith Jr., H. Ducklow, and J. J. McCarthy (2000), Temperature effects on export production in the open ocean, *Global Biogeochemical Cycles*, *14*(4), 1231-1246, doi:10.1029/1999GB001229.

Laws, E. A., E. D'Sa, and P. Naik (2011), Simple equations to estimate ratios of new or export production to total production from satellite-derived estimates of sea surface temperature and primary production, *Limnology and Oceanography: Methods*, *9*(12), 593-601, doi:10.4319/lom.2011.9.593.

Le Moigne, F. A. C., K. Pabortsava, C. L. J. Marcinko, P. Martin, and R. J. Sanders (2014), Where is mineral ballast important for surface export of particulate organic carbon in the ocean?, *Geophysical Research Letters*, *41*(23), 8460-8468, doi:10.1002/2014GL061678.

Lee, C., M. L. Peterson, S. G. Wakeham, R. A. Armstrong, J. K. Cochran, J. C. Miquel, S. W. Fowler, D. Hirschberg, A. Beck, and J. Xue (2009), Particulate organic matter and ballast fluxes measured using time-series and settling velocity sediment traps in the northwestern Mediterranean Sea, *Deep Sea Research Part II: Topical Studies in Oceanography*, *56*(18), 1420-1436, doi:10.1016/j.dsr2.2008.11.029.

Lopez-Urrutia, A., and X. A. G. Moran (2007), Rsource Limitation of Bacterial Production Distorts the Temperrature Dependence of Oceanic Carbon Cycling, *Ecology*, *88*(4), 817-822, doi:10.1890/06-1641.

Maerz, J., K. D. Six, I. Stemmler, S. Ahmerkamp, and T. Ilyina (2020), Microstructure and composition of marine aggregates as co-determinants for vertical particulate organic carbon transfer in the global ocean, *Biogeosciences*, *17*(7), 1765–1803, doi:10.5194/bg-17-1765-2020.

Maiti, K., M. A. Charette, K. O. Buesseler, and M. Kahru (2013), An inverse relationship between production and export efficiency in the Southern Ocean, *Geophysical Research Letters*, *40*(8), 1557-1561, doi:10.1002/grl.50219.

Markussen, T. N., C. Konrad, C. Waldmann, M. Becker, G. Fischer, and M. H. Iversen (2020), Tracks in the Snow – Advantage of Combining Optical Methods to Characterize Marine Particles and Aggregates, *Frontiers in Marine Science*, *7*, doi:10.3389/fmars.2020.00476.

Marsay, C. M., R. J. Sanders, S. A. Henson, K. Pabortsava, E. P. Achterberg, and R. S. Lampitt (2015), Attenuation of sinking particulate organic carbon flux through the mesopelagic ocean, *Proceedings of the National Academy of Sciences*, *112*(4), 1089-1094, doi:10.1073/pnas.1415311112.

Moore, J. K., K. Lindsay, S. C. Doney, M. C. Long, and K. Misumi (2013), Marine Ecosystem Dynamics and Biogeochemical Cycling in the Community Earth System Model [CESM1(BGC)]: Comparison of the 1990s with the 2090s under the RCP4.5 and RCP8.5 Scenarios, *Journal of Climate*, *26*(23), 9291 - 9312, doi:10.1175/JCLI-D-12-00566.1.

Moriarty, R., and T. D. O'Brien (2013), Distribution of mesozooplankton biomass in the global ocean, *Earth System Science Data*, *5*(1), 45–55, doi:10.5194/essd-5-45-2013.

Moriarty, R., E. T. Buitenhuis, and C. Le Quéré (2013), Distribution of known macrozooplankton abundance and biomass in the global ocean, *Earth System Science Data*, *5*(2), 241–257, doi:10.5194/essd-5-241-2013.

Mouw, C. B., A. Barnett, G. A. McKinley, L. Gloege, and D. Pilcher (2016), Global ocean particulate organic carbon flux merged with satellite parameters, *Earth System Science Data*, *8*(2), 531–541, doi:10.5194/essd-8-531-2016.

Omand, M. M., R. Govindarajan, J. He, and A. Mahadevan (2020), Sinking flux of particulate organic matter in the oceans: Sensitivity to particle characteristics, *Scientific Reports*, *10*(1), 5582, doi:10.1038/s41598-020-60424-5.

Palevsky, H. I., and S. C. Doney (2018), How Choice of Depth Horizon Influences the Estimated Spatial Patterns and Global Magnitude of Ocean Carbon Export Flux, *Geophysical Research Letters*, *45*(9), 4171-4179, doi:10.1029/2017GL076498.

Parekh, P., S. Dutkiewicz, M. J. Follows, and T. Ito (2006), Atmospheric carbon dioxide in a less dusty world, *Geophysical Research Letters*, *33*(3), L03610, doi:10.1029/2005GL025098.

Passow, U., and C. Carlson (2012), The biological pump in a high CO_2 world, *Marine Ecology Progress Series*, *470*(2), 249–271, doi:10.3354/meps09985.

Schoofs, S., R. Trompert, and U. Hansen (2000), Thermochemical convection in and beneath intracratonic basins: Onset and effects, *Journal of Geophysical Research: Solid Earth*, *105*(B11), 25567-25585, doi:10.1029/2000JB900272.

Schourup-Kristensen, V., D. Sidorenko, D. A. Wolf-Gladrow, and C. Völker (2014), A skill assessment of the biogeochemical model REcoM2 coupled to the Finite Element Sea Ice–Ocean Model (FESOM 1.3), *Geoscientific Model Development*, *7*(6), 2769–2802, doi:10.5194/gmd-7-2769-2014.

Sidorenko, D., Q. Wang, S. Danilov, and J. Schröter (2011), FESOM under coordinated ocean-ice reference experiment forcing, *Ocean Dynamics*, *61*(7), 881–890, doi:10.1007/s10236-011-0406-7.

Siegel, D. A., K. O. Buesseler, S. C. Doney, S. F. Sailley, M. J. Behrenfeld, and P. W. Boyd (2014), Global assessment of ocean carbon export by combining satellite observations and food-web models, *Global Biogeochemical Cycles*, *28*(3), 181-196, doi:10.1002/2013GB004743.

Siegel, D. A., K. O. Buesseler, M. J. Behrenfeld, C. R. Benitez-Nelson, E. Boss, M. A. Brzezinski, A. Burd, C. A. Carlson, E. A. D'Asaro, S. C. Doney, M. J. Perry, R. H. R. Stanley, and D. K. Steinberg (2016), Prediction of the Export and Fate of Global Ocean Net Primary Production: The EXPORTS Science Plan, *Frontiers in Marine Science*, *3*, doi:10.3389/fmars.2016.00022.

Steinberg, D. K., and M. R. Landry (2017), Zooplankton and the Ocean Carbon Cycle, *Annual Review of Marine Science*, *9*(1), 413–444, doi:10.1146/annurev-marine-010814-015924.

Taucher, J., L. T. Bach, U. Riebesell, and A. Oschlies (2014), The viscosity effect on marine particle flux: A climate relevant feedback mechanism, *Global Biogeochemical Cycles*, *28*(4), 415-422, doi:10.1002/2013GB004728.

Turner, J. T. (2015), Zooplankton fecal pellets, marine snow, phytodetritus and the ocean's biological pump, *Progress in Oceanography*, *130*, 205–248, doi:10.1016/j.pocean.2014.08.005.

Uitz, J., H. Claustre, B. Gentili, and D. Stramski (2010), Phytoplankton class-specific primary production in the world's oceans: Seasonal and interannual variability from satellite observations, *Global Biogeochemical Cycles*, *24*(3), doi:10.1029/2009GB003680.

Volk, T., and M. I. Hoffert (1985), *Ocean Carbon Pumps: Analysis of Relative Strengths and Efficiencies in Ocean-Driven Atmospheric CO2 Changes*, pp. 99–110, American Geophysical Union (AGU), doi:10.1029/GM032p0099.

Wang, Q., S. Danilov, D. Sidorenko, R. Timmermann, C. Wekerle, X. Wang, T. Jung, and J. Schröter (2014), The Finite Element Sea Ice-Ocean Model (FESOM) v.1.4: formulation of an ocean general circulation model, *Geoscientific Model Development*, *7*(2), 663–693, doi:10.5194/gmd-7-663-2014.

Weber, T., J. A. Cram, S. W. Leung, T. DeVries, and C. Deutsch (2016), Deep ocean nutrients imply large latitudinal variation in particle transfer efficiency, *Proceedings of the National Academy of Sciences*, *113*(31), 8606-8611, doi:10.1073/pnas.1604414113.

Wilson, J. D., S. Barker, and A. Ridgwell (2012), Assessment of the spatial variability in particulate organic matter and mineral sinking fluxes in the ocean interior: Implications for the ballast hypothesis, *Global Biogeochemical Cycles*, *26*(4), GB4011, doi:10.1029/2012GB004398.

SUPPORTING INFORMATION

Contents of this file

1. Table 4.S1: Parameters for the new sinking routine in REcoM-3ZOO.
2. Figure 4.S1: The contribution of slow and fast-sinking particles to total sinking particles in the euphotic zone.
3. Figure 4.S2: The density of particles, seawater viscosity and scaling factors in the model.
4. Figure 4.S3: Productivity and export efficiency regimes in the different simulations.
5. Figure 4.S4: Profiles of sinking speeds of slow and fast-sinking particles.
6. Figure 4.S5: Spatial patterns of the mean sinking speed of the slow- and fast-sinking particles.
7. Figure 4.S6: Comparison of POC flux with available data.
8. Figure 4.S7: The spatial distribution of differrent depth horizons.
9. Figure 4.S8: The spatial distribution of temporal mean export production in the different simulations.
10. Figure 4.S9: Drivers of e-ratio and T_{eff} and comparison with empirical equations,

INTRODUCTION

This Appendix firstly presents the contribution of slow and fast-sinking particles to the total sinking particles across the euphotic depth.

Text for the Figures

Figure 4.S1 shows the contribution (%) of slow and fast-sinking particles to average total sinking particles in the euphotic zone in REcoM-3ZOO. In the model, sinking particles are dominated by the slow-sinking particles (Fig. 4.S1a). The fast-sinking particles contribute mainly in the North Atlantic and North Pacific, and in the Equatorial Pacific. In addition, the fast-sinking particles dominate the total sinking particles (up to 74%) in parts of the southern high latitudes.

Figure 4.S2 shows the density of particles, seawater viscosity and scaling factors in the model. Slow sinking particles have a higher density compared to fast-sinking particles since the shares of opal and $CaCO_3$ are higher compared to the fast-sinking particles (Fig. 4.S2a,b). We see this effect in the density scaling (Fig. 4.S2c,d). The high density of the particle enhances the scaling factor. Seawater viscosity is higher in the colder regions and decreases towards the equator (Fig. 4.S2c). As a result, the viscosity scaling increases the sinking speed and reduces the sinking speed in the high latitudes.

Figure 4.S3 shows the productivity and export efficiency regimes in four simulations. Although there are minor changes, the distribution of large regions is similar in the model.

Figure 4.S4 shows the mean profiles of sinking speeds of slow and fast sinking particles. The average surface sinking speed of slow-sinking particles varies between 9 and 22 m d^{-1} in four regions. The average slow-sinking particles reach a maximum of 135 m d^{-1} at 5000 m in the LPLE region. The average surface sinking speed of fast-sinking particles varies between 91 and

125 m d^{-1}. The mean sinking speed of fast-sinking particles reaches a maximum of 250 m d^{-1} at 5000 m in the LPLHE.

Figure 4.S5 shows the 5-year mean sinking speed of the slow and fast-sinking particles at the surface. Due to the parameter choices, fast-sinking particles have higher sinking rates than slow-sinking particles. The temporal mean sinking speed of fast-sinking particles varies between a minimum 51 m d^{-1} in South Pacific and a maximum of 250 m d^{-1} in the Southern Ocean. The surface sinking speed of slow-sinking particles varies between 3 m d^{-1} in polar regions and a maximum of 100 m d^{-1} in the subtropical gyres.

Figure 4.S6 shows the comparison of POC flux in the model and available data (*Mouw et al.*, 2016). The spatial distribution of POC flux observations is shown in Figure 4.S6a. There are 14748 observations, and 83 % of the observations are from the northern hemisphere. The rest, 17%, is from the southern hemisphere. The POC flux in the model was plotted against the observations, and observations were colored according to depth (4.S6b). This comparison gives a root mean square error (RMSE) of 2.39 mmol C m^{-2} d^{-1}. In the northern and southern hemispheres, the RMSE is 2.15 and 3.52 mmol C m^{-2} d^{-1}, respectively.

Figure 4.S7 shows the spatial distribution of different depth horizons in the reference simulation.

Figure 4.S8 shows the annual mean export flux in the reference simulation (REF) and the effects of ballasting, viscosity and oxygen-dependent remineralization as derived by the difference between REF and the specific simulations NO_DENSITY, NO_VISCOSITY, and NO_OXYGEN.

Figure 4.S9 shows the plankton composition in the low latitudes and high latitudes. In addition, it shows the relationship between primary production, export efficiency, transfer efficiency, and sea surface temperature. Further, it shows the comparison with the empirical equations that are used in the literature.

Calculation of the particle density and seawater viscosity

Sinking particles (slow- or fast-sinking) are represented by four state variables: carbon, nitrogen, $CaCO_3$ and silicate (opal). Density of the particle ($\rho_{particle}$) is calculated from the densities (ρ_{POC}, ρ_{PON}, ρ_{CaCO_3}, ρ_{opal}, see Table 4.S1) and volumetric proportions of organic matter (V_{POC}, V_{PON}), carbonate (V_{CaCO_3}), and silicate (V_{opal}) that make up the particles, as follows:

$$\rho_{particle} = V_{POC} \cdot \rho_{POC} + V_{PON} \cdot \rho_{PON} + V_{CaCO_3} \cdot \rho_{CaCO_3} + V_{opal} \cdot \rho_{opal} \tag{4.5}$$

The modeled seawater viscosity (μ) is calculated by using in situ temperature (T, °C) (in equation 4.6, *Schoofs et al.*, 2000):

$$\mu = 2.414 \cdot 10^{-5} \cdot 10^{247.8/(T+133.15)} \tag{4.6}$$

The $\rho_{particle}$ and μ are used in Equation 1 in the main text to calculate the varying particle sinking speed.

Parameter (Unit)	Symbol	Value	Reference
POC density (kg m^{-3})	ρ_C	1033	*Cram et al.* (2018)
PON density (kg m^{-3})	ρ_N	1033	*Cram et al.* (2018)
$CaCO_3$ density (kg m^{-3})	ρ_{CaCO_3}	2830	*Cram et al.* (2018)
Opal density (kg m^{-3})	ρ_{opal}	2090	*Cram et al.* (2018)
Reference particle density (kg m^{-3})	ρ_{ref}	1230	*Cram et al.* (2018)
Reference seawater density (kg m^{-3})	ρ_{swref}	1027	*Cram et al.* (2018)
Reference seawater viscosity (kg m^{-1} s^{-1})	μ_{ref}	0.00156	*Cram et al.* (2018)
Reference sinking speed of slow-sinking particles (m d^{-1})	w_{ref_1}	10	—
Reference sinking speed of fast-sinking particles (m d^{-1})	w_{ref_2}	200	—
Depth scaling factor (d^{-1})	d_s	0.01	—
Maximum sinking velocity (d^{-1})	w_{max}	250	—
Reference remineralization rate (d^{-1})	r_{ref}	0.15	—
Half-saturation coefficient for oxygen dependent remineralization (mmol m^{-3})	k_{O_2}	15	*Cram et al.* (2018)

TABLE 4.S1: Parameters for the new sinking routine in REcoM-3ZOO.

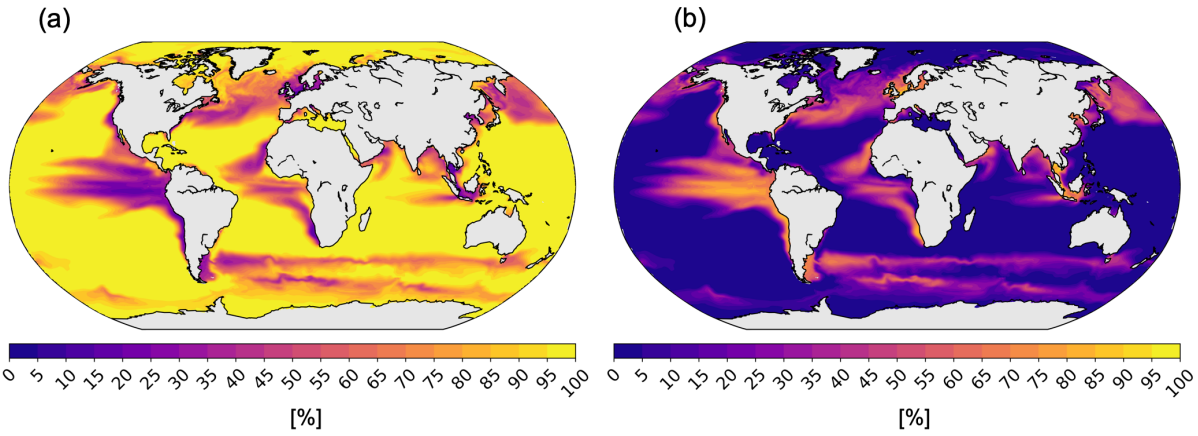

FIGURE 4.S1: The contribution (%) of slow and fast-sinking particles to the temporal average total sinking particles across the euphotic depth in the biogeochemical model REcoM-3ZOO. (a) Slow-sinking particles, (b) fast-sinking particles.

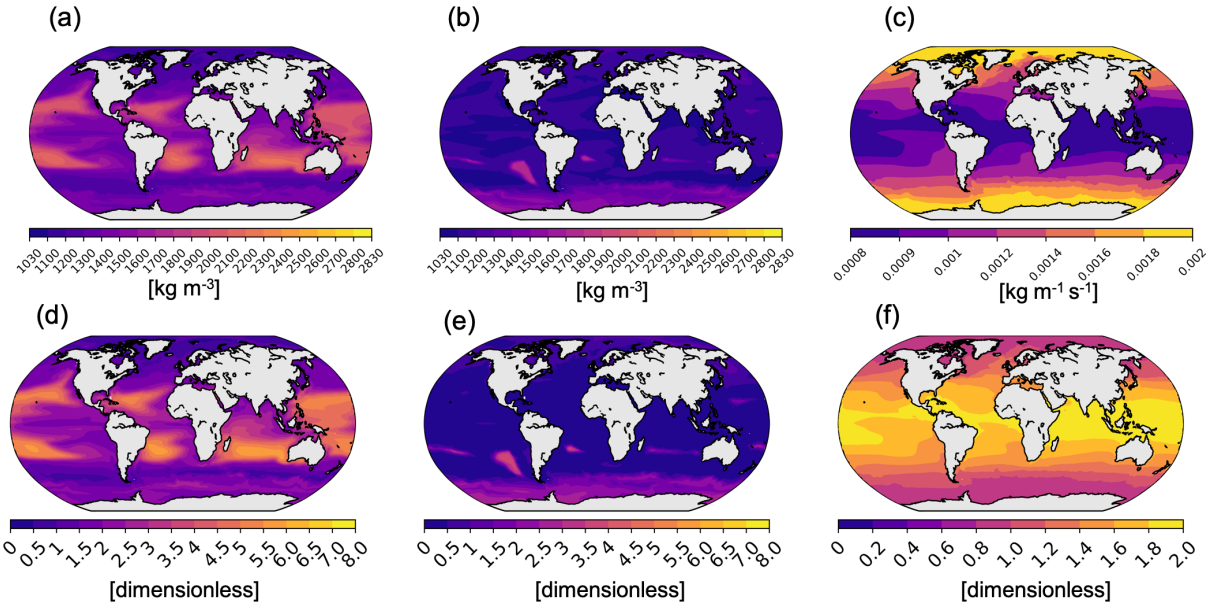

FIGURE 4.S2: The density of particles, seawater viscosity and scaling factors in the model. The first row is (a) the density of slow-sinking particles (kg m^{-3}), (b) the density of fast-sinking particles (kg m^{-3}) and (c) seawater viscosity (kg m^{-1}). The second row depicts the scaling factors: (d) density scaling for slow-sinking particles, (e) density scaling for fast-sinking particles, and (f) viscosity scaling for both particle types.

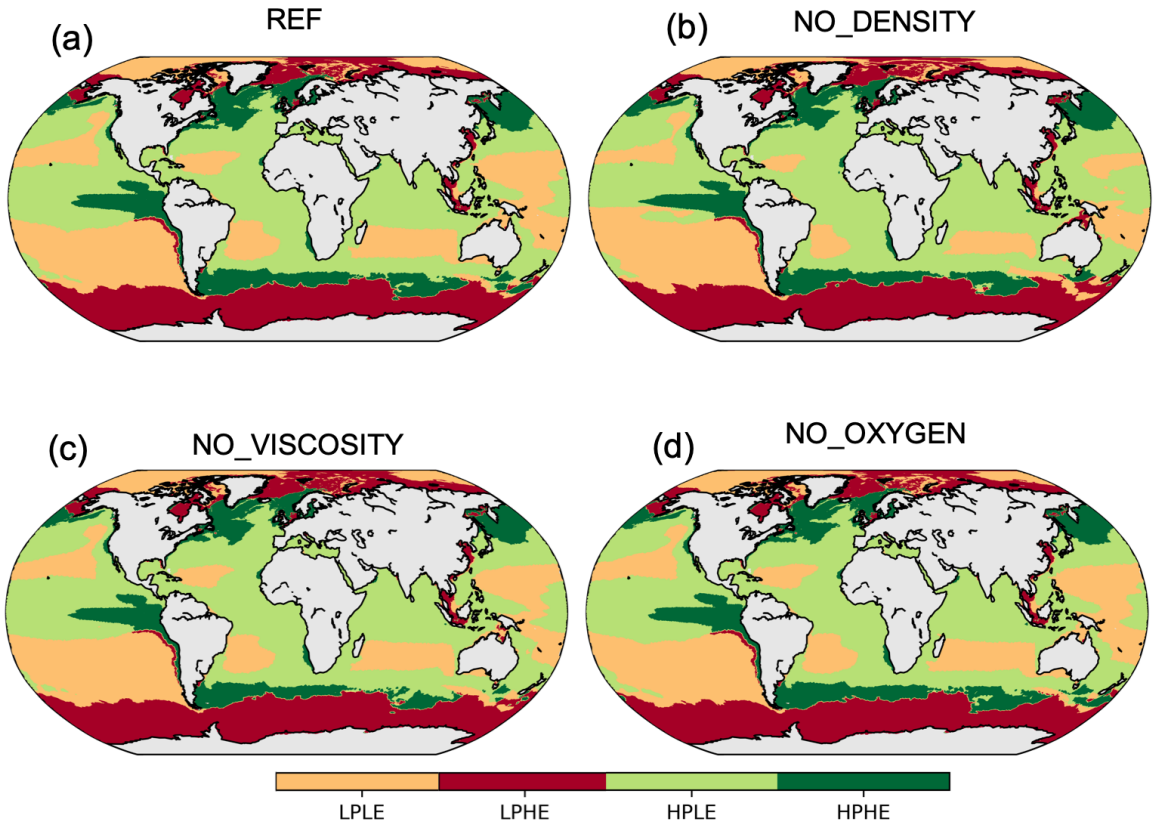

FIGURE 4.S3: Productivity and export efficiency regimes are presented for the four different simulations, see figure titles. Locations of modeled regimes are marked as low net primary production (NPP), high export efficiency (LPHE, dark red), low NPP, low export efficiency (LPLE, orange), high NPP, low export efficiency (HPLE, light green), and high NPP, high export efficiency (HPHE, dark green).

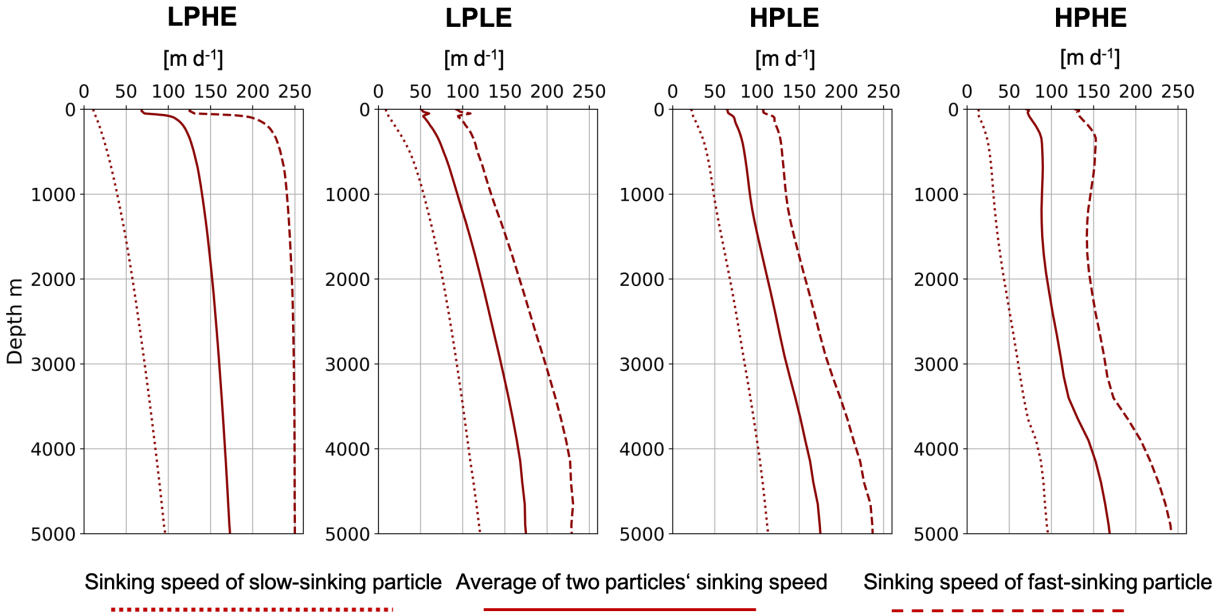

FIGURE 4.S4: Profiles of sinking speeds of slow (dark red dotted line) and fast-sinking particles (dark red, dashed line) are shown in four productivity and export efficiency regimes. The solid dark red line shows the average of slow and fast-sinking particles.

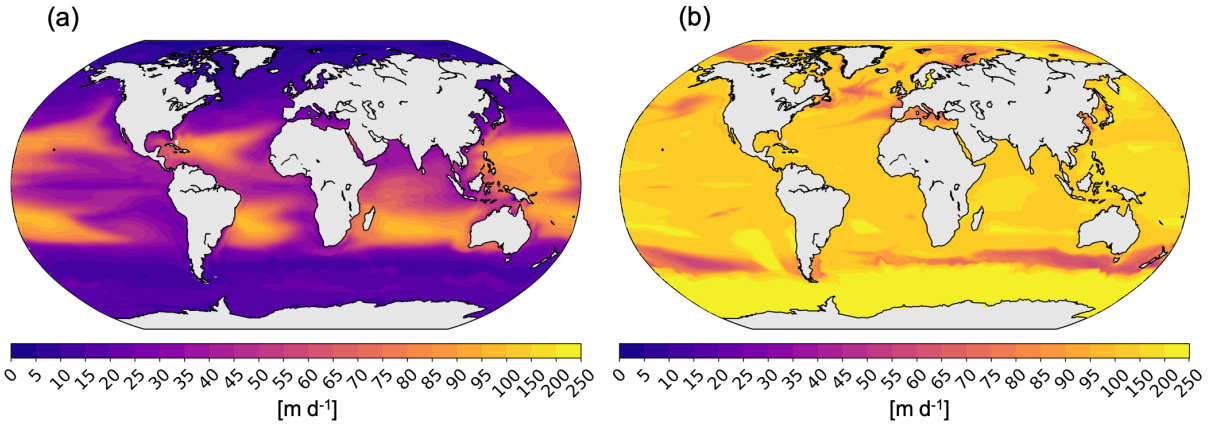

FIGURE 4.S5: The 5-year mean sinking speed (m d^{-1}) of the slow- and fast- sinking particles at the surface: (a) slow-sinking and (b) fast-sinking particles.

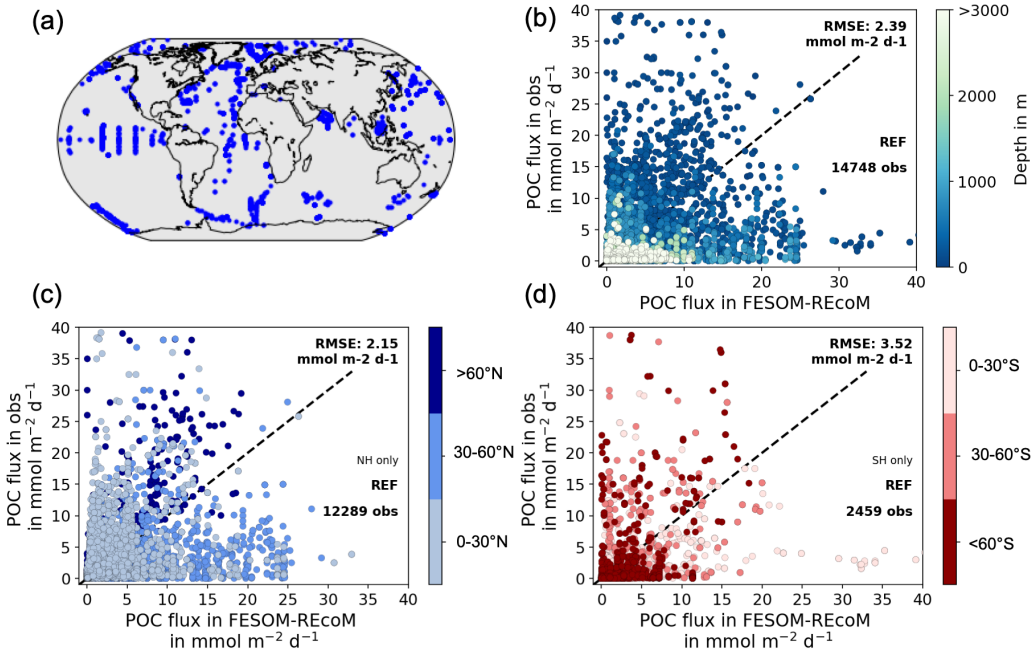

FIGURE 4.S6: Comparison of modeled and observed POC flux (a) the spatial distribution of data compiled by (*Mouw et al.*, 2016), (b) Comparison of particulate organic carbon (POC) flux (mmol C m^{-2} d^{-1}) sorted by depth (m), (c) Comparison of POC flux (mmol C m^{-2} d^{-1}) sorted by three subregions in the northern hemisphere and (d) Comparison of POC flux (mmol C m^{-2} d^{-1}) sorted by three subregions in the southern hemisphere

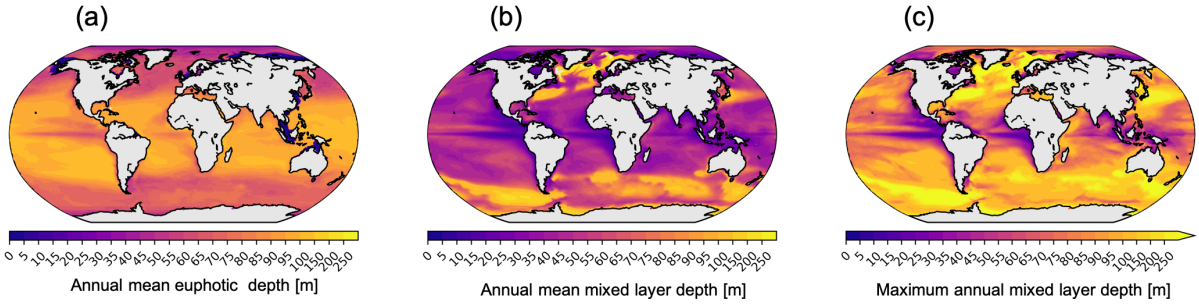

FIGURE 4.S7: Spatial distribution of different depth horizons: (a) Annual mean of euphotic depth, (b) annual meean of mixed layer depth (MLD), and (c) maximum annual MLD in the REF simulation.

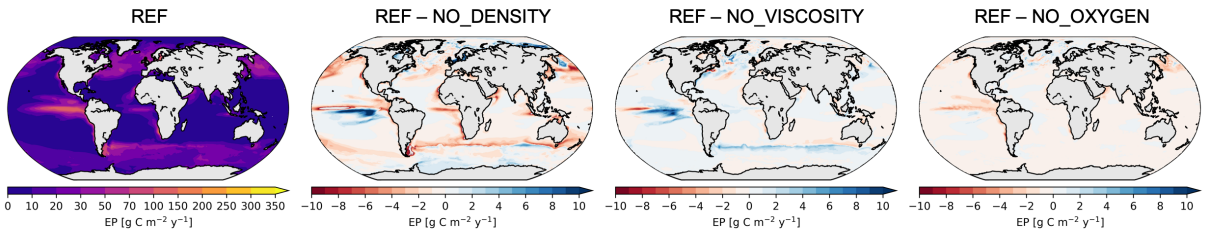

FIGURE 4.S8: The temporal mean of POC export production (EP, g C m^{-2} yr^{-1}) across euphotic depth in the baseline simulation REF (first column) and the effects of ballasting, viscosity and oxygen-dependent remineralization as derived by the difference between REF and the specific simulations NO_DENSITY, NO_VISCOSITY, and NO_OXYGEN.

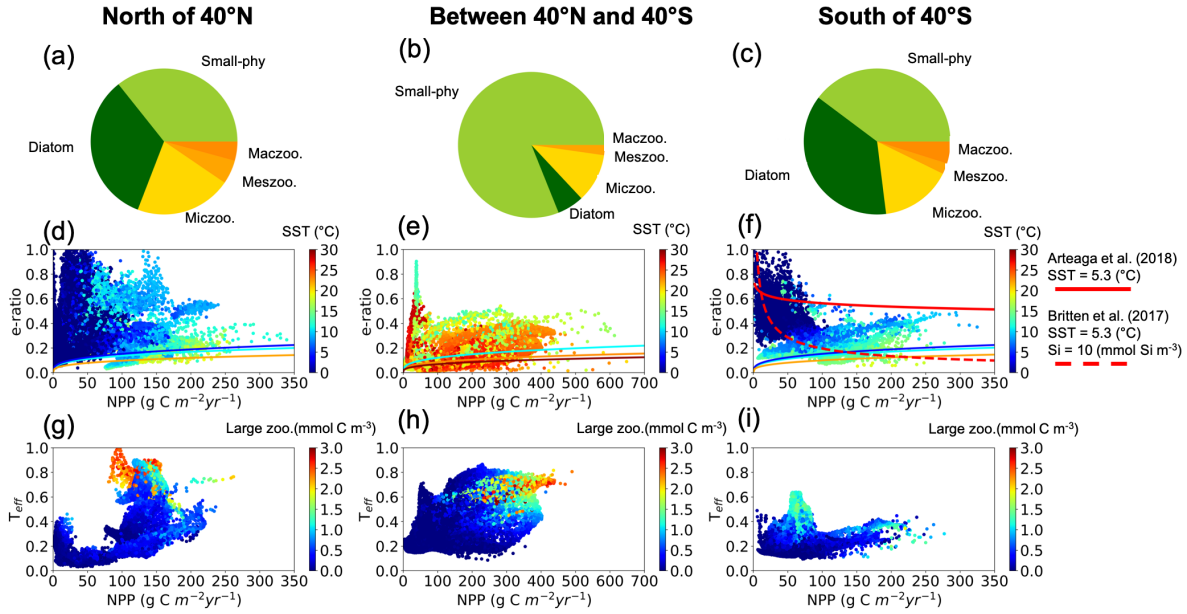

FIGURE 4.S9: Export efficiency (e-ratio) and transfer efficiency (T_{eff}) in relation to community composition, net primary production (NPP) and sea surface temperature (SST). The first row illustrates the share (%) of biomass of each plankton functional type to the total plankton biomass within the euphotic zone. Diatom, small phytoplankton, microzooplankton,mesozooplankton, and macrozooplankton are represented with dark green, light green, yellow, orange, and dark orange, respectively. The second row shows the e-ratio versus modeled total net primary production (NPP), with points colored by temporal mean SST (°C). Also, the relationship between NPP and e-ratio was calculated by using the empirical equation from *Laws et al.* (2011) and are plotted as solid lines (at temperatures of 5.3, 18, 30°). The colors of lines correspond to SST colors in the color bar. The two red lines in panel f show the results from the empirical equations suggested by *Arteaga et al.* (2018) and *Britten et al.* (2017). The third row shows the transfer efficiency (T_{eff}) versus the modelled total net primary production (NPP) , with points colored by temporal mean surface large zooplankton (meso- and macrozooplankton biomass, mmol C m^{-3}) biomass.

SYNTHESIS AND OUTLOOK

Biogeochemical models are powerful tools for researching global biogeochemical cycles and pelagic ecosystems (*Le Quéré et al.*, 2005; *Hood et al.*, 2006). Researchers have used such models to study carbon and nutrient cycling (*Henson et al.*, 2015; *Le Quéré et al.*, 2016) and phytoplankton dynamics (*Hashioka et al.*, 2013) for more than two decades. By design, all of these models are simplifications of complex natural ecosystems. Therefore, it is not possible to represent all organisms and processes that occur in the natural environment in these models. As a compromise, key species and processes are implemented in the framework of 'Plankton Functional Type (PFT) modeling' to simulate ocean biogeochemistry and plankton diversity to the extent needed (*Le Quéré et al.*, 2005; *Hood et al.*, 2006). Most PFT models in the literature represent several phytoplankton functional types such as coccolithophores, diatoms, *Phaeocystis* (*Moore et al.*, 2004; *Romanou et al.*, 2014; *Wright et al.*, 2021). However, zooplankton functional types are less well represented in these models. Except for recent examples from PlankTOM and COBALT (*Le Quéré et al.*, 2016; *Stock et al.*, 2020; *Wright et al.*, 2021), PFT models usually represent zooplankton with only one or two zooplankton functional types (*Séférian et al.*, 2020). The limited amount of zooplankton functional types can be one reason for the misrepresentation of zooplankton-related processes such as fecal pellet production, dissolved organic carbon and nutrient excretion, respiration, and grazing, which all play important roles for ocean biogeochemical cycles and food webs. Therefore, there is a growing body of work including multiple zooplankton functional types in biogeochemical models (e.g., *Buitenhuis et al.*, 2006, 2010; *Le Quéré et al.*, 2016; *Stock et al.*, 2020; *Wright et al.*, 2021)

In this thesis, I used a global setup of a physical-biogeochemical model to quantitatively assess the role of zooplankton functional types on the carbon export and sequestration flux, nutrient recycling, and phytoplankton bloom phenology. Besides, I used the model to investigate the role of mineral ballasting, seawater viscosity, and oxygen-dependent remineralization on carbon export efficiency and transfer efficiency and set these processes in perspective to the role of phytoplankton and zooplankton community composition. I will first summarize the major scientific findings of the thesis (section 5.1), and then I will discuss the scientific progress and the limitations of the results (section 5.2). Lastly, I will discuss future research ideas (section 5.3) emerging from the work presented in this thesis.

5.1 MAJOR FINDINGS AND CONCLUSION

In the pelagic ecosystem, zooplankton plays an important role due to its functions, such as recycling of carbon and nutrients and grazing on phytoplankton. The focus of this Ph.D. project was to investigate the role of zooplankton in global biogeochemical cycles and, in particular, to assess the sensitivity of biogeochemical model results to the representation of multiple zooplankton functional types. For this purpose, it was necessary to conduct literature research and define the key processes of zooplankton functional types before implementing them in the biogeochemical model REcoM. Throughout the Ph.D. project, three zooplankton functional types and a new fast-sinking detritus class were implemented (*Publication I* and *II*) into the biogeochemical model REcoM (Fig. 5.2), which originally only contained single generic zooplankton and a single detritus group. After the parametrization of the new zooplankton functional types, this new model version was used to explore the drivers of carbon export and transfer efficiencies. To this end, a new sinking routine was implemented in the model in *Publication III*. Scientifically, this thesis has contributed to addressing the following research questions by using a biogeochemical model:

- What is the role of zooplankton in carbon export and nutrient recycling?
- How does zooplankton grazing affect phytoplankton bloom phenology?

- What are the relative roles of plankton community composition and of mineral ballasting, seawater viscosity, and oxygen-dependent remineralization on carbon export efficiency and transfer efficiency?

In the following, the contribution of this thesis to address each of these questions will be summarized:

What is the role of zooplankton in carbon export and nutrient recycling?

Publication I presented and evaluated the global biogeochemical model REcoM after implementing a polar macrozooplankton and associated fast-sinking detritus class. The model reproduces the high biomass of macrozooplankton in the Southern Ocean as known from observations (*Moriarty et al.*, 2013). Our model results reveal a macrozooplankton-related contribution of up to 14% to total carbon export in the Southern Ocean south of 50°S. Besides its contribution to the carbon export, the transfer efficiency of carbon reaches up to 50% in the regions where high macrozooplankton biomass occurs. Similarly, I showed that the high mesozooplankton and macrozooplankton abundance enhances carbon transfer efficiency (reaching up to 80%) in the equatorial upwelling regions and the Southern Ocean (*Publication III*). These findings imply that models benefit from representing additional zooplankton functional types and their fast-sinking fecal pellets to better capture the mechanistic processes of carbon export.

The role of zooplankton in nutrient recycling was mainly discussed in *Publication II*. In that study, I presented a new model version with three zooplankton functional types (REcoM-3ZOO). Our model reproduces the global biomass and spatial distribution of micro-, meso- and macrozooplankton (*Buitenhuis et al.*, 2010; *Moriarty et al.*, 2013; *Moriarty and O'Brien*, 2013) and their expected roles in the carbon cycle reasonably well. In *Publication I* and particularly in *Publication II*, I illustrated that nutrient recycling by zooplankton stimulates the net primary production in the biogeochemical model REcoM. The new food web structure of the model leads to a 25% increase in annual net primary production compared to the original version of the model. This resulted from the role of zooplankton in the partitioning of primary production between recycled production, export, and standing stocks of organic matter. The findings imply that the mean state of nutrients and primary production in the model and comparability of the results with observations can benefit from the representation of zooplankton functional types.

How does zooplankton grazing affect phytoplankton bloom phenology?

In *Publication II*, I use the global biogeochemical model to assess the bloom phenology of phytoplankton in the Atlantic sector of the Southern Ocean. This publication compared the phytoplankton bloom phenology in two model versions (REcoM-2 and REcoM-3ZOO) and evaluated it with satellite data (*Johnson et al.*, 2013). These comparisons showed that a parameterization that resulted in weak grazing pressure causes an early start of the phytoplankton bloom in the model. Enhancing zooplankton grazing delays the start of the phytoplankton bloom by three weeks and controls the magnitude of the bloom peak in the Southern Ocean. Furthermore, our results suggest that the increase in the phytoplankton loss rate due to zooplankton grazing changes the mechanism behind the start of the phytoplankton bloom. In the original version of the model with one zooplankton group and weak grazing pressure, the start of the spring bloom in the Southern Ocean depends on bottom-up control (light availability) as in Sverdrup's 'Critical Depth Hypothesis' (*Sverdrup*, 1953). In contrast, in the model version with three zooplankton functional types, the spring bloom is initialized when the mixed layer depth is at its maximum. The underlying cause is the dilution of grazers due to the deepening

of the mixed layer, and this model state mirrors Behrenfeld's 'Dilution–Recoupling Hypothesis' (*Behrenfeld*, 2010). The model results now align with the current theories about phytoplankton bloom initiation, but foremost this highlights the sensitivity of phytoplankton bloom phenology to the zooplankton representation in the model.

What are the relative roles of plankton community composition and of mineral ballasting, seawater viscosity, and oxygen-dependent remineralization on export efficiency and transfer efficiency?

In this thesis, I used three different versions of the biogeochemical model REcoM for global-scale carbon export analysis (Fig. 5.1). In the original version of REcoM with one zooplankton group, the global export efficiency across the euphotic depth is 19.2% and the transfer efficiency amounts to 10.6%. In the version with three zooplankton functional types (REcoM-3ZOO, *Publication II*), the export efficiency decreases to 12.7% across the euphotic depth and the transfer efficiency of carbon increases to 29.6 %. This indicates that both global export efficiency and transfer efficiency change substantially with the number of plankton functional types in the model. Further, in *Publication III*, I implemented a new sinking routine (modified version of *Cram et al.*, 2018) into the biogeochemical model REcoM-3ZOO. The new configuration allowed me to separately quantify the effect of previously omitted processes on carbon export and sequestration flux in the models (*Henson et al.*, 2022). In *Publication III*, I focused particularly on the effect of the three processes, namely seawater viscosity, mineral ballasting, and oxygen-dependent remineralization, on carbon export efficiency and transfer efficiency. Our results show that the global mean export efficiency across the euphotic depth stays similar (13.7$\pm$0.2%) whether or not the effects of seawater viscosity, mineral ballasting, and oxygen-dependent remineralization were included in the model. However, the global mean carbon transfer efficiency is more sensitive and varies between 25% and 32% in the different simulations. The magnitude of the effect of each process shows spatial variability. While the effect of ballast minerals increases the transfer efficiency by a factor of nine in high latitudes and subtropical gyres, including oxygen-dependent remineralization increases the transfer efficiency by 28% in low latitudes. The influence of seawater viscosity on transfer efficiency is smaller than the other effects, with the largest effect being an increase of the transfer efficiency by 8% in subtropical gyres. These findings contribute to a previous study that summarized different estimates of present-day particle export fluxes depending on which processes are included in a model (*Henson et al.*, 2022).

Model Developments in this Thesis

In addition to examining the previously listed questions, the work contributes to the ongoing development of REcoM. Throughout this Ph.D. project, three zooplankton functional types and a fast-sinking detritus class were implemented in the model (Fig. 5.2). The model now differs from other models in the literature, notably by representing the polar macrozooplankton group, which has a high biomass in the Southern Ocean. Furthermore, a new sinking routine was implemented into the model (*Publication III*). This is an important first step in order to assess the global particulate organic carbon (POC) flux and underlying processes in follow-up studies of the present-day and future biological carbon pump.

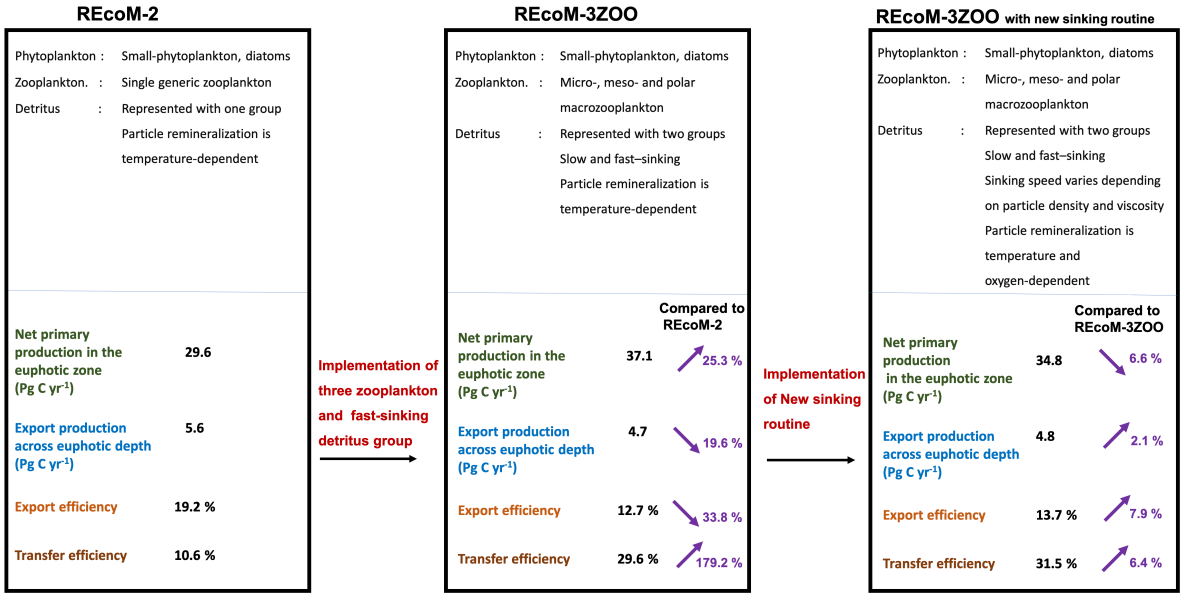

FIGURE 5.1: Summary of global integrated net primary production, export production, export efficiency and transfer efficiency in the different versions of REcoM.

5.2 LIMITATIONS AND IMPLICATIONS OF THE NEW PARAMETRIZATIONS IN RECOM

There are still many ways in which biogeochemical models can be improved. Previous studies reported the sensitivity of the biogeochemical model results to parameter values (*Hill Cruz et al.*, 2021), process formulations (*Gentleman and Neuheimer*, 2008), physics (*Couespel et al.*, 2021), or new plankton functional types (*Le Quéré et al.*, 2016). In this thesis, I demonstrated the sensitivity of one biogeochemical model to the implementation of new zooplankton functional types. In my studies, it is shown that "structuring and parameterizing biogeochemical models based on observations without tuning is a strategy that works," as suggested by *Buitenhuis et al.* (2006). I showed that the model's mean state is improved by the representation of zooplankton functional types and related processes. Nevertheless, the parametrizations of zooplankton functional types and sinking particles have limitations and caveats that will be discussed in the following.

Parametrization of Zooplankton Functional Types

In *Publication I* and *II*, we parameterized three zooplankton functional types: micro-, meso- and macrozooplankton. Microzooplankton is parametrized as a fast-growing herbivore group that is closely coupled to the growth of phytoplankton, whereas the mesozooplankton group has a lower grazing rate and produces fast-sinking fecal pellets. The macrozooplankton group was parametrized close to polar macrozooplankton, which produce fast-sinking fecal pellets with a high carbon to nitrogen ratio. Thus, the main differences between the zooplankton functional types are their temperature sensitivities and the group-specific parameter values reflecting their main roles as outlined above (see *Publication II* supplementary). In REcoM-3ZOO, the same grazing and mortality formulations are used for all zooplankton functional types. Here, I will discuss the possible effects of different grazing, mortality, and grazing preference formulations on our results.

There is a long list of publications since the 1960s that describe the influence of different grazing formulations on single (e.g., *Holling*, 1965; *Steele*, 1974; *Gentleman and Neuheimer*, 2008)

and multiple prey systems (e.g., *Gentleman et al.*, 2003; *Anderson et al.*, 2010). The most common results of these studies are the drastic change in phytoplankton composition and biomass due to the different formulations. A very robust example is from *Anderson et al.* (2010). The authors illustrated that the global diatom biomass changed by a factor of five when using different grazing formulations. In this thesis, we have used the same ingestion function (Holling Type III, *Holling*, 1959) for all three zooplankton functional types and did not test the effect of Holling Type I and II ingestion formulations. The sigmoidal (Holling Type III) type of response can occur for the whole population even when the individual zooplankton species is non-sigmoidal (Holling Type I or II) (*Lampert*, 2005; *Morozov and Arashkevich*, 2008). However, Holling Type I and II responses are common for filter feeders (*Jeschke et al.*, 2002, 2004). Therefore, further tests of using the Holling Type II ingestion function for the herbivorous microzooplankton group could be done in the future in REcoM. I expect that using a Holling type II grazing function for microzooplankton would not change the main findings regarding the role of zooplankton functional types on carbon export and nutrient recycling. Still, the magnitude of these processes could be affected when the sensitivity of phytoplankton and consequently zooplankton biomass to the chosen equation is considered (*Anderson et al.*, 2010).

Another aspect is the grazing preference of the zooplankton functional types on different prey. The preference for multiple prey can be constant or variable. While the constant preference reflects given prey palatability or is related to predator–prey size ratios, variable preference is a way to describe how zooplankton select preferentially the most abundant prey (*Vallina et al.*, 2014). When the variable preference option is used, passive or active switching between the preys can be used. While active switching depends on the relative densities of the multiple prey, passive switching is associated with the single resource responses (*Gentleman et al.*, 2003; *Vallina et al.*, 2014). The choice of the grazing preference formula affects the model results, however, the effect is much smaller than using a different grazing equation. For instance, (*Vallina et al.*, 2014) illustrated that the choice of different grazing preference formulations can decrease phytoplankton biomass by up to 10%. In our model, I used the variable grazing formulation from *Fasham et al.* (1990). In the case of implementing new phytoplankton functional types to the model, future users of the model should reassess the performance of the current equation because it was shown that the feeding probability on each phytoplankton group decreases with the increasing number of phytoplankton groups (*Vallina et al.*, 2014).

Zooplankton mortality represents the death of individuals and loss of their associated biomass due to predation, starvation, genetic malfunction, and disease (*Carlotti et al.*, 2000). Different mathematical functions (linear, quadratic, hyperbolic, sigmoidal) are used, and their choice by modelers is generally based on theoretical arguments rather than specific mechanisms or observations (*Mitra et al.*, 2014). Similar to the ingestion function, the use of different mortality functions can influence the results of the models. *Mitra et al.* (2014) did a detailed analysis by using NPZD-type (*Fasham et al.*, 1990) models. The authors showed that nutrients, bacteria, and especially zooplankton biomass are sensitive (decrease or increase) to the choice of the zooplankton mortality function. A recent example analysed the sensitivity of zooplankton and phytoplankton biomass to a change of zooplankton's mortality parameter values by $\pm 50\%$ (*Hill Cruz et al.*, 2021). We used the quadratic mortality function in our parametrizations and did not perform a systematic sensitivity test for the mortality equations and parameter values. The mortality term remains to be a parameter that needs tuning due to difficulties in obtaining realistic mortality estimates from the field, laboratory, or mesocosm studies *Mitra et al.* (2014).

Finally, a representation of zooplankton diel and/or seasonal vertical migration is lacking in REcoM. Large-scale biogeochemical models still include this behavioral feature only rarely, because of difficulties to parameterize this process (*Archibald et al.*, 2019). For instance, none of the biogeochemical components of CMIP6 Earth System Models represents vertical migration

of zooplankton (*Henson et al.*, 2022). However, including vertical migration of zooplankton may enhance present-day export estimates by 14% to 40% globally (*Aumont et al.*, 2018; *Archibald et al.*, 2019). Thus, the importance of zooplankton in carbon fluxes might be even more prominent than what we have shown in this thesis. The limited number of models including zooplankton vertical migration indicates a research gap in this field. Therefore, developing the representation of zooplankton vertical migration in REcoM and using the model to investigate its impact on present-day, and future carbon export flux estimates might be an interesting aspect in the future.

Parametrization of Detritus Classes

I used REcoM versions with two detritus classes in *Publication I, II,* and *III*. The reason behind implementing the new fast-sinking particles is the observed high sinking rates of zooplankton fecal pellets (*Turner*, 2002). In the literature, a large range of sinking speeds of zooplankton fecal pellets is reported (5 to 2700 m d^{-1}, *Turner*, 2002). The sinking speed of fecal pellets depends on the species. For example, while the sinking speed of copepod fecal pellets ranges from 5 to 200 m d^{-1}, pellets of euphausiids may sink with velocities between 16 and 862 m d^{-1} (for the complete set of ranges of other zooplankton groups, see Table 2 in *Turner*, 2002). It remains a challenge to capture this wide variety of particle sinking speeds in biogeochemical models. Therefore, having a fast-sinking detritus class and associating it with zooplankton groups is an improvement for REcoM. However, the explicit division of the spectrum of sinking particles into two pools gives a strong geographical separation between the two sinking particle pools. For instance, while the fast-sinking particles dominate the upper ocean only in the regions with high meso- and macrozooplankton biomass, the slow-sinking particles can make up to 100% of total sinking particles in some regions such as the subtropical gyres (see supplementary Figure 4.S1 in *Publication III*). Hence, the model design inherently makes a strong assumption about the spatial distribution of the particle classes. We see this effect directly in *Publication III* in the regions with high meso- and macrozooplankton abundance. These regions are characterized by high transfer efficiencies of carbon.

In the literature, the sinking rates of various types of particles were reported to lie between 5 and 2700 m d^{-1} (*Turner*, 2002). The ocean biogeochemical models are far from covering this range of sinking speeds (see supplementary Table 1 in *Henson et al.*, 2022) and there is no consensus about the pre-defined sinking speed parameter. The particle sinking speeds vary between 1 m d^{-1} and 200 m d^{-1} (sometimes varying with depth) among the models. If a biogeochemical model represents the explicit sinking of particles, the particles generally have a constant sinking speed. In *Publication III*, I implement the tested one-dimensional particle sinking model (*Cram et al.*, 2018) in REcoM. This application does not come at the expense of high computational demand and provides large variability of particle sinking speed. It provides insights into the underlying processes of export flux, as shown in *Publication III*. Therefore, I suggest using the new sinking routine for the future users of the model.

5.3 DIRECTIONS OF THE FUTURE RESEARCH

In the following section, possible topics of future research regarding future model development in FESOM-REcoM will be discussed, resulting from the limitations of the results presented in this thesis. Also, other open questions in the field of zooplankton and PFT modeling will be addressed.

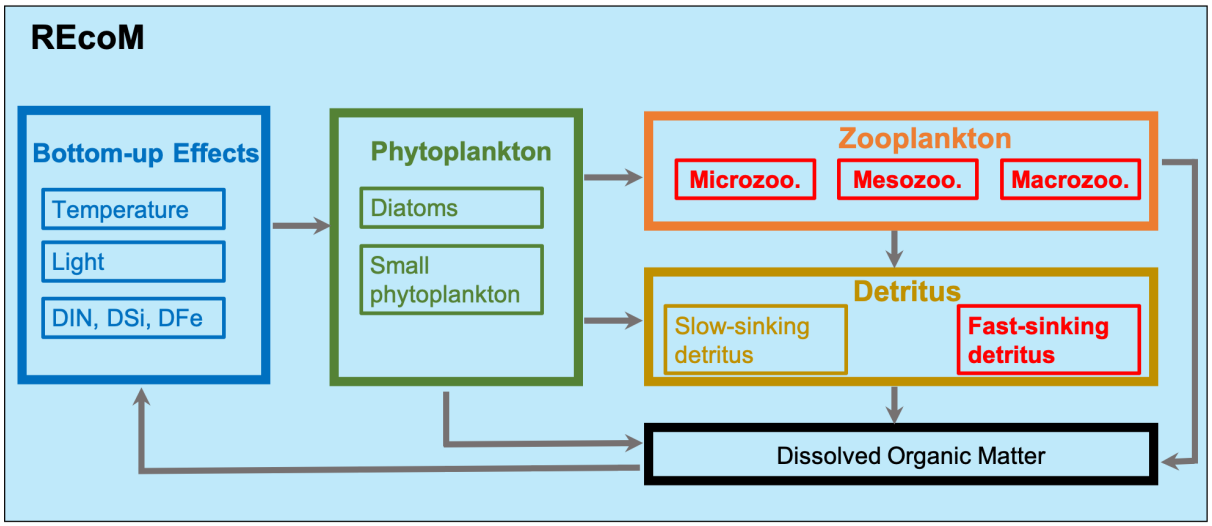

FIGURE 5.2: Simplified schematic figure of the main components and links in the Regulated Ecosystem Model (*Hauck et al.*, 2013; *Karakuş et al.*, 2021). Compartments and processes that were implemented during the work on this thesis (micro-, meso- and macrozooplankton and fast-sinking detritus) are highlighted in red.

Do we need multiple zooplankton functional types in PFT Models?

There is a large spread in the number, name, equations, and parameter values of zooplankton functional types in the biogeochemical models (Chapter 1). As to the balance between model simplicity and complexity, it is still a valid question whether we should implement more zooplankton functional types into the models or not? Are the additional computational costs justified (*Kriest et al.*, 2010; *Kwiatkowski et al.*, 2014)? The answer certainly depends on the scientific question posed. The main decisive factor is whether processes (grazing, nutrient recycling, or fecal pellet production) via which zooplankton impacts global biogeochemical cycles are well represented. This is important because in PFT models we primarily model processes and not organisms. Hence, a critical question is whether it is possible to capture all of these processes and their effects on ocean biogeochemistry by a single generic zooplankton group. According to results in *Publication II*, at least two zooplankton functional types must be present in global models to realistically model the zooplankton-related processes. A single generic zooplankton group parametrized is not enough to reproduce the global zooplankton biomass. And even if the biomass is captured well in the global ocean after tuning experiments, the rates of loss (fecal pellet productions, excretion, respiration) or gain (grazing) terms are probably unrealistic (*Publication II*). Thus, there will be an under- or overestimation of the role of zooplankton for biogeochemical cycles on a global scale. Therefore, improvement of parameterizations of new zooplankton functional types remains essential despite all the difficulties in finding the right parameter values. The improvement of the model's mean state after parametrization of three zooplankton functional types as shown in this thesis makes us confident to suggest to modelers to parametrize at least three zooplankton functional types in global biogeochemical models.

Our findings clearly show that the bulk properties (nutrients, net primary production) of the global biogeochemical model REcoM have benefited from the parametrization of three zooplankton functional types. Now, the model represents the most important zooplankton groups to mimic important biogeochemical functions. In further steps they could be separated

into additional size classes, but that would possibly be computationally expensive for our purposes to use them in an Earth System Model.

PFT models and/or Trait-based models

Since certain plankton functional types account for the most important biogeochemical processes (e.g., calcification, fecal pellet production, nitrogen fixation), the reason why we need PFT models is clear. Although there was a productive discussion about the usefulness of increasing complexity in the models in the first decade of PFT modeling (*Anderson*, 2005; *Le Quéré*, 2006; *Flynn*, 2006), today PFT models are widely accepted and used by the research community for questions such as carbon cycling and phytoplankton bloom phenology (e.g., *Le Quéré et al.*, 2016; *Stock et al.*, 2020; *Hashioka et al.*, 2013). The acceptance of these types of models is partly related to the increase of knowledge and data on plankton functional types (*Buitenhuis et al.*, 2013), but also to the need for understanding the response of phytoplankton, zooplankton, and export fluxes to a changing climate (*Bopp et al.*, 2013; *Séférian et al.*, 2020; *Henson et al.*, 2022). There is, therefore, no doubt about the usefulness of these models.

In the Plankton Functional Type models, one of the ways to represent complex interactions in the ocean is by implementing new processes and/or plankton functional types. In principle, both strategies are valuable for answering questions about carbon export or biogeochemical cycles. However, things get more complicated when these models are used to investigate more ecological topics, such as competition between plankton functional types or future projections of zooplankton and phytoplankton biomass and of net primary production. It should not be forgotten that these models are built on each functional group's traits which are fixed characteristics of a functional group that describes its growth or fitness (*Kiørboe et al.*, 2018). In other words, the method that is used in PFT models is based on defining the trophic network by prescribing who consumes what and at what rates (*Kiørboe et al.*, 2018). Therefore, model results are always strongly dependent on the prescription of the rates or structure of the model.

Trait-based models have been used simultaneously with PFT models for years to study plankton ecology. These models are designed for microbial communities to mimic the plankton diversity by using simple formulations and the basic principle of survival of the fittest (*Kiørboe et al.*, 2018). Trait-based models consider individuals with key traits described by few parameters and characterized by environmentally dependent trade-offs, which are the costs and benefits of particular physiological characteristics (*Follows et al.*, 2007; *Kiørboe et al.*, 2018). Therefore, they can better predict the competition between marine microbial communities caused by future environmental changes. This approach is already used by modelers on a global scale, mainly to describe competitive interactions between marine phytoplankton (*Follows et al.*, 2007; *Ward et al.*, 2012; *Dutkiewicz et al.*, 2014). In contrast, there are only a few trait-based studies in which the focus lies on marine zooplankton, although the global distribution of zooplankton traits (e.g., body size, feeding mode, egg size, spawning strategy and respiration rate) is well-documented (*Kiørboe*, 2011; *Litchman et al.*, 2013; *Brun et al.*, 2016). However, the use of traits to define the main zooplankton groups and their implementation in models continues to attract interest from the scientific community. For instance, a recent study identifies eleven copepod functional groups that are built on a species trait dataset in the global ocean (*Benedetti et al.*, 2022, in review). In this context, it is important to note the modeling work from *Serra-Pompei et al.* (2020) who present a new model type (Nutrients–Unicellular–Multicellular (NUM)) that considers the size and trait distribution. The new concept (NUM) was recently embedded within a representation of the global ocean circulation, using the "transport matrix method" (*Khatiwala*, 2007), and it was used to investigate carbon export efficiency (*Serra-Pompei et al.*, 2022). The authors showed that carbon export correlates well with copepod biomass and calculated trophic levels in the

model(*Serra-Pompei et al.*, 2022). To sum up, the availability of data on zooplankton traits and the use of these data in models are increasing. Therefore, implementing a trait-based approach could be a potential avenue for future research on the role of zooplankton in biogeochemical cycles in global ocean models. It should be noted that these models consist of a large number of tracers (*Ward et al.*, 2012). Thus, they are computationally costly to use coupled to climate models for now.

The Evaluation of Zooplankton Functional Types in the Models

Biological complexity, namely the number of plankton functional types and nutrients, can be increased in ocean biogeochemical models to represent the lower trophic levels of the ecosystem more realistically. However, when we increase the complexity of the models, we also need to assess the model results with the observations quantitatively. Although this is the general rule, the zooplankton component of models is rarely assessed in detail due to the different temporal and spatial resolutions of observations and model outputs (*Everett et al.*, 2017). In addition, the observations and model outputs are often reported in different formats. For instance, field studies generally report abundance of zooplankton rather than mass of nitrogen or carbon, as used in models (*Everett et al.*, 2017). However, data wrangling (*Kandel et al.*, 2011), which is the transformation of one format to a more useful format for modellers, does make the comparison and evaluation possible. For example, the MAREDAT data products (also used for for the assessment of zooplankton biomass in this thesis, *Buitenhuis et al.*, 2010; *Moriarty and O'Brien*, 2013; *Moriarty et al.*, 2013) are an excellent example of data wrangling. While these data sets were a big step forward to facilitate model evaluation, they are still far away to be a real 'constraint' comparable to surface chlorophyll and nutrient concentrations (*Everett et al.*, 2017). Any model which produces reasonable chlorophyll and nutrient concentrations will give a similar global spatial distribution of zooplankton biomass (*Petrik et al.*, 2022, in review).

More rarely, satellite products are also used to study zooplankton directly to detect swarms (*Basedow et al.*, 2019) or indirectly as an indicator for zooplankton biomass (*Strömberg et al.*, 2009). Such estimates based on chlorophyll concentration result in similar mean zooplankton biomass and spatial distribution as large-scale biogeochemical models (*Strömberg et al.*, 2009). Recently, *Belcher et al.* (2021) reported the reflectance spectra of freshly caught krill as a base for future remote detection by satellites. In addition, *Menden-Deuer et al.* (2021b) hypothesized that grazing affects the absorption coefficients and scattering functions of seawater, and this could allow scientists to use remote sensing to detect herbivorous grazing. Future innovation in this field will make the evaluation of zooplankton components of biogeochemical models easier.

Zooplankton in Earth System Models

Several studies assessed the outputs of biogeochemical models that are coupled to Earth System Models (ESMs) used for climate simulations (*Bopp et al.*, 2013; *Kwiatkowski et al.*, 2020; *Séférian et al.*, 2020). The focus of these studies was mainly the assessment of future warming, deoxygenation, and acidification in Coupled Model Intercomparison Project 5 (CMIP5) (*Bopp et al.*, 2013), and CMIP6 models (*Kwiatkowski et al.*, 2020). Additionally, *Séférian et al.* (2020) mapped the changes or updates in ocean biogeochemistry components of ESMs between CMIP5 and CMIP6 model versions. However, none of these studies reported a detailed analysis of zooplankton biomass. Recently, *Petrik et al.* (2022) assessed the mesozooplankton representation in six ESMs from CMIP6. The study's main findings were: (1) On the global scale, five out of six models represent mesozooplankton moderately well compared to observations, (2) the

mesozooplankton and chlorophyll relationship can be an emergent constraint to zooplankton projections, and (3) more attention needs to be paid to prey preferences, food web structure and temperature sensitivity. A close look at this valuable analysis shows that historic area-weighted mean mesozooplankton biomass in the models ranges between 291 and 646 mg C m^{-2} globally. The seasonal cycle of the mesozooplankton biomass differs between models and future changes of mesozooplankton biomass follow the direction of changes in chlorophyll concentrations. Although these kinds of studies are precious to track differences among models, they mainly report the same message, namely that the food web structure and the parametrizations in the biogeochemical models lead to a large spread in the model results (*Bopp et al.*, 2013; *Frölicher et al.*, 2016; *Petrik et al.*, 2022).

In this Ph.D. thesis, I worked on the mean zooplankton biomass and underlying processes in REcoM. The current state of the zooplankton functional types in the model compares reasonably well with the observations of biomass and of global and regional fluxes. Hence, this model is well suited for future scenario simulations. The next step in the future could be using the model to examine the response of zooplankton functional types to future environmental changes.

Processes Related to Export Fluxes in Biogeochemical Models

The deep ocean is the long-term storage of carbon, and the particulate export flux is the mechanism carrying carbon from the upper ocean to the deep ocean (*Passow and Carlson*, 2012). Global ocean biogeochemical models are commonly used to quantify the export flux and analyze its large-scale spatial pattern (*Henson et al.*, 2015; *Palevsky and Doney*, 2018). The gravitational sinking of particles is an important component of export flux and is represented in all climate models with a marine biogeochemistry module (*Buesseler et al.*, 2020; *Henson et al.*, 2022). However, the representation of processes that affect sinking particle generation and transformation (e.g., fragmentation, the viscosity of seawater, mineral ballasting, zooplankton vertical migration) vary widely among the models (*Henson et al.*, 2022). Omitting these processes does affect not only the export flux but also the net primary production and export ratio in the models (*Kwiatkowski et al.*, 2020; *Séférian et al.*, 2020).

In this regard, the representation of particle fragmentation and vertical migration through zooplankton in the models is worth highlighting. It is known that zooplankton play a quantitatively important role in the vertical carbon flux due to particle fragmentation and vertical migration (*Banse*, 1990; *Steinberg and Landry*, 2017). Numerous small copepods are associated with detrital particles on which they feed and are identified as "gatekeepers" for the particle flux through the euphotic zone (*Gonzalez and Smetacek*, 1994; *Koski et al.*, 2020). Several studies particularly point to the role of particle-associated copepods in particle fragmentation rather than ingestion of detrital particles (*Lampitt et al.*, 1990; *Noji et al.*, 1991). Similarly, migration by zooplankton may be a significant flux component as carbon is transported from the upper ocean directly to the mesopelagic (*Steinberg and Landry*, 2017). These two processes are not represented in any CMIP6 model, despite their potentially large effect on export flux (*Henson et al.*, 2022). In the future, the Global Ocean Observing System's Essential Ocean Variables (GOOS EOVs), may provide valuable observational data for a better understanding and, hence, model parametrization of these two processes. The recent increase in the use of autonomous platforms such as mooring lines and floats may provide new insights into export processes, including particle fragmentation and vertical migration (*Henson et al.*, 2022). Therefore, the implementation of these two known and quantitatively important export processes (*Banse*, 1990; *Mayor et al.*, 2014, 2020) should be prioritized for future biogeochemical model development.

In this PhD thesis, three new processes, namely mineral ballast, seawater viscosity, and oxygen-dependent remineralization, were implemented in the model (*Publication III*) because

the effects of these three factors are well understood from observational and experimental studies. This was the first step in representing the missing processes affecting sinking particle dynamics in REcoM. The next step in the future could be the implementation of particle fragmentation and vertical migration of zooplankton.

5.4 CONCLUSION

Zooplankton form an important component of the ocean ecosystem (*Steinberg and Landry*, 2017). However, it is generally treated as a top closure term and represented relatively simple in global biogeochemical models (*Edwards and Yool*, 2000; *Mitra et al.*, 2014). This was a result of limited global datasets about zooplankton features and biomass. However, the availability of increasingly detailed global datasets about zooplankton biomass (*Buitenhuis et al.*, 2010; *Moriarty et al.*, 2013; *Moriarty and O'Brien*, 2013) and traits (*Brun et al.*, 2016) increased remarkably over the last decades, and these were used to assess the biogeochemical models. In this thesis, I highlight the role of zooplankton in nutrient recycling, carbon export, and phytoplankton bloom phenology. Thus, our results suggest that zooplankton should be treated as more than a closure term in global biogeochemical models. This will not only increase the understanding of the underlying processes of biogeochemical cycles but also lead to more robust projections of the future biological carbon pump and lower trophic levels to climate change.

BIBLIOGRAPHY

Anderson, L. A., and J. L. Sarmiento (1995), Global ocean phosphate and oxygen simulations, *Global Biogeochemical Cycles*, *9*(4), 621-636, doi:10.1029/95GB01902.

Anderson, T. R. (2005), Plankton functional type modelling: running before we can walk?, *Journal of Plankton Research*, *27*(11), 1073-1081, doi:10.1093/plankt/fbi076.

Anderson, T. R., W. C. Gentleman, and B. Sinha (2010), Influence of grazing formulations on the emergent properties of a complex ecosystem model in a global ocean general circulation model, *Progress in Oceanography*, *87*(1), 201-213, doi:10.1016/j.pocean.2010.06.003.

Anderson, T. R., D. O. Hessen, A. Mitra, D. J. Mayor, and A. Yool (2013), Sensitivity of secondary production and export flux to choice of trophic transfer formulation in marine ecosystem models, *Journal of Marine Systems*, *125*, 41-53, doi:10.1016/j.jmarsys.2012.09.008.

Archibald, K. M., D. A. Siegel, and S. C. Doney (2019), Modeling the Impact of Zooplankton Diel Vertical Migration on the Carbon Export Flux of the Biological Pump, *Global Biogeochemical Cycles*, *33*(2), 181-199, doi:10.1029/2018GB005983.

Armstrong, R. A., C. Lee, J. I. Hedges, S. Honjo, and S. G. Wakeham (2001a), A new, mechanistic model for organic carbon fluxes in the ocean based on the quantitative association of POC with ballast minerals, *Deep Sea Research Part II: Topical Studies in Oceanography*, *49*(1), 219-236, doi:10.1016/S0967-0645(01)00101-1.

Armstrong, R. A., C. Lee, J. I. Hedges, S. Honjo, and S. G. Wakeham (2001b), A new, mechanistic model for organic carbon fluxes in the ocean based on the quantitative association of POC with ballast minerals, *Deep Sea Research Part II: Topical Studies in Oceanography*, *49*(1), 219-236, doi:10.1016/S0967-0645(01)00101-1.

Atkinson, A., V. Siegel, E. Pakhomov, and P. Rothery (2004), Long-term decline in krill stock and increase in salps within the Southern Ocean, *Nature*, *432*(7013), 100–103, doi:10.1038/nature02996.

Atkinson, A., K. Schmidt, S. Fielding, S. Kawaguchi, and P. Geissler (2012), Variable food absorption by Antarctic krill: Relationships between diet, egestion rate and the composition and sinking rates of their fecal pellets, *Deep Sea Research Part II: Topical Studies in Oceanography*, *59-60*, 147-158, doi:10.1016/j.dsr2.2011.06.008.

Aumont, O., C. Ethé, A. Tagliabue, L. Bopp, and M. Gehlen (2015), PISCES-v2: an ocean biogeochemical model for carbon and ecosystem studies, *Geoscientific Model Development*, *8*(8), 2465–2513, doi:10.5194/gmd-8-2465-2015.

Aumont, O., O. Maury, S. Lefort, and L. Bopp (2018), Evaluating the Potential Impacts of the Diurnal Vertical Migration by Marine Organisms on Marine Biogeochemistry, *Global Biogeochemical Cycles*, *32*(11), 1622-1643, doi:10.1029/2018GB005886.

Bandara, K., O. Varpe, L. Wijewardene, V. Tverberg, and K. Eiane (2021), Two hundred years of zooplankton vertical migration research, *Biological Reviews*, *96*(4), 1547-1589, doi:10.1111/brv.12715.

Banse, K. (1990), New views on the degradation and disposition of organic particles as collected by sediment traps in the open sea, *Deep Sea Research Part A. Oceanographic Research Papers*, *37*(7), 1177-1195, doi:10.1016/0198-0149(90)90058-4.

Banse, K. (1992), Grazing, temporal changes of phytoplankton concentrations, and the microbial loop in the open sea, in *Primary Productivity and Biogeochemical Cycles in the Sea*, edited by K. V. P.G. Falkowski, A.D. Woodhead, Springer, Boston, MA, doi:10.1007/978-1-4899-0762-2_22.

Banse, K. (1994), Grazing and Zooplankton Production as Key Controls of Phytoplankton Production in the Open Ocean, *Oceanography*, *7*(1), 13–20, doi:10.5670/oceanog.1994.10.

Banse, K. (2002), Steemann Nielsen and the zooplankton, *Hydrobiologia*, *480*, 15–28, doi:10.1023/A:1021220714899.

Banse, K. (2013), Reflections about chance in my career, and on the top-down regulated world, *Annual Review of Marine Science*, *5*, 1–19, doi:10.1146/annurev-marine-121211-172359.

Basedow, S. L., D. McKee, I. Lefering, A. Gislason, M. Daase, E. Trudnowska, E. S. Egeland, M. Choquet, and S. Falk-Petersen (2019), Remote sensing of zooplankton swarms, *Scientific Reports*, *9*(1), 686, doi:10.1038/s41598-018-37129-x.

Beaugrand, G., P. C. Reid, F. Ibanez, J. A. Lindley, and M. Edwards (2002), Reorganization of North Atlantic marine copepod biodiversity and climate, *Science*, *296*(5573), 1692–1694, doi:10.1126/science.1071329.

Beaugrand, G., C. Luczak, and M. Edwards (2009), Rapid biogeographical plankton shifts in the North Atlantic Ocean, *Global Change Biology*, *15*(7), 1790-1803, doi:10.1111/j.1365-2486.2009.01848.x.

Behrenfeld, M. J. (2010), Abandoning Sverdrup's Critical Depth Hypothesis on phytoplankton blooms, *Ecology*, *91*(4), 977–989, doi:10.1890/09-1207.1.

Behrenfeld, M. J., E. Boss, D. A. Siegel, and D. M. Shea (2005), Carbon based ocean productivity and phytoplankton physiology from space, *Global Biogeochemical Cycles*, *19*(1), doi:10.1029/2004GB002299.

Behrenfeld, M. J., S. C. Doney, I. Lima, E. S. Boss, and D. A. Siegel (2013), Annual cycles of ecological disturbance and recovery underlying the subarctic Atlantic spring plankton bloom, *Global Biogeochemical Cycles*, *27*(2), 526–540, doi:10.1002/gbc.20050.

Belcher, A., S. Fielding, A. Gray, L. Biermann, G. Stowasser, P. Fretwell, L. Ireland, and G. A. Tarling (2021), Experimental determination of reflectance spectra of Antarctic krill (*Euphausia superba*) in the Scotia Sea, *Antarctic Science*, *33*(4), 402–414, doi:10.1017/S0954102021000262.

Benedetti, F., J. Wydler, and M. Vogt (2022), Copepod functional traits and groups show contrasting biogeographies in the global ocean, *bioRxiv*, doi:10.1101/2022.02.24.481747.

Besiktepe, S., and H. G. Dam (), Coupling of ingestion and defecation as a function of diet in the calanoid copepod *Acartia tonsa* , *Marine Ecology Progress Series*, pp. 151–164, doi:10.3354/meps229151.

Bochdansky, Alexander B. and Deibel, Don and Rivkin, Richard B. (1999), Absorption Efficiencies and Biochemical Fractionation of Assimilated Compounds in the Cold Water Appendicularian Oikopleura vanhoeffeni, *Limnology and Oceanography*, *44*(2), 415–424, doi:10.4319/Lo.1999.44.2.0415.

Böckmann, S., F. Koch, B. Meyer, F. Pausch, M. Iversen, R. Driscoll, L. M. Laglera, C. Hassler, and S. Trimborn (2021), Salp fecal pellets release more bioavailable iron to Southern Ocean phytoplankton than krill fecal pellets, *Current Biology*, *31*(13), 2737–2746.e3, doi:10.1016/j.cub.2021.02.033.

Bopp, L., L. Resplandy, J. C. Orr, S. C. Doney, J. P. Dunne, M. Gehlen, P. Halloran, C. Heinze, T. Ilyina, R. Séférian, J. Tjiputra, and M. Vichi (2013), Multiple stressors of ocean ecosystems in the 21st century: projections with CMIP5 models, *Biogeosciences*, *10*(10), 6225–6245, doi: 10.5194/bg-10-6225-2013.

Boyd, P. W., H. Claustre, M. Levy, D. A. Siegel, and T. Weber (2019), Multi-faceted particle pumps drive carbon sequestration in the ocean, *Nature*, *568*(7752), 327–335, doi:10.1038/s41586-019-1098-2.

Brewin, R. J., S. Sathyendranath, T. Platt, H. Bouman, S. Ciavatta, G. Dall'Olmo, J. Dingle, S. Groom, B. Jönsson, T. S. Kostadinov, G. Kulk, M. Laine, V. Martínez-Vicente, S. Psarra, D. E. Raitsos, K. Richardson, M.-H. Rio, C. S. Rousseaux, J. Salisbury, J. D. Shutler, and P. Walker (2021), Sensing the ocean biological carbon pump from space: A review of capabilities, concepts, research gaps and future developments, *Earth-Science Reviews*, *217*, 103604, doi: 10.1016/j.earscirev.2021.103604.

Bruland, K. W., and M. W. Silver (1981), Sinking rates of fecal pellets from gelatinous zooplankton (Salps, Pteropods, Doliolids), *Marine Biology*, *63*(3), 295–300, doi:10.1007/BF00395999.

Brun, P., M. R. Payne, and T. Kiørboe (2016), Trait biogeography of marine copepods – an analysis across scales, *Ecology Letters*, *19*(12), 1403-1413, doi:10.1111/ele.12688.

Brussaard, C. P. D. (2004), Viral Control of Phytoplankton Populations—a Review, *Journal of Eukaryotic Microbiology*, *51*(2), 125-138, doi:10.1111/j.1550-7408.2004.tb00537.x.

Bryan, K. (1968), A Numerical Method for the Study of the Circulation of the World Ocean, *Journal of Computational Physics*, *135*(2), 154-169, doi:10.1006/jcph.1997.5699.

Buesseler, K. O., P. W. Boyd, E. E. Black, and D. A. Siegel (2020), Metrics that matter for assessing the ocean biological carbon pump, *Proceedings of the National Academy of Sciences*, *117*(18), 9679-9687, doi:10.1073/pnas.1918114117.

Buitenhuis, E., C. Le Quéré, O. Aumont, G. Beaugrand, A. Bunker, A. Hirst, T. Ikeda, T. O'Brien, S. Piontkovski, and D. Straile (2006), Biogeochemical fluxes through mesozooplankton, *Global Biogeochemical Cycles*, *20*(2), doi:10.1029/2005GB002511.

Buitenhuis, E., R. B. Rivkin, S. Sailley, and C. Le Quéré (2010), Biogeochemical fluxes through microzooplankton, *Global Biogeochemical Cycles*, *24*(4), doi:10.1029/2009GB003601.

Buitenhuis, E., M. Vogt, R. Moriarty, N. Bednaršek, S. C. Doney, K. Leblanc, C. Le Quéré, Y.-W. Luo, C. O'Brien, T. O'Brien, J. Peloquin, R. Schiebel, and C. Swan (2013), MAREDAT: towards a world atlas of MARine Ecosystem DATa, *Earth System Science Data*, *5*(2), 227–239, doi:10.5194/essd-5-227-2013.

Burd, A. B., and G. A. Jackson (2009), Particle Aggregation, *Annual Review of Marine Science*, *1*(1), 65-90, doi:10.1146/annurev.marine.010908.163904.

Calbet, A. (2001), Mesozooplankton grazing effect on primary production: A global comparative analysis in marine ecosystems, *Limnology and Oceanography*, *46*(7), 1824-1830, doi:10.4319/lo.2001.46.7.1824.

Calbet, A. (2008), The trophic roles of microzooplankton in marine systems, *ICES Journal of Marine Science*, *65*(3), 325-331, doi:10.1093/icesjms/fsn013.

Calbet, A., and M. R. Landry (2004), Phytoplankton growth, microzooplankton grazing, and carbon cycling in marine systems, *Limnology and Oceanography*, *49*(1), 51-57, doi:10.4319/lo.2004.49.1.0051.

Capone, D. G., J. P. Zehr, H. W. Paerl, B. Bergman, and E. J. Carpenter (1997), *Trichodesmium* a Globally Significant Marine Cyanobacterium, *Science*, *276*(5316), 1221-1229, doi:10.1126/science.276.5316.1221.

Carlotti, F., J. Giske, and F. Werner (2000), 12 - Modeling zooplankton dynamics, in *ICES Zooplankton Methodology Manual*, edited by R. Harris, P. Wiebe, J. Lenz, H. R. Skjoldal, and M. Huntley, pp. 571–667, Academic Press, London, doi:10.1016/B978-012327645-2/50013-X.

Carlson, C. A., and D. A. Hansell (2015), Chapter 3 - DOM Sources, Sinks, Reactivity, and Budgets, in *Biogeochemistry of Marine Dissolved Organic Matter (Second Edition)*, edited by D. A. Hansell and C. A. Carlson, pp. 65–126, Academic Press, Boston, doi:10.1016/B978-0-12-405940-5.00003-0.

Caron, D. A., L. P. Madin, and J. J. Cole (1989), Composition and degradation of salp fecal pellets: Implications for vertical flux in oceanic environments, *Journal of Marine Research*, *47*, 829-850, doi:10.1357/002224089785076118.

Carr, M.-E., M. A. Friedrichs, M. Schmeltz, M. Noguchi Aita, D. Antoine, K. R. Arrigo, I. Asanuma, O. Aumont, R. Barber, M. Behrenfeld, R. Bidigare, E. T. Buitenhuis, J. Campbell, A. Ciotti, H. Dierssen, M. Dowell, J. Dunne, W. Esaias, B. Gentili, W. Gregg, S. Groom, N. Hoepffner, J. Ishizaka, T. Kameda, C. Le Quéré, S. Lohrenz, J. Marra, F. Mélin, K. Moore, A. Morel, T. E. Reddy, J. Ryan, M. Scardi, T. Smyth, K. Turpie, G. Tilstone, K. Waters, and Y. Yamanaka (2006), A comparison of global estimates of marine primary production from ocean color, *Deep Sea Research Part II: Topical Studies in Oceanography*, *53*(5), 741-770, doi:10.1016/j.dsr2.2006.01.028.

Cavan, E. L., F. A. C. Le Moigne, A. J. Poulton, G. A. Tarling, P. Ward, C. J. Daniels, G. M. Fragoso, and R. J. Sanders (2015), Attenuation of particulate organic carbon flux in the Scotia Sea, Southern Ocean, is controlled by zooplankton fecal pellets, *Geophysical Research Letters*, *42*(3), 821-830, doi:10.1002/2014GL062744.

Chenillat, F., P. Rivière, and M. D. Ohman (2021), On the sensitivity of plankton ecosystem models to the formulation of zooplankton grazing, *PLOS ONE*, *16*(5), 1-27, doi:10.1371/journal.pone.0252033.

Coello-Camba, A., M. Llabrés, C. M. Duarte, and S. Agustí (2017), Zooplankton excretion metabolites stimulate Southern Ocean phytoplankton growth, *Polar Biology*, *40*(10), 2035–2045, doi:10.1007/s00300-017-2123-2.

Couespel, D., M. Lévy, and L. Bopp (2021), Oceanic primary production decline halved in eddy-resolving simulations of global warming, *Biogeosciences*, *18*(14), 4321–4349, doi:10.5194/bg-18-4321-2021.

Cram, J. A., T. Weber, S. W. Leung, A. M. P. McDonnell, J.-H. Liang, and C. Deutsch (2018), The Role of Particle Size, Ballast, Temperature, and Oxygen in the Sinking Flux to the Deep Sea, *Global Biogeochemical Cycles*, *32*(5), 858-876, doi:10.1029/2017GB005710.

Dagg, M. J., J. Urban-Rich, and J. O. Peterson (2003), The potential contribution of fecal pellets from large copepods to the flux of biogenic silica and particulate organic carbon

in the Antarctic Polar Front region near 170°W, *Deep-Sea Research Part II: Topical Studies in Oceanography*, *50*(3-4), 675–691, doi:10.1016/S0967-0645(02)00590-8.

del Giorgio, P. A., and C. M. Duarte (2002), Respiration in the open ocean, *Nature*, *420*(6914), 379–384, doi:10.1038/nature01165.

Devol, A. H., and H. E. Hartnett (2001), Role of the oxygen-deficient zone in transfer of organic carbon to the deep ocean, *Limnology and Oceanography*, *46*(7), 1684-1690, doi:10.4319/lo.2001.46.7.1684.

DeVries, T., and T. Weber (2017), The export and fate of organic matter in the ocean: New constraints from combining satellite and oceanographic tracer observations, *Global Biogeochemical Cycles*, *31*(3), 535-555, doi:10.1002/2016GB005551.

Doney, S. C. (1999), Major challenges confronting marine biogeochemical modeling, *Global Biogeochemical Cycles*, *13*(3), 705-714, doi:10.1029/1999GB900039.

Dunne, J., J. John, E. Shevliakova, R. Stouffer, J. Krasting, S. Malyshev, P. Milly, L. Sentman, A. Adcroft, W. Cooke, et al. (2013), GFDL's ESM2 global coupled climate-carbon Earth System Models. Part II: carbon system formulation and baseline simulation characteristics, *Journal of Climate*, *26*(7), 2247–2267, doi:10.1175/JCLI-D-11-00560.1.

Dunne, J. P., I. Bociu, B. Bronselaer, H. Guo, J. G. John, J. P. Krasting, C. A. Stock, M. Winton, and N. Zadeh (2020), Simple Global Ocean Biogeochemistry With Light, Iron, Nutrients and Gas Version 2 (BLINGv2): Model Description and Simulation Characteristics in GFDL's CM4.0, *Journal of Advances in Modeling Earth Systems*, *12*(10), e2019MS002008, doi:10.1029/2019MS002008.

Durkin, C. A., B. A. S. Van Mooy, S. T. Dyhrman, and K. O. Buesseler (2016), Sinking phytoplankton associated with carbon flux in the Atlantic Ocean, *Limnology and Oceanography*, *61*(4), 1172-1187, doi:10.1002/lno.10253.

Dutkiewicz, S., B. A. Ward, J. R. Scott, and M. J. Follows (2014), Understanding predicted shifts in diazotroph biogeography using resource competition theory, *Biogeosciences*, *11*(19), 5445–5461, doi:10.5194/bg-11-5445-2014.

Ebersbach, F., and T. W. Trull (2008), Sinking particle properties from polyacrylamide gels during the KErguelen Ocean and Plateau compared Study (KEOPS): Zooplankton control of carbon export in an area of persistent natural iron inputs in the Southern Ocean, *Limnology and Oceanography*, *53*(1), 212–224, doi:10.4319/lo.2008.53.1.0212.

Edwards, A. M., and A. Yool (2000), The role of higher predation in plankton population models, *Journal of Plankton Research*, *22*(6), 1085-1112, doi:10.1093/plankt/22.6.1085.

Edwards, M., D. Johns, P. Licandro, A. John, and D. Stevens (2006), Ecological Status Report: results from the CPR Survey 2004/2005, *SAHFOS Technical Report*, (3), 1–8.

Edwards, M., P. Hélaouët, E. Goberville, A. Lindley, G. A. Tarling, M. T. Burrows, and A. Atkinson (2021), North Atlantic warming over six decades drives decreases in krill abundance with no associated range shift, *Communications Biology*, *4*(1), 644, doi:10.1038/s42003-021-02159-1.

Everett, J. D., M. E. Baird, P. Buchanan, C. Bulman, C. Davies, R. Downie, C. Griffiths, R. Heneghan, R. J. Kloser, L. Laiolo, A. Lara-Lopez, H. Lozano-Montes, R. J. Matear, F. McEnnulty, B. Robson, W. Rochester, J. Skerratt, J. A. Smith, J. Strzelecki, I. M. Suthers, K. M.

Swadling, P. van Ruth, and A. J. Richardson (2017), Modeling What We Sample and Sampling What We Model: Challenges for Zooplankton Model Assessment, *Frontiers in Marine Science*, *4*, doi:10.3389/fmars.2017.00077.

Fasham, M. (1995), Variations in the seasonal cycle of biological production in subarctic oceans: A model sensitivity analysis, *Deep Sea Research Part I: Oceanographic Research Papers*, *42*(7), 1111-1149, doi:10.1016/0967-0637(95)00054-A.

Fasham, M. J., H. W. Ducklow, and S. M. McKelvie (1990), A nitrogen-based model of plankton dynamics in the oceanic mixed layer, *Journal of Marine Research*, *48*(3), 591–639, doi:10.1357/002224090784984678.

Fennel, W., and T. Neumann (2015), Chapter 1 - introduction, in *Introduction to the Modelling of Marine Ecosystems (Second Edition)*, edited by W. Fennel and T. Neumann, second edition ed., pp. 1–12, Elsevier, Boston, doi:10.1016/B978-0-444-63363-7.00001-5, ISBN: 978-0-444-63363-7.

Field, C., M. J. Behrenfeld, J. T. Randerson, and P. Falkowski (1998), Primary Production of the Biosphere: Integrating Terrestrial and Oceanic Components, *Science*, *281*(5374), 237-240, doi:10.1126/science.281.5374.237.

Field, D., T. R. Baumgartner, C. D. Charles, V. Ferreira-Bartrina, and M. D. Ohman (2006), Planktonic foraminifera of the California Current reflect 20th-century warming, *Science*, *311*(5757), 63–66, doi:10.1126/science.1116220.

Fleming, R. H. (1939), The Control of Diatom Populations by Grazing, *ICES Journal of Marine Science*, *14*(2), 210-227, doi:10.1093/icesjms/14.2.210.

Flynn, K. J. (2006), Reply to Horizons Article 'Plankton functional type modelling: running before we can walk' Anderson (2005): II. Putting trophic functionality into plankton functional types, *Journal of Plankton Research*, *28*(9), 873-875, doi:10.1093/plankt/fbl015.

Follows, M., S. Dutkiewicz, S. Grant, and S. Chisholm (2007), Emergent Biogeography of Microbial Communities in a Model Ocean, *Science*, *315*(5820), 1843-1846, doi:10.1126/science.1138544.

Foote, E. (1856), Circumstances affecting the Heat of the Sun's Rays, *The American Journal of Science and Arts*, *XXII*, 382–383.

Frost, B. W. (1991), The role of grazing in nutrient-rich areas of the open sea, *Limnology and Oceanography*, *36*(8), 1616–1630, doi:10.4319/lo.1991.36.8.1616.

Frost, B. W. (1993), A modelling study of processes regulating plankton standing stock and production in the open subarctic Pacific Ocean, *Progress in Oceanography*, *32*(1-4), 17–56, doi:10.1016/0079-6611(93)90008-2.

Frölicher, T. L., K. B. Rodgers, C. A. Stock, and W. W. L. Cheung (2016), Sources of uncertainties in 21st century projections of potential ocean ecosystem stressors, *Global Biogeochemical Cycles*, *30*(8), 1224-1243, doi:10.1002/2015GB005338.

Gentleman, W., and A. Neuheimer (2008), Functional responses and ecosystem dynamics: how clearance rates explain the influence of satiation, food-limitation and acclimation, *Journal of Plankton Research*, *30*(11), 1215–1231, doi:10.1093/plankt/fbn078.

Gentleman, W., A. Leising, B. Frost, S. Strom, and J. Murray (2003), Functional responses for zooplankton feeding on multiple resources: a review of assumptions and biological dynamics, *Deep Sea Research Part II: Topical Studies in Oceanography*, *50*(22), 2847-2875, doi: 10.1016/j.dsr2.2003.07.001.

Goldthwait, S., J. Yen, J. Brown, and A. Alldredge (2004), Quantification of marine snow fragmentation by swimming *euphausiids*, *Limnology and Oceanography*, *49*(4), 940-952, doi: 10.4319/lo.2004.49.4.0940.

Gonzalez, H., and V. Smetacek (1994), The possible role of the cyclopoid copepod Oithona in retarding vertical flux, *PoLAR*, *113*(1982), 233–246, doi:10.3354/meps113233.

Greene, C. H., and P. H. Wiebe (1990), Bioacoustical Oceanography: New Tools for Zooplankton and Micronekton Research in the 1990s, *Oceanography*, doi:10.5670/oceanog.1990.15.

Halfter, S., E. L. Cavan, K. M. Swadling, R. S. Eriksen, and P. W. Boyd (2020), The Role of Zooplankton in Establishing Carbon Export Regimes in the Southern Ocean – A Comparison of Two Representative Case Studies in the Subantarctic Region, *Frontiers in Marine Science*, *7*, 1–8, doi:10.3389/fmars.2020.567917.

Hansen, B. W., P. K. Bjørnsen, and P. J. Hansen (1994), The size ratio between planktonic predators and their prey, *Limnology and Oceanography*, *39*, 395-403, doi:10.4319/lo.1994.39.2.0395.

Hashioka, T., M. Vogt, Y. Yamanaka, C. Le Quéré, E. T. Buitenhuis, M. N. Aita, S. Alvain, L. Bopp, T. Hirata, I. Lima, S. Sailley, and S. C. Doney (2013), Phytoplankton competition during the spring bloom in four plankton functional type models, *Biogeosciences*, *10*(11), 6833–6850, doi:10.5194/bg-10-6833-2013.

Hauck, J., C. Völker, T. Wang, M. Hoppema, M. Losch, and D. A. Wolf-Gladrow (2013), Seasonally different carbon flux changes in the Southern Ocean in response to the southern annular mode, *Global Biogeochemical Cycles*, *27*(4), 1236–1245, doi:10.1002/2013GB004600.

Hedges, J. I. (1992), Global biogeochemical cycles: progress and problems, *Marine Chemistry*, *39*(1), 67-93, doi:10.1016/0304-4203(92)90096-S.

Henson, S., R. Sanders, and E. Madsen (2012), Global patterns in efficiency of particulate organic carbon export and transfer to the deep ocean, *Global Biogeochemical Cycles*, *26*(1), doi:10.1029/2011GB004099.

Henson, S., F. Le Moigne, and S. Giering (2019), Drivers of Carbon Export Efficiency in the Global Ocean, *Global Biogeochemical Cycles*, *33*(7), 891-903, doi:10.1029/2018GB006158.

Henson, S., C. Laufkötter, S. Leung, S. L. C. Giering, H. I. Palevsky, and E. L. Cavan (2022), Uncertain response of ocean biological carbon export in a changing world, *Nature Geoscience*, doi:10.1038/s41561-022-00927-0.

Henson, S. A., J. P. Dunne, and J. L. Sarmiento (2009), Decadal variability in North Atlantic phytoplankton blooms, *Journal of Geophysical Research: Oceans*, *114*(4), 1–11, doi:10.1029/2008JC005139.

Henson, S. A., R. Sanders, E. Madsen, P. J. Morris, F. Le Moigne, and G. D. Quartly (2011), A reduced estimate of the strength of the ocean's biological carbon pump, *Geophysical Research Letters*, *38*(4), doi:10.1029/2011GL046735.

Henson, S. A., A. Yool, and R. Sanders (2015), Variability in efficiency of particulate organic carbon export: A model study, *Global Biogeochemical Cycles*, *29*(1), 33-45, doi: 10.1002/2014GB004965.

Herman, A. W., B. Beanlands, and E. F. Phillips (2004), The next generation of Optical Plankton Counter: the Laser-OPC, *Journal of Plankton Research*, *26*(10), 1135-1145, doi:10.1093/plankt/fbh095.

Hernandez-Leon, S., and T. Ikeda (2005), Zooplankton respiration, in *Respiration in Aquatic Ecoystems*, edited by P. de Giorgio, pp. 57–82, Oxford Univ. Press.

Hernández-León, S., R. Koppelmann, E. Fraile-Nuez, A. Bode, C. Mompeán, X. Irigoien, M. P. Olivar, F. Echevarría, M. L. Fernández de Puelles, J. I. González-Gordillo, A. Cózar, J. L. Acuña, S. Agustí, and C. M. Duarte (2020), Large deep-sea zooplankton biomass mirrors primary production in the global ocean, *Nature Communications*, *11*(1), 6048, doi: 10.1038/s41467-020-19875-7.

Hernández-León, S., and T. Ikeda (2005), A global assessment of mesozooplankton respiration in the ocean, *Journal of Plankton Research*, *27*(2), 153-158, doi:10.1093/plankt/fbh166.

Hernández-León, S., C. Fraga, and T. Ikeda (2008), A global estimation of mesozooplankton ammonium excretion in the open ocean, *Journal of Plankton Research*, *30*(5), 577-585, doi: 10.1093/plankt/fbn021.

Hill Cruz, M., I. Kriest, Y. S. José, R. Kiko, H. Hauss, and A. Oschlies (2021), Zooplankton mortality effects on the plankton community of the northern Humboldt Current System: sensitivity of a regional biogeochemical model, *Biogeosciences*, *18*(9), 2891–2916, doi:10.5194/bg-18-2891-2021.

Hirst, A., J. Roff, and R. Lampitt (2003), A synthesis of growth rates in marine epipelagic invertebrate zooplankton, pp. 1–142, Academic Press, doi:10.1016/S0065-2881(03)44002-9.

Hirst, A. G., and T. Kiorboe (2002), Mortality of marine planktonic copepods: global rates and patterns, *Marine Ecology Progress Series*, *230*, 195–209, doi:10.3354/meps230195.

Holligan, P. M., E. Fernández, J. Aiken, W. M. Balch, P. Boyd, P. H. Burkill, M. Finch, S. B. Groom, G. Malin, K. Muller, D. A. Purdie, C. Robinson, C. C. Trees, S. M. Turner, and P. van der Wal (1993), A biogeochemical study of the coccolithophore, *Emiliania huxleyi*, in the North Atlantic, *Global Biogeochemical Cycles*, *7*(4), 879-900, doi:10.1029/93GB01731.

Holling, C. (1959), The Components of Predation as Revealed by a Study of Small-Mammal Predation of the European Pine Sawfly, *The Canadian Entomologist*, *91*(5), 293 – 320, doi: 10.4039/Ent91293-5.

Holling, C. (1965), The functional response of predators to prey density and its role in mimicry and population regulation, *The Memoirs of the Entomological Society of Canada*, *97*(S45), 5–60.

Hood, R. R., E. A. Laws, R. A. Armstrong, N. R. Bates, C. W. Brown, C. A. Carlson, F. Chai, S. C. Doney, P. G. Falkowski, R. A. Feely, M. A. Friedrichs, M. R. Landry, J. Keith Moore, D. M. Nelson, T. L. Richardson, B. Salihoglu, M. Schartau, D. A. Toole, and J. D. Wiggert (2006), Pelagic functional group modeling: Progress, challenges and prospects, *Deep Sea Research Part II: Topical Studies in Oceanography*, *53*(5), 459-512, doi:10.1016/j.dsr2.2006.01.025.

Hopkins, J., S. A. Henson, A. J. Poulton, and W. M. Balch (2019), Regional Characteristics of the Temporal Variability in the Global Particulate Inorganic Carbon Inventory, *Global Biogeochemical Cycles*, *33*(11), 1328-1338, doi:10.1029/2019GB006300.

Ikeda, T. (2014), Respiration and ammonia excretion by marine metazooplankton taxa: synthesis toward a global-bathymetric model, *Marine Biology*, *161*(12), 2753–2766, doi:10.1007/s00227-014-2540-5.

Ilyina, T., K. D. Six, J. Segschneider, E. Maier-Reimer, H. Li, and I. Núñez-Riboni (2013), Global ocean biogeochemistry model HAMOCC: Model architecture and performance as component of the MPI-Earth system model in different CMIP5 experimental realizations, *Journal of Advances in Modeling Earth Systems*, *5*(2), 287-315, doi:10.1029/2012MS000178.

IPCC (2021), *Climate Change 2021: The Physical Science Basis. Contribution of Working Group I to the Sixth Assessment Report of the Intergovernmental Panel on Climate Change*, V. Masson-Delmotte, P. Zhai, A. Pirani, S. L. Connors, C. Pean, S. Berger, N. Caud, Y. Chen, L. Goldfarb, M. I. Gomis, M. Huang, K. Leitzell, E. Lonnoy, J. B. R. Matthews, T. K. Maycock, T. Waterfield, O. Yelekçi, R. Yu, B. Zhou (eds), Cambridge University Press, doi:10.1017/9781009157896.

Iversen, M. H., and H. Ploug (2013), Temperature effects on carbon-specific respiration rate and sinking velocity of diatom aggregates - potential implications for deep ocean export processes, *Biogeosciences*, *10*(6), 4073–4085, doi:10.5194/bg-10-4073-2013.

Iversen, M. H., E. A. Pakhomov, B. P. Hunt, H. van der Jagt, D. Wolf-Gladrow, and C. Klaas (2017), Sinkers or floaters? Contribution from salp pellets to the export flux during a large bloom event in the Southern Ocean, *Deep-Sea Research Part II: Topical Studies in Oceanography*, *138*(December 2016), 116–125, doi:10.1016/j.dsr2.2016.12.004.

Ivlev, V. S. (1961), *Experimental ecology of the feeding of fishes*, Yale University Press.

Jackson, G. A. (1990), A model of the formation of marine algal flocs by physical coagulation processes, *Deep Sea Research Part A. Oceanographic Research Papers*, *37*(8), 1197-1211, doi:10.1016/0198-0149(90)90038-W.

Jeschke, J. M., M. Kopp, and R. Tollrian (2002), Predator functional responses: Discriminating between handling and digesting prey, *Ecological Monographs*, *72*(1), 95-112, doi:10.1890/0012-9615(2002)072[0095:PFRDBH]2.0.CO;2.

Jeschke, J. M., M. Kopp, and R. Tollrian (2004), Consumer-food systems: why type I functional responses are exclusive to filter feeders, *Biological Reviews*, *79*(2), 337-349, doi:10.1017/S1464793103006286.

Johnson, R., P. G. Strutton, S. W. Wright, A. McMinn, and K. M. Meiners (2013), Three improved satellite chlorophyll algorithms for the Southern Ocean, *Journal of Geophysical Research: Oceans*, *118*(7), 3694-3703, doi:10.1002/jgrc.20270.

Kandel, S., J. Heer, C. Plaisant, J. Kennedy, F. van Ham, N. H. Riche, C. Weaver, B. Lee, D. Brodbeck, and P. Buono (2011), Research Directions in Data Wrangling: Visuatizations and Transformations for Usable and Credible Data, *Information Visualization*, *10*(4), 271–288, doi:10.1177/1473871611415994.

Karakuş, O., C. Völker, M. Iversen, W. Hagen, D. Wolf-Gladrow, B. Fach, and J. Hauck (2021), Modeling the Impact of Macrozooplankton on Carbon Export Production in the Southern Ocean, *Journal of Geophysical Research: Oceans*, *126*(12), e2021JC017315, doi:10.1029/2021JC017315.

Karl, D. M. (2007), Microbial oceanography: paradigms, processes and promise, *Nature Reviews Microbiology*, *5*(10), 759–769, doi:10.1038/nrmicro1749.

Kawamiya, M., T. Hajima, K. Tachiiri, S. Watanabe, and T. Yokohata (2020), Two decades of Earth system modeling with an emphasis on Model for Interdisciplinary Research on Climate (MIROC), *Progress in Earth and Planetary Science*, *7*(1), 64, doi:10.1186/s40645-020-00369-5.

Khatiwala, S. (2007), A computational framework for simulation of biogeochemical tracers in the ocean, *Global Biogeochemical Cycles*, *21*(3), doi:10.1029/2007GB002923.

Kiorboe, T. (1997), Population regulation and role of mesozooplankton in shaping marine pelagic food webs, *Hydrobiologia*, *363*, 13–27, doi:10.1023/A:1003173721751.

Kiørboe, T., and J. L. Hansen (1993), Phytoplankton aggregate formation: observations of patterns and mechanisms of cell sticking and the significance of exopolymeric material, *Journal of Plankton Research*, *15*(9), 993-1018, doi:10.1093/plankt/15.9.993.

Kiørboe, T., K. P. Andersen, and H. G. Dam (1990), Coagulation efficiency and aggregate formation in marine phytoplankton, *Marine Biology*, *107*(2), 235–245, doi:10.1007/BF01319822.

Kiørboe, T. (2011), How zooplankton feed: mechanisms, traits and trade-offs, *Biological Reviews*, *86*(2), 311-339, doi:10.1111/j.1469-185X.2010.00148.x.

Kiørboe, T., A. Visser, and K. H. Andersen (2018), A trait-based approach to ocean ecology, *ICES Journal of Marine Science*, *75*(6), 1849-1863, doi:10.1093/icesjms/fsy090.

Koski, M., B. Valencia, R. Newstead, and C. Thiele (2020), The missing piece of the upper mesopelagic carbon budget? Biomass, vertical distribution and feeding of aggregate-associated copepods at the PAP site, *Progress in Oceanography*, *181*, 102243, doi:10.1016/j.pocean.2019.102243.

Kriest, I., S. Khatiwala, and A. Oschlies (2010), Towards an assessment of simple global marine biogeochemical models of different complexity, *Progress in Oceanography*, *86*(3), 337-360, doi:10.1016/j.pocean.2010.05.002.

Kulk, G., T. Platt, J. Dingle, T. Jackson, B. F. Jönsson, H. A. Bouman, M. Babin, R. J. W. Brewin, M. Doblin, M. Estrada, F. G. Figueiras, K. Furuya, N. González-Benítez, H. G. Gudfinnsson, K. Gudmundsson, B. Huang, T. Isada, z. Kovac, V. A. Lutz, E. Marañón, M. Raman, K. Richardson, P. D. Rozema, W. H. v. d. Poll, V. Segura, G. H. Tilstone, J. Uitz, V. v. Dongen-Vogels, T. Yoshikawa, and S. Sathyendranath (2020), Primary production, an index of climate change in the ocean: Satellite-based estimates over two decades, *Remote Sensing*, *12*(5), doi:10.3390/rs12050826.

Kwiatkowski, L., A. Yool, J. I. Allen, T. R. Anderson, R. Barciela, E. T. Buitenhuis, M. Butenschön, C. Enright, P. R. Halloran, C. Le Quéré, L. De Mora, M. F. Racault, B. Sinha, I. J. Totterdell, and P. M. Cox (2014), IMarNet: An ocean biogeochemistry model intercomparison project within a common physical ocean modelling framework, *Biogeosciences*, *11*(24), 7291–7304, doi:10.5194/bg-11-7291-2014.

Kwiatkowski, L., O. Torres, L. Bopp, O. Aumont, M. Chamberlain, J. R. Christian, J. P. Dunne, M. Gehlen, T. Ilyina, J. G. John, A. Lenton, H. Li, N. S. Lovenduski, J. C. Orr, J. Palmieri, Y. Santana-Falcón, J. Schwinger, R. Séférian, C. A. Stock, A. Tagliabue, Y. Takano, J. Tjiputra, K. Toyama, H. Tsujino, M. Watanabe, A. Yamamoto, A. Yool, and T. Ziehn (2020), Twenty-first century ocean warming, acidification, deoxygenation, and upper-ocean nutrient and

primary production decline from CMIP6 model projections, *Biogeosciences*, *17*(13), 3439–3470, doi:10.5194/bg-17-3439-2020.

Laglera, L. M., A. Tovar-Sánchez, M. Iversen, H. González, H. Naik, G. Mangesh, P. Assmy, C. Klaas, M. Mazzocchi, M. Montresor, S. Naqvi, V. Smetacek, and D. Wolf-Gladrow (2017), Iron partitioning during LOHAFEX: Copepod grazing as a major driver for iron recycling in the Southern Ocean, *Marine Chemistry*, *196*, 148-161, doi:10.1016/j.marchem.2017.08.011.

Lampert, W. (2005), Vertical distribution of zooplankton: density dependence and evidence for an ideal free distribution with costs, *BMC Biology*, *3*(1), 10, doi:10.1186/1741-7007-3-10.

Lampitt, R., T. Noji, and B. von Bodungen (1990), What happens to zooplankton faecal pellets? Implications for material flux, *Marine Biology*, *104*(1), 15–23, doi:10.1007/BF01313152.

Laufkötter, C., M. Vogt, N. Gruber, O. Aumont, L. Bopp, S. C. Doney, J. P. Dunne, J. Hauck, J. G. John, I. D. Lima, R. Seferian, and C. Völker (2016), Projected decreases in future marine export production: The role of the carbon flux through the upper ocean ecosystem, *Biogeosciences*, *13*(13), 4023–4047, doi:10.5194/bg-13-4023-2016.

Laufkötter, C., J. G. John, C. A. Stock, and J. P. Dunne (2017), Temperature and oxygen dependence of the remineralization of organic matter, *Global Biogeochemical Cycles*, *31*(7), 1038-1050, doi:10.1002/2017GB005643.

Laurenceau-Cornec, E. C., T. W. Trull, D. M. Davies, S. G. Bray, J. Doran, F. Planchon, F. Carlotti, M.-P. Jouandet, A.-J. Cavagna, A. M. Waite, and S. Blain (2015), The relative importance of phytoplankton aggregates and zooplankton fecal pellets to carbon export: insights from free-drifting sediment trap deployments in naturally iron-fertilised waters near the Kerguelen Plateau, *Biogeosciences*, *12*(4), 1007–1027, doi:10.5194/bg-12-1007-2015.

Laws, E. A., P. G. Falkowski, W. O. Smith Jr., H. Ducklow, and J. J. McCarthy (2000), Temperature effects on export production in the open ocean, *Global Biogeochemical Cycles*, *14*(4), 1231-1246, doi:10.1029/1999GB001229.

Laws, E. A., E. D'Sa, and P. Naik (2011), Simple equations to estimate ratios of new or export production to total production from satellite-derived estimates of sea surface temperature and primary production, *Limnology and Oceanography: Methods*, *9*(12), 593-601, doi:10.4319/lom.2011.9.593.

Le Moigne, F. A. C., K. Pabortsava, C. L. J. Marcinko, P. Martin, and R. J. Sanders (2014), Where is mineral ballast important for surface export of particulate organic carbon in the ocean?, *Geophysical Research Letters*, *41*(23), 8460-8468, doi:10.1002/2014GL061678.

Le Moigne, F. A. C., S. A. Henson, E. Cavan, C. Georges, K. Pabortsava, E. P. Achterberg, E. Ceballos-Romero, M. Zubkov, and R. J. Sanders (2016), What causes the inverse relationship between primary production and export efficiency in the Southern Ocean?, *Geophysical Research Letters*, *43*(9), 4457-4466, doi:10.1002/2016GL068480.

Le Quéré, C., E. T. Buitenhuis, R. Moriarty, S. Alvain, O. Aumont, L. Bopp, S. Chollet, C. Enright, D. J. Franklin, R. J. Geider, S. P. Harrison, A. G. Hirst, S. Larsen, L. Legendre, T. Platt, I. C. Prentice, R. B. Rivkin, S. Sailley, S. Sathyendranath, N. Stephens, M. Vogt, and S. M. Vallina (2016), Role of zooplankton dynamics for Southern Ocean phytoplankton biomass and global biogeochemical cycles, *Biogeosciences*, *13*(14), 4111–4133, doi:10.5194/bg-13-4111-2016.

Le Quéré, C. (2006), Reply to Horizons Article 'Plankton functional type modelling: running before we can walk' Anderson (2005): I. Abrupt changes in marine ecosystems?, *Journal of Plankton Research*, *28*(9), 871-872, doi:10.1093/plankt/fbl014.

Le Quéré, C., S. P. Harrison, I. Colin Prentice, E. T. Buitenhuis, O. Aumont, L. Bopp, H. Claustre, L. Cotrim Da Cunha, R. Geider, X. Giraud, C. Klaas, K. E. Kohfeld, L. Legendre, M. Manizza, T. Platt, R. B. Rivkin, S. Sathyendranath, J. Uitz, A. J. Watson, and D. Wolf-Gladrow (2005), Ecosystem dynamics based on plankton functional types for global ocean biogeochemistry models, *Global Change Biology*, *11*(11), 2016-2040, doi:10.1111/j.1365-2486.2005.1004.x.

Leblanc, K., J. Arístegui, L. Armand, P. Assmy, B. Beker, A. Bode, E. Breton, V. Cornet, J. Gibson, M.-P. Gosselin, E. Kopczynska, H. Marshall, J. Peloquin, S. Piontkovski, A. J. Poulton, B. Quéguiner, R. Schiebel, R. Shipe, J. Stefels, M. A. van Leeuwe, M. Varela, C. Widdicombe, and M. Yallop (2012), A global diatom database – abundance, biovolume and biomass in the world ocean, *Earth System Science Data*, *4*(1), 149–165, doi:10.5194/essd-4-149-2012.

Leblanc, K., B. Quéguiner, F. Diaz, V. Cornet, M. Michel-Rodriguez, X. Durrieu de Madron, C. Bowler, S. Malviya, M. Thyssen, G. Grégori, M. Rembauville, O. Grosso, J. Poulain, C. de Vargas, M. Pujo-Pay, and P. Conan (2018), Nanoplanktonic diatoms are globally overlooked but play a role in spring blooms and carbon export, *Nature Communications*, *9*(1), 953, doi:10.1038/s41467-018-03376-9.

Lenz, J. (2000), 1 - introduction, in *ICES Zooplankton Methodology Manual*, edited by R. Harris, P. Wiebe, J. Lenz, H. R. Skjoldal, and M. Huntley, pp. 1–32, Academic Press, London, doi:10.1016/B978-012327645-2/50002-5.

Lindley, J., and S. Daykin (2005), Variations in the distributions of Centropages chierchiae and Temora stylifera (Copepoda: Calanoida) in the north-eastern Atlantic Ocean and western European shelf waters, *ICES Journal of Marine Science*, *62*(5), 869–877, doi:10.1016/j.icesjms.2005.02.009.

Litchman, E., M. D. Ohman, and T. Kiørboe (2013), Trait-based approaches to zooplankton communities, *Journal of Plankton Research*, *35*(3), 473-484, doi:10.1093/plankt/fbt019.

Llort, J., M. Lévy, J.-B. Sallée, and A. Tagliabue (2015), Onset, intensification, and decline of phytoplankton blooms in the Southern Ocean, *ICES Journal of Marine Science*, *72*(6), 1971-1984, doi:10.1093/icesjms/fsv053.

Longhurst, A., A. Bedo, W. Harrison, E. Head, and D. Sameoto (1990), Vertical flux of respiratory carbon by oceanic diel migrant biota, *Deep Sea Research Part A. Oceanographic Research Papers*, *37*(4), 685-694, doi:10.1016/0198-0149(90)90098-G.

Lutz, M., R. Dunbar, and K. Caldeira (2002), Regional variability in the vertical flux of particulate organic carbon in the ocean interior, *Global Biogeochemical Cycles*, *16*(3), 11-1-11-18, doi:10.1029/2000GB001383.

Mackas, D. L., R. Goldblatt, and A. G. Lewis (1998), Interdecadal variation in developmental timing of *Neocalanus plumchrus* populations at Ocean Station P in the subarctic North Pacific, *Canadian Journal of Fisheries and Aquatic Sciences*, *55*(8), 1878-1893, doi:10.1139/f98-080.

Maerz, J., K. D. Six, I. Stemmler, S. Ahmerkamp, and T. Ilyina (2020), Microstructure and composition of marine aggregates as co-determinants for vertical particulate organic carbon transfer in the global ocean, *Biogeosciences*, *17*(7), 1765–1803, doi:10.5194/bg-17-1765-2020.

Maier-Reimer, E. (1993), Geochemical cycles in an ocean general circulation model. Preindustrial tracer distributions, *Global Biogeochemical Cycles*, *7*(3), 645-677, doi:10.1029/93GB01355.

Maier-Reimer, E., and K. Hasselmann (1987), Transport and storage of CO_2 in the ocean –an inorganic ocean-circulation carbon cycle model, *Climate Dynamics*, *2*(2), 63–90, doi:10.1007/BF01054491.

Maiti, K., M. A. Charette, K. O. Buesseler, and M. Kahru (2013), An inverse relationship between production and export efficiency in the Southern Ocean, *Geophysical Research Letters*, *40*(8), 1557-1561, doi:10.1002/grl.50219.

Marsay, C. M., R. J. Sanders, S. A. Henson, K. Pabortsava, E. P. Achterberg, and R. S. Lampitt (2015), Attenuation of sinking particulate organic carbon flux through the mesopelagic ocean, *Proceedings of the National Academy of Sciences*, *112*(4), 1089-1094, doi:10.1073/pnas.1415311112.

Martin, J. H., G. A. Knauer, D. M. Karl, and W. W. Broenkow (1987), VERTEX: carbon cycling in the northeast Pacific, *Deep Sea Research Part A. Oceanographic Research Papers*, *34*(2), 267-285, doi:10.1016/0198-0149(87)90086-0.

Mayor, D. J., R. Sanders, S. L. C. Giering, and T. R. Anderson (2014), Microbial gardening in the ocean's twilight zone: Detritivorous metazoans benefit from fragmenting, rather than ingesting, sinking detritus, *BioEssays*, *36*(12), 1132-1137, doi:10.1002/bies.201400100.

Mayor, D. J., W. C. Gentleman, and T. R. Anderson (2020), Ocean carbon sequestration: Particle fragmentation by copepods as a significant unrecognised factor?, *BioEssays*, *42*(12), 2000149, doi:10.1002/bies.202000149.

Menden-Deuer, S., E. J. Lessard, J. Satterberg, and D. Grünbaum (2005), Growth rates and starvation survival of three species of the pallium-feeding, thecate dinoflagellate genus Protoperidinium, *Aquatic Microbial Ecology*, *41*(2), 145–152, doi:10.3354/ame041145.

Menden-Deuer, S., W. H. Slade, and H. Dierssen (2021a), Promoting Instrument Development for New Research Avenues in Ocean Science: Opening the Black Box of Grazing, *Frontiers in Marine Science*, *8*, doi:10.3389/fmars.2021.695938.

Menden-Deuer, S., W. H. Slade, and H. Dierssen (2021b), Promoting Instrument Development for New Research Avenues in Ocean Science: Opening the Black Box of Grazing, *Frontiers in Marine Science*, *8*, doi:10.3389/fmars.2021.695938.

Mitra, A. (2009), Are closure terms appropriate or necessary descriptors of zooplankton loss in nutrient-phytoplankton-zooplankton type models?, *Ecological Modelling*, *220*(5), 611–620, doi:10.1016/j.ecolmodel.2008.12.008.

Mitra, A., C. Castellani, W. C. Gentleman, S. H. Jónasdóttir, K. J. Flynn, A. Bode, C. Halsband, P. Kuhn, P. Licandro, M. D. Agersted, A. Calbet, P. K. Lindeque, R. Koppelmann, E. F. Møller, A. Gislason, T. G. Nielsen, and M. St. John (2014), Bridging the gap between marine biogeochemical and fisheries sciences; configuring the zooplankton link, *Progress in Oceanography*, *129*, 176-199, doi:10.1016/j.pocean.2014.04.025.

Moeller, H. V., C. Laufkötter, E. M. Sweeney, and M. D. Johnson (2019), Light-dependent grazing can drive formation and deepening of deep chlorophyll maxima, *Nature Communications*, *10*(1), 1978, doi:10.1038/s41467-019-09591-2.

Møller, E. F. (2005), Sloppy feeding in marine copepods: prey-size-dependent production of dissolved organic carbon, *Journal of Plankton Research*, *27*(1), 27-35, doi:10.1093/plankt/fbh147.

Møller, E. F. (2007), Production of dissolved organic carbon by sloppy feeding in the copepods *Acartia tonsa*, Centropages typicus, and Temora longicornis, *Limnology and Oceanography*, *52*(1), 79–84, doi:10.4319/lo.2007.52.1.0079.

Møller, E. F., P. Thor, and T. G. Nielsen (2003), Production of DOC by *Calanus finmarchicus, C. glacialis and C. hyperboreus* through sloppy feeding and leakage from fecal pellets, *Marine Ecology Progress Series*, *262*, 185–191.

Montagnes, D. J., and A. Fenton (2012), Prey-abundance affects zooplankton assimilation efficiency and the outcome of biogeochemical models, *Ecological Modelling*, *243*, 1-7, doi: 10.1016/j.ecolmodel.2012.05.006.

Moore, J. K., S. C. Doney, and K. Lindsay (2004), Upper ocean ecosystem dynamics and iron cycling in a global three-dimensional model, *Global Biogeochemical Cycles*, *18*(4), doi: 10.1029/2004GB002220.

Moriarty, R., and T. D. O'Brien (2013), Distribution of mesozooplankton biomass in the global ocean, *Earth System Science Data*, *5*(1), 45–55, doi:10.5194/essd-5-45-2013.

Moriarty, R., E. T. Buitenhuis, and C. Le Quéré (2013), Distribution of known macrozooplankton abundance and biomass in the global ocean, *Earth System Science Data*, *5*(2), 241–257, doi: 10.5194/essd-5-241-2013.

Morozov, A., and E. Arashkevich (2008), Patterns of Zooplankton Functional Response in Communities with Vertical Heterogeneity: a Model Study, *Math. Model. Nat. Phenom.*, *3*(3), 131-148, doi:10.1051/mmnp:2008061.

Najjar, R. G., J. L. Sarmiento, and J. R. Toggweiler (1992), Downward transport and fate of organic matter in the ocean: Simulations with a general circulation model, *Global Biogeochemical Cycles*, *6*(1), 45-76, doi:10.1029/91GB02718.

Noji, T., K. W. Estep, F. Macintyre, and F. Norrbin (1991), Image Analysis of Faecal Material Grazed Upon by Three Species Of Copepods: Evidence For Coprorhexy, Coprophagy and Coprochaly, *Journal of the Marine Biological Association of the United Kingdom*, *71*(2), 465–480, doi:10.1017/S0025315400051717.

Ohman, M. D., B. W. Frost, and E. B. Cohen (1983), Reverse Diel Vertical Mig.ration: An Escape from Invertebrate Predators, *Science*, *220*(4604), 1404-1407, doi:10.1126/science.220.4604.1404.

Omand, M. M., R. Govindarajan, J. He, and A. Mahadevan (2020), Sinking flux of particulate organic matter in the oceans: Sensitivity to particle characteristics, *Scientific Reports*, *10*(1), 5582, doi:10.1038/s41598-020-60424-5.

Palevsky, H. I., and S. C. Doney (2018), How Choice of Depth Horizon Influences the Estimated Spatial Patterns and Global Magnitude of Ocean Carbon Export Flux, *Geophysical Research Letters*, *45*(9), 4171-4179, doi:10.1029/2017GL076498.

Parsons, T., and C. Lalli (2002), Jellyfish population explosions: revisiting a hypothesis of possible causes, *La mer*, *40*(3), 111–121.

Passow, U., and C. Carlson (2012), The biological pump in a high CO_2 world, *Marine Ecology Progress Series*, *470*(2), 249–271, doi:10.3354/meps09985.

Petrik, C. M., J. Y. Luo, R. Heneghan, J. D. Everett, C. S. Harrison, and A. Richardson (2022), Assessment and constraint of mesozooplankton in CMIP6 Earth system models, *Earth and Space Science Open Archive*, p. 40, doi:10.1002/essoar.10510705.1.

Prowe, A. F., M. Pahlow, S. Dutkiewicz, M. Follows, and A. Oschlies (2012), Top-down control of marine phytoplankton diversity in a global ecosystem model, *Progress in Oceanography*, *101*(1), 1–13, doi:10.1016/j.pocean.2011.11.016.

Purcell, J. E. (1983), Digestion rates and assimilation efficiencies of siphonophores fed zooplankton prey, *Marine Biology*, *73*(3), 257–261, doi:10.1007/BF00392251.

Purcell, J. E. (2005), Climate effects on formation of jellyfish and ctenophore blooms: a review, *Journal of the Marine Biological Association of the United Kingdom*, *85*(3), 461–476, doi:10.1017/S0025315405011409.

Racault, M. F., C. Le Quéré, E. Buitenhuis, S. Sathyendranath, and T. Platt (2012), Phytoplankton phenology in the global ocean, *Ecological Indicators*, *14*(1), 152–163, doi:10.1016/j.ecolind.2011.07.010.

Redfield, A. C., B. H. Ketchum, and F. A. Richards (1963), *The influence of organisms on the composition of sea-water, In: The Composition of Seawater: Comparative and Descriptive Oceanography. The Sea: Ideas and Observations on Progress in the Study of the Seas*, 26–77 pp., M. N. Hill (ed.), Wiley-Interscience.

Rembauville, M., C. Manno, G. Tarling, S. Blain, and I. Salter (2016), Strong contribution of diatom resting spores to deep-sea carbon transfer in naturally iron-fertilized waters downstream of South Georgia, *Deep Sea Research Part I: Oceanographic Research Papers*, *115*, 22-35, doi:10.1016/j.dsr.2016.05.002.

Richardson, A. (2008), In hot water: zooplankton and climate change, *ICES Journal of Marine Science*, *65*(3), 279-295, doi:10.1093/icesjms/fsn028.

Richardson, A., A. Walne, A. John, T. Jonas, J. Lindley, D. Sims, D. Stevens, and M. Witt (2006), Using continuous plankton recorder data, *Progress in Oceanography*, *68*(1), 27-74, doi:10.1016/j.pocean.2005.09.011.

Riley, G. A. (1949), Quantitative ecology of the plankton of the western North Atlantic, *Bull. Bingham Oceanogr. Collection*, *12*, 1–169.

Riley, G. A., and D. F. Bumpus (1946), Phytoplankton-zooplankton relationships on Georges Bank, *Journal of Marine Research*, *480*, 15–28.

Riley, J. S., R. Sanders, C. Marsay, F. A. C. Le Moigne, E. P. Achterberg, and A. J. Poulton (2012), The relative contribution of fast and slow sinking particles to ocean carbon export, *Global Biogeochemical Cycles*, *26*(1), doi:10.1029/2011GB004085.

Romanou, A., J. Romanski, and W. W. Gregg (2014), Natural ocean carbon cycle sensitivity to parameterizations of the recycling in a climate model, *Biogeosciences*, *11*(4), 1137–1154, doi:10.5194/bg-11-1137-2014.

Ryther, J., and J. Sanders (1980), Experimental Evidence of Zooplankton Control of the Species Composition and Size Distribution of Marine Phytoplankton, *Marine Ecology Progress Series*, *3*, 279–283, doi:10.3354/meps003279.

Saba, G. K., D. K. Steinberg, and D. A. Bronk (2009), Effects of diet on release of dissolved organic and inorganic nutrients by the copepod *Acartia tonsa*, *Marine Ecology Progress Series*, *386*, 147–161, doi:10.3354/meps08070.

Saba, G. K., D. K. Steinberg, and D. A. Bronk (2011), The relative importance of sloppy feeding, excretion, and fecal pellet leaching in the release of dissolved carbon and nitrogen by *Acartia tonsa* copepods, *Journal of Experimental Marine Biology and Ecology*, *404*(1), 47-56, doi:10.1016/j.jembe.2011.04.013.

Sarmiento, J. L., and N. Gruber (2006), *Ocean Biogeochemical Dynamics*, Princeton University Press, ISBN:0-691-01707-7.

Sarmiento, J. L., R. D. Slater, M. J. R. Fasham, H. W. Ducklow, J. R. Toggweiler, and G. T. Evans (1993), A seasonal three-dimensional ecosystem model of nitrogen cycling in the North Atlantic Euphotic Zone, *Global Biogeochemical Cycles*, *7*(2), 417-450, doi:10.1029/93GB00375.

Sato, M., S. Takeda, and K. Furuya (2007), Iron regeneration and organic iron (III) - binding ligand production during in situ zooplankton grazing experiment, *Marine Chemistry*, *106*(3), 471-488, doi:10.1016/j.marchem.2007.05.001.

Savoca, M. S., M. F. Czapanskiy, S. R. Kahane-Rapport, W. T. Gough, J. A. Fahlbusch, K. C. Bierlich, P. S. Segre, J. Di Clemente, G. S. Penry, D. N. Wiley, J. Calambokidis, D. P. Nowacek, D. W. Johnston, N. D. Pyenson, A. S. Friedlaender, E. L. Hazen, and J. A. Goldbogen (2021), Baleen whale prey consumption based on high-resolution foraging measurements, *Nature*, *599*(7883), 85–90, doi:10.1038/s41586-021-03991-5.

Schmidt, K., C. Schlosser, A. Atkinson, S. Fielding, H. Venables, C. Waluda, and E. Achterberg (2016), Zooplankton Gut Passage Mobilizes Lithogenic Iron for Ocean Productivity, *Current Biology*, *26*(19), 2667-2673, doi:10.1016/j.cub.2016.07.058.

Schmoker, C., S. Hernández-León, and A. Calbet (2013), Microzooplankton grazing in the oceans: impacts, data variability, knowledge gaps and future directions, *Journal of Plankton Research*, *35*(4), 691-706, doi:10.1093/plankt/fbt023.

Schnack-Schiel, S., and W. Hagen (1994), Life cycle strategies and seasonal variations in distribution and population structure of four dominant calanoid copepod species in the eastern Weddell Sea, Antarctica, *Journal of Plankton Research*, *16*(11), 1543-1566, doi:10.1093/plankt/16.11.1543.

Schourup-Kristensen, V., D. Sidorenko, D. A. Wolf-Gladrow, and C. Völker (2014), A skill assessment of the biogeochemical model REcoM2 coupled to the Finite Element Sea Ice–Ocean Model (FESOM 1.3), *Geoscientific Model Development*, *7*(6), 2769–2802, doi:10.5194/gmd-7-2769-2014.

Séférian, R., S. Berthet, A. Yool, J. Palmiéri, L. Bopp, A. Tagliabue, L. Kwiatkowski, O. Aumont, J. Christian, J. Dunne, M. Gehlen, T. Ilyina, J. G. John, H. Li, M. C. Long, J. Y. Luo, H. Nakano, A. Romanou, J. Schwinger, C. Stock, Y. Santana-Falcón, Y. Takano, J. Tjiputra, H. Tsujino, M. Watanabe, T. Wu, F. Wu, and A. Yamamoto (2020), Tracking Improvement in Simulated Marine Biogeochemistry Between CMIP5 and CMIP6, *Current Climate Change Reports*, *6*(3), 95–119, doi:10.1007/s40641-020-00160-0.

Serra-Pompei, C., F. Soudijn, A. W. Visser, T. Kiørboe, and K. H. Andersen (2020), A general size- and trait-based model of plankton communities, *Progress in Oceanography*, *189*, 102473, doi:10.1016/j.pocean.2020.102473.

Serra-Pompei, C., B. A. Ward, J. Pinti, A. W. Visser, T. Kiørboe, and K. H. Andersen (2022), Linking plankton size spectra and community composition to carbon export and its efficiency, *Global Biogeochemical Cycles*, *n/a*(n/a), e2021GB007275, doi:10.1029/2021GB007275.

Sieburth, J. M., V. Smetacek, and J. Lenz (1978), Pelagic ecosystem structure: Heterotrophic compartments of the plankton and their relationship to plankton size fractions, *Limnology and Oceanography*, *23*(6), 1256-1263, doi:10.4319/lo.1978.23.6.1256.

Siegel, D. A., S. C. Doney, and J. A. Yoder (2002), The North Atlantic Spring Phytoplankton Bloom and Sverdrup's Critical Depth Hypothesis, *Science*, *296*(5568), 730–733, doi:10.1126/science.1069174.

Siegel, D. A., K. O. Buesseler, M. J. Behrenfeld, C. R. Benitez-Nelson, E. Boss, M. A. Brzezinski, A. Burd, C. A. Carlson, E. A. D'Asaro, S. C. Doney, M. J. Perry, R. H. R. Stanley, and D. K. Steinberg (2016), Prediction of the Export and Fate of Global Ocean Net Primary Production: The EXPORTS Science Plan, *Frontiers in Marine Science*, *3*, doi:10.3389/fmars.2016.00022.

Siegenthaler, U., T. F. Stocker, E. Monnin, D. Lüthi, J. Schwander, B. Stauffer, D. Raynaud, J.-M. Barnola, H. Fischer, V. Masson-Delmotte, and J. Jouzel (2005), Stable Carbon Cycle - Climate Relationship During the Late Pleistocene, *Science*, *310*(5752), 1313-1317, doi:10.1126/science.1120130.

Smetacek, V. (1985), Role of sinking in diatom life-history cycles: ecological, evolutionary and geological significance, *Marine Biology*, *84*(3), 239–251, doi:10.1007/BF00392493.

Smetacek, V. (2012), Making sense of ocean biota: How evolution and biodiversity of land organisms differ from that of the plankton, *Journal of Biosciences*, *37*(4), 589–607, doi:10.1007/s12038-012-9240-4.

Soppa, M. A., C. Völker, and A. Bracher (2016), Diatom phenology in the Southern Ocean: Mean patterns, trends and the role of climate oscillations, *Remote Sensing*, *8*(5), 1–17, doi:10.3390/rs8050420.

Steele, J. H. (1958), Plant Production in the northern North Sea, *HM Stationary Office*.

Steele, J. H. (1959), Quantitative ecology of Marine phytoplankton, *Biol. Rev.*

Steele, J. H. (1974), The structure of marine ecosystems, in *The Structure of Marine Ecosystems*, Harvard University Press.

Steele, J. H., and E. W. Henderson (1992), The role of predation in plankton models, *Journal of Plankton Research*, *14*(1), 157-172, doi:10.1093/plankt/14.1.157.

Steinberg, D. K., and M. R. Landry (2017), Zooplankton and the Ocean Carbon Cycle, *Annual Review of Marine Science*, *9*(1), 413–444, doi:10.1146/annurev-marine-010814-015924.

Steinberg, D. K., C. A. Carlson, N. R. Bates, S. A. Goldthwait, L. P. Madin, and A. F. Michaels (2000), Zooplankton vertical migration and the active transport of dissolved organic and inorganic carbon in the Sargasso Sea, *Deep Sea Research Part I: Oceanographic Research Papers*, *47*(1), 137-158, doi:10.1016/S0967-0637(99)00052-7.

Stock, C. A., J. P. Dunne, S. Fan, P. Ginoux, J. John, J. P. Krasting, C. Laufkötter, F. Paulot, and N. Zadeh (2020), Ocean Biogeochemistry in GFDL's Earth System Model 4.1 and Its Response to Increasing Atmospheric CO_2, *Journal of Advances in Modeling Earth Systems*, *12*(10), e2019MS002043, doi:10.1029/2019MS002043.

Stramska, M. (2009), Particulate organic carbon in the global ocean derived from SeaWiFS ocean color, *Deep Sea Research Part I: Oceanographic Research Papers*, *56*(9), 1459-1470, doi: 10.1016/j.dsr.2009.04.009.

Stramska, M., and A. Cieszyńska (2015), Ocean colour estimates of particulate organic carbon reservoirs in the global ocean – revisited, *International Journal of Remote Sensing*, *36*(14), 3675-3700, doi:10.1080/01431161.2015.1049380.

Strömberg, K. P., T. J. Smyth, J. I. Allen, S. Pitois, and T. D. O'Brien (2009), Estimation of global zooplankton biomass from satellite ocean colour, *Journal of Marine Systems*, *78*(1), 18-27, doi:10.1016/j.jmarsys.2009.02.004.

Suess, E. (1980), Particulate organic carbon flux in the oceans—surface productivity and oxygen utilization, *Nature*, *288*(5788), 260–263, doi:10.1038/288260a0.

Sundquist, E. T. (1985), Geological Perspectives on Carbon Dioxide and the Carbon Cycle, in *The Carbon Cycle and Atmospheric CO2: Natural Variations Archean to Present*, pp. 55–59, American Geophysical Union (AGU), doi:10.1029/GM032p0005.

Sverdrup, H. U. (1953), On Conditions for the Vernal Blooming of Phytoplankton, *ICES Journal of Marine Science*, *18*(3), 287-295, doi:10.1093/icesjms/18.3.287.

Taucher, J., L. T. Bach, U. Riebesell, and A. Oschlies (2014), The viscosity effect on marine particle flux: A climate relevant feedback mechanism, *Global Biogeochemical Cycles*, *28*(4), 415-422, doi:10.1002/2013GB004728.

Thor, P., H. G. Dam, and D. Rogers (2003), Fate of organic ca rbon released from decomposing copepod fecal pellets in relation to bacterial production and ectoenzymatic activity, *Aquat. Microb. Ecol.*, *33*, 279-288, doi:10.1016/S0022-0981(98)00104-X.

Tovar-Sanchez, A., C. M. Duarte, S. Hernández-León, and S. A. Sañudo-Wilhelmy (2007), Krill as a central node for iron cycling in the Southern Ocean, *Geophysical Research Letters*, *34*(11), doi:10.1029/2006GL029096.

Turner, J. T. (2002), Zooplankton fecal pellets, marine snow and sinking phytoplankton blooms., *Aquatic Microbial Ecology*, *27*, 57–102, doi:10.3354/Ame027057.

Turner, J. T. (2015), Zooplankton fecal pellets, marine snow, phytodetritus and the ocean's biological pump, *Progress in Oceanography*, *130*, 205–248, doi:10.1016/j.pocean.2014.08.005.

Urban-Rich, J. (1999), Release of dissolved organic carbon from copepod fecal pellets in the Greenland Sea, *Journal of Experimental Marine Biology and Ecology*, *232*(1), 107-124, doi: 10.1016/S0022-0981(98)00104-X.

Vallina, S., B. Ward, S. Dutkiewicz, and M. Follows (2014), Maximal feeding with active prey-switching: A kill-the-winner functional response and its effect on global diversity and biogeography, *Progress in Oceanography*, *120*, 93-109, doi:10.1016/j.pocean.2013.08.001.

Verity, P. G. (1985), Grazing, respiration, excretion, and growth rates of tintinnids, *Limnology and Oceanography*, *30*(6), 1268-1282, doi:10.4319/lo.1985.30.6.1268.

Verity, P. G., and V. Smetacek (1996), Organism life cycles, predation, and the structure of marine pelagic ecosystems, *Marine Ecology Progress Series*, *130*(1-3), 277–293, doi:10.3354/meps130277.

Villareal, T. A., S. Woods, J. Moore, and K. CulverRymsza (1996), Vertical migration of Rhizosolenia mats and their significance to NO_3 fluxes in the central North Pacific gyre, *Journal of Plankton Research*, *18*(7), 1103-1121, doi:10.1093/plankt/18.7.1103.

Volk, T., and M. I. Hoffert (1985), Ocean Carbon Pumps: Analysis of Relative Strengths and Efficiencies in Ocean-Driven Atmospheric CO_2 Changes, in *The Carbon Cycle and Atmospheric CO2: Natural Variations Archean to Present*, pp. 99–110, American Geophysical Union (AGU), doi:10.1029/GM032p0099.

Wang, Q., S. Danilov, D. Sidorenko, R. Timmermann, C. Wekerle, X. Wang, T. Jung, and J. Schröter (2014), The Finite Element Sea Ice-Ocean Model (FESOM) v.1.4: formulation of an ocean general circulation model, *Geoscientific Model Development*, *7*(2), 663–693, doi:10.5194/gmd-7-663-2014.

Ward, B., S. Dutkiewicz, O. Jahn, and M. J. Follows (2012), A size-structured food-web model for the global ocean, *Limnology and Oceanography*, *57*(6), 1877-1891, doi:10.4319/lo.2012.57.6.1877.

Weber, T., J. A. Cram, S. W. Leung, T. DeVries, and C. Deutsch (2016), Deep ocean nutrients imply large latitudinal variation in particle transfer efficiency, *Proceedings of the National Academy of Sciences*, *113*(31), 8606-8611, doi:10.1073/pnas.1604414113.

Wiebe, P. H., and M. C. Benfield (2003), From the Hensen net toward four-dimensional biological oceanography, *Progress in Oceanography*, *56*(1), 7-136, doi:10.1016/S0079-6611(02)00140-4.

Wilson, J. D., S. Barker, and A. Ridgwell (2012), Assessment of the spatial variability in particulate organic matter and mineral sinking fluxes in the ocean interior: Implications for the ballast hypothesis, *Global Biogeochemical Cycles*, *26*(4), doi:10.1029/2012GB004398.

Wright, R. M., C. Le Quéré, E. Buitenhuis, S. Pitois, and M. J. Gibbons (2021), Role of jellyfish in the plankton ecosystem revealed using a global ocean biogeochemical model, *Biogeosciences*, *18*(4), 1291–1320, doi:10.5194/bg-18-1291-2021.

Yool, A., E. E. Popova, and T. R. Anderson (2013), MEDUSA-2.0: an intermediate complexity biogeochemical model of the marine carbon cycle for climate change and ocean acidification studies, *Geoscientific Model Development*, *6*(5), 1767–1811, doi:10.5194/gmd-6-1767-2013.

Zahariev, K., J. R. Christian, and K. L. Denman (2008), Preindustrial, historical, and fertilization simulations using a global ocean carbon model with new parameterizations of iron limitation, calcification, and N_2 fixation, *Progress in Oceanography*, *77*(1), 56-82, doi:10.1016/j.pocean.2008.01.007.

Zeebe, R. E., and D. Wolf-Gladrow (2001), *CO2 in seawater: Eqilibrium, kinetics, isotopes*, vol. 65, Elsevier, ISBN:9780444509468.

Zeebe, R. E., and D. A. Wolf-Gladrow (2009), Carbon dioxide, dissolved (ocean), in *Encyclopedia of Paleoclimatology and Ancient Environments*, edited by V. Gornitz, pp. 123–127, Springer Netherlands, Dordrecht, doi:10.1007/978-1-4020-4411-3_30.

DECLARATION

Versicherung an Eides Statt

Ich, Onur Karakuş,

versichere an Eides Statt durch meine Unterschrift, dass ich die vorstehende Arbeit selbständig und ohne fremde Hilfe angefertigt und alle Stellen, die ich wörtlich dem Sinne nach aus Veröffentlichungen entnommen habe, als solche kenntlich gemacht habe, mich auch keiner anderen als der angegebenen Literatur oder sonstiger Hilfsmittel bedient habe.

Ich versichere an Eides Statt, dass ich die vorgenannten Angaben nach bestem Wissen und Gewissen gemacht habe und dass die Angaben der Wahrheit entsprechen und ich nichts verschwiegen habe.

Die Strafbarkeit einer falschen eidesstattlichen Versicherung ist mir bekannt, namentlich die Strafandrohung gemäß § 156 StGB bis zu drei Jahren Freiheitsstrafe oder Geldstrafe bei vorsätzlicher Begehung der Tat bzw. gemäß § 161 Abs. 1 StGB bis zu einem Jahr Freiheitsstrafe oder Geldstrafe bei fahrlässiger Begehung.

Ort, Datum

Unterschrift

Declaration on the contribution of the candidate to a multi-author article/manuscript which is included as a chapter in the submitted doctoral thesis

Chapter: **"Modeling the Impact of Macrozooplankton on Carbon Export Production in the Southern Ocean"**

Contribution of the candidate in % of the total work load (up to 100% for each of the following categories):

Experimental concept and design:	ca. 60 %
Experimental work and/or acquisition of (experimental) data:	ca.100%
Data analysis and interpretation:	ca. 70 %
Preparation of Figures and Tables:	ca. 70%
Drafting of the manuscript:	ca. 60%

Chapter: **"The Role of Zooolankton Grazing and Nutrient Recycling for Global Ocean Biogeochemistry and Phytoplankton Phenology"**

Contribution of the candidate in % of the total work load (up to 100% for each of the following categories):

Experimental concept and design:	ca. 70 %
Experimental work and/or acquisition of (experimental)	ca.100%
data: Data analysis and interpretation:	ca. 80 %
Preparation of Figures and Tables:	ca. 90 %
Drafting of the manuscript:	ca. 70%

Chapter: **"The Role of Ballasting, Seawater Viscosity and Oxygen for Carbon Export and Transfer Efficiencies in the Global Ocean"**

Contribution of the candidate in % of the total work load (up to 100% for each of the following categories):

Experimental concept and design:	ca. 90 %
Experimental work and/or acquisition of (experimental) data:	ca.100%
Data analysis and interpretation:	ca. 70%
Preparation of Figures and Tables:	ca. 90%
Drafting of the manuscript:	ca. 80 %

Date:

Signatures: